PRINCETON UNIVERSITY

DEPARTMENT OF AERONAUTICAL ENGINEERING

DEPARTMENT OF THE NAVY
BUREAU OF NAVAL WEAPONS
Contract No. NOas 60-6078c

COMBUSTION INSTABILITY

IN

LIQUID PROPELLANT ROCKET MOTORS

TECHNICAL REPORT:

AN INVESTIGATION OF TRANSVERSE MODE COMBUSTION INSTABILITY IN LIQUID PROPELLANT ROCKET MOTORS

Aeronautical Engineering Report No. 550

Prepared by: Frederick H Reardon
F. H. Reardon, Research Aide

Approved by: Luigi Crocco
L. Crocco, Professor-in-Charge

and David T. Harrje
D. T. Harrje, Research Engineer

1 June 1961

Department of Aeronautical Engineering
PRINCETON UNIVERSITY
Princeton, New Jersey

ABSTRACT

The transverse modes of high frequency combustion instability in liquid propellant rocket motors are studied both theoretically and experimentally. The nature of the phenomenon is described, and previous experimental and theroretical work on the problem is discussed. A preliminary exploratory series of experiments demonstrates the need for additional theoretical analysis in order to explain three effects: (1) the influence on stability of the orientation of the elements of the injection pattern with respect to the radial direction, (2) the greater tendency to instability of the spinning forms of tangential modes as compared to the standing forms. (3) the effect of the distribution of injection across the injector face.

The basic theory is derived for the case of a circularly cylindrical combustion chamber with uniformly distributed injection. Following Crocco, the concept of a sensitive time lag is introduced. However, dependence of the time lag on the radial and tangential velocity components as well as on the thermodynamic state properties (represented by the pressure) is assumed. Small perturbation theory is used, in conjunction with an approximate order of magnitude analysis, to derive a characteristic equation relating the frequency of neutral oscillation at the stability limits to the parameters describing the combustion process. Extensions of the basic theory are made to cover the cases of (1) nonuniformly distributed injection, (2) a variable angle sector motor, and (3) more general time lag formulations. The use of the sector motor in the study of tangential modes of instability is discussed. Calculations for an idealized rocket motor are presented in order to illustrate the results of the theoretical analysis.

A series of experiments using both sector and full cylindrical motors is described. It is shown that partial and qualitative verification is obtained

for the theoretical predictions that (1) the standing form of a tangential mode is more stable than the spinning form because the tangential velocity effects are inoperative in the former, (2) the radial velocity fluctuations cause a shift of the unstable ranges of the sensitive time lag, (3) increasing stability is obtained as the propellant injection is moved toward the center of the chamber, (4) the pressure dependent combustion parameters correspond to those which govern the longitudinal modes of instability. The validity of the linearized approach is assessed and areas for further theoretical and experimental work are indicated.

ACKNOWLEDGMENTS

I am indeed grateful to Professor Luigi Crocco, my Faculty Advisor and the Professor-in-Charge of the Combustion Instability Research Program, for his many valuable suggestions and constructive criticisms, both in the course of the investigation and in the writing of this dissertation. Other members of the faculty, notably Professors M. Summerfield and S. I. Cheng, contributed to the final result through stimulating discussions.

It is a pleasure to acknowledge the aid and encouragement which were freely given by Mr. D. T. Harrje, the Research Engineer directing the instability program. The assembly and operation of the rocket motors were carried out by an efficient staff of technicians under the direction of Mr. K. J. Gadsby, who also did much of the primary data reduction. The Jet Propulsion computation group, headed by Messrs. W. H. Dodge and R. N. Deeter, provided important assistance in the performing of the numerical calculations, for many of which the digital computer of the Plasma Physics Laboratory was utilized. The design of the experimental equipment and the drawing of the illustrations for this dissertation were carried out under the direction of Messrs. H. Burkert and T. Poli. I am indebted to Miss Frances Allison and her secretarial staff for the preparation of the manuscript.

Finally, the financial assistance of the Department of the Navy, Bureau of Naval Weapons, under contract numbers NOas 53-817-c and NOas 60-6078-c, is gratefully acknowledged.

TABLE OF CONTENTS

LIST OF ILLUSTRATIONS

List of Illustrations

List of Illustrations (continued)

List of Illustrations (continued)

Nomenclature

A_{pq}	Expansion coefficient for pressure dependent combustion process
$\mathcal{A}$	First transverse nozzle admittance coefficient
a	Droplet momentum function as defined in text
B_{pq}	Expansion coefficient for radial velocity dependent combustion process
$B, \tilde{B}_{pq}$	Modified pressure perturbation axial distribution functions as defined in text
$\mathcal{B}$	Second transverse nozzle admittance function
b_n	Auxiliary function defined in nozzle admittance analysis
C_{pq}	Expansion coefficient for tangential velocity dependent combustion process
$\mathcal{C}$	Third transverse nozzle admittance coefficient
c	Velocity of sound
c^*	Characteristic velocity of experimental rocket motor
f	Velocity distribution term as defined in text
$D, \tilde{D}_{pq}$	Modified velocity perturbation axial distribution functions as defined in text
d	Thickness of spray produced by doublet injector
d	Droplet momentum function as defined in text
E', E'_{pq}	Functions defined in analysis of axially concentrated combustion distribution
$\mathcal{E}$	Combined transverse nozzle admittance coefficient as defined in text
F	Thrust of experimental rocket motor
F', F'_{pq}	Functions defined in analysis of axially concentrated combustion distribution
$F(z)$	Axial distribution of velocity sensitive combustion terms
f	Reduced frequency of neutral oscillations

Nomenclature (continued)

f	Overall rate of processes occurring during combustion of liquid bipropellants in rocket combustion chamber
$G(r,\theta)$	Transverse distribution of velocity sensitive combustion terms
$g(\omega)$	Function expressing effect of non-combustion fluid mechanical processes in solution for velocity parameters
g_n	Auxiliary function defined in nozzle admittance analysis
H	Normalizing factor in eigenfunction expansions as defined in text
H_{pq}	Integrated axial distribution functions for burning rate perturbation as defined in text
$h(\omega)$	Function expressing effect of non-combustion fluid mechanical processes in solution for pressure parameters
h	Index counting the number of cylindrical nodal surfaces in transverse oscillation pattern
h	Specific enthalpy
h_n	Auxiliary function defined in nozzle admittance analysis
J_ν	Bessel function of first kind of order ν
j_n	Function defined in nozzle admittance analysis
K	Dimensionless velocity gradient at nozzle throat
$K_{Apq}, K_{Bpq}, \cdots K_0$	Integration constants
k	Droplet momentum interchange coefficient
$k'(\varepsilon)$	Liquid velocity proportionality factor as defined in text
k_n	Auxiliary function defined in nozzle admittance analysis
L_c	Length of rocket motor combustion chamber
ℓ_r	Radial velocity interaction index
ℓ_θ	Tangential velocity interaction index
$\dot{m}_i$	Mass injection flow rate
$\dot{m}_b$	Mass burning rate

Nomencla ure (continued)

n	Pressure interaction index
n_M	Minimum value of pressure interaction index
$P_{pq}(z)$	Pressure perturbation axial distribution functions
p	Pressure
$\mathcal{P}$	Proportionality factor relating burning rate perturbation to pressure perturbation as defined in text
Q	Mass burning rate per unit volume
r	Radius coordinate in cylindrical system
r_c	Radius of combustion chamber
r_i	Injection radius for concentrated injection distribution
R	Mixture ratio
R_{des}	Design mixture ration of experimental injector
$\mathcal{R}$	Proportionality factor relating burning rate perturbation to radial velocity perturbation
$S_{pq}(z)$	Entropy perturbation axial distribution functions
s	Specific entropy
s	Generalized oscillation frequency, $s=\lambda+i\omega$
t	Time; time at which transformation from reactants to products occurs
$\mathcal{T}$	Proportionality factor relating burning rate perturbation to tangential velocity perturbation
$U_{pq}(z)$	Axial velocity perturbation axial distribution functions
u	Axial velocity
$V_{pq}(z)$	Radial velocity perturbation axial distribution functions
v	Radial velocity
$W_{pq}(z)$	Tangential velocity perturbation axial distribution functions
w	Tangential velocity

Nomenclature (continued)

X	Variable defined in nozzle admittance analysis
Y_x	Local mass fraction of oxidizer vapor in burning droplet spray
Y_ν	Bessel function of second kind of order ν
y	Auxiliary function defined in analysis of droplet dynamics
z	Axial distance coordinate
z_m	Location of concentrated combustion front
$\mathcal{Z}$	Chamber length parameter as defined in text
α	Sector angle
α_n	Longitudinal nozzle admittance coefficient
β_i	Angle of orientation of injector spud with respect to tangential position
β	Droplet drag parameter as defined in text
γ	Ratio of specific heats of gaseous combustion products
Δ	Laplacian operator, $\Delta = \frac{\partial^2}{\partial z^2} + \frac{\partial^2}{\partial r^2} + \frac{1}{r}\frac{\partial}{\partial r} + \frac{1}{r^2}\frac{\partial^2}{\partial \theta^2}$
ξ^0	Auxiliary function defined in nozzle admittance analysis
η_{ij}	Fraction of total injection rate injected at (r_i, θ_j)
θ	Angular coordinate in cylindrical system
θ'	Angular coordinate in sector motor analysis, $\theta' = \frac{\pi}{\alpha}\theta$
θ_i	Angle of injection for tangentially concentrated injection distribution
$\Theta_\nu(\theta)$	Tangential distribution functions for pressure perturbation
λ	Amplification factor
$\mu(r,\theta)$	Transverse combustion distribution function
ν	Index counting the number of diametral nodal surfaces in transverse oscillation pattern
ξ_0, ξ_2	Auxiliary functions defined in nozzle admittance analysis
ρ	Mass density

Nomenclature (continued)

σ	Injection density, i.e., mass injection flow rate per unit area
τ	Sensitive time lag in "common time lag" formulation
τ_T	Total time lag
τ_i	Insensitive time lag in "common" formulation
τ_p	Pressure sensitive time lag
τ_v	Velocity sensitive time lag
$\tau_1, \tau_2, \tau_3, \tau_4$	Insensitive time lags in generalized formulation
τ_M	Sensitive time lag corresponding to minimum interaction index
ϕ	Steady state velocity potential in nozzle analysis
φ	Departure of frequency from acoustic frequency, $\varphi = \frac{\omega}{\omega_0} - 1$
$\Psi_{pq}(r)$	Radial distribution functions for pressure perturbation
ω	Oscillation frequency
ω_M	Frequency corresponding to minimum interaction index

Subscripts

o	Injector face conditions
e	Chamber exit (nozzle entrance)
L	Liquid
m	Mean value
r	Real part of complex quantity
i	Imaginary part of complex quantity
s	Stagnation conditions
0	Zeroth order perturbation solution (acoustic)
1	First order perturbation solution
A	Solution corresponding to pressure effects on combustion process

Nomenclature (continued)

B	Solution corresponding to radial velocity effects on combustion process
C	Solution corresponding to tangential velocity effects on combustion process
D	Solution corresponding to non-combustion fluid mechanical processes

Superscripts

/	Complex, space dependent part of perturbation
—	Steady state
→	Vectorial quantity
*	Dimensional quantity

CHAPTER I

Introduction

A Description of the Phenomenon

In a liquid propellant rocket motor, the combustion process is never entirely smooth. During the steady state period between starting and cutoff, fluctuations occur in all important properties (pressure, temperature, velocity, etc.) around the desired operating values. The amplitude of such fluctuations can vary over a wide range, from motor to motor and in one motor for different operating conditions. When the fluctuations are completely random, the operation is classified as "rough" combustion. A qualitative distinction can be made between "rough" and "smooth" combustion on the basis of the root-mean-square amplitude of the fluctuations.

Combustion instability, on the other hand, consists of organized oscillations, which are maintained and amplified by the combustion process itself. It is generally agreed that there are three kinds of instability, differentiated by the frequency of the resulting oscillations. These are referred to as low, intermediate and high frequency instability.

Low frequency unstable combustion has received much theoretical and experimental study (1,2,3,4)*. It is now rather well understood and comparatively easy to avoid or cure. A theoretical analysis exists for the intermediate frequency case (5), but the phenomenon is rarely observed. This dissertation is concerned with the high frequency type of combustion instability, which is by far the most destructive type and the most difficult to control.

---

* Numbers in parentheses refer to References listed on pp. 120, 121

High frequency instability is a forced oscillation of the combustion chamber gases, driven by the combustion process interacting with the resonance effects of the chamber geometry, with damping supplied by the exhaust nozzle. The resulting oscillation patterns are very similar to those of the acoustic modes of the chamber. For a cylindrical chamber, one can distinguish between longitudinal and transverse acoustic modes. In a longitudinal mode the property variations occur in the axial direction, while conditions are uniform on a section normal to the axis. Purely transverse modes involve uniformity of the properties along the axis, but variations in the radial and circumferential directions. Figure 1 shows the acoustic oscillation patterns for several purely transverse modes for a circular cross section. The most commonly observed modes, in order of increasing frequency, are the first tangential, second tangential, first radial, and the first combined radial tangential. In the "P" diagrams, several typical isobars are drawn, for a given instant, with the solid lines indicating values in excess of the mean pressure level. The "V" diagrams show streamlines at the same instant. Each acoustic mode has a characteristic frequency, which is related to the S number shown with the diagrams (the significance of this number will be discussed more fully in a later section). It has been observed that the frequencies of fully developed pure transverse mode combustion oscillations fall within few percent of the acoustic frequencies for the corresponding modes. Each tangential or combined mode can exist in two forms: the standing form, in which the nodal sufaces (indicated by the solid diametral lines of Figure 1) are stationary, and the spinning form, in which the nodal surfaces rotate at the angular frequency of the oscillation. The two forms of the first tangential mode are illustrated in Figure 2 which shows schematically pressure and velocity patterns at four instants during a period of oscillation.

Purely longitudinal modes occur in chambers with large length to diameter ratios ($L/D \gg 1$); purely transverse modes, for $L/D \ll \frac{1}{2}$; combined longitudinal-transverse modes may be observed when $L/D \sim 1$; provided in all cases that certain requirements for instability are met. The derivation and discussion of these requirements is the substance of this dissertation.

A linearized theoretical analysis will be employed; although such a theory is capable of predicting the onset of instability, it is entirely unable to determine the characteristics of the fully developed oscillations. In particular the amplitude of the fluctuations, which is set by various competing non-linear processes, may be small or large, depending on the mode and the operating conditions. The amplitudes of purely transverse modes have been observed in most cases to be very large; peak-to-peak values of up to 300% of steady state chamber pressure were measured in the course of this investigation. One of the most detrimental consequences of such oscillations is the burnout of combustion chamber hardware because of the abnormally high heat transfer rates associated with instability. In one series of tests (6) a jump in wall heat flux from 3 up to 13 Btu/in^2-sec, was measured accompanying the onset of a transverse mode oscillation. Such effects provide a strong motivation for investigations leading to a better understanding and control of this phenomenon.

B. Previous experimental work

A considerable amount of experimental work has been done on combustion instability in rocket motors. However, very little of this effort has been of a systematic nature, or has been connected with theoretical considerations. The initial studies of Berman and Cheney (7) of longitudinal modes of oscillation used slit window photographic methods. They detected the buildup of small disturbances into high amplitude shock type waves, and showed that the frequencies of oscillation approximated the

acoustic frequencies within the combustion chamber. Ellis and his associates (8) correlated measurements of pressure fluctuations with the optical methods used almost exclusively by Berman and Cheney in their initial studies.

Later work by Ellis extended the optical studies to transverse modes (9). These investigations showed high particle velocities (of the order of 2000 fps) and spiral particle trajectories (in a plane normal to the combustion chamber axis). The changes in the oscillation patterns observed in using chambers of different diameters and different injector configurations were explained qualitatively by means of a "propellant preparation time" and its relation to the "wave travel time", the latter being a function of the chamber size.

Various methods have been developed by the industry to compare the stability of different motor configurations by pulsing during steady state rocket operation. In one method, a series of calibrated powder charges is fired tangentially into the chamber in order to disturb the combustion and flow patterns. Each charge is stronger than the preceding one. Shutdown of the rocket motor is effected automatically following the onset of instability. The number of charges fired is thus a measure of the relative stability of the motor at the particular operating conditions of the test. While such studies are of undoubted value in the development of a rocket engine system, they contribute relatively little to the fundamental understanding of the phenomenon of instability.

Male, Kerslake, and Tischler (10) at the NASA Lewis Research Center made optical studies which corroborated those of other experimenters (7, 8). In addition, they noted some interaction effects between longitudinal and transverse modes of oscillation, as well as the greatly increased heat transfer to the combustion chamber walls which is associated with transverse modes of

instability. Other interesting aspects of combustion instability involving chamber geometry were investigated by this group (1). However, no attempt was made to determine the underlying mechanisms.

Investigations by Osborn and Bonnell (12, 13) using a gas rocket system have sought to assess the effects of such parameters as chamber geometry, chamber pressure, and propellant chemistry on combustion instability. Working with a constant diameter, variable length motor, they have noted with some propellants sharp changes in the stability behavior for transverse modes when the chamber length is increased to the point where longitudinal mode instability is possible, thus indicating important interaction effects between longitudinal and transverse modes. They have also reported widened instability regions with propellants of higher heat release rates.

All of the investigations described above were restricted to the purely empirical approach, rather than attempting fundamental, systematic studies based on a quantitative theory.

C. Previous theoretical work

Probably the first theoretical investigation of the interaction of pressure waves and combustion was that made by Rayleigh in his explanation of Rijke tones (11). He concluded that in order for heat to drive a standing wave, the heat input should maximize with time when the pressure is at its local maximum. Subsequent investigations have extended Rayleigh's analysis to more general combustion systems.

The concept of a combustion time lag as a coordinating influence to excite organized oscillations in a liquid propellant rocket combustion chamber originated in von Karman's group at the Jet Propulsion Laboratory in 1941. Gunder and Friant (2), Yachter (3) and Summerfield (4) made analyses of low frequency instability (which depends upon the interaction between the feed system and combustion process) based on a constant time lag. However, it was

impossible to explain high frequency combustion instability using a constant time lag.

Crocco (15) introduced the time varying combustion time lag in his analysis of high frequency instability. He represented the total time lag τ_T as the sum of two parts; the constant "insensitive" time lag τ_i , and the "sensitive" time lag τ , which varies with time, responding to fluctuations in the chamber conditions. Thus

$$\tau_T = \tau_i + \tau$$

Rather than trying to describe quantitatively the effect of each of the chamber conditions on the time lag, the simplifying assumption was made that the variations of all physical factors could be correlated with values of the local pressure. For small amplitude perturbations, the rate at which the sensitive time lag is affected can be expressed by

$$\tau - \bar{\tau} = \frac{n}{\bar{p}} \int_{t-\bar{\tau}}^{t} (p - \bar{p})\, dt'$$

where the barred quantities correspond to steady state. The factor n was called by Crocco the "interaction index".

The synthetic representation of the combustion process by means of the time lag concept eliminates the need for information on any of the specific processes occurring in the chamber, such as atomization, vaporization, mixing, chemical kinetics, etc. This fact constitutes the primary advantage of the time lag type analysis, since very little quantitative information is available concerning the details of these various processes.

The application to the sensitive time lag theory to the longitudinal mode was first made by Crocco in 1951 (15). The expanded and generalized theory of longitudinal mode combustion instability was published, but without experimental verification, in 1956 by Crocco and Cheng (1). The validity of the theory was shown in a series of experiments reported by Crocco, Grey and Harrje (16).

In the latter paper, a simple means for measuring the combustion parameters and through stability limits tests was presented. The first application of the sensitive time lag theory to transverse modes was made by Scala (5), who considered the stability of general three dimensional perturbations on a one dimensional steady state flow situation. He was able to present only limited results calculated from his theory, and no experimental results, although he was able to show theoretically the destabilizing effect of increasing the nozzle entrance Mach number. The above mentioned investigations of Crocco and his associates (1,5,15,16) provided an important foundation for the present study of transverse mode combustion instability.

Maslen and Moore (17) investigated theoretically the effects of viscous damping in a chamber without combustion. Their results showed that large amplitude non-shock type waves could exist in the spinning form of the tangential mode, but that the standing mode was subject to damping proportional to the amplitude. The damping of the fundamental longitudinal mode was shown to exceed that of the first tangential mode for low values of the ratio of chamber length to diameter.

Recently, Pickford and Peoples (18) have attempted to analyze the stability of liquid rocket combustion by means of an available energy concept, in an attempt at an a priori calculation of stability behavior from knowledge of the physical and chemical nature of the propellants, the injection process, etc. However, it appears that the accomplishment of this objective still lies in the future.

D. Preliminary exploratory testing

At the time of the initiation of the experimental phase of this investigation of transverse mode instability, the theoretical analysis had not been carried beyond that of Reference 2, and because of the complexitity

of the computations required, very little guidance was available from that source. Therefore, the experimental program began with a series of exploratory tests designed to reveal the most significant parameters, on which the later, more systematic tests were to concentrate. The first series of exploratory tests was in the form of a parameter survey. Later, a second group of experiments using half chambers and diametral barriers was made in order to evaluate a proposed method of stability limits testing.

The experimental apparatus consisted of a sectioned, uncooled, copper rocket motor and its associated hardware and instrumentation (Figures 3 and 4). The three parts of the motor--the spud type injector, the four inch long cylindrical chamber section, and the nozzle--were held together by a hydraulic cylinder arrangement to facilitate parameter changes. This system had been used successfully on the longitudinal program. The length of the cylindrical section was fixed by the so-called "critical length" of the propellant-injector combination (the length below which longitudinal mode instability is not possible), since it was desired to study purely transverse modes. The nozzle consisted of a 30° half-angle convergent part blending into a circular arc throat and followed by a 15° half-angle divergent cone. The throat diameter and the subsonic length were determined by the combination of thrust level, chamber pressure, and chamber diameter. All surfaces exposed to the hot combustion gases were ceramic coated (0.012" zirconium oxide over 0.003" nicket-chromium) to reduce heat transfer. Starting was accomplished by means of a solid propellant squib which ignited a gaseous hydrogen preflow. The hydrogen flow was terminated at the time of fuel introduction. The pressurized feed system made use of cavitating venturis for flow regulation. Run durations varied between one-half and three seconds.

Instrumentation included the usual steady-state equipment (propellant

flow rates, chamber and injector pressures, etc.) and high response water cooled strain-gage pressure transducers (19) flush mounted in the chamber. Six locations were provided for the high frequency transducers in the cylindrical chamber section, in two axial and three meridianal planes, in order to investigate the oscillation wave patterns. The steady and fluctuating components of each pressure signal were separated, the steady state portion appearing on a recording potentiometer and the fluctuating portion on a seven channel FM magnetic tape recorder. Amplitudes and frequencies of the recorded pressure oscillations were then measured electronically from the tape recording. A special run cutoff device provided rapid shutdown in the event of a large amplitude instability, in order to minimize burnout of the hardware. A detailed discussion of the instrumentation is found in (20).

The exploratory tests were designed to investigate the following parameters, each of which was to be varied independently of the others:

(1) Chamber diameter--In the transverse mode theory, it was shown that the chamber diameter (or radius) is the characteristic length associated with transverse modes of oscillation. For the exploratory tests, three diameters were chosen, in a range practical for testing at the Forrestal Research Center rocket test facility. These diameters were 3, 6, and 9 inches. However, it was found that the three inch diameter equipment could not be designed with the flexibility required by the exploratory series. Most of the experiments were conducted, therefore, with the two larger diameters.

(2) Chamber pressure--The effect of this parameter was largely unknown at the start. Although some effect on the combustion parameters (time lag and interaction index) was expected, no clear trends had been shown by longitudinal mode testing. The levels selected for testing were 150, 500, and 900 psia.

(3) Thrust--The effect of the thrust level was also unknown.

Injection velocities were kept constant, and the thrust was varied by means of the injector hole size. Some effect on the combustion parameters could be expected from the hole size changes because of differences in the atomization characteristics of the injectors. In addition, the thrust level, chamber pressure, and chamber diameter determine the chamber Mach number, which had been shown to be of importance in the limited results presented in Reference 2. Tests were made at thrust levels of 100, 500 and 1000 pounds.

(4) Mixture ratio---The longitudinal stability limits testing demonstrated that the combustion parameters were strongly dependent on mixture ratio. The exact physical nature of this dependence remains to be determined. Mixture ratios from 1.0 to 2.2 were surveyed. Included in this range were the maximum characteristic velocity (c*) ratio (1.4 for the propellants used) and the stoichiometric ratio (2.09).

(5) Design mixture ratio---This parameter was defined as that ratio at which the bipropellant injection velocities were equal and the net momentum of the spray produced by the doublet injector was axial. Varying the design mixture ratio over the values of 1.0, 1.4, 1.8, and 2.2 resulted in changes in injector hole size as well as in the angles of the injector passages with respect to the combustion chamber axis, with important effects on atomization and mixing to be expected. However, the influence of such effects could not be predicted. Most of the tests were made using the 1.4 design mixture ratio injectors.

(6) Injector type---A simple unlike impinging doublet type injector, with impingement at the injector face and 12 orifice pairs, was chosen for the initial tests of the exploratory series. Although the combustion parameters had been clearly shown to be strong functions of injector type, the greatest amount of longitudinal experience had been obtained with such an injector.

(7) Propellants---As in the case of the type of injector, the propellant combination was known to have a strong influence on stability. The combination of liquid oxygen and 95 percent ethyl alcohol (Solox) was chosen for the first series, again on the basis of greatest instability testing experience.

(8) Injection diameter---In the exploratory test series, the 12 injection points were equally spaced around the circumference of a single circle. Other experimenters had noted a destabilizing trend as the diameter of the injection circle approached the chamber diameter. Injectors were designed for 2 - 1/4, 5, and 8 inch circles. However, the smallest of these proved to be impractical.

(9) Orientation---For maximum experimental flexibility, spud type injectors were used (Figures 5 and 6). Each doublet pair was contained in a single spud, which could be oriented in either of two ways, 90° apart (see Figure 7). In the "radial" orientation, each spud was arranged so that the line of centers of the injection orifices lay along a radius. With the spud rotated through 90° to the "tangential" orientation, the line of centers was tangential to the injection circle. The spud orientation proved to be one of the most important parameters.

The exploratory testing was begun at the 100 pound thrust level. However, the results were somewhat indeterminate When oscillations were present, the amplitudes were very small. In addition, reliable starting was a problem because the small throat diameters necessitated the use of a spark igniter rather than the solid propellant squib used in longitudinal mode stability tests (16). Also, with the small propellant flows involved in these tests, considerable trouble was had with clogging of the cavitating venturis. Therefore, after a limited number of tests, the 100 pound level was discarded in favor of the more reasonable 500 pound thrust level.

Six series of tests comprised the exploratory testing at the 500 pound thrust level. These series were as follows:

1 - 9" chamber, 5" injector, spuds tangential

2 - 9" chamber, 8" injector, spuds tangential

3 - 6" chamber, 5" injector, spuds tangential

4 - 9" chamber, 5" injector, spuds radial

5 - 9" chamber, 8" injector, spuds radial

6 - 6" chamber, 5" injector, spuds radial

In each series, a mixture ratio survey was made (the design mixture ratio was 1.4 for all series) at each of three chamber pressure levels, 150, 500, and 900 psia. The results of these tests are shown in Figures 8 and 9.

In Figure 8, the test points of series 1 to 3 are plotted on the chamber pressure, mixture ratio plane, with the nature of the oscillation shown by the shading of the point. It can be seen that all tests with the tangential orientation were unstable in the first tangential mode. Many of the tests caused destruction of the pressure transducer or of chamber or injector parts, in spite of the run shutdown device. The peak-to-peak amplitudes of the pressure flutuations varied between 170 and 330 psi on these tests. Figure 10 shows the wave shapes, and indicates the use of multiple pickups to determine the wave pattern within the combustion chamber. It was observed that the oscillations in these tests were all of the spinning type. This fact can be seen in Figure 10 in that the 90° phase lag of trace 2 with respect to trace 1 corresponds exactly to the spacing of the two pressure transducers around the circumference of the chamber. In addition, it can be seen that the pressure oscillation near the nozzle is smaller and less steepened than, and lags slightly behind, the oscillation near the injector. This result is to be expected, since it has been shown that the combustion zone, with this particular injector and propellant combination, is concentrated

within 2" of the injector face. None of the waves, even close to the injector, showed steepening into shock-type waves, in contrast with those observed on longitudinal tests (Figure 11). Although all tests with the tangential orientation were unstable, the amplitudes of the fully developed oscillations were greater when the propellants were injected near the chamber wall (Figure 8), thus showing one effect of the injection diameter.

Quite different results were obtained with the radial spud orientation as shown in Figure 9. The first observation which can be made is that the radial orientation tests were more stable than the tangential. Only the 9" chamber with the 8" injector gave well defined zones of instability. The first tangential mode was observed at the lowest pressure level for mixture ratios in the vicinity of the design point (1.4). The disappearance of the first tangential mode can be explained qualitatively by the fact (determined by the analysis of Reference 5) that decrease in the chamber Mach number is stabilizing. Since all tests of this series were made at the 500 pound thrust level, the higher pressures were obtained by decreasing the size of the nozzle throat, thus decreasing the chamber Mach number. At higher pressures, the second tangential mode was observed, but with very much smaller amplitudes. No calculations were made in Reference 2 for the second tangential mode. However, the presence of the second mode in these tests agrees well with theoretical results presented in a later section. It can be seen that only for this series (5) were well defined stability limits observed, to which a linear theory could be applied.

Injection of the propellant nearer to the center of the combustion chamber was seen in series 4 tests (9" chamber, 5" injector, radial orientation) to have a stabilizing effect, a result which agrees qualitatively with the reduced amplitudes of the corresponding tangential orientation tests (series 1). The results of the 6" chamber, 5" injector tests (radial orientation) were not clear. At the low pressure level stability was observed. At higher

pressures the traces showed several modes present intermittently, including the first and second tangential and first radial modes. The stability of the 6" motor as contrasted to the instability observed for similar operating conditions with the 9" motor can be explained qualitatively by noting that while the resonance properties of the 9" chamber were matched to the time lag of the combustion process, the decrease in diameter destroyed the resonant coupling.

At this point, the need for more systematic experiments, involving the determination of stability limits, which could be compared quantitatively with the theory being developed, became clear. In the longitudinal program, the primary experiment is that of determining limits of stability on the mixture ratio-chamber length plane. Because of the fact that the length of the chamber (above a certain minimum) has little effect on the combustion pattern but a great effect on the resonance properties of the chamber, such limits can be used to deduce values of the combustion parameters, the sensitive time lag τ and the interaction index n (16).

For the case of the tangential modes of transverse instability, the "sector motor" concept was evolved. In this type of test, only one sector of the motor is operated, the rest of the chamber and nozzle (to the throat) are filled in with a copper insert. Such a motor is shown schematically in Figure 12(b) and in Figure 13.

A 180° or half chamber, formed by means of an insert, can oscillate only in the standing form of a tangential mode. On the other hand, a full 360° chamber can sustain either the standing or spinning form of the mode. As in the tests discussed above, the spinning form is the one normally observed in an unstable full chamber. According to the pressure sensitive time lag theory of (5), the stability behavior should be the same for both the full and half chambers, as long as the operating conditions are the same. A series of tests was made in order to test this conclusion. The results are

presented in Table I. All tests were made at the same conditions of chamber pressure and mixture ratio, but it is clear that the stability behavior of the two forms of first tangential mode is not the same.

Further tests in this series made use of barriers, of 1/4" thick steel and of various lengths, placed in the chamber along a diametral surface, instead of the 180° sector insert (see Figure 12(a)). Such barriers were found to be capable of producing the same stable operation as the full 180° insert. It was also determined that stable operation resulted with a barrier only 5/8" long, if the barrier was placed against the injector face. If a space was left between the injector and barrier, instability was observed, even though a longer barrier was used. The conclusions to be drawn are that the pressure sensitivity theory of (5) is not sufficient to explain completely transverse modes of instability, and that the additional effects, which cause the spinning form to be much more unstable than the standing form, are concentrated near the injector face, in the early combustion zone.

In order to investigate the transition from the stable standing form of the tangential modes to the unstable spinning form, the permanent steel barrier was replaced with a destructible one. The latter was made of aluminum, 1/8" thick by 1" long, and was placed against the injector face. Experiments showed that the aluminum barrier remained essentially intact for the first second of operation, but disappeared quickly at that time. Thus each aluminum barrier test could show motor operation under both stable and unstable conditions.

A comparison of the stability of the standing and spinning modes using the tangential spud orientation is shown in Figure 14. The first and second lines represent the whole and half chamber tests, respectively, which were discussed above. The third and fourth lines present the results of the aluminum barrier tests. It can be seen that the early portion of these tests

corresponded to the 180° sector tests, and that as soon as the constraint to the standing mode was removed, the rocket operation became unstable. In the transition period a smooth increase in amplitude from the combustion noise level to that of the fully developed oscillation was observed.

Results of a similar series of experiments using the radial spud orientation are presented in Figure 15. Just as in the tangential orientation tests, the unstable region observed with full chamber operation was not present in the half chamber tests. The aluminum barrier tests reproduced the half chamber test results during the early portion of each run ($t < 1$ second). However, unlike the corresponding tangential orientation tests, when the barrier burned away, the rocket motor operation remained stable. Such anomalous behavior may indicate the existence of non-linear effects during the starting transient period of the radial orientation tests.

The exploratory test program demonstrated three effects not predicted by previous theories. They were: (1) the marked difference in stability behavior between the tangential and radial spud orientations, (2) the greater tendency to instability of the spinning mode compared to the standing mode, and (3) the effect of the injection diameter in an injection pattern concentrated on a single circle. It then became necessary to modify the existing theory in an attempt to explain the effects noted.

These modifications are developed in the following two chapters. In Chapter II, the stability analysis is made for a one dimensional steady state flow, which implies that the injection is uniformly distributed. The geometry of the combustion chamber is that of a circular cylinder, corresponding to the full chamber used in the exploratory tests. The analysis is extended in Chapter III to cover cases of non-uniformly distributed injection and is also applied to the sector motor. Chapter IV presents experimental data which is compared with the theoretical predictions; the validity of the modified theory is then assessed.

CHAPTER II

Instability Analysis for a Circular Cylindrical Combustion Chamber with Uniform Injection

A. Governing Equations

The analysis which follows is based on the consideration of the stability of small perturbations. Each of the quantities describing the flow in the rocket motor is assumed to oscillate about a given steady state value. For certain operating conditions, the oscillation amplitudes will increase with time, even for arbitrarily small initial amplitudes. Since random fluctuations of small but finite amplitude (generally referred to as "combustion noise") are always present in a rocket motor, such unstable operating conditions must be avoided. The approach which will be used in the determination of the stability of a rocket combustion system is the following. Conditions will be established for the existence of neutral oscillations, the amplitudes of which neither increase nor decrease with time. The assemblage of the operating points of the system which satisfy the conditions for neutral oscillation form the "stability limits" which divide the unstable from the stable regions of operation. The complete stability behavior of the rocket is described by specifying the stability limits and indicating the unstable regions.

The rocket motor to be considered consists of a circular cylindrical combustion chamber of length L_c and radius r_c, followed by a converging-diverging expansion nozzle. The walls are assumed to be rigid, impervious, and adiabatic. The medium within the chamber consists of gaseous products of combustion in which are distributed burning droplets of the liquid propellants. The volume occupied by the liquid is taken to be negligibly small. In this two phase flow, the burning droplets act as distributed sources of mass, momentum, and energy. It is assumed that combustion is

completed within the combustion chamber and that the gas velocity in the chamber is so small that the square of the Mach number is negligible compared to unity. Thus, in this ideal rocket motor, the flow is divided into two parts, a low speed combustion process and an expansion to supersonic velocity without combustion.

It is convenient to carry out the analysis in terms of the following dimensionless variables:

$$
\begin{aligned}
&\text{pressure} && p = \frac{p^*}{\bar{p}_0^*} \\
&\text{density} && \rho = \frac{\rho^*}{\bar{\rho}_0^*} \\
&\text{temperature} && T = \frac{T^*}{\bar{T}_0^*} \\
&\text{enthalpy} && h = \frac{(\gamma-1)h^*}{\gamma R^* \bar{T}_0^*} \\
&\text{entropy} && s = \frac{s^*}{c_p^*} \\
&\text{velocity} && \vec{V} = \frac{\vec{V}^*}{\bar{c}_0^*} \\
&\text{mass burning rate per unit volume} && Q = \frac{Q^* r_c^*}{\bar{p}_0^* \bar{c}_0^*} \\
&\text{time} && t = \frac{t^* \bar{c}_0^*}{r_c^*} \\
&\text{axial distance} && z = \frac{z^*}{r_c^*} \\
&\text{radial distance} && r = \frac{r^*}{r_c^*}
\end{aligned}
\qquad (2.1)
$$

where c^* is the velocity of sound, C_p^* is the constant pressure specific heat, $\gamma = \frac{C_p^*}{C_v^*}$ is the ratio of specific heats, and R^* is the gas constant. The

subscript o denotes values at the injector face, * indicates a dimensional quantity, a superposed arrow indicates a vector, and barred quantities correspond to steady state. Droplet properties will be denoted by the subscript L. It should be noted that the droplet density ρ_L^* is the total mass of droplets per unit volume of gas. Since the steady state gas velocity must vanish at the injector face, $\bar{p}_o^*$, $\bar{\rho}_o^*$, $\bar{T}_o^*$ and $\bar{c}_o^*$ are stagnation quantities. The cylindrical coordinate system is shown in Figure 16.

The equations stating the conservation of mass, momentum, and energy for the system of burning droplets and combustion products will be presented here without derivation. For a more complete discussion, the reader is referred to References(1) and (5). The continuity equations are

$$\frac{\partial \rho}{\partial t} + \nabla \cdot (\rho \vec{v}) = \Omega = -\frac{\partial \rho_L}{\partial t} - \nabla \cdot (\rho_L \vec{V}_L) \tag{2.2a}$$

Neglecting viscous effects, the conservation of momentum takes the form

$$\frac{\partial}{\partial t}(\rho \vec{v} + \rho_L \vec{V}_L) + \rho \vec{v}(\nabla \cdot \vec{v}) + (\vec{v} \cdot \nabla)\rho \vec{v}$$

$$+ \rho_L \vec{V}_L (\nabla \cdot \vec{V}_L) + (\vec{V}_L \cdot \nabla)\rho_L \vec{V}_L = -\frac{1}{\gamma} \nabla p \tag{2.2b}$$

In the energy conservation equation, terms expressing the work done by viscous stresses and heat transferred by conduction or diffusion will be neglected. Then the energy equation in terms of the stagnation enthalpy, $h_s = h + \frac{\gamma-1}{2} v^2$ is

$$\rho \left[\frac{\partial h_s}{\partial t} + (\vec{v} \cdot \nabla) h_s \right] = \frac{\gamma-1}{\gamma} \frac{\partial p}{\partial t} - \Omega (h_s - h_{Ls}) \tag{2.2c}$$

where h_{LS} includes the chemical energy of the propellants.

The momentum interchange between the liquid and gaseous phases can be expressed by the equation

$$\frac{\partial \vec{V}_L}{\partial t} + (\vec{V}_L \cdot \nabla)\vec{V}_L = k(\vec{V} - \vec{V}_L) \tag{2.2d}$$

where the coefficient k is related to the frictional drag. The equation describing the energy transfer between phases will, following Crocco (1), be replaced by the simple relation

$$\frac{\partial h_{LS}}{\partial t} + (\vec{V}_L \cdot \nabla) h_{LS} = 0 \tag{2.2e}$$

The equation of state of the combustion gases is taken as

$$p = \rho T \tag{2.2f}$$

The set of equations to be solved must be completed by an expression for the burning rate Q, to be derived in a later section, and appropriate boundary conditions on all of the variables.

Each quantity is now written as the sum of a steady state part and a time varying perturbation. Thus the pressure is expressed as

$$p = \bar{p} + p' e^{st} \tag{2.3}$$

where $\bar{p}$ is the steady state pressure and p' is the complex, space dependent perturbation amplitude. (For simplicity in the analysis below the term "pressure perturbation" will be understood to mean p' only).

In the time dependent factor e^{st}, $s=\lambda+i\omega$, in which the real part λ is the amplification factor and the imaginary part is the frequency of oscillation.* The condition $\lambda=0$ corresponds to neutral oscillation at a stability limit, while $\lambda<0$, $\lambda>0$ represent stability and instability, respectively. As mentioned above, the analysis will be directed toward the determination of the conditions which prevail when $\lambda=0$ or $s=i\omega$. It is assumed that the perturbations are sufficiently small that the squares and products of perturbations can be neglected in comparison to the steady state values.

The components of the vectorial gas and droplet velocities $\vec{V}$ and $\vec{V}_L$, are represented as follows:

axial components u, u_L

radial components v, v_L

tangential components w, w_L

The steady state flow is assumed to be one dimensional, although the perturbations will be considered in three dimensions, thus

$$\left.\begin{aligned} \bar{\vec{V}} &= \bar{u}\,, \quad \bar{\vec{V}}_L = \bar{u}_L \\ \bar{v} &= \bar{w} = \bar{v}_L = \bar{w}_L = 0 \end{aligned}\right\} \tag{2.4}$$

and the time and transverse space derivatives vanish in the steady state governing equations.

---

*In the complex representation of oscillating quantities, used in this analysis, the actual physical value of a quantity is given by the real part of the corresponding complex expression.

The system of steady state equations is then

$$\frac{d}{dz}(\bar{\rho}\bar{u}) = \bar{Q} = -\frac{d}{dz}(\bar{\rho}_L \bar{u}_L) \tag{2.5a}$$

$$\frac{d}{dz}(\bar{\rho}\bar{u}^2) + \frac{d}{dz}(\bar{\rho}_L \bar{u}_L^2) = -\frac{1}{\gamma}\frac{d\bar{p}}{dz} \tag{2.5b}$$

$$\bar{\rho}\bar{u}\frac{d\bar{h}_s}{dz} = -\bar{Q}(\bar{h}_s - \bar{h}_{Ls}) \tag{2.5c}$$

$$\bar{p} = \bar{\rho}\bar{T} \tag{2.5d}$$

$$\bar{u}_L \frac{d\bar{u}_L}{dz} = k(\bar{u} - \bar{u}_L) \tag{2.5e}$$

$$\frac{d\bar{h}_{Ls}}{dz} = 0 \tag{2.5f}$$

with the following boundary conditions at $\bar{z} = 0$:

$$\bar{u} = 0\,, \quad \bar{u}_L = \bar{u}_{L0}\,, \quad \bar{\rho}_L = \bar{\rho}_{L0}$$

$$\bar{p} = \bar{\rho} = \bar{T} = 1$$

$$\bar{h}_s = \bar{h}_{s0}\,, \quad \bar{h}_{Ls} = \bar{h}_{Ls0}\,, \quad \bar{Q} = 0$$

The continuity equations are integrated to give

$$\bar{\rho}\bar{u} = \int_0^{\bar{z}} \bar{Q}(\bar{z}')\,d\bar{z}' = \bar{\rho}_{L0}\bar{u}_{L0} - \bar{\rho}_L \bar{u}_L \tag{2.6}$$

where $\bar{\rho}_{L0}\bar{u}_{L0}$ is the propellant injection rate. The momentum equation yields

$$\bar{p} = 1 - \gamma(\bar{\rho}\bar{u}^2 + \bar{\rho}_L\bar{u}_L^2 - \bar{\rho}_{L0}\bar{u}_{L0}^2) \tag{2.7}$$

Then, since $\bar{T} = \frac{\bar{T}^*}{\bar{T}_0^*} = 1 - (\frac{\gamma-1}{2})\bar{u}^2$, the steady state gas density is given by

$$\bar{\rho} = \frac{\bar{p}}{1 - (\frac{\gamma-1}{2})\bar{u}^2} = \frac{1 - \gamma(\bar{\rho}\bar{u}^2 + \bar{\rho}_L\bar{u}_L^2 - \bar{\rho}_{L0}\bar{u}_{L0}^2)}{1 - (\frac{\gamma-1}{2})\bar{u}^2} \tag{2.8}$$

The dimensionless gas velocity $\bar{u}$, which is very nearly equal to the Mach number, increases from zero at the injector face to a maximum value $\bar{u}_e$ at the chamber exit (or nozzle entrance) station, $z = z_e = \frac{L_c^*}{r_c^*}$. It is assumed that the exit velocity $\bar{u}_e$ is small enough that its square is negligible compared to unity. That is, the analysis will be carried out to include terms of the same order of magnitude as the exit velocity (written symbolically as $O(\bar{u}_e)$), but terms of the order of $\bar{u}_e^2$ will be neglected.

The order of magnitude comparisons to be made in the following analysis are not intended to be mathematically exact, but rather to express relations which are approximately true in the range of parameter values considered.

Liquid injection velocities are typically somewhat less than the chamber exit velocities. Initially, the droplet velocity decreases because the gas velocity is very nearly zero in the vicinity of the injector. For injection into stagnant gas, equation (2.5e) gives

$$\frac{d\bar{u}_L}{dz} = -k$$

The distance which the droplet penetrates into gas is then

$$z_p = \frac{u_{L0}}{k}$$

A reasonable assumption is that the "penetration distance" z_p is $O(1)$, so that the droplet coefficient k is $O(\bar{u}_e)$. Therefore, the droplet velocity decreases gradually, as the gas velocity increases due to combustion, until the two velocities are equal. Then $\bar{u}_L$ increases again as the droplets are carried along with the gas stream toward the nozzle. The droplet velocity is always less than the gas velocity and approaches it asymptotically. It is clear that the momentum interchange coefficient k will increase as the droplet vaporizes and burns. Rather than take this variation into account specifically a constant, effective value will be used.

The steady state values of pressure, temperature, and density are, to $O(\bar{u}_e)$,

$$\bar{p} = \bar{T} = \bar{\rho} = 1 \tag{2.9}$$

The relation between the gas velocity and the burning rate is

$$\bar{u} = \int_0^{\bar{z}} \bar{Q}(\bar{z}')\, d\bar{z}' \tag{2.10a}$$

or

$$\bar{Q} = \frac{d\bar{u}}{d\bar{z}} \tag{2.10b}$$

Integration of equation (2.5f) yields

$$\bar{h}_{LS} = \text{constant} = \bar{h}_{LSo}$$

Introducing this result into the energy equation (2.5c) gives

$$\bar{u}\frac{d\bar{h}_s}{d\bar{z}} = -\frac{d\bar{u}}{d\bar{z}}(\bar{h}_s - \bar{h}_{LSo})$$

which can be written as

$$\frac{d}{d\bar{z}}\left[\bar{u}(\bar{h}_{LS} - \bar{h}_{LSo})\right] = 0$$

and integrates to

$$\bar{u}(\bar{h}_s - \bar{h}_{LSo}) = \text{constant}$$

The only constant value which will satisfy this relation is zero. Therefore

$$\bar{h}_s = \bar{h}_{LSo} = \bar{h}_{LS} = \bar{h}_{so} \tag{2.11}$$

In order to investigate the stability problem for a particular rocket motor, it is necessary to have specified the steady state combustion distribution function $\bar{Q}(\bar{z})$, equivalently, the gas velocity distribution $\bar{u}(\bar{z})$. The liquid droplet velocity can be found in terms of the gas velocity from equation (2.5e), as discussed in Appendix A. Then, since it is assumed that combustion is complete at the chamber exit, the liquid density is

obtained from the continuity equation by the relation

$$\bar{\rho}_L(z) = \frac{\bar{u}_e - \bar{u}(z)}{\bar{u}_L(z)} \tag{2.12}$$

In order to obtain the solution for the unsteady flow, the steady state solution, equations (2.9) to (2.12), is perturbed by writing

$$\left.\begin{aligned}
&p = 1 + p' e^{st}, \quad \rho = 1 + \rho' e^{st}, \quad T = 1 + T' e^{st}, \\
&u = \bar{u} + u' e^{st}, \quad v = v' e^{st}, \quad w = w' e^{st}, \\
&\rho_L = \bar{\rho}_L + \rho_L' e^{st}, \quad u_L = \bar{u}_L + u_L' e^{st}, \quad w_L = v_L' e^{st}, \\
&w_L = w_L' e^{st}, \quad Q = \frac{d\bar{u}}{dz} + Q' e^{st}, \quad h_s = \bar{h}_{LSo} + h_s' e^{st}, \\
&h_{LS} = \bar{h}_{LSo} + h_{LS}'
\end{aligned}\right\} \tag{2.13}$$

as discussed above. The exp[illegible]s (2.13) are then inserted into the equations governing the flow, equations (2.2a) to (2.2f), the indicated differentiations and multiplications are carried out, and the terms involving squares and products of perturbations are neglected. Then subtraction of the steady state equations and cancellation of the factor e^{st} give the equations to be satisfied by the perturbations (i. e., the space dependent perturbation amplitudes). These steps are presented in detail in (5) and will not be repeated here. The resulting perturbation equations (in cylindrical coordinates) are the following:

continuity,

$$\left.\begin{aligned}
&s\rho' + \frac{\partial u'}{\partial z} + \frac{\partial v'}{\partial r} + \frac{v'}{r} + \frac{1}{r}\frac{\partial w'}{\partial \theta} + \bar{u}\frac{\partial \rho'}{\partial z} + \frac{d\bar{u}}{dz}\rho' = Q' \\
&= -s\rho_L' - \bar{\rho}_L\left(\frac{\partial u_L'}{\partial z} + \frac{\partial v_L'}{\partial r} + \frac{v_L'}{r} + \frac{1}{r}\frac{\partial w_L'}{\partial \theta}\right) - \bar{u}_L\frac{\partial \rho_L'}{\partial z} - \frac{d\bar{u}_L}{dz}\rho_L' - \frac{d\bar{\rho}_L}{dz}u_L'
\end{aligned}\right\} \tag{2.14a}$$

axial component of moment n,

$$s(u'+\bar{u}\rho') + \bar{u}\left(\frac{\partial v'}{\partial r} + \frac{v'}{r} + \frac{1}{r}\frac{\partial w'}{\partial \theta}\right) + 2\bar{u}\frac{\partial u'}{\partial z} + 2\frac{d\bar{u}}{dz}u' + 2\bar{u}\frac{d\bar{u}}{dz}\rho' = -\frac{1}{\gamma}\frac{\partial p'}{\partial z}$$
$$-s(\bar{\rho}_L u_L' + \bar{u}_L \rho_L') - \bar{\rho}_L \bar{u}_L\left(\frac{\partial v_L'}{\partial r} + \frac{v_L'}{r} + \frac{1}{r}\frac{\partial w_L'}{\partial \theta}\right) - 2\bar{\rho}_L \bar{u}_L \frac{\partial u_L'}{\partial z} - 2\bar{\rho}_L \frac{d\bar{u}_L}{dz} u_L' \qquad (2.14b)$$
$$- 2\bar{u}_L \frac{d\bar{\rho}_L}{dz} u_L' - 2\bar{u}_L \frac{d\bar{u}_L}{dz} \rho_L'$$

radial component of moementum

$$s(v' + \bar{\rho}_L v_L') + \frac{d\bar{u}}{dz} v' + \bar{u}\frac{\partial v'}{\partial z} + \bar{\rho}_L \frac{d\bar{u}_L}{dz} v_L'$$
$$+ \bar{\rho}_L \bar{u}_L \frac{\partial v_L'}{\partial z} + \bar{u}_L \frac{d\bar{\rho}_L}{dz} v_L' = -\frac{1}{\gamma}\frac{\partial p'}{\partial r} \qquad (2.14c)$$

tangential component of momentum,

$$s(w' + \bar{\rho}_L w_L') + \frac{d\bar{u}}{dz} w' + \bar{u}\frac{\partial w'}{\partial z} + \bar{\rho}_L \frac{d\bar{u}_L}{dz} w_L'$$
$$+ \bar{\rho}_L \bar{u}_L \frac{\partial w_L'}{\partial z} + \bar{u}_L \frac{d\bar{\rho}_L}{dz} w_L' = -\frac{1}{\gamma r}\frac{\partial p'}{\partial \theta} \qquad (2.14d)$$

energy,

$$s\, h_s' + \bar{u}\frac{\partial h_s'}{\partial z} = \frac{\gamma-1}{\gamma} s\, p' - \frac{d\bar{u}}{dz}(h_s' - h_{Ls}') \qquad (2.14e)$$

droplet dynamics,

$$\left.\begin{aligned} s u_L' + \bar{u}_L \frac{\partial u_L'}{\partial z} + \frac{d\bar{u}_L}{dz} u_L' &= k(u' - u_L') \\ s v_L' + \bar{u}_L \frac{\partial v_L'}{\partial z} &= k(v' - v_L') \\ s w_L' + \bar{u}_L \frac{\partial w_L'}{\partial z} &= k(w' - w_L') \end{aligned}\right\} \qquad (2.14f)$$

state,

$$p' = \rho' + T' \qquad (2.14g)$$

and droplet energy,

$$s\, h_{Ls}' + \bar{u}_L \frac{\partial h_{Ls}'}{\partial z} = 0 \qquad (2.14h)$$

This last equation is satisfied by

$$h_{Ls}' = h_{Ls_0}'(0, r, \theta)\, e^{-\int_0^z \frac{s}{\bar{u}_L} dz'}$$

Assuming that the enthalpy (or energy) of the liquid propellants supplied to the rocket motor is constant, $h'_{LS_0} = 0$, and thus $h'_{LS} = 0$. Introducing this result into the energy equation and replacing the stagnation enthalpy perturbation by

$$h'_s = p' - \rho' + (\gamma-1)\bar{u}u'$$

(since $h' = T'$ for the nondimensionalization scheme used, and the equation of state gives $T' = p' - \rho'$) yields a modified energy equation.

$$s\left[p' - \rho' + (\gamma-1)\bar{u}u'\right] + \frac{\partial}{\partial z}\left\{\bar{u}\left[p' - \rho' + (\gamma-1)\bar{u}u'\right]\right\} = \frac{\gamma-1}{\gamma} s p' \qquad (2.14i)$$

The equations describing the dynamics of the liquid droplets are discussed in Appendix A. Solutions are obtained of the form

$$\left.\begin{aligned} u_L' &= \frac{k}{s}u' \\ v_L' &= \frac{k'(z)}{s}v' \\ w_L' &= \frac{k'(z)}{s}w' \end{aligned}\right\} \qquad (2.15)$$

where $k'(z) = \frac{s}{k}\left(1 - e^{-(k+s)\int_0^z \frac{dz'}{\bar{u}_L}}\right)$. Since k and k' are $O(\bar{u}_e)$, the liquid velocity oscillations are an order of magnitude smaller than the corresponding gas velocity oscillations.

B. Burning Rate Perturbation

The system of perturbation equations is not complete without an expression for the burning rate perturbation, Q'. The relation for Q' derived by Crocco (1) and later used by Scala (5) made use of the concept of the combustion time lag. That is, the gradual evolution of combustion products from an element of propellant mixture traveling through the combustion chamber after injection was approximated by a discontinuous conversion from reactants to products after a certain time, called the time lag, had elapsed. By this approximation, the impossible task of describing the combustion process

through the quantitative knowledge of its intermediate history was greatly simplified. It was recognized that if the combustion chamber conditions fluctuate, the time lage must also vary. An additional approximation was introduced to simplify the description of the effect of the chamber conditions on the time lag. The total time lag τ_T was taken as the sum of an insensitive time lag τ_i and a sensitive time lag τ. The various physical conditions were assumed to affect the combustion processes only during the sensitive portion of the total time lag. Thus, during fluctuating operation of the rocket motor, the time variation of the total combustion time lag is taken up completely by the sensitive time lag; the insensitive time lag is constant.

The burning rate perturbation can be related to the rate of change of the time lag by considering a small fractional element $\delta \dot{m}_b$ of the propellants burning at a given location at the time t. The burning rate of such an element is related to the local burning rate per unit volume by

$$\delta \dot{m}_b(z, r, \theta, t) = Q(z, r, \theta, t) \cdot r\, dr\, d\theta\, dz$$

This element was injected $\tau_T(z, r, \theta, t)$ seconds before combustion, as a fraction of the total injection rate

$$\delta \dot{m}_i\left(t - \tau_T[z, r, \theta, t]\right)$$

Then, since the element burning during the time interval dt was injected during the interval $d(t-\tau_T)$, continuity requires that

$$\delta \dot{m}_i (t-\tau_T)\, d(t-\tau_T) = \delta \dot{m}_b(t)\, dt$$

or

$$\delta \dot{m}_b (z, r, \theta, t) = \delta \dot{m}_i \left(t - \tau_T[z, r, \theta, t]\right) \cdot \left(1 - \frac{d\tau_T}{dt}\right)$$

Introducing the division of the total time lag into its sensitive and insensitive parts,

$$\tau_T = \tau_i + \tau$$

where, by definition, $\frac{d\tau_i}{dt} = 0$, gives

$$\delta \dot{m}_b(t) = \delta \dot{m}_i(t-\tau_T) \cdot \left(1 - \frac{d\tau}{dt}\right)$$

Under steady state conditions, this last relation reduces to

$$\delta \overline{\dot{m}_b} = \delta \overline{\dot{m}_i}$$

In the following analysis, attention will be concentrated on intrinsic instability, that is, instability occurring when the injection rate is constant. Then

$$\delta \dot{m}_i = \delta \overline{\dot{m}_i} = \delta \overline{\dot{m}_b}$$

and

$$\delta \dot{m}_b = \delta \overline{\dot{m}_b} \left(1 - \frac{d\tau}{dt}\right)$$

In terms of the burning rate per unit volume,

$$Q = \bar{Q}\left(1 - \frac{d\tau}{dt}\right) + \text{higher order terms}$$

or

$$Q' e^{st} = Q - \bar{Q} = -\frac{d\bar{u}}{dz} \cdot \frac{d\tau}{dt} \qquad (2.16)$$

Spatial effects due to the fluctuations of the total time lag and liquid droplet velocity contribute terms of the same order of magnitude as $\bar{u}\frac{d\bar{u}}{dz}$. While $\frac{d\bar{u}}{dz}$ may be O(1) locally, the effect of this factor integrated over the entire chamber is only $O(\bar{u}_e)$. This result is demonstrated Appendix B. The terms introduced by spatial variations are therefore $O(\bar{u}_e^2)$ and have been neglected.

In the original formulation by Crocco, the time lag was defined by noting that the transformation for burnt gases takes place only when the processes occurring during the time lag have accumulated up to a well determined level, $\bar{E}_a$. This condition was expressed by the equation

$$\int_{t-\tau_T}^{t} f(x_i[t'])dt' = \bar{E}_a = \int_{t-\bar{\tau}_T}^{t} \bar{f}(x_i[t'])dt' \tag{2.17}$$

where f is the overall rate of the various processes involved in the combustion of the liquid bipropellants, and t is the time at which the transformation to burned gases occurs. In the integrals, the rate f must be computed using the instantaneous values of the physical conditions at each instant t' at the location x_i (representing the spatial variables z, r, θ) where the element is at that instant. The sensitivity of the rate f to variations in chamber conditions (correlated to the local pressure) was expressed by the interaction index n, defined by

$$n = \frac{\bar{p}}{\bar{f}}\left(\frac{\partial f}{\partial p} + \frac{\partial f}{\partial T}\frac{\partial T}{\partial p} + \cdots\right) \tag{2.18}$$

where the parenthetical expression is evaluated at the steady state operating conditions. The assumption was made that the sensitive portion of the time lag occurrs just before the conversion to combustion products. Then during the insensitive time lag the unsteady process rate is equal to the steady state rate,

$$f = \bar{f}, \qquad t - \tau_T \le t' \le t - \tau \tag{2.19}$$

Since the unsteady pressure is of the form $p = \bar{p} + p'e^{st}$, the process rate during the sensitive time lag is given by

$$f = \bar{f}(1 + n p' e^{st'}), \qquad t - \tau \le t' \le t \tag{2.20}$$

Introducing these expressions for $\bar{f}$ into equation (2.17) gives

$$\int_{t-\tau_T}^{t} \bar{f}\,dt' = \int_{t-\tau_T}^{t-\tau} \bar{f}\,dt' + \int_{t-\tau}^{t} \bar{f}\,(1+n\,p'e^{st'})\,dt' = \bar{E}_a$$

or

$$\int_{t-\tau_T}^{t} \bar{f}\,dt' + \int_{t-\tau}^{t} \bar{f}\,n p' e^{st'}\,dt' = \bar{E}_a \tag{2.21}$$

The first term in this equation can be written as

$$\int_{t-\tau_T}^{t-\bar{\tau}_T} \bar{f}\,dt' + \int_{t-\bar{\tau}_T}^{t} \bar{f}\,dt'$$

which, by equation (2.17) is

$$\int_{t-\tau_T}^{t-\bar{\tau}_T} \bar{f}\,dt' + \bar{E}_a$$

Then equation (2.21 becomes

$$\int_{t-\tau_T}^{t-\bar{\tau}_T} \bar{f}\,dt' = -n \int_{t-\tau}^{t} \bar{f}\,p' e^{st'}\,dt' \tag{2.22}$$

Assuming the spatial nonuniformity of $\bar{f}$ to be negligible, the integral on the left side of equation (2.22) can be written as $\bar{f}\cdot(\tau_T - \bar{\tau}_T)$, and

$$\tau_T - \bar{\tau}_T = \tau - \bar{\tau} = -\int_{t-\bar{\tau}}^{t} n p' e^{st'}\,dt' \tag{2.23}$$

neglecting higher order terms. Differentiation of equation (2.23) with respect to time gives

$$\frac{d\tau}{dt} = -n\left\{p'(x_i[t])\,e^{st} - p'(x_i[t-\bar{\tau}])\,e^{s(t-\bar{\tau})}\right\}$$

which can be rewritten as

$$\frac{d\tau}{dt} = -n\,p'(x_i[t])\,e^{st}\left\{1 - \frac{p'(x_i[t-\bar{\tau}])}{p'(x_i[t])}\,e^{-s\bar{\tau}}\right\} \tag{2.24}$$

Finally, combining equations (2.16 and (2.24), the burning rate perturbation is given by

$$Q' = \frac{d\bar{u}}{d\bar{z}}\,n\left\{1 - \frac{p'(x_i[t-\bar{\tau}])}{p'(x_i[t])}\,e^{-s\bar{\tau}}\right\} p'(x_i[t]) \tag{2.25a}$$

which is of the form

$$Q' = \frac{d\bar{u}}{dz}\,\rho\,p'(x_i[t]) \qquad (2.25b)$$

In the preliminary exploratory tests, the orientation of the spray fans (produced by unlike impinging doublets arranged around the circumference of a circle) was found to be critical with regard to transverse mode instability. Such a result could not be predicted using the burning rate expression of equation (2.25a), in the derivation of which it was assumed that all quantities affecting the combustion process could be correlated to the local pressure. While this assumption can be applied to thermodynamic state properties such as temperature and density, it can not be applied to the components of the gas velocity, which may be of equal importance in the combustion process. The effects of the velocity perturbations must therefore be taken into account separately from the effects of those quantities which can be correlated with the pressure.

Only the transverse (i. e., radial and tangential) components of the velocity perturbation can be significant in the explanation of the orientation effect. For purely transverse modes of oscillation, the longitudinal component is always much smaller than the transverse components. In addition, the longitudinal velocity perturbation vanishes at the injector face and has its smallest magnitude in the early combustion region, the zone in which the diametral barriers were seen in the preliminary testing to have the greatest influence on stability.

Of the various intermediate processes occurring during the combustion of liquid bipropellants, those most sensitive to velocity are the vaporization of the liquid droplets and the mixing of the vaporized propellants which must precede chemical reaction. In the process of vaporization, the important

quantity is the absolute magnitude of the velocity of the hot gases relative to the liquid droplet. The differences in the velocity patterns of the standing and spinning forms of tangential modes of oscillation (which were observed to have strikingly different stability characteristics) could result in differences in the local and overall vaporization rates. However, since the direction of the relative velocity is immaterial, the oscillation effect is not explainable by means of the vaporization process. In addition, the theoretical study of Wieber and Mickelsen (21) indicates that the oscillating velocity effect on droplet vaporization is essentially nonlinear, because of the dependence of the evaporation rate on the absolute magnitude of the relative velocity. On the other hand, the mixing of the propellants by the oscillating velocities is very strongly dependent on the orientation of the liquid spray fans (produced by the unlike impinging doublet injector). Although no detailed description of such a complex phenomenon is now possible, the following schematic discussion illustrates one process by which the burning rate may be caused to oscillate by an oscillating transverse velocity.

Consider the mixture of gaseous combustion products, vaporized propellants (oxidizer and fuel), and liquid propellant droplets at some axial station downstream of an injector doublet. For an unlike impinging injector, liquid mixing is imperfect and some degree of stratification exists in the mixture. For concreteness, the area of interest is shown in Figure 17 (a) for a doublet spud oriented with the line of centers of its orifices tangential to the injection circle. Then the stratification is almost entirely in the tangential direction, as shown by the lines of constant mass fraction of vaporized oxidizer in the gas mixture, Y_x. The exact shape of the constant Y_x contours will be dependent on the design and operating mixture ratios, the propellant characteristics, etc. Because of the turbulence in the combustion chamber, the stratification pattern shown

schematically in Figure 17 (a) represents only a mean condition.

A typical fuel rich droplet is shown at position A in the region which is relatively rich in vaporized fuel. A corresponding oxidizer rich droplet is shown at B in the oxidizer rich region of the mixture. As a droplet evaporates, the vapors diffuse away and must mix with the other vaporized propellant in the proper proportions for chemical raction. In a rocket combustion chamber, the transport and mixing of the vapors is most likely to be carried out primarily by turbulence rather than molecular diffusion. The overall burning rate of a fuel rich droplet, f_F , will therefore be a function of the amount of oxidizer vapor near the droplet, $f_F = f_F[(Y_x)_A]$, where subscript A indicates conditions in the vicinity of the fuel rich droplet at position A (the subscript B will be used similarly to denote conditions near the oxidized drop at B).

In the presence of small, periodic, transverse gas velocity oscillations $v'e^{i\omega t}$, $w'e^{i\omega t}$, the gaseous mixture will be transported relative to the droplets, causing oscillations of the local mass fractions of oxidizer and fuel. The perturbation in the rate f_F can then be written.

$$f_F - \bar{f}_F = f_F' = \left(\frac{\partial f_F}{\partial Y_x} \right)_A (Y_x')_A \tag{2.26}$$

where the proportionality factor $\frac{\partial f_F}{\partial Y_x})_A$ depends on $(Y_x)_A$ and on the propellant physical and chemical characteristics. The dependence is not necessarily that determined by investigators of laminar droplet burning (22). The change in the local oxidizer mass fraction due to the tangential velocity perturbation is

$$\begin{aligned} (Y_x')_A &= -\frac{1}{r} \left(\frac{\partial Y_x}{\partial \theta} \right)_A \int_0^t (\Delta w')_A e^{\omega t'} dt' \\ &= -\frac{1}{i\omega r} \left(\frac{\partial Y_x}{\partial \theta} \right)_A (\Delta \omega')_A e^{i\omega t} \end{aligned} \tag{2.27}$$

where $\Delta\omega'$ is the relative velocity of the gases with respect to the droplet.

The motion of the larger droplets is small compared to the gas motion, while the smaller droplets tend to move with the gas. Therefore the discussion here pertains to the larger droplets. As a droplet evaporates, the effect on it of the transverse velocity decreases. Thus the velocity effect described here can be expected to be most important in the early combustion region, in agreement with the results of the exploratory testing.

Combining equations (2.26) and (2.27) gives an expression for the rate perturbation for the fuel rich droplet at A,

$$f_F' = -\left(\frac{\partial f_F}{\partial Y_x}\right)_A \left(\frac{1}{r}\frac{\partial Y_x}{\partial \theta}\right)_A \frac{(\Delta w')_A}{i\omega} e^{i\omega t} \qquad (2.28a)$$

For the corresponding oxidizer rich droplet at B, the expression is

$$f_x' = -\left(\frac{\partial f_x}{\partial Y_x}\right)_B \left(\frac{1}{r}\frac{\partial Y_x}{\partial \theta}\right)_B \frac{(\Delta w')_B}{i\omega} e^{i\omega t} \qquad (2.28b)$$

Since the fuel rich droplet is in an oxidant deficient region, an increase in the oxidizer mass fraction will increase its contribution to the overall burning rate, that is, $\frac{\partial f_F}{\partial Y_x} > 0$. The opposite is true for the oxidizer rich droplet; $\frac{\partial f_F}{\partial Y_x} < 0$ since an increase in the local oxidizer fraction is accompanied by a decrease in the local fuel fraction. A perturbation velocity in the positive θ -direction will increase the oxidizer rich droplet burning rate and decrease the fuel rich droplet burning rate. Therefore the effects on the two droplets will tend to cancel.

The net burning rate perturbation is given approximately by

$$f_{net}' = f_x' + f_F' \cong -\left[\frac{\partial f_F}{\partial Y_x} + \frac{\partial f_x}{\partial Y_x}\right]_o \left(\frac{1}{r}\frac{\partial Y_x}{\partial \theta}\right)_o \frac{(\Delta w')_o}{i\omega} e^{i\omega t} \qquad (2.29)$$

where the subscript o denotes conditions at the center of the spray. Then $\frac{f_{net}'}{(\Delta w')_o} \lesseqgtr 0$ as $\left|\frac{\partial f_F}{\partial Y_x}\right| \gtreqless \left|\frac{\partial f_x}{\partial Y_x}\right|$. That is, for a positive velocity perturbation, the sign of the net rate perturbation depends on the relative magnitudes of $\frac{\partial f_F}{\partial Y_x}$ and $\frac{\partial f_x}{\partial Y_x}$. In order to determine the effects of the velocity perturbation on

the entire spray, the summation must include all of the propellant droplets.

If one of the propellants vaporizes at a greater rate than the other, most of the droplets in the mixture will be of the slower evaporating propellant. Therefore, there will be no cancellation of opposing effects and the overall velocity effect will be determined by the characteristics of the less volatile propellant. For the liquid oxygen-ethyl alcohol combination used in the experimental phase of the present investigation, it can be estimated, using the spray evaporation calculations of Priem and Heidmann (23) and the relative vaporization rate data of Pass and Tischler (24), that at any station, twice as much oxidant as fuel will have been vaporized. Thus an important velocity effect can be expected. For propellant combinations using non-cryogenic oxidizers, the evaporation rates of the fuel and oxidizer should not be so different, and the velocity mixing effect should be considerably reduced.

The analysis of liquid droplet dynamics presented in Appendix A shows that the relative velocity perturbation $\Delta w'$ is proportional to the gas velocity perturbation w'. Then the net rate perturbation can be written in the form

$$f'_{net} = \ell\, w' e^{i\omega t} \qquad (2.29b)$$

where

$$\ell \cong -\frac{1}{i\omega}\left(\frac{\partial \bar{\rho}_r}{\partial Y_x} + \frac{\partial \bar{\rho}_x}{\partial Y_x}\right)_0 \left(\frac{1}{r}\frac{\partial Y_x}{\partial \theta}\right)_0 \left(\frac{\Delta w'}{\bar{w}}\right)$$

is a velocity interaction index analogous to the pressure interaction index defined originally by Crocco (equation 2.18). A spray thickness d can be defined as the distance between two reference contours of constant oxidizer fraction (e. g. lines 1 and 2 in Figure 17 (a)). Then

$$\left(\frac{1}{r}\frac{\partial Y_x}{\partial \theta}\right)_0 \cong \frac{Y_{x_1} - Y_{x_2}}{d} = \frac{\Delta Y_x}{d}$$

and the velocity index ℓ is seen to be inversely proportional to the spray thickness. In general, the net combustion process rate perturbation will depend on both the radial and tangential velocities,

$$\dot{q}'_{net} = \left(\ell_r v' + \ell_\theta w'\right) e^{i\omega t} \qquad (2.29c)$$

where ℓ_r and ℓ_θ are the radial and the tangential velocity indices.

If the injector doublet which produces the mixture discussed above is rotated through an angle β_i from the tangential orientation, the resulting mixture will also be rotated, and will appear as shown in Figure 17 (b). The spray thicknesses in the radial and tangential directions are then

$$d_r = \frac{d}{\sin\beta_i}, \qquad d_\theta = \frac{d}{\cos\beta_i}$$

Each velocity index is inversely proportional to the corresponding spray thickness, or

$$\ell_r \sim \frac{\sin\beta}{d}, \qquad \ell_\theta \sim \frac{\cos\beta_i}{d}$$

For the tangential spud orientation, $\beta_i = 0$ and $\ell_r = 0$; for the radial orientation, $\beta_i = \frac{\pi}{2}$ so that $\ell_\theta = 0$. For a given injector spud, producing a spray with a given thickness d, the sum of the squares of the velocity indices will be a constant, independent of the angle of orientation.

The simple argument presented above is intended to suggest how the transverse velocity oscillations can affect the mixing of the vaporized propellants and produce oscillations in the overall burning rate. For the unlike impinging doublet, it is seen that the perturbation of the combustion process rate is a linear function of the radial and tangential components of the velocity perturbation, assuming that the perturbation is very small. Other injector types will not exhibit this linear velocity effect; some will be insensitive to oscillating velocities while other will show a velocity dependence which cannot be linearized.

At the present time, the magnitudes of the velocity indices and

their variations with axial distance cannot be calculated because of the lack of quantitative knowledge of the processes involved in liquid bipropellant combustion under turbulent rocket combustion chamber conditions.

In this chapter, it will be assumed that the velocity effects occur during the same time interval (the sensitive time lag) as the pressure effects. Although this is the simplest manner in which the velocity effects can be introduced, it is not necessarily the proper one. Consideration is given to alternative formulations and their implications in Chapter III. It should be noted, however, that the alternative burning rate expressions involve additional parameters which, like , , , and , cannot at present be calculated a priori from a consideration of physical and chemical processes. Resort to experimental techniques will be necessary in order to determine the proper description of the unsteady combustion process, including both pressure and velocity effects. Assuming, then, a linear dependence of the perturbation of the overall rate of the processes occurring during the sensitive time lag on the perturbations of pressure and radial and tangential velocity, equation (2.20) becomes

$$\frac{p_b'(t')}{\bar{p}_b} = \left(\quad + \quad e^{s\tau} - \quad e^{s\tau} + \quad e^{s\tau} \right), \qquad t - \tau \le t' \le t \tag{2.30}$$

The time rate of change of the sensitive time lag is found, by the same procedure as used previously, to be

$$\frac{d\tau}{dt} = \quad \left\{ \quad - \frac{\quad}{\quad} e^{-s\tau} \right\} \quad \left\{ \quad - \frac{\quad}{\quad} e^{-s\tau} \right\} \quad \left\{ \quad - \frac{\quad}{\quad} e^{-s\tau} \right\} \tag{2.31}$$

Then the burning rate perturbation can be written as

$$\frac{m_b'}{\bar{m}_b} = \quad \frac{p_b'}{\bar{p}_b} + \quad \frac{u_r'}{\bar{u}_r} + \quad \frac{u_\theta'}{\bar{u}_\theta} \tag{2.32}$$

where

$$\mathcal{P} = n\left\{1 - \frac{p'(x_i[t-\bar{\tau}])}{p'(x_i[t])}e^{-s\bar{\tau}}\right\}$$

$$\mathcal{Q} = l_r\left\{1 - \frac{v'(x_i[t-\bar{\tau}])}{v'(x_i[t])}e^{-s\bar{\tau}}\right\}$$

$$\mathcal{J} = l_\theta\left\{1 - \frac{w'(x_i[t-\bar{\tau}])}{w'(x_i[t])}e^{-s\bar{\tau}}\right\}$$

In general, $\bar{\tau}=\bar{\tau}(t)$ varies from one propellant element to another. The effect on combustion instability of such a spread in the sensitive time lag has been evaluated by Crocco and Cheng (1). In this analysis, it is assumed that all propellant elements have equal mean sensitive time lags, so that $\bar{\tau}$ = constant.

C. Solution for the Perturbations

The addition of velocity terms to the burning rate perturbation expression makes separation of the variables impossible. Therefore a different approach is used. The solution is asuumed to take the form of a series; the pressure perturbation, for example, is

$$p' = p_0 + p_1 + p_2 + \cdots \tag{2.33}$$

where p_1 is assumed to be $O(\bar{u}_e p_c)$, p_2 is $O(\bar{u}_e^2 p_c)$, etc. Since the governing equations were derived neglecting terms of $O(\bar{u}_e^2)$, the solution will be carried only as far as the first order correction, p_1. As discussed previously, it is assumed that the combustion process produces a through velocity in the combustion chamber which is small compared to the velocity of sound, and that the droplet drag, and hence the droplet oscillation amplitude, is also small. Therefore, the zeroth order solution corresponds to acoustic oscillations, and the first order correction includes the effects of the combustion process, the liquid gas interaction, and the exhaust nozzle.

The zeroth order equations are

$$s\rho_0 + \frac{\partial u_0}{\partial z} + \frac{\partial v_0}{\partial r} + \frac{1}{r} v_0 + \frac{1}{r}\frac{\partial w_0}{\partial \theta} = 0 \tag{2.34a}$$

$$s u_0 = -\frac{1}{\gamma}\frac{\partial p_0}{\partial z} \tag{2.34b}$$

$$s v_0 = -\frac{1}{\gamma}\frac{\partial p_0}{\partial r} \tag{2.34c}$$

$$s w_0 = -\frac{1}{\gamma r}\frac{\partial p_0}{\partial \theta} \tag{2.34d}$$

$$\frac{p_0}{\gamma} = \rho_0 \tag{2.34e}$$

The boundary conditons at the combustion chamber walls are that the velocity perturbation normal to the wall must vanish; that is, $u' = 0$ at $z = 0$ and $v' = 0$ at $r = 1$. In addition, it is necessary to impose conditions of boundedness and periodicity in order to obtain a solution. At the combustion chamber exit, $z = z_e$, the proper boundary condition is a relation between the perturbations of pressure, velocity, and entropy. (This "nozzle admittance relation" is discussed more fully later in this chapter and in Appendix C.) However, the oscillations in a closed end cylinder are quite similar to those in a rocket combustion chamber. Therefore, it is instructive to consider the zeroth order solution with the solid wall boundary condition imposed at the nozzle entrance,

$$u'(z=z_e) = 0$$

Equations (2.34a) to (2.34e) can be solved for p_0 to give

$$\Delta p_0 - s^2 p_0 = 0 \tag{2.35}$$

where Δ is the Laplacian operator

$$\Delta = \frac{\partial^2}{\partial z^2} + \frac{\partial^2}{\partial r^2} + \frac{1}{r}\frac{\partial}{\partial r} + \frac{1}{r^2}\frac{\partial^2}{\partial \theta^2}$$

The solution is obtained by assuming p_0 in the form

$$p_0 = P_0(z)\,\Psi_0(r)\,\Theta_0(\theta) \tag{2.36a}$$

so that the other perturbation quantities become

$$\rho_0 = \frac{1}{\gamma} P_0(z)\, \Psi_0(r)\, \Theta_0(\theta) \tag{2.36b}$$

$$u_0 = -\frac{1}{\gamma s} \frac{dP_0(z)}{dz} \Psi_0(r)\, \Theta_0(\theta) \tag{2.36c}$$

$$v_0 = -\frac{1}{\gamma s} P_0(z) \frac{d\Psi_0}{dr}\, \Theta_0(\theta) \tag{2.36d}$$

$$w_0 = -\frac{1}{\gamma s} P_0(z) \frac{1}{r} \Psi_0(r) \frac{d\Theta_0}{d\theta} \tag{2.36e}$$

Substitution of the expression (2.36a) into equation (2.35) yields the following three ordinary differential equations:

$$\frac{d^2 P_0}{dz^2} - (s^2 + s_{\nu h}^2) P_0 = 0 \tag{2.37a}$$

$$r^2 \frac{d^2 \Psi_0}{dr^2} + r \frac{d\Psi_0}{dr} + (s_{\nu h}^2 r^2 - \nu^2) \Psi_0 = 0 \tag{2.37b}$$

$$\frac{d^2 \Theta_0}{d\theta^2} + \nu^2 \Theta_0 = 0 \tag{2.37c}$$

where $s_{\nu h}^2$ and ν^2 are separation constants.

Equation (2.37b) is a Bessel equation of order , for which the solutions are

$$J_\nu(s_{\nu h} r), \qquad Y_\nu(s_{\nu h} r)$$

The boundary condition at $r = 1$ is the solid wall condition, $v_0 = \frac{d\Psi_0}{dr} = 0$. At $r = 0$, which is a singular point for the differential equation, the condition is that the perturbations must be finite; i. e., Ψ_0 is to be regular. Therefore the Bessel function of the second kind, $Y_\nu(s_{\nu h} r)$, is excluded because of its logarithmic singularity at $r = 0$. The first condition determines the value of the constant $s_{\nu h}$. That is, $s_{\nu h}$ is the solution of the equation

$$\frac{dJ_\nu}{dr}(s_{\nu h}) = 0$$

For each value of the parameter ν, there are an infinite number of zeros $s_{\nu h}$, counted by the index h. Physically, h is the number of cylindrical

surfaces, including the outer solid wall, on which the radial velocity perturbation vanishes; $h = 1$ corresponds to a purely tangential mode, $h = 2$ to the first radial mode, $h = 3$ to the second radial mode, etc.

The solutions of the harmonic oscillator equation (2.36c) are

$$e^{i\nu\theta}, \quad e^{-i\nu\theta}$$

The first of these solutions, $e^{i\nu\theta}$, represents a wave moving in the negative θ direction since

$$p_0 \sim e^{i(\omega t + \nu\theta)}$$

and the phase velocity is $-\frac{\omega}{\nu}$. Similarly, the second solution, $e^{-i\nu\theta}$, represents a wave moving at the same speed in the positive direction. The combination of the two oppositely moving waves produces a standing oscillation pattern, with

$$p_0 \sim \cos \nu\theta \, e^{i\omega t}, \quad \omega_0 \sim \sin \nu\theta \, e^{i\omega t}$$

Both the spinning and standing solutions must be periodic, since the directions represented by $\theta = 0$ and $\theta = 2\pi$ are physically identical. Thus

$$p_0(\theta) = p_0(\theta + 2\pi)$$

Moreover, the standing mode tangential velocity perturbation vanishes on ν stationary diametral surfaces (nodal surfaces) which can then be replaced by solid surfaces (e. g., barriers or sector inserts) without disturbing the oscillation pattern. In a spinning mode the nodal surfaces rotate at the oscillation frequency. For $\nu = 0$, the solution of equation (2.36c) is simply

$$\omega_0 = \text{constant}$$

which represents a purely radial mode, since there is no variation in the tangential direction. The first tangential mode corresponds to $\nu = 1$, the second tangential mode to $\nu = 2$, and so on.

The solution of equation (2.36a) which satisifies the solid wall boundary condition at the injector ($z = 0$) is

$$P_0(z) = P_{00} \cosh \sqrt{s^2 + s_{yh}^2}\, z$$

where $P_{oo} = P_o(0)$ is an arbitrary constant. The solid wall condition at the nozzle end of the combustion chamber,

$$\frac{dP_o}{dz}(z=z_e) = 0$$

can be satisfied if $s = i\omega$. Then

$$P_o(z) = P_{oo} \cos \sqrt{\omega^2 - s_{\nu h}^2}\, z$$

and the boundary condition becomes

$$\sin \sqrt{\omega^2 - s_{\nu h}^2}\, z_e = 0$$

which implies that

$$\sqrt{\omega^2 - s_{\nu h}^2}\, z_e = j\pi \,, \qquad j = 0, 1, 2, \cdots$$

or

$$\omega = \sqrt{s_{\nu h}^2 + \frac{j^2\pi^2}{z_e^2}} \tag{2.38}$$

Thus the acoustic oscillations in a closed bylinder are neutral ($\lambda=0$) with discrete, well defined frequencies. The purely longitudinal modes correspond to $s_{\nu h} = s_{01} = 0$, $j = 1, 2, \cdots$ so that $\omega = \frac{j\pi}{z_e}$ and

$$p_o = P_o(z) = P_{oo} \cos j\pi\left(\frac{z}{z_e}\right) \,, \qquad v_o = w_o = 0$$

Purely transverse modes are obtained when $j = 0$, $s_{\nu h} \neq 0$. Then the frequency of oscillation is $\omega = s_{\nu h}$. As discussed above, $s_{\nu h}$ is a function of the indices ν and h which specify the mode. Isobar and streamline patterns for several transverse (standing) modes, with the corresponding values of $s_{\nu h}$, are shown in Figure 1. For these modes,

$$P_o(z) = P_{oo} \,, \qquad U_o(z) = 0$$

The most general three dimensional oscillations involve combinations of longitudinal and transverse modes, in which both the axial and transverse velocity perturbations are of the same order of magnitude as the pressure perturbation. The oscillation frequency in the general case is given by equation (2.38) with both $s_{\nu h}$ and j having nonzero values.

The present investigation is concerned only with the purely transverse modes. By this restriction of attention, considerable reduction in

complexity is obtained and the properties peculiar to the transverse oscillations may more easily be seen. However, important effects can be expected to result from the interaction of longitudinal and transverse modes, and ultimately the analysis of general three dimensional oscillations should be made.

The oscillations in a rocket combustion chamber differ from the acoustic vibrations just discussed for two reasons. The first is the presence of the liquid propellant combustion process with the resulting small nonzero through velocity. Second, the boundary condition at the chamber exit imposed by the exhaust nozzle in supercritical operation is significantly different from the solid wall condition used in the acoustic solution. The nozzle boundary condition for transverse modes of neutral oscillations was derived by Crocco; an analytical discussion of this derivation is given in (25).

Let the perturbations of pressure, velocity, and entropy be given by

$$\left.\begin{aligned} p' &= P(z)\,\Psi_{\nu h}(r)\,\Theta_\nu(\theta) \\ u' &= U(z)\,\Psi_{\nu h}(r)\,\Theta_\nu(\theta) \\ v' &= V(z)\,\frac{d\Psi_{\nu h}}{dr}\,\Theta_\nu(\theta) \\ w' &= W(z)\,\frac{1}{r}\,\Psi_{\nu h}(r)\,\frac{d\Theta_\nu}{d\theta} \\ s' &= S(z)\,\Psi_{\nu h}(r)\,\Theta_\nu(\theta) \end{aligned}\right\} \qquad (2.39)$$

where $\Psi_{\nu h} = J_\nu(s_{\nu h} r)$, $\Theta_\nu = \cos\nu\theta$ or $e^{-i\nu\theta}$ are the transverse distribution functions discussed above, and the time dependence is harmonic, $e^{i\omega t}$. From the transverse momentum conservation equations it follows that $V = W$. Then the boundary condition at the nozzle entrance, which by analogy with acoustical terminology was called by Crocco the nozzle admittance relation,

takes the form

$$\frac{U(z_e)}{P(0)} + \mathcal{A}\frac{P(z_e)}{P(0)} + \mathcal{B}s_{vh}\frac{\gamma V(z_e)}{P(0)} + \mathcal{C}\frac{\gamma S(z_e)}{P(0)} = 0 \qquad (2.40)$$

The admittance coefficients $\mathcal{A}$, $\mathcal{B}$, and $\mathcal{C}$ are complex functions of the mode, frequency, chamber exit velocity, and nozzle convergent section geometry. A discussion of the calculation of the admittance coefficients for an axisymmetric nozzle is included as Appendix C of this dissertation.

The computations which have been made indicate that the admittance coefficients are approximately $O(\bar{u}_e)$, or slightly larger, for frequencies in the vicinity of the acoustic oscillation frequency. For transverse modes, $\frac{P(z_e)}{P(0)}$ and $\frac{V(z_e)}{P(0)}$ are O(1). It will be shown later that if combustion is complete at the nozzle entrance the entropy perturbation $\frac{S(z_e)}{P(0)}$ is at most $O(\bar{u}e^2)$. Then from the admittance relation it can be seen that the axial velocity perturbation $\frac{U(z_e)}{P(0)}$ is not zero as in the acoustic case, but is really approximately $O(\bar{u}_e)$.

By definition,

$$\frac{p'}{P_{00}} = \frac{P_0(z)}{P_{00}}\Psi_0(r)\,\omega_n(\theta) + O(\bar{u}_e)$$

and from the discussion above

$$\frac{u'}{P_{00}} = -\frac{1}{\gamma S}\frac{d}{dz}\left(\frac{P_0}{P_{00}}\right)\Psi_0\,\omega_0 + O(\bar{u}_e) \cong O(\bar{u}_e)$$

That is,

$$\frac{d}{dz}\left(\frac{P_0}{P_{00}}\right) = \sqrt{s^2+s_{vh}^2}\,\sinh\sqrt{s^2+s_{vh}^2}\,z \cong O(\bar{u}_e)$$

Expanding the function $\sinh\sqrt{s^2+s_{vh}^2}\,z$ and neglecting higher order terms gives the not unexpected result

$$s^2 + s_{vh}^2 \cong O(\bar{u}_e)$$

since z_e is O(1). Thus, for purely transverse modes, the combustion process and exhaust nozzle give rise to a small axial velocity perturbation and a small shift in frequency from the corresponding acoustic frequency. In addition, the oscillations in a rocket motor may be unstable, whereas

the acoustic oscillations are always neutral.

It should be noted that the series expansion used for the perturbations,

$$p' = p_0 + p_1 + \cdots \quad , \quad u' = u_0 + u_1 + \cdots$$

cannot be applied to the admittance coefficients $\mathcal{A}$, $\mathcal{B}$, and $\mathcal{C}$. An expansion of the form

$$\mathcal{A} = \mathcal{A}_0 + \mathcal{A}_1 + \cdots$$

requires that $\frac{\mathcal{A}_1}{\mathcal{A}_0} = O(\bar{u}_e)$. Since $\mathcal{A}_0 = O(\bar{u}_e)$, the requirements is that $\mathcal{A}_1$ must be $O(\bar{u}_e^2)$. The admittance coefficients are functions of the frequency ω; therefore the terms in the series expansion can be written

$$\mathcal{A}_0 = \mathcal{A}(\omega = s_{vh}) \quad , \quad \mathcal{A}_1 = \left(\frac{\partial \mathcal{A}}{\partial \omega}\right)_{\omega = s_{vh}} \cdot (\omega - s_{vh}) \quad , \quad \cdots$$

Thus, since $\omega - s_{vh}$ is $O(\bar{u}_e)$, the derivative $\frac{\partial \mathcal{A}}{\partial \omega}$ must be $O(\bar{u}_e)$ also. The curves presented in Figure 18, which show a frequency dependence typical of the admittance coefficients in general, demonstrate that $\frac{\partial \mathcal{A}}{\partial \omega}$ can be $O(1)$, so that the series expansion breaks down. In this analysis, therefore, the application of the nozzle boundary condition will be deferred until the first order solution is obtained.

The equations governing the first order solution for the perturbations will now be derived. In this derivation the simplifying assumption will be made that the gradient of a quantity is of the same order of magnitude as the quantity itself. However, an exception must be made in the case of the steady state axial gas velocity, $\bar{u}(\bar{z})$. In order to allow for the case of a relatively concentrated combustion zone, the velocity gradient $\frac{d\bar{u}}{d\bar{z}}$ must be allowed to be $O(1)$ locally, rather than $O(\bar{u}_e)$. The chamber length $\bar{z}_e$ is assumed to be $O(1)$; therefore the axial distance over which $\frac{d\bar{u}}{d\bar{z}}$ is $O(1)$ can only be $O(\bar{u}_e)$. The determination of the first order solution is much simplified by requiring the steady state velocity gradient to be of the same

order of magnitude as the exit velocity. It is demonstrated in Appendix B that the same solution results when the magnitude restriction on the velocity gradient is removed, although the analysis is considerably more complicated.

Assuming, then, that $\frac{d\bar{u}}{dz}$ is $O(\bar{u}_e)$, the first order equations are obtained as follows. The perturbations are given by

$$\left.\begin{aligned}
p' &= p_0 + p_1 \\
\rho' &= \frac{1}{\gamma} p_0 + \rho_1 \\
u' &= -\frac{1}{\gamma s}\frac{\partial p_0}{\partial z} + u_1 = O(\bar{u}_e \cdot p_0) \\
v' &= -\frac{1}{\gamma s}\frac{\partial p_0}{\partial r} + v_1 \\
w' &= -\frac{1}{\gamma s r}\frac{\partial p_0}{\partial \theta} + w_1 \\
\rho_L' &= \rho_{L1} = O(\bar{u}_e \cdot p_0) \\
u_L' &= \frac{k}{s} u' = O(\bar{u}_e^2 p_0) \\
v_L' &= \frac{k'(z)}{s} v' = -\frac{k'(z)}{\gamma s^2}\frac{\partial p_0}{\partial r} + O(\bar{u}_e^2 \cdot p_0) \\
w_L' &= \frac{k'(z)}{s} w' = -\frac{k'(z)}{\gamma s^2 r}\frac{\partial p_0}{\partial \theta} + O(\bar{u}_e^2 \cdot p_0)
\end{aligned}\right\} \qquad (2.41)$$

where the first order solution p_0 has been found to be

$$p_0 = P_{00}\left[1 + (s^2 + s_{\nu h}^2)\frac{z^2}{2}\right]\Psi_{\nu h}(r)\,\Theta_\nu(\theta) \qquad (2.41a)$$

with $\Psi_{\nu h}(r) = J_\nu(s_{\nu h} r)$, $\Theta_\nu = \cos \nu\theta$ (standing mode) or $e^{-i\nu\theta}$ (spinning mode), and $s^2 + s_{\nu h}^2 = O(\bar{u}_e)$. The expressions (2.41) are inserted into equations (2.14a), (2.14b), (2.14d), and (2.14i) and the zeroth order relations are subtracted off. The resulting system of partial differential equations is:

$$s\rho_1 + \frac{\partial u_1}{\partial z} + \frac{\partial v_1}{\partial r} + \frac{v_1}{r} + \frac{1}{r}\frac{\partial w_1}{\partial \theta} = \frac{d\bar{u}}{dz}\left[\mathcal{P} p_0 - \mathcal{R}\frac{1}{\gamma s}\frac{\partial p_0}{\partial r} - \mathcal{T}\frac{1}{\gamma s r}\frac{\partial p_0}{\partial \theta} - \frac{p_0}{\gamma}\right] \qquad (2.42a)$$

$$s u_1 = -\frac{1}{\gamma}\frac{\partial p_1}{\partial z} \qquad (2.42b)$$

$$s v_1 = -\frac{1}{\gamma}\frac{\partial p_1}{\partial r} + \frac{1}{\gamma s}\left(k'\bar{\rho}_1 + \frac{d\bar{u}}{dz}\right)\frac{\partial p_0}{\partial r} \qquad (2.42c)$$

$$s w_1 = -\frac{1}{\gamma r}\frac{\partial p_1}{\partial \theta} + \frac{1}{\gamma s r}\left(k'\bar{\rho}_1 + \frac{d\bar{u}}{dz}\right)\frac{\partial p_0}{\partial \theta} \qquad (2.42d)$$

$$\frac{s p_1}{\gamma} - s\rho_1 = -\frac{d\bar{u}}{dz}\left(\frac{\gamma - 1}{\gamma}\right) p_0 \qquad (2.42e)$$

The boundary conditions on thes equations are those which were applied to the zeroth order solution, namely, the solid wall condition at $z = 0$ and $r = 1$, the condition of regularity at $r = 0$, and the periodicity condition in the circumferential direction, including the same distinction between the standing and the spinning forms of tangential modes. The nozzle boundary condition will be applied to the overall solution, that is, to the sum of the zeroth and first order solutions.

The systems of first order equations can be solved for p_1, giving

$$\Delta p_1 - s^2 p_1 = \left[k'\bar{\rho}_L + (\gamma+1)\frac{d\bar{u}}{dz}\right] s p_0 - \gamma s \rho \frac{d\bar{u}}{dz} p_0 + Q \frac{d\bar{u}}{dz}\frac{\partial p_0}{\partial r} + J \frac{d\bar{u}}{dz}\cdot\frac{1}{r}\frac{\partial p_0}{\partial \theta} \tag{2.43}$$

where $\Delta = \frac{\partial^2}{\partial z^2} + \frac{\partial^2}{\partial r^2} + \frac{1}{r}\frac{\partial}{\partial r} + \frac{1}{r^2}\frac{\partial^2}{\partial \theta^2}$. Since equation (2.43) is linear, the solution can be found by superposition. Let

$$p_1 = p_A + p_B + p_C + p_D \tag{2.44}$$

where the partial solutions p_A, p_B, p_C and p_D are solutions of the following equations

$$\Delta p_A - s^2 p_A = -\gamma s \rho \frac{d\bar{u}}{dz} P_{00} \Psi_{\nu h} \Theta_\nu \tag{2.45a}$$

$$\Delta p_B - s^2 p_B = Q \frac{d\bar{u}}{dz} P_{00} \frac{d\Psi_{\nu h}}{dr} \Theta_\nu \tag{2.45b}$$

$$\Delta p_C - s^2 p_C = J \frac{d\bar{u}}{dz} P_{00} \frac{\Psi_{\nu h}}{r} \frac{d\Theta_\nu}{d\theta} \tag{2.45c}$$

$$\Delta p_D - s^2 p_D = \left[k'\bar{\rho}_L + (\gamma+1)\frac{d\bar{u}}{dz}\right] s P_{00} \Psi_{\nu h} \Theta_\nu \tag{2.45d}$$

The partial solution p_A can be obtained by letting

$$p_A = P_A(z)\ \Psi_{\nu h}(r)\ \Theta_\nu(\theta)$$

Then equation (2.45a) becomes

$$\frac{d^2 P_A}{dz^2}\Psi_{\nu h}\Theta_\nu + P_A\left(\frac{\partial^2}{\partial r^2} + \frac{1}{r}\frac{\partial}{\partial r} + \frac{1}{r^2}\frac{\partial^2}{\partial \theta^2}\right)\Psi_{\nu h}\Theta_\nu - s^2 P_A \Psi_{\nu h}\Theta_\nu = -\gamma s \rho \frac{d\bar{u}}{dz}\Psi_{\nu h}\Theta_\nu P_{00} \tag{2.46}$$

The transverse distribution functions satisfy the relation

$$\left(\frac{\partial^2}{\partial r^2} + \frac{1}{r}\frac{\partial}{\partial r} + \frac{1}{r^2}\frac{\partial^2}{\partial \theta^2} \right) \Psi_{\nu h} \Theta_\nu = - s_{\nu h}^2 \Psi_{\nu h} \Theta_\nu \tag{2.47}$$

Making use of this relation, equation (2.46) becomes

$$\frac{d^2}{dz^2}\left(\frac{P_A}{P_{oo}} \right) + (s^2 + s_{\nu h}^2) \frac{P_A}{P_{oo}} = - \gamma s \mathcal{P} \frac{d\bar{u}}{dz}$$

However, since $s^2 + s_{\nu h}^2$ and $\frac{P_A}{P_{oo}}$ are both $O(\bar{u}_e)$, the differential equation for P_A reduces to

$$\frac{d^2}{dz^2}\left(\frac{P_A}{P_{oo}} \right) = - \gamma s \mathcal{P} \frac{d\bar{u}}{dz} + O(\bar{u}_e^2) \tag{2.48}$$

This equation is easily integrated to give

$$\frac{P_A(z)}{P_{oo}} = - \gamma s \mathcal{P} \int_0^z \bar{u}\, dz' + K_A \tag{2.49}$$

where the integration constand K_A represents the value of $\frac{P_A}{P_{oo}}$ at the injector face, $z = 0$; therefore $K_A = O(\bar{u}_e)$.

The partial solution ϕ_D is obtained in the same manner from equation (2.45d) with $\phi_D = P_D(z) \Psi_{\nu h}(r) \Theta_\nu(\theta)$ and

$$\frac{P_D(z)}{P_{oo}} = s \int_0^z dz' \int_0^{z'} k'(z'') \bar{P}_i(z'')\, dz'' + (\gamma+1) s \int_0^z \bar{u}(z')\, dz' + K_D \tag{2.50}$$

where again $K_D = \frac{P_D(0)}{P_{oo}} = O(\bar{u}_e)$.

A different procedure must be adopted in order to obtain the partial solutions ϕ_B and ϕ_C because equations (2.45b) ar (2.45c) are not separable. These equations are of the form

$$\Delta \phi - s^2 \phi = F(z) \cdot G(r, \theta) \tag{2.51}$$

The solutions (eigenfunctions) of the corresponding homogeneous equation we determined previously in the discussion of the zeroth order perturbation solution. The transverse distribution functions for these solutions were

found to be

$$\Psi_{pq}(r) = J_p(s_{pq} r), \quad \Theta_p(\theta) = \begin{cases} \cos p\theta \\ e^{-ip\theta} \end{cases}$$

$$p = 0, 1, 2, 3, \cdots \quad ; \quad q = 1, 2, 3, \cdots$$

These transverse eigenfunctions form a complete, orthogonal set. A solution of equation (2.51) can be obtained, therefore, by expanding $G(r,\theta)$ in a series of the transverse eigenfunctions.*

$$G = \sum_{p=0}^{\infty} \sum_{q=1}^{\infty} A_{pq} \Psi_{pq}(r) \Theta_p(\theta)$$

Write the solution of equation (2.51) in the form

$$\phi = \sum_{p=0}^{\infty} \sum_{q=1}^{\infty} a_{pq} P_{pq}(z) \Psi_{pq}(r) \Theta_p(\theta) \tag{2.52a}$$

The transverse eigenfunctions must satisfy the relation stated previously in equation (2.49). Then equation (2.51) yields

$$a_{pq}\left[\frac{d^2 P_{pq}}{dz^2} - (s^2 + s_{pq}^2) P_{pq} \right] = A_{pq} F(z) \quad \text{for all} \quad p,q$$

Let $a_{pq} = A_{pq}$. Then the partial differential equation (2.51) has been reduced to the set of linear, second order, inhomogeneous, ordinary differential equations

$$\frac{d^2 P_{pq}}{dz^2} - (s^2 + s_{pq}^2) P_{pq} = F(z) \tag{2.53a}$$

The expansion coefficients are given by

$$A_{pq} = \frac{1}{H} \int_{\theta=0}^{2\pi} \int_{r=0}^{1} G(r,\theta) \Psi_{pq} \Theta_p^* \, r\,dr\,d\theta \tag{2.54a}$$

where H is a normalizing factor, defined by

$$H = \int_0^{2\pi} \int_0^1 \Psi_{pq}^2 \Theta_p \Theta_p^* \, r\,dr\,d\theta$$

and Θ_p^* is the complex conjugate of Θ_p.

---

* The validity of the expansion depends on the existence of Green's function for the boundary condition $\partial\phi/\partial r(r=1) = 0$, which follows the existence of Green's function for the boundary condition $\phi(r=1) = 0$. (26,27)

Consider first the partial solution ϕ_B , given by

$$\phi_B = \sum_{p=0}^{\infty} \sum_{q=1}^{\infty} B_{pq} P_{Bpq}(z) \Psi_{pq}(r) \Theta_p(\theta) \tag{2.52b}$$

where the axial distribution functions P_{Bpq} satisfy the differential equations

$$\frac{d^2}{dz^2}\left(\frac{P_{Bpq}}{P_{oo}}\right) - (s^2 + s_{pq}^2)\frac{P_{Bpq}}{P_{oo}} = \mathcal{R}\frac{d\bar{u}}{dz} \tag{2.53b}$$

The mode of instability under consideration is specified by the pair of indices ν, h. If $p = \nu$, $q = h$, equation (2.53b) reduces to

$$\frac{d^2}{dz^2}\left(\frac{P_{B\nu h}}{P_{oo}}\right) = \mathcal{R}\frac{d\bar{u}}{dz}$$

exactly as for the partial solutions ϕ_A and ϕ_D . Then

$$\frac{P_{B\nu h}}{P_{oo}} = \mathcal{R}\int_0^z \bar{u}(z')dz' + K_{B\nu h} \tag{2.55a}$$

as before. For all other values of p and q , equation (2.53b) becomes

$$\frac{d^2}{dz^2}\left(\frac{P_{Bpq}}{P_{oo}}\right) - (s_{pq}^2 - s_{\nu h}^2)\frac{P_{Bpq}}{P_{oo}} = \mathcal{R}\frac{d\bar{u}}{dz}$$

since $s^2 = -s_{\nu h}^2 + O(\bar{u}_e)$. The solution of this equation is obtained by the method of variation of constants as

$$\frac{P_{Bpq}}{P_{oo}} = \mathcal{R}\int_0^z \frac{d\bar{u}}{dz}(z')\frac{\sinh\sqrt{s_{pq}^2 - s_{\nu h}^2}\,(z-z')}{\sqrt{s_{pq}^2 - s_{\nu h}^2}}dz' + K_{Bpq}\cosh\sqrt{s_{pq}^2 - s_{\nu h}^2}\,z$$

The expansion coefficients B_{pq} are given by

$$B_{pq} = \frac{\int_0^{2\pi}\int_0^1 \frac{d\Psi_{\nu h}}{dr}\Psi_{pq}\Theta_\nu\Theta_p^* r\,dr\,d\theta}{\int_0^{2\pi}\int_0^1 \Psi_{pq}^2\Theta_p\Theta_p^* r\,dr\,d\theta}$$

For a spinning mode, $\Theta_p = e^{-ip\theta}$. Then, denoting $\frac{dJ_\nu(x)}{dx}$ by $J_\nu'(x)$,

$$B_{pq} = \frac{\int_0^{2\pi} e^{-i\nu\theta}e^{ip\theta}d\theta \int_0^1 s_{\nu h}J_\nu'(s_{\nu h}r)J_p(s_{pq}r)\,r\,dr}{\int_0^{2\pi}d\theta\int_0^1 J_p^2(s_{pq}r)\,r\,dr}$$

From this expression, since the functions $e^{-i\nu\theta}$ and $e^{ip\theta}$ are orthogonal, it can be seen that

$$B_{pq} = 0,\ p \neq \nu\ ;\ B_{\nu q} = \frac{s_{\nu h}\int_0^1 J_\nu'(s_{\nu h}r)J_\nu(s_{\nu q}r)\,r\,dr}{\int_0^1 J_\nu^2(s_{\nu q}r)\,r\,dr} \tag{2.56}$$

The same result is obtained for the standing mode, because $\cos\nu\theta$ and $\cos p\theta$ $(0 \le \theta \le 2\pi)$ are also orthogonal.

The partial solution ψ_c is obtained by the same precedure as used for ψ_B. Thus let

$$\psi_c = \sum_{p=0}^{\infty} \sum_{q=1}^{\infty} C_{pq} P_{cpq}(z) \Psi_{pq}(r) \Theta_p(\theta) \tag{2.52c}$$

where the axial distribution functions are

$$\frac{P_{c\nu h}}{P_{oo}} = J \int_0^z \bar{u}(z')dz' + K_{c\nu h} \tag{2.57a}$$

$$\frac{P_{cpq}}{P_{oo}} = J \int_0^z \frac{d\bar{u}}{dz}(z') \frac{\sinh\sqrt{s_{pq}^2 - s_{\nu h}^2}\,(z-z')}{\sqrt{s_{pq}^2 - s_{\nu h}^2}} dz' + K_{cpq} \cosh\sqrt{s_{pq}^2 - s_{\nu h}^2}\, z \tag{2.57b}$$

The expansion coefficients for ψ_c are given by the expression

$$C_{pq} = \frac{\int_0^{2\pi}\int_0^1 \frac{1}{r} \Psi_{\nu h} \Psi_{pq} \Theta_\nu' \Theta_p^* \, r\,dr\,d\theta}{\int_0^{2\pi}\int_0^1 \Psi_{pq}^2 \Theta_p \Theta_p^* \, r\,dr\,d\theta}$$

For a spinning mode $\Theta_\nu = e^{i\nu\theta}$. Then $\Theta_\nu' = -i\nu e^{-i\nu\theta}$ is orthogonal to all of the functions $\Theta_p^* = e^{ip\theta}$ except Θ_ν^*, so that

$$\left.\begin{aligned} C_{pq} &= 0, \quad p \neq \nu \\ \text{and} \quad C_{\nu q} &= -i\nu \frac{\int_0^1 J_\nu(s_{\nu h} r)\, J_\nu(s_{\nu q} r)\, dr}{\int_0^1 J_\nu^2(s_{\nu q} r)\, r\,dr} \end{aligned}\right\} \tag{2.58a}$$

In particular, for $q = h$, the second of equations (2.58a) becomes

$$C_{\nu h} = -i\nu \frac{\int_0^1 J_\nu^2(s_{\nu h} r)\, dr}{\int_0^1 J_\nu^2(s_{\nu h} r\; r\,dr} = -i\tilde{C}_{\nu h} \tag{2.58b}$$

where $\tilde{C}_{\nu h}$ is a positive real number. Thus, the expansion coefficient corresponding to the mode of instability under consideration is a negative purely imaginary number.

However, for a standing mode of oscillation, $\Theta_\nu = \cos p\theta$, and the derivative $\Theta_\nu' = -\nu \sin\nu\theta$ is orthogonal to $\Theta_p^* = \cos p\theta$ for all p, over the interval $0 \le \theta \le 2\pi$. In order to obtain expressions for the expansion

coefficients, the interval of definition of the eigenfunction expansion is changed from $0 \le \theta \le 2\pi$ to $0 \le \theta \le \pi$. Since the standing mode oscillation pattern is symmetrical about $\theta = 0$, (or $\theta = \pi$), the other half of the solution can be obtained by reflection. Then for a standing mode,

$$C_{pq} = -\nu \frac{\int_0^{\pi} \sin \nu\theta \cos p\theta \, d\theta \int_0^1 J_\nu(s_{\nu h} r) J_p(s_{pq} r) \, dr}{\int_0^{\pi} \cos^2 p\theta \, d\theta \int_0^1 J_p^2(s_{pq} r) \, r \, dr}$$

or

$$\left.\begin{aligned} C_{pq} &= 0, \quad \text{for } p - \nu = 2m, \quad m = 0, \pm 1, \pm 2, \cdots \\ C_{pq} &= -\frac{4\nu^2}{\pi(p^2 - \nu^2)} \cdot \frac{\int_0^1 J_\nu(s_{\nu h} r) J_p(s_{pq} r) \, dr}{\int_0^1 J_p^2(s_{pq} r) \, r \, dr}, \quad \text{for } p - \nu = 2m + 1 \end{aligned}\right\} \quad (2.58c)$$

The most important result here is that the eigenfunction expansion for ψ_t does not include a term corresponding to the mode the stability of which is being considered.

It should also be noted that whereas the expansions for ψ_B and for ψ_C in the case of a spinning mode are uniformly convergent, the standing mode series for ψ_C ,

$$\psi_C = \sum_{\substack{p-\nu \\ \text{odd}}} \sum_{q=1}^{\infty} C_{pq} P_{cpq}(z) J_p(s_{pq} r) \cos p\theta$$

is not uniformly convergent. This result follows from the fact that the tangential part of the nonhomogeneous term of equation (2.45c),

$$\frac{d\Theta_\nu}{d\theta} = -\nu \sin \nu\theta$$

vanishes at $\theta = 0$ and π . On the contrary, the eigenfunctions $\Theta_p = \cos p\theta$ do not vanish, but have vanishing derivatives Θ_p' at the endpoints. Thus the expansion

$$G(r,\theta) = -\frac{1}{r} J_\nu(s_{\nu h} r) \nu \sin \nu\theta = \sum_{\substack{p-\nu \\ \text{odd}}} \sum_{q=1}^{\infty} C_{pq} J_p(s_{pq} r) \cos p\theta$$

does not converge at the boundaries, $\theta = 0, \pi$. However, the eigenfunction series for ψ_t does satisfy the tangential boundary condition, $\left(\frac{\partial \psi_t}{\partial \theta}\right)_{\theta=0,\pi} = 0$,

and does represent the partial solution ϕ_c away from the tangential boundaries.

In summary, the solution for the pressure perturbation has been found to be

$$p' = \left\{ \left[P_0(z) + P_A(z) + B_{\nu h} P_{B\nu h}(z) - i \tilde{C}_{\nu h} P_{C\nu h}(z) + P_D(z) \right] J_\nu(s_{\nu h} r) + \sum_{q \neq h} \left[B_{\nu q} P_{B\nu q}(z) + C_{\nu q} P_{C\nu q}(z) \right] J_\nu(s_{\nu q} r) \right\} e^{-i\nu\theta} \tag{2.59a}$$

for the spinning mode, and

$$p' = \left\{ \left[P_0(z) + P_A(z) + B_{\nu h} P_{B\nu h}(z) + P_D(z) \right] J_\nu(s_{\nu h} r) + \sum_{q \neq h} B_{\nu q} P_{B\nu q}(z) J_\nu(s_{\nu q} r) \right\} \cos \nu\theta + \sum_{\substack{p=\nu \\ \text{odd}}} \sum_{q=1}^{\infty} C_{pq} J_p(s_{pq} r) \cos p\theta \tag{2.59b}$$

for the standing mode. Both of these solutions are of the form

$$p' = \left[P_0(z) + P_{1\nu h}(z) \right] \Psi_{\nu h}(r) \Theta_\nu(\theta) + \sum_{p,q \neq \nu,h} \sum P_{1pq}(z) \Psi_{pq}(r) \Theta_p(\theta) \tag{2.60a}$$

so that the velocity perturbations can be written as

$$u' = -\frac{1}{\gamma s} \left[\left(\frac{dP_0}{dz} + \frac{dP_{1\nu h}}{dz} \right) \Psi_{\nu h} \Theta_\nu + \sum_p \sum_q \frac{dP_{1pq}}{dz} \Psi_{pq} \Theta_p \right] \tag{2.60b}$$

$$v' = -\frac{1}{\gamma s} \left\{ \left[\left(1 + \frac{k' \beta_c}{s} + \frac{1}{s} \frac{d\bar{u}}{dz} \right) P_0 + P_{1\nu h} \right] \Psi'_{\nu h} \Theta_\nu + \sum_p \sum_q P_{1pq} \Psi'_{pq} \Theta_p \right\} \tag{2.60c}$$

$$w' = -\frac{1}{\gamma s} \left\{ \left[\left(1 + \frac{k' \beta_c}{s} + \frac{1}{s} \frac{d\bar{u}}{dz} \right) P_0 + P_{1\nu h} \right] \frac{\Psi_{\nu h}}{r} \Theta'_\nu + \sum_p \sum_q P_{1pq} \frac{\Psi_{pq}}{r} \Theta'_p \right\} \tag{2.60d}$$

The entropy perturbation must be evaluated before the nozzle boundary condition can be imposed. The fundamental identical relation of thermodynamics can be written in dimensionless form as

$$T\, ds = dh - \frac{\gamma - 1}{\gamma} \frac{dp}{\rho}$$

In terms of steady state and perturbation quantities, this relation becomes

$$\bar{T} s' = h' - \frac{\gamma-1}{\gamma} \frac{p'}{\bar{\rho}}$$

It has been shown that $\bar{T} = \bar{p} = \bar{\rho} = 1$ and $h' = T'$. Then the entropy perturbation is given by

$$s' = T' - \frac{\gamma-1}{\gamma} p'$$

or, making use of the equation of state (2.14g) to eliminate the temperature perturbation,

$$s' = \frac{p'}{\gamma} - \rho' \tag{2.61}$$

The perturbations of all unsteady quantities have been assumed to be represented by series expansions. Thus for the entropy

$$s' = s_0 + s_1 + \cdots$$

where from equation (2.61)

$$s_0 = \frac{p_0}{\gamma} - \rho_0 \quad , \quad s_1 = \frac{p_1}{\gamma} - \rho_1 \, , \quad \cdots$$

The zeroth order energy equation (2.34e) shows that

$$s_0 = 0$$

From the first order energy equation (2.42e) it can be seen that

$$s_1 = -\frac{1}{S} \frac{d\bar{u}}{dz} \left(\frac{\gamma-1}{\gamma} \right) p_0$$

or

$$s' = s_1 = -\frac{1}{S} \frac{d\bar{u}}{dz} \left(\frac{\gamma-1}{\gamma} \right) P_{00} \Psi_{\nu\lambda}(r) \Theta_\nu(\theta) + O(\bar{u}_e^2) \tag{2.62}$$

Thus, the entropy perturbation is largest in the region where the combustion is most intense. At the nozzle entrance, where combustion is assumed complete, the entropy perturbation vanishes.

It is now possible to examine the stability behavior of the rocket

motor by applying the chamber exit boundary condition, which is the nozzle admittance relation. The conditions at the stability limits, which bound the regions of unstable operation, will be derived by setting the amplification factor λ equal to zero. Then the complex time parameter s is purely imaginary, $s = i\omega$, where ω is the frequency of oscillation.

E. Characteristic Equation

The boundary condition imposed by the exhaust nozzle upon the oscillatory flow in the rocket combustion chamber has been presented in equation (2.40) in a form appropriate to the zeroth order solution. Because of the distortion of the wave pattern introduced by the effects on the combustion process of the transverse velocity fluctuations, it has been necessary to make use of eigenfunction expansions in the perturbation solution, which has been found to take the following form:

$$\left.\begin{aligned}
p' &= \sum_{p=0}^{\infty}\sum_{q=1}^{\infty} P_{pq}(\bar{t})\,\Psi_{pq}(r)\,\Theta_p(\theta) \\
u' &= \sum_{p=0}^{\infty}\sum_{q=1}^{\infty} U_{pq}(\bar{t})\,\Psi_{pq}(r)\,\Theta_p(\theta) \\
v' &= \sum_{p=0}^{\infty}\sum_{q=1}^{\infty} V_{pq}(\bar{t})\,\Psi'_{pq}(r)\,\Theta_p(\theta) \\
w' &= \sum_{p=0}^{\infty}\sum_{q=1}^{\infty} V_{pq}(\bar{t})\,\frac{1}{r}\Psi_{pq}(r)\,\Theta'_p(\theta) \\
s' &= \sum_{p=0}^{\infty}\sum_{q=1}^{\infty} S_{pq}(\bar{t})\,\Psi_{pq}(r)\,\Theta_p(\theta)
\end{aligned}\right\} \qquad (2.63)$$

Then, imposing the nozzle boundary conditions results in not one relation as in equation (2.40), but infinitely many relations of the form

$$\frac{\gamma U_{pq}(\bar{t}_e)}{P_{oo}} + A\,\frac{P_{pq}(\bar{t}_e)}{P_{oo}} + B\,S_{pq}\,\frac{i\,V_{pq}(\bar{t}_e)}{P_{oo}} + C\,\frac{\gamma S_{pq}(\bar{t}_e)}{P_{oo}} = 0 \qquad (2.64)$$

There is thus an admittance relation corresponding to each term in the eigenfunction expansions.

Since combustion is assumed to be complete at the entrance to the nozzle,

$$\frac{d\bar{u}}{d\bar{z}}(\bar{z}_e) = \bar{\rho}_L(\bar{z}_e) = 0$$

Hence, the axial distribution functions become, using equations (2.59) and (2.60),

$$\left.\begin{aligned}
P_{\nu h}(\bar{z}_e) &= P_0(\bar{z}_e) + P_A(\bar{z}_e) + B_{\nu h} P_{B\nu h}(\bar{z}_e) - i\tilde{C}_{\nu h} P_{C\nu h}(\bar{z}_e) + P_D(\bar{z}_e) \\
P_{pq}(\bar{z}_e) &= B_{pq} P_{Bpq}(\bar{z}_e) + C_{pq} P_{Cpq}(\bar{z}_e) \\
U_{pq}(\bar{z}_e) &= -\frac{1}{\gamma S}\frac{dP_{pq}(\bar{z}_e)}{d\bar{z}} \\
V_{pq}(\bar{z}_e) &= -\frac{1}{\bar{\nu} S} P_{pq}(\bar{z}_e) \\
S_{pq}(\bar{z}_e) &= 0
\end{aligned}\right\} \qquad (2.65)$$

where

$$\left.\begin{aligned}
P_0(\bar{z}) &= P_{oo}\left[1 + (S^2 + S_{\nu h}^2)\frac{\bar{z}^2}{2}\right] \\
P_A(\bar{z}) &= P_{oo}\left[-\gamma S \mathcal{P}\int_0^{\bar{z}} \bar{u}\, d\bar{z}' + K_A\right] \\
P_{B\nu h}(\bar{z}) &= P_{oo}\left[\mathcal{R}\int_0^{\bar{z}} \bar{u}\, d\bar{z}' + K_{B\nu h}\right] \\
P_{C\nu h}(\bar{z}) &= P_{oo}\left[\mathcal{J}\int_0^{\bar{z}} \bar{u}\, d\bar{z}' + K_{C\nu h}\right] \\
P_D(\bar{z}) &= P_{oo}\left[S\int_0^{\bar{z}} d\bar{z}'\int_0^{\bar{z}'} \bar{k}'\bar{\rho}_L\, d\bar{z}'' + (\gamma+1)S\int_0^{\bar{z}} \bar{u}\, d\bar{z}' + K_D\right] \\
P_{Bpq}(\bar{z}) &= P_{oo}\left[\mathcal{R}\int_0^{\bar{z}} \frac{d\bar{u}}{d\bar{z}}\frac{\sinh\sqrt{S_{pq}^2 - S_{\nu h}^2}\,(\bar{z}-\bar{z}')}{\sqrt{S_{pq}^2 - S_{\nu h}^2}}\, d\bar{z}' + K_{Bpq}\cosh\sqrt{S_{pq}^2 - S_{\nu h}^2}\,\bar{z}\right] \\
P_{Cpq}(\bar{z}) &= P_{oo}\left[\mathcal{J}\int_0^{\bar{z}} \frac{d\bar{u}}{d\bar{z}}\frac{\sinh\sqrt{S_{pq}^2 - S_{\nu h}^2}\,(\bar{z}-\bar{z}')}{\sqrt{S_{pq}^2 - S_{\nu h}^2}}\, d\bar{z}' + K_{Cpq}\cosh\sqrt{S_{pq}^2 - S_{\nu h}^2}\,\bar{z}\right]
\end{aligned}\right\} \qquad (2.66)$$

Substituting the relations (2.65) into the nozzle admittance equation (2.64), and defining a combined admittance coefficient $\mathcal{E}$ by

$$\mathcal{E} = \mathcal{E}_r + i\mathcal{E}_i = \left(\frac{\omega}{S_{pq}}\right)\mathcal{A} + i\mathcal{B} \qquad (2.67)$$

there results the equation

$$\left(\frac{d}{dz} - i\, s_{pq}\, \varepsilon\right) \frac{P_{pq}}{P_{so}}(z_e) = 0 \tag{2.68}$$

Each of the partial solutions making up the pressure perturbation p' includes a constant resulting from the integration in the axial direction. For each pair of indices p, q (that is, for each term in the eigenfunction expansion), the several integration constants can be combined into one. Then the axial distribution functions $P_{pq}(z)$ take the following form:

$$P_{pq}(z) = P_{oo}\left[\tilde{P}_{pq}(z) + K_{pq}\cosh\sqrt{s_{pq}^2 - s_{\nu h}^2}\, z\right] \tag{2.69}$$

where the function $\tilde{P}_{pq}$ does not include any integration constant and the constants K_{pq} are all $O(\bar{u}e)$. In particular, the axial function corresponding to the mode of oscillation under consideration can be written as

$$P_{\nu h}(z) = P_{oo}\left(1 + K_{\nu h} + \tilde{P}_{1\nu h}(z)\right) \tag{2.70}$$

The function $\tilde{P}_{1\nu h}$, which from equations (2.65 and (2.66) is given by

$$\tilde{P}_{1\nu h}(z) = (s^2 + s_{\nu h}^2)\frac{z^2}{2} + s\int_0^z dz' \int_0^{z'} \frac{\bar{u}}{\bar{\rho}_u} dz'' + \left[(\gamma+1)s - \gamma s\mathcal{P} + B_{\nu h}\mathcal{Q} - i\tilde{C}_{\nu h} J\right]\int_0^z \bar{u}\, dz' \tag{2.71}$$

is $O(\bar{u}_e)$. The integration constant $K_{\nu h}$ can be absorbed into the constant P_{oo}, as can be seen from the following discussion. Equation (2.69) is divided through by $\tilde{P}_{oo} = P_{oo}(1 + K_{\nu h})$ giving

$$\frac{P_{\nu h}}{\tilde{P}_{oo}} = 1 + \frac{\tilde{P}_{1\nu h}}{1 + K_{\nu h}} = 1 + \tilde{P}_{1\nu h}(1 - K_{\nu h}) + O(\bar{u}_e^3)$$

or

$$\frac{P_{\nu h}}{\tilde{P}_{oo}} = 1 + \tilde{P}_{1\nu h} - K_{\nu h}\tilde{P}_{1\nu h} + O(\bar{u}_e^3)$$

Since both $K_{\nu h}$ and $\tilde{P}_{1\nu h}$ are $O(\bar{u}_e)$, their product is $O(\bar{u}_e^2)$, and thus

$$P_{\nu h}(z) = \tilde{P}_{oo}\left(1 + \tilde{P}_{1\nu h}\right) + O(\bar{u}_e^2) \tag{2.70a}$$

Similarly, replacing P_{00} with $\tilde{P}_{00}$ in equation (2.69) results in an error of $O(\tilde{u}_e^2)$, which in this analysis has been assumed to be negligible.

The solution for the pressure perturbation, equation (2.60a) can thus be written

$$p'(z,r,\theta) = \tilde{P}_{00}\left\{\left[1+\tilde{P}_{1\nu h}(z)\right]\Psi_{\nu h}(r)\Theta_{\nu}(\theta) + \right.$$
$$\left. + \sum_{p,q\neq\nu,h}\sum \left(\tilde{P}_{1pq}(z) + K_{pq}\cosh\sqrt{s_{pq}^2 - s_{\nu h}^2}\, z\right)\Psi_{pq}(r)\Theta_p(\theta)\right\} \tag{2.72}$$

The constant $\tilde{P}_{00}$, which represents the perturbation amplitude level, will not affect the stability solution. For each $p,q \neq \nu,h$, the nozzle boundary condition

$$\frac{d\tilde{P}_{pq}}{dz}(z_e) + K_{pq}\sqrt{s_{pq}^2 - s_{\nu h}^2}\,\sinh\sqrt{s_{pq}^2 - s_{\nu h}^2}\, z_e - $$
$$- i s_{pq}\mathcal{E}(\omega, s_{pq})\left[\tilde{P}_{pq}(z_e) + K_{pq}\cosh\sqrt{s_{pq}^2 - s_{\nu h}^2}\, z_e\right] = 0 \tag{2.73a}$$

can be used to determine the integration constant K_{pq}. Application of the remaining boundary condition,

$$\frac{d\tilde{P}_{\nu h}}{dz}(z_e) - i s_{\nu h}\mathcal{E}(\omega, s_{\nu h})\left[1 + \tilde{P}_{1\nu h}(z_e)\right] = 0 \tag{2.73b}$$

results in an eigenvalue problem. That is, equation (2.73b) is the characteristic equation for the eigenvalues $s = \lambda + i\omega$. The following discussion will be concerned with the neutral oscillations occurring at the stability limits, for which $\lambda = 0$.

By use of the expression for $P_{\nu h}(z)$ obtained from equations (2.70) and (2.71), the characteristic equation (2.73b) can be written as

$$P + i\left(\frac{B_{\nu h}}{\gamma\omega}\right)R + \left(\frac{C_{\nu h}}{\gamma\omega}\right)J = h \tag{2.74}$$

where the right hand side is of the form

$$h = \frac{\gamma+1}{\gamma} + \frac{h_2}{h_1} \tag{2.75a}$$

with
$$h_1 = \gamma\bar{u}_e - i\gamma s_{\nu h}\mathcal{E}\int_0^{z_e}\bar{u}\,dz \tag{2.75b}$$

$$h_2 = \int_0^{z_e} -k'\bar{p}_i\,dz + i s_{\nu h} z_e\left(f - \frac{1}{f}\right)$$
$$- \mathcal{E}\left[\frac{1}{f} - \frac{s_{\nu h}^2 z_e^2}{2}\left(f - \frac{1}{f}\right) + i s_{\nu h}\int_0^{z_e} dz \int_0^{z} k'\bar{p}_i\,dz'\right] \tag{2.75c}$$

In the expressions for h_1 and h_2 a reduced frequency $f = \frac{\omega}{S_{yh}}$ has been introduced. Since $\omega^2 - S_{yh}^2 = O(\bar{u}_e)$ for a purely transverse mode, the reduced frequency takes on values near unity.

It is convenient in discussing the characteristic equation to define several auxiliary functions:

$$\left.\begin{aligned} a &= a_r + i a_i = \frac{S_{yh}}{\bar{u}_e} \int_0^{z_e} dz \int_0^z k'(z) \bar{p}_i(z')\, dz' \\ \varepsilon &= S_{yh} \int_0^{z_e} (\bar{u}/\bar{u}_e)\, dz \\ d &= d_r + i d_i = \frac{1}{\bar{u}_e} \int_0^{z_e} k'(z) \bar{p}_i(z)\, dz \\ \gamma &= S_{yh} z_e \end{aligned}\right\} \qquad (2.76a)$$

The functions h_1 and h_2 in equation (2.76) can be written in terms of these auxiliary functions as

$$\left.\begin{aligned} h_1 &= \gamma \bar{u}_e (1 - i\varepsilon) \\ h_2 &= \bar{u}_e \left\{ d + i \frac{\gamma}{\bar{u}_e} \left(f - \frac{1}{f}\right) - \frac{\varepsilon}{\bar{u}_e} \left[\frac{1}{f} - \frac{1}{2}\gamma^2 \left(f - \frac{1}{f}\right) \right] - i\varepsilon a \right\} \end{aligned}\right\} \qquad (2.76b)$$

As written in equation (2.74) above, the characteristic equation exhibits the balance which exists at the stability limits. In order for neutral oscillations to be maintained, the energy supplied by the combustion process, represented by the left side of equation (2.74), must be completely absorbed by the fluid mechanical processes, which are represented by the function h on the right side of the characteristic equation. If more than sufficient energy is supplied, the oscillation amplitude will grow. Such an oscillation is linearly unstable. Eventually, nonlinear energy-absorbing processes will restore the energy balance at some high level of amplitude. The importance of the oscillation to the proper operation of the rocket motor depends upon the amplitude level finally attained. However, it has been observed that nearly all transverse mode instabilities grow to very high levels, causing rapid combustion chamber destruction. Stable operation results in the case that the energy release is insufficient to balance the energy absorbed by the oscillation. The fact that the characteristic equation is

complex implies that there is a phase condition, as well as the amplitude condition, relating the oscillating rates of energy release and energy absorption for neutral oscillations.

Assuming that the pressure and velocity effects are characterized by the same mean sensitive time lag τ , the definitions of the burning rate parameters are

$$\left.\begin{aligned} \mathcal{P} &= n\,(1-e^{-i\omega\tau}) \\ \mathcal{R} &= \ell_r\,(1-e^{-i\omega\tau}) \\ \mathcal{J} &= \ell_e\,(1-e^{-i\omega\tau}) \end{aligned}\right\} \qquad (2.77)$$

Then the characteristic equation takes the form

$$\left[1+i\left(\frac{B_{vh}}{\gamma\omega}\right)\frac{\ell_r}{n}+\left(\frac{\tilde{C}_{vh}}{\gamma\omega}\right)\frac{\ell_e}{n}\right] n\,(1-e^{-i\omega\tau}) = h(\omega) \qquad (2.78)$$

This complex equation is equivalent to two real equations. Therefore, for neutral oscillations of a given rocket motor, the four combustion parameters, n, τ, $\frac{\ell_r}{n}$, and $\frac{\ell_e}{n}$, are not independent. If any three are known, then the fourth, together with the oscillation frequency, can be determined from equation (2.78). Because the frequency dependence of $h(\omega)$ is quite complicated, it is most convenient to regard the frequency as one of the independent variables. In order that the present investigation may be related more easily to previous studies of both longitudinal and transverse modes, the two dependent variables will be taken to be the mean sensitive time lag τ and the pressure interaction index n . Thus,

$$n = n\left(\omega, \frac{\ell_r}{n}, \frac{\ell_e}{n}\right)$$

$$\tau = \tau\left(\omega, \frac{\ell_r}{n}, \frac{\ell_e}{n}\right)$$

will be determined from the characteristic equation, which can be written as

$$n\,(1-e^{-i\omega\tau}) = \frac{h}{1+i\left(\frac{B_{vh}}{\gamma\omega}\right)\frac{\ell_r}{n}+\left(\frac{\tilde{C}_{vh}}{\gamma\omega}\right)\frac{\ell_e}{n}} = \tilde{h} = \tilde{h}_r + i\,\tilde{h}_i \qquad (2.79)$$

At present, none of the combustion parameters can be calculated

a priori, although a method has been developed for measuring n and τ experimentally (16). Since very little is known about the velocity parameters their effect will be shown by calculating n and τ for assumed real values of the ratios $\frac{\ell_r}{n}$ and $\frac{\ell_\theta}{n}$. The modifications introduced by the assumed velocity effects will then be noted and compared with the results of appropriate experiments.

The real and imaginary parts of equation (2.79),

$$\left.\begin{aligned} n(1-\cos\omega\tau) &= \tilde{h}_r \\ n\sin\omega\tau &= \tilde{h}_i \end{aligned}\right\} \tag{2.80}$$

comprise a simultaneous pair of equations for n and τ . The solution is found to be

$$n = \frac{\tilde{h}_r^2 + \tilde{h}_i^2}{2\tilde{h}_r}$$

$$\tau = \frac{1}{\omega}\sin^{-1}\left(\frac{\tilde{h}_i}{n}\right) = \frac{1}{\omega}\cos^{-1}\left(1-\frac{\tilde{h}_r}{n}\right) \tag{2.81}$$

where τ is determined modulo 2π . When $\omega\tau=\pi$, $\sin\omega\tau = \tilde{h}_i = 0$ and $(1-\cos\omega\tau) = 2$. Then

$$\left.\begin{aligned} n &= \tfrac{1}{2}\tilde{h}_r = n_M \\ \tau &= \frac{\pi}{\omega} = \tau_M \end{aligned}\right\} \tag{2.82}$$

For physically realizable systems, $\tilde{h}_r > 0$, so that $n \geq n_M > 0$

It can be seen that n_M is the minimum value of the interaction index, for when $\omega\tau \neq \pi$, $\tilde{h}_i \neq 0$ and

$$n = \frac{1}{2}\tilde{h}_r + \frac{1}{2}\frac{\tilde{h}_i^2}{\tilde{h}_r}$$

which is greater than n_M since $\tilde{h}_r$ and $\tilde{h}_i^2$ are positive. For $n_1 > n_M$, there are two solutions for τ , namely.

$$\tau_1 = \frac{1}{\omega_1}\sin^{-1}\left(-\frac{\sqrt{\tilde{h}_i^2}}{n_1}\right), \quad \tau_2 = \frac{1}{\omega_2}\sin^{-1}\left(+\frac{\sqrt{\tilde{h}_i^2}}{n_1}\right)$$

with $\tau_1 > \tau_M > \tau_2$ and $\omega_1 < \omega_M < \omega_2$.

A typical solution for $n(\omega)$ and $\tau(\omega)$ for assumed values of l_f/n and l_o/n is shown in Figure 19. This solution applies at the stability limits, where $\lambda = 0$. It can be seen that for any given value of the time lag, only one value of the pressure interaction index is consistent with neutral oscillations. For the same τ, a larger value of n corresponds to instability ($\lambda > 0$), a smaller value to stability ($\lambda < 0$). Thus the n, τ-plane is divided by the loci of $\lambda = 0$ into stable and unstable regions, as shown in Figure 20.

A given rocket motor system at given operating conditions is assumed to be characterized by a set of values of the combustion parameters n, τ, $\frac{l_f}{n}$ and $\frac{l_o}{n}$. If the point on the n, τ-plane representing this motor falls within one of the unstable regions (i. e., above the stability limit curve) corresponding to one of the transverse modes and to the appropriate values of l_f/n and l_o/n, then the operation of the rocket will be unstable, and large amplitude oscillations can be expected to result. Therefore, any effect which increases the size of the unstable areas on the n, τ-plane (e.g., by shifting the stability limits to smaller n for all τ, or by flattening the limit curves without changing n_M) is a destabilizing effect.

Since the function $h(\omega)$ in equation (2.79) depends on s_{vh}, there is a different stability pattern for each mode of oscillation. In Figure 21, stability limits are presented for several purely transverse modes. For a given interaction index value, the value of the time lag at the stability limit is nearly inversely proportional to the acoustic frequency s_{vh}. Thus higher modes are associated with smaller sensitive time lags. By definition,

$$\tau = \frac{\tau^* \bar{c}_o^*}{c^*}$$

Hence, a shorter time lag is obtained by a decrease in the stagnation

sound velocity of the combustion gases, by an increase in the combustion chamber diameter, or by a decrease in the dimensional time lag itself.

The nature of the functional relationships involved in the characteristic equation precludes a general analytical solution. Therefore, it is necessary to rely on numerical solutions for specific cases. A large volume of calculations is thus required to explore the dependence of the stability patterns on each physical parameter. In this situation, many important insights can be gained by considering a very much simplified rocket motor system, for which some analytical results are also possible.

The simplest steady state combustion distribution is that in which all of the combustion occurs at a single axial station. This ideal combustion pattern is actually a good approximation to that produced by an efficient injector (such as the unlike impinging doublet type used in the experimental phase of this investigation), which provides good atomization and rapid mixing of the liquid propellants. The steady state axial velocity distribution for concentrated combustion is given by

$$\bar{u} = 0, \quad 0 \le z \le z_m$$

$$\bar{u} = \bar{u}_e, \quad z_m \le z \le z_e$$

where z_m is the location of the combustion front and z_e is the nozzle entrance station. The other simplification to be introduced is

$$\bar{u}_L \simeq \bar{u}_{Lm} = \text{Constant}$$

which is applicable when the droplet momentum coefficient k is not too large.

For this simple model, the auxiliary functions defined in

equation (2.75a) become

$$\left.\begin{aligned} a_r &= \tfrac{1}{2}\beta(\kappa+\zeta) + \beta\kappa\sigma_r + O(\bar{u}_e^2) \\ a_i &= \beta\kappa\sigma_i + O(\bar{u}_e^2) \\ \kappa &= S_{vn}(z_e - z_m) \\ d_r &= \beta(1+\sigma_r) \\ d_i &= \beta\sigma_i \end{aligned}\right\} \qquad (2.83)$$

where

$$\beta = \frac{-k z_m}{\bar{u}_{Lm}}$$

$$\sigma_r = e^{-\beta}\,\frac{\cos\mu}{\beta+i\mu}$$

$$\sigma_i = -e^{-\beta}\,\frac{\sin\mu}{\beta+i\mu}$$

$$\mu = f\cdot\frac{S_{vn} z_m}{\bar{u}_{Lm}}$$

Since the frequency corresponding to the minimum interaction index is close to the acoustic frequency, the reduced frequency f can be approximated by $1+\varphi$, where $\varphi^2 << 1$.

Consider first the case in which there are no velocity effects on combustion, only pressure effects. Then $n_M = \frac{h_r}{2}$ and $h_i = 0$ where h_r and h_i are the real and imaginary parts of the function h defined in equation (2.75) as

$$h = \frac{\gamma+1}{\gamma} + \frac{h_2}{h_1}$$

Then

$$\left.\begin{aligned} h_r &= \frac{\gamma+1}{\gamma} + \frac{h_{1r}h_{2r} + h_{1i}h_{2i}}{h_{1r}^2 + h_{1i}^2} \\ h_i &= \frac{h_{1r}h_{2i} - h_{1i}h_{2r}}{h_{1r}^2 + h_{1i}^2} \end{aligned}\right\} \qquad (2.84)$$

Introducing the expressions (2.83) into the definitions of h_1 and h_2 of equation (2.75) gives

$$\left.\begin{aligned} h_{1r} &= \gamma \bar{u}_e (1+\rho\varepsilon_i) \\ h_{1i} &= -\gamma \bar{u}_e \rho \varepsilon_r \\ h_{2r} &= \bar{u}_e \left[\alpha_r - \frac{\varepsilon_r}{\bar{u}_e}(1-\varphi-\varphi\gamma^2) + \varepsilon_i a_r + \varepsilon_r a_i \right] \\ h_{2i} &= \bar{u}_e \left[\alpha_i + \frac{2\varphi\gamma}{\bar{u}_e} - \frac{\varepsilon_i}{\bar{u}_e}(1-\varphi-\varphi\gamma^2) + \varepsilon_i a_i - \varepsilon_r a_r \right] \end{aligned}\right\} \quad (2.85)$$

These expressions can be simplified by noting the order of magnitude of each term and neglecting the higher order terms. It can be seen from equation (2.83) that, since $\frac{l}{k}$ and $\bar{u}_m$ are $O(\bar{u}_e)$ while z_e, z_m, and $s_{\varphi i}$ are $O(1)$,

β, a_r, α_r, ρ are $O(1)$

$\mu = O(1/\bar{u}_e)$

σ_r, σ_i, a_i, α_i are $O(\bar{u}_e)$

The real part of the combined admittance coefficient, ε_r, is at most $O(\bar{u}_e)$ However, the imaginary part can take on somewhat greater values, so that ε_i^2 is $O(\bar{u}_e)$ in the range of exit velocities considered here.

Straightforward calculation, making use of the above order of magnitude observations, yields

$$\bar{u}_M = \frac{\gamma+1}{2\gamma} + \frac{\beta}{2\gamma(1+\rho\varepsilon_i)^2}\left\{[1+\rho\varepsilon_i]\left[1+\tfrac{1}{2}\varepsilon_i(\gamma+\rho)\right] + \sigma_r\right\} - \frac{\varepsilon_r/\bar{u}_e}{2\gamma(1+\rho\varepsilon_i)^2}\left\{1-\varphi\left[(1+\gamma^2)(1-\rho\varepsilon_i) - 2\rho\gamma\right]\right\} \quad (2.86)$$

where from the condition $h_i = 0$ the frequency is given by

$$\varphi = \frac{1}{1+\gamma^2+\frac{2\gamma}{\varepsilon_i}} \quad (2.87)$$

The important quantities governing the stability limits are the chamber exit velocity $\bar{u}_e$, through the admittance coefficients ε_r and ε_i (which are also frequency dependent), the droplet drag factor β, and the length parameter γ. The quantity ρ, which measures the volume occupied completely by gaseous products of combustion, has a very small

influence on n_M. The derivative

$$\frac{\partial n_M}{\partial f} = \frac{\beta\left[\frac{3}{2}\varepsilon_i + \frac{1}{2}\varepsilon_i^2(3+2f)\right] - p\,\frac{\varepsilon_r}{\bar{u}_e}\left[(1+3^2)\varepsilon_i + n_3\right] - 4\gamma\varepsilon_i\left(n_M - \frac{\gamma+1}{2\gamma}\right)(1+f\varepsilon_i)}{2\gamma\,(1+f\varepsilon_i)^2}$$

is at most $O(\bar{u}_e)$. The function σ_r, which is given approximately by

$$\sigma_r \cong -\left(\frac{\bar{u}_{im}}{f S_{vh} z_m}\right) \sin\left(\frac{f S_{vh}}{\bar{u}_{im}} z_m\right)$$

oscillates very rapidly with respect to z_m (in general, $f\frac{S_{vh}}{\bar{u}_{im}}$ is at least 35). Thus, the small spreading of the combustion front which must be present in any actual rocket chamber will cause the effect of σ to be cancelled.

Figure 22 shows the variation of the nozzle admittance coefficients with the combustion chamber exit velocity for two frequencies, $\omega = S_{vh}$ and $\omega = 1.05\ S_{vh}$. For longitudinal modes, the nozzle admittance, defined by

$$\alpha_n \bar{u}_e = \frac{\gamma U(z_e)}{P(z_e)}$$

is positive. It has been shown (1) that the nozzle exerts a strong damping effect. On the other hand, for transverse modes, the admittance is, from equation (2.68),

$$\mathcal{E} = -f\,\frac{\gamma U(z_e)}{P(z_e)}$$

so that

$$\mathcal{E} \sim -\int \alpha_n \bar{u}_e$$

For all but the smallest nozzle entrance velocities, the transverse mode nozzle admittance ratio is positive. Therefore, in transverse modes, the exhaust nozzle exerts negative damping, i.e. it has a destabilizing effect.

At the lower velocities ($\bar{u}_e < 0.10$), ε_i is nearly constant, but $\varepsilon_r/\bar{u}_e$ increases rapidly with increasing velocity. Therefore, the minimum interaction index shows a sharp decrease with increasing exit velocity in this range, as can be seen from equation (2.86). Figure 23

shows that the entire stability limit curve is shifted downward when the exit velocity is increased from 0.05 to 0.10. For larger velocities, $\varepsilon_r/\bar{u}_e$ levels off and then decreases, but the stabilizing effect of the $\frac{\varepsilon_r}{a_e}$ decrease is offset by the destabilizing effect of the decrease of ε_i. The result is that n_M continues to decrease with increasing $\bar{u}_e$, although much more slowly. Some combustion chamber configurations show an increase in n_M with velocity for $\bar{u}_e > 0.30$. However, these results cannot be trusted because the $O(\bar{u}_e^2)$ terms which have been neglected may be very important. Hence, in the range of exit velocities appropriate to the small Mach number assumption, increasing the combustion chamber exit velocity (decreasing the nozzle contraction ratio) always has a destabilizing effect.

The nozzle admittance coefficients shown in Figure 22 correspond to a nozzle with a linear velocity profile in the subsonic section. For a nozzle with a conical converging part, the coefficients show similar trends, but the values of $\frac{\varepsilon_r}{\bar{u}_e}$ for the "conical" nozzle are much larger than those for the "linear" nozzle, especially the range $\bar{u}_e \leq 0.15$. For higher exit velocities, the coefficients for the two types of nozzle tend to converge. Therefore, the minimum interaction index is smaller for the conical nozzle than for the linear for corresponding combustion chamber conditions, as shown in Figure 24.

The droplet drag coefficient β is, by equation (2.83), the product of the momentum interchange coefficient $\mathcal{R}$, which represents the rate at which energy is transferred into the oscillatory motion of the liquid propellant droplets, and the droplet lifetime, $\tau_m/\bar{u}_{1_m}$, that is, the time interval during which the droplets can absorb energy from the oscillations of the gases in the combustion chamber. From equation (2.86),

$$\frac{\partial n_M}{\partial \beta} = \frac{(1+\kappa\varepsilon_i)(1+\frac{1}{2}\varepsilon_i[3+\kappa])}{2\gamma(1+\kappa\varepsilon_i)^2}$$

which is positive and O(1). Thus, increasing β has an appreciable stabilizing effect, as shown in Figure 25. The quantity β can also be considered as the ratio of the distance of the combustion front from the injector face, z_m, to the distance of droplet penetration into stagnant combustion gas, $z_p = \frac{\bar{u}_{Lm}}{k}$, based on a mean droplet velocity and an effective momentum coefficient. Then β can be seen to depend on the injector spray characteristics, including the droplet size distribution and the effectiveness of liquid mixing, and on the droplet vaporization characteristics. The β range for these calculations ($0.2 \leq \beta \leq 0.7$) was chosen so as to include values which are likely to be found in actual rocket motors. However, further basic information is needed to establish the value of β more definitely.

The effect of the chamber length parameter, $\zeta = \epsilon_{yh} \cdot z_e$, can be seen from equation (2.86) by calculating the derivative,

$$\frac{\partial n_M}{\partial \zeta} = \frac{1}{2\gamma(1+\rho\xi_i)^2} \left\{ \frac{1}{2}\beta\xi_i(1+\rho\xi_i) + 2\rho\frac{\xi_r}{\bar{u}_e}\left[\zeta(1-\rho\xi_i)-\rho\right] \right.$$
$$\left. -2\frac{\xi_r}{\bar{u}_e}\frac{\left[(1+\zeta^2)(1-\rho\xi_i)-2\rho\zeta\right]\left[\zeta+1/\xi_i\right]}{\left[1+\zeta^2+2\zeta/\xi_i\right]^2} \right.$$

For most cases the positive terms dominate, so that an increase in combustion chamber length has a stabilizing effect. The only exceptions are cases with low β values and very low exit velocities ($\bar{u}_e \leq 0.05$), for which $\xi_r/\bar{u}_e$ is negative (linear nozzle). However, $\frac{\partial n_M}{\partial \zeta}$ is only $O(\bar{u}_e)$ in any case, so that a large change in length is required to produce a significant shift in the stability limits. In Figure 26, stability limits are shown for the first tangential mode for two lengths which are in the ratio of 2 to 1. Because of the factor S_{mn}, changes in length are more significant for higher transverse modes than for the first tangential. If the length is increased beyond the critical length, longitudinal and mixed longitudinal-transverse modes will

also be unstable, and the present theory will not be applicable.

The preceding discussion has been concerned only with pressure effects. If now the tangential (but not radial) velocity fluctuations are also assumed to affect the combustion process, the characteristic equation becomes

$$n\left(1-e^{-i\omega\tau}\right) = \bar{h} = \frac{h}{1+\left(\frac{\tilde{c}_{vh}}{r\omega}\right)\frac{\ell_\theta}{n}}$$

The ratio of the minimum interaction index including tangential velocity effects, n_{MT}, to that for pressure effects alone, n_{MP}, is then

$$\frac{n_{MT}}{n_{MP}} = \frac{\tilde{h}_r}{h_r} = \frac{1}{1+\left(\frac{\tilde{c}_{vh}}{r\omega}\right)\frac{\ell_\theta}{n}}$$

Therefore, since $\frac{\tilde{c}_{vh}}{r\omega} > 0$, a positive value of the tangential velocity interaction index causes a downward shift of the stability limit curve on the n,τ- plane by contracting the ordinates of the limit points, which is a destabilizing trend. Since $\frac{\tilde{h}}{h}$ is real, there is no effect on the time lag value at the minimum point. Figure 27 shows the influence of the tangential velocity effect on the stability limits for the first tangential spinning mode. For other modes of oscillation, the effects will be qualitatively the same. The magnitude of the velocity effect, for a given $\frac{\ell_\theta}{n}$ value, depends on the ratio of the expansion coefficient $\tilde{c}_{vh}$ to the frequency $\omega = f s_{vh}$. This ratio is approximately equal to $\frac{\tilde{c}_{vh}}{s_{vh}}$, values of which are given in Table II for several modes. The second tangential mode is seen to be slightly more influenced by the tangential velocity oscillations than the other modes. It should be recalled that the expansion coefficient $\tilde{c}_{vh}$ vanishes for a standing tangential mode, so that there are no tangential velocity effects for such an oscillation.

The velocity index ℓ_θ is positive in the case that the burning rate is increased by a positive velocity. For the tangential velocity, the

positive direction is not fixed with respect to the rocket combustion chamber, but is the direction in which a spinning wave travels. Assuming that the injector is characterized by a positive ℓ_θ direction (determined by the orientation of the injection pattern), the velocity effect of a wave moving in the positive direction will augment the pressure effect. However, for a wave moving in the other direction, the velocity effect will oppose that of the pressure. It is apparent, therefore, that the preferred wave travel direction with respect to the physical frame of reference is the same as the positive ℓ_θ direction of the injector. Without more detailed knowledge of the combustion process than is presently available, this direction cannot be determined a priori, but must be established by experimental evidence.

Consider now the effect of the radial velocity coupled with the pressure, i. e., $\ell_r \neq 0$ but $\ell_\theta = 0$. Then the characteristic equation is

$$n(1 - e^{-i\omega\tau}) = \tilde{h} = \frac{h}{1 + i\left(\frac{B_{vh}}{\gamma\omega}\right)\frac{\ell_r}{n}}$$

Since the ratio $\tilde{h}/h$ is complex, one can expect an influence on τ as well as on n. At the minimum pressure interaction index point,

$$n_{MR} = \frac{\tilde{h}_r}{2} = \frac{1}{2}\,\frac{h_r + \left(\frac{B_{vh}}{\gamma\omega}\frac{\ell_r}{n}\right)h_i}{1 + \left(\frac{B_{vh}}{\gamma\omega}\frac{\ell_r}{n}\right)^2} \quad ; \quad \tilde{h}_i = \frac{h_i - \left(\frac{B_{vh}}{\gamma\omega}\frac{\ell_r}{n}\right)h_r}{1 + \left(\frac{B_{vh}}{\gamma\omega}\frac{\ell_r}{n}\right)^2} = 0$$

Thus, when the radial velocity effect is included, the condition at the minimum is

$$h_i = \left(\frac{B_{vh}}{\gamma\omega}\frac{\ell_r}{n}\right)h_r$$

rather than $h_i = 0$. Then $\tilde{h}_r = h_r$ or $n_{MR} = \frac{1}{2}h_r(\omega_M)$, as before. From Figure 28 it can be seen that a positive radial velocity index implies a higher frequency at any n than that corresponding to pressure effects

alone. The flatness of the $h_r(\omega)$ curve indicates that the minimum value of the pressure index will not be significantly altered by the addition of radial velocity effects. Since $\tau \sim \frac{1}{\omega}$, a positive value of ℓ_r corresponds to a shift of the minimum point toward smaller τ . However, the magnitude of the shift is very small, as a result of the strong variation of h_t with ω and the low values taken by the ratio $\frac{B_{sh}}{S_{sh}}$, listed in Table II. For $n > n_M$, the shift of the stability limits reverses, because a positive radial velocity index brings about an increase in $\omega\tau$ which is slightly greater than the increase in ω . Thus, except for the near vicinity of the minimum point, the limit curve is shifted in the direction of longer time lags for a positive index ℓ_r . These results are shown in Figure 29. In the cylindrical coordinate system, the positive radial direction is from the center of the chamber toward the outer wall. If a positive velocity increases the burning rate, ℓ_r is positive and the stability limit curve is shifted toward longer τ , and vice versa. However, it can be seen that the magnitude of the radial velocity effect is much smaller than that of the tangential velocity effect for equal velocity interaction indices.

CHAPTER III

Extensions of Instability Analysis

A. Instability Analysis with Nonuniform Injection

In the preceding analysis it was assumed that the steady state flow in the combustion chamber was one dimensional. That is, the injection of the liquid propellants, their conversion to combustion products, and all fluid properties were taken to be uniformly distributed across each transverse section. The analysis of longitudinal modes of instability developed in (1) has demonstrated that the axial distribution of the combustion relative to the pressure perturbation distribution is of great importance in determining the stability behavior of the rocket motor. According to the combustion model used in that analysis, the fluctuating energy release is proportional to the amplitude of the pressure fluctuation. At a pressure node, the pressure oscillation vanishes. Therefore, if all of the combustion is concentrated at an axial station corresponding to a node for a given longitudinal mode, no oscillation in the burning rate will result and the rocket motor operation will be stable with respect to the given mode. For a combustion front located a short distance from the nodal point, the pressure perturbation amplitude is not zero, and instability is possible if the sensitivity of the combustion process to pressure variations (measured by the interaction index) is sufficiently large. As the combustion front is moved away from the node, the magnitude of the interaction index required for instability decreases, reaching a minimum value when the combustion front is located at the pressure antinode. If the combustion is not concentrated, but is spread over a certain axial distance, then the stability behavior depends on the mean sensitivity over the combustion zone.

For purely transverse modes of instability, the most important variations in the oscillating quantities occur in the lateral rather than in the

axial direction. Therefore, the transverse distribution of the combustion relative to the transverse pertubation distributions is of great significance. Of necessity, some nonuniformity in the injection distribution is present in any liquid propellant rocket motor. Although the flow in a rocket thrust chamber is highly turbulent, there is definite evidence of stratification of the combustion, which persists throughout the flow, even past the sonic throat This stratification, observed optically using both rectangular (26) and circular sector motors (9) with transparent walls, has been clearly identified with a nonuniform propellant injection distribution.

The exact treatment of unsteady, axisymmetric, two phase turbulent flow, with combustion distributed arbitrarily in three dimensions, is quite a formidable problem. The steady state solution appears to offer the greatest difficulties, since the solution for the perturbations can be based on an expansion method similar to that used in Chapter II.. Little quantitative data is presently available concerning the processes which are important in rocket motor combustion or the three dimensional distribution of combustion which exists in a typical motor. Thus it is likely that the exact solution of the general problem will be difficult to interpret in terms of actual motor designs.

Therefore, because of the problems associated with the exact solution and in view of the observed stratification of combustion, the following approximate approach is used in the present analysis. The one dimensional nature of the steady state flow is retained. The effect of the nonuniform transverse distribution of combustion appears only as a variation in the sensitivity of the combustion process to the effects of pressure and velocity. This variation is described by a distribution function $\psi(r,\theta)$. Thus the burning rate perturbation for nonuniform injection is related to that for uniform injection by

$$\dot{Q} = \dot{Q}_{\text{uniform injection}} \psi(r,\theta) \tag{3.1}$$

The distribution function is identified with the injection density $\sigma(r,\theta)$, defined by

$$\dot{m}_i = \bar{\dot{m}}_i = \int_{r=0}^{1}\int_{\theta=0}^{2\pi} \sigma(r,\theta)\, r\,dr\,d\theta \tag{3.2}$$

where $\dot{m}_i$ is the total mass injection rate. Then $\mu(r,\theta)$ can be defined as the ratio of the local injection density σ to the mean injection density σ_m, where

$$\sigma_m \int_0^1\int_0^{2\pi} r\,dr\,d\theta = \pi\,\sigma_m = \int_0^1\int_0^{2\pi} \sigma(r,\theta)\, r\,dr\,d\theta \tag{3.3}$$

That is, the burning rate distribution function is defined by

$$\mu(r,\theta) = \frac{\sigma(r,\theta)}{\sigma_m} \tag{3.4}$$

with the normalizing condition

$$\int_0^1\int_0^{2\pi} \mu(r,\theta)\, r\,dr\,d\theta = \pi = \int_0^1\int_0^{2\pi} r\,dr\,d\theta \tag{3.5}$$

For uniform injection, $\mu(r,\theta) = 1$.

It is clear that this approach involves a contradiction in that the steady state solution assumes that all fluid properties are uniform across every section whereas the perturbation solution is based on a non-uniform transverse combustion distribution. However, it was found previously that the major part of the oscillation corresponds to that of a homogeneous gas, because the Mach number in the chamber is small compared to unity. The presence of the combustion introduces a higher order correction which is primarily due to the sensitivity of the combustion process to fluctuations of pressure and velocity.

The identification of the burning rate distribution μ with the injection density σ neglects the spreading of the streams of injected propellants as they are atomized, vaporized, and undergo turbulent mixing with the hot combustion products prior to the final chemical reaction. Unfortunately, it is not possible with present knowledge to calculate the spreading of the propellant streams. However, the effect of spreading on stability can be estimated by introducing appropriate burning rate distribution functions into the analysis.

Accordingly, the steady state solution for the case of nonuniformly distributed combustion is taked to be that given by equations (2.9) through (2.12). The zeroth order perturbation solution, equation (2.41a), is also unchanged, since it does not involve the combustion at all. However, the differential equation for the first order pressure perturbation becomes

$$\Delta p_1 - s^2 p_1 = \left[k' \bar{\rho}_L + (\gamma+1) \frac{d\bar{u}}{dz} \right] + \mu(r,\theta) \left[-\gamma_s \rho \frac{d\bar{u}}{dz} p_0 + R \frac{d\bar{u}}{dz} \frac{\partial p_0}{\partial r} + J \frac{d\bar{u}}{dz} \cdot \frac{1}{r} \frac{\partial p_0}{\partial \theta} \right] \tag{3.6}$$

The boundary conditions are unchanged by the introduction of the burning rate distribution. Therefore, as before, the solution is obtained by superposition, so that

$$p_1 = p_A + p_B + p_C + p_D \tag{3.7}$$

where

$$\Delta p_A - s^2 p_A = -\gamma_s \rho \frac{d\bar{u}}{dz} P_{00} \Psi_{\nu h}(r) \Theta_\nu(\theta) \mu(r,\theta) \tag{3.8a}$$

$$\Delta p_B - s^2 p_B = R \frac{d\bar{u}}{dz} P_{00} \frac{d\Psi_{\nu h}}{dr} \Theta_\nu(\theta) \mu(r,\theta) \tag{3.8b}$$

$$\Delta \psi_C - s^2 \psi_C = J \frac{d\bar{u}}{d\bar{z}} P_{oo} \frac{1}{r} \Psi_{vh}(r) \frac{d\Theta_v}{d\theta} \mu(r,\theta) \tag{3.8c}$$

$$\Delta \psi_D - s^2 \psi_D = \left[k \bar{\rho}_L + (\gamma+1) \frac{d\bar{u}}{d\bar{z}} \right] s P_{oo} \Psi_{vh}(r) \Theta_v(\theta) \mu_s(r,\theta) \tag{3.8d}$$

Since equation (3.8a) is identical to equation (2.45d), the solution is that given by equation (2.50).

Because of the presence of the distribution function $\mu(r,\theta)$, it is necessary to apply the eigenfunction expansion method to ψ_A as well as to ψ_B and ψ_C. Thus, let

$$\psi_A = \sum_{p=0}^{\infty} \sum_{q=1}^{\infty} A_{pq} P_{Apq}(z) \Psi_{pq}(r) \Theta_p(\theta) \tag{3.9a}$$

$$\psi_B = \sum_{p=0}^{\infty} \sum_{q=1}^{\infty} B_{pq} P_{Bpq}(z) \Psi_{pq}(r) \Theta_p(\theta) \tag{3.9b}$$

$$\psi_C = \sum_{p=0}^{\infty} \sum_{q=1}^{\infty} C_{pq} P_{Cpq}(z) \Psi_{pq}(r) \Theta_p(\theta) \tag{3.9c}$$

where

$$A_{pq} = \frac{\int_0^1 \int_0^{2\pi} \mu(r,\theta) \Psi_{vh} \Psi_{pq} \Theta_v \Theta_p^* \, r\,dr\,d\theta}{\int_0^1 \int_0^{\pi} \Psi_{pq}^2 \Theta_p \Theta_p^* \, r\,dr\,d\theta} \tag{3.10a}$$

$$B_{pq} = \frac{\int_0^1 \int_0^{2\pi} \mu(r,\theta) \Psi_{vh}' \Psi_{pq} \Theta_v \Theta_p^* \, r\,dr\,d\theta}{\int_0^1 \int_0^{2\pi} \Psi_{pq}^2 \Theta_p \Theta_p^* \, r\,dr\,d\theta} \tag{3.10b}$$

$$C_{pq} = \frac{\int_0^1 \int_0^{2\pi} \mu(r,\theta) \frac{1}{r} \Psi_{\nu h} \Psi_{pq} \Theta_\nu' \Theta_p^* \, r\,dr\,d\theta}{\int_0^1 \int_0^{2\pi} \Psi_{pq}^2 \Theta_p \Theta_p^* \, r\,dr\,d\theta} \tag{3.10c}$$

The differential equation to be satisfied by the $P_{Apq}(z)$ is

$$\frac{d^2}{dz^2}\left(\frac{P_{Apq}}{P_{oo}}\right) - (S^2 + S_{pq}^2)\left(\frac{P_{Apq}}{P_{oo}}\right) = -\gamma s \mathcal{P} \frac{d\bar{u}}{dz} \tag{3.11}$$

which has the solutions

$$\frac{P_{A\nu h}}{P_{oc}} = -\gamma s \mathcal{P} \int_0^z \bar{u}(z')\,dz' + K_{A\nu h} \tag{3.12a}$$

$$\frac{P_{Apq}}{P_{oo}} = -\gamma s \mathcal{P} \int_0^z \frac{d\bar{u}}{dz}(z') \frac{\sinh\sqrt{s_{pq}^2 - s_{\nu h}^2}\,(z-z')}{\sqrt{s_{pq}^2 - s_{\nu h}^2}}\,dz' + K_{Apq}\cosh\sqrt{s_{pq}^2 - s_{\nu h}^2}\,z \tag{3.12b}$$

The solutions for P_{Bpq} and P_{Cpq} are of this same form, and are given by equations (2.55) and 2.57). Thus the pressure perturbation becomes

$$p' = \left[P_0(z) + A_{\nu h} P_{A\nu h}(z) + B_{\nu h} P_{B\nu h}(z) + C_{\nu h} P_{C\nu h}(z) + P_D(z)\right] \Psi_{\nu h}(r)\,\Theta_\nu(\theta) \tag{3.13}$$

$$+ \sum_{p,q \neq \nu,h} \sum \left[A_{pq} P_{Apq}(z) + B_{pq} P_{Bpq}(z) + C_{pq} P_{Cpq}(z)\right] \Psi_{pq}(r)\,\Theta_p(\theta)$$

Equation (3.13) is of the same form as equation (2.60a), so that the velocity perturbations are given by equations (2.60b), (2.60c), and (2.60d) in this case also.

The only modifications introduced by the nonuniformity of the injection and combustion are the introduction of the expansion coefficients A_{pq} and the redefining of B_{pq} and C_{pq} to include the distribution function $\mu(r,\theta)$. Therefore, the characteristic equation takes the form

$$A_{\nu h}\mathcal{P} + i\frac{B_{\nu h}}{\gamma\omega}\mathcal{Q} + i\frac{C_{\nu h}}{\gamma\omega}\mathcal{J} = h \tag{3.14}$$

in which the function h is unchanged from the uniform case and is given by

the expressions of equation (2.75).

The effect of the nonuniformities can be seen immediately by considering the case in which only pressure variations affect the burning rate. Then

$$n\left(1-e^{-i\omega\tau}\right) = \frac{h}{A_{\nu h}} \tag{3.15}$$

The coefficient $A_{\nu h}$ is always real, so that only the value of the interaction index is changed. Thus, for all ω,

$$\frac{n}{n_{uniform}} = \frac{1}{A_{\nu h}} \tag{3.16a}$$

and

$$\tau = \tau_{uniform} \tag{3.16b}$$

For a combustion distribution characterized by $A_{\nu h} > 1$, $n < n_{uniform}$. That is, the ordinates of stability limit curve on the n,τ-plane are contracted, increasing the area of the unstable region above the curve. Therefore, an injection distribution for which $A_{\nu h} > 1$ is more unstable than a uniform one, for corresponding mean combustion chamber conditions.

Consider first the case in which the only nonuniformity is in the radial direction, so that $\mu = \mu(r)$. This case is of the greatest interest in this investigation because in the rocket motors used for the experimental phase the injection of the propellants was concentrated at a single radius, thus providing a highly nonuniform distribution. Then

$$A_{\nu h} = \frac{\int_0^1 \mu(r) J_\nu^2(s_{\nu h} r) r\,dr}{\int_0^1 J_\nu^2(s_{\nu h} r)\, r\,dr}$$

The integral in the denominator gives

$$\int_0^1 J_\nu^2(s_{\nu h} r)\, r\,dr = \frac{1}{2}\left[J_\nu^2(s_{\nu h}) - J_{\nu-1}(s_{\nu h})\, J_{\nu+1}(s_{\nu h})\right],$$

so that the pressure coefficient $A_{\nu h}$ becomes

$$A_{\nu h} = \frac{\int_0^1 \mu(r)\, J_\nu^2(s_{\nu h} r)\, r\, dr}{\frac{1}{2}\left[J_\nu^2(s_{\nu h}) - J_{\nu-1}(s_{\nu h}) J_{\nu+1}(s_{\nu h})\right]} \tag{3.17}$$

The limiting case of concentration corresponds to a distribution function in the form of a pulse at a single radius r_i

$$\left.\begin{aligned} \mu(r) &= 0 \quad , \quad r \neq r_i \\ \mu(r) &\neq 0 \quad , \quad r = r_i \end{aligned}\right\} \tag{3.18}$$

The normalizing condition, equation (3.5), is, for $\mu = \mu(r)$,

$$\int_0^1 \mu(r)\, r\, dr = \frac{1}{2}$$

then

$$A_{\nu h} = A_{\nu h}(r_i) = \frac{J_\nu^2(s_{\nu h} r_i)}{J_\nu^2(s_{\nu h}) - J_{\nu-1}(s_{\nu h}) J_{\nu+1}(s_{\nu h})} \tag{3.19}$$

Figure 30 shows the radial variation of the pressure coefficient $A_{\nu h}(r_i)$ for the first and second tangential modes and the first radial mode. It can be seen that a rocket motor with injection concentrated on a circle the radius of which is greater than approximately six tenths of the chamber radius is more unstable in the tangential modes than a corresponding motor with uniformly distributed combustion. The most unstable configuration for these modes is that for which the injection radius equals the chamber radius. For this case, for the first tangential mode,

$$n = 0.7\, n_{uniform}$$

On the other hand, the first radial mode is absolutely stable when $r_i \cong 0.63$ (pressure node); and concentrated combustion is more unstable than uniform only for $r_i < 0.45$.

An estimate of the effect of the spreading of the propellant streams on the stability behavior can be obtained by considering a rectangular injection distribution,

$$\left.\begin{aligned} &\mu(r)=0, \quad 0\le r \le r_i-\tfrac{1}{2}\Delta r_i \\ &\mu(r)=\frac{1}{2r_i\Delta r_i}, \quad r_i-\tfrac{1}{2}\Delta r_i \le r \le r_i+\tfrac{1}{2}\Delta r_i \\ &\mu(r)=0, \quad r_i+\tfrac{1}{2}\Delta r_i \le r \le 1 \end{aligned}\right\} \qquad (3.20)$$

where $\Delta r_i=0$ corresponds to the pulse distribution. In Figure 31, the coefficient A_{11}, which corresponds to the first tangential mode, is shown as a function of the extent of the spreading, Δr_i, for three values of the mean radius r_i. For this distribution, coefficients greater than unity are reduced and those less than unity are increased as Δr_i is increased. For moderate amounts of spreading, the changes in the coefficients are not large. Therefore, since the actual burning rate distribution is not known for a rocket motor with radially concentrated injection, a good approximation to the stability limits in such a case can be obtained by using a pulse type distribution function.

A more uniform combustion distribution can be achieved by injecting at more than one radius. If the spreading of the propellant streams is neglected, the burning rate distribution function can be taken as

$$\mu(r) = \sum_{i=1}^{j} \eta_i \, \delta(r_i) \qquad (3.21)$$

where $\delta(r_i)$ is the Dirac delta function, i.e., a pulse at radius r_i, and η_i is the fraction of the total propellant flow rate which is injected at $r=r_i$. Then

$$A_{nh} = \frac{\int_0^1 \sum_{i=1}^{j} \eta_i \delta(r_i) J_n^2(s_{nh} r)\, r\,dr}{\frac{1}{2}\left[J_n^2(s_{nh}) - J_{n-1}(s_{nh}) J_{n+1}(s_{nh})\right]} = \frac{\sum_{i=1}^{j} \eta_i \int_0^1 \delta(r_i) J_n^2(s_{nh} r)\, r\,dr}{\frac{1}{2}\left[J_n^2(s_{nh}) - J_{n-1}(s_{nh}) J_{n+1}(s_{nh})\right]}$$

$$= \sum_{i=1}^{j} \eta_i \, A_{nh}(r_i) \qquad (3.22)$$

Consider an injector for which $\eta_i = \eta = \frac{i}{j}$. Then

$$A_{\nu h} = \frac{1}{j} \sum_{i=1}^{j} A_{\nu h}(r_i) \tag{3.22a}$$

In order to obtain the most uniform injection density distribution, the injection radii must be such that the areas corresponding to the r_i are all equal. It may be verified that

$$r_i = \sqrt{\frac{2i-1}{2j}}$$

For such an injector, the variations with the number of injection radii of the pressure coefficients for the first and second tangential modes and the first radical mode are given in the following table:

j = 1	A_{11} = 1.142	A_{21} = 1.110	A_{02} = 0.133
2	1.036	1.009	0.600
3	1.011	1.003	0.811

Thus, for the tangential modes, as few as three injection circles can produce a pressure sensitivity substantially equivalent to that of an absolutely uniform injection distribution. However, the first radial mode requires a larger number of circles in order to accomplish a similar result.

With regard to pressure sensitivity, nonuniformity of the injection density in the tangential direction is not significant for radial modes or for the spinning forms of tangential modes. The reasons are that there are no diametral nodal surfaces for radial modes, and in the tangential modes, the nodal surfaces rotate with respect to the injector. Thus, in the definition of $A_{\nu h}$, equation (3.10a), the product $\Theta_\nu \Theta_\nu^* = 1$ identically for radial and spinning tangential modes.

Assuming that the injection distribution is uniform radially, $\mu(r,\theta) = \mu(\theta)$. For a standing mode, $\Theta_\nu = \cos \nu\theta$, so that

$$A_{\nu h} = \frac{\int_0^{2\pi} \mu(\theta) \cos^2 \nu\theta \, d\theta}{\int_0^{2\pi} \cos^2 \nu\theta \, d\theta} = \frac{1}{\pi} \int_0^{2\pi} \mu(\theta) \cos^2 \nu\theta \, d\theta \tag{3.23}$$

The normalizing condition on $\mu(\theta)$ is

$$\int_0^{2\pi} \mu(\theta)\, d\theta = 2\pi$$

If all injection is concentrated along a single radius $\theta = \theta_i$,

$$\mu(\theta) = \delta(\theta_i) \tag{3.24}$$

Then

$$A_{\nu h}(\theta_i) = 2\cos^2 \nu\theta_i \tag{3.25}$$

In a standing tangential mode, the pressure nodal surfaces are located at $\theta = \frac{\pi}{2\nu}$ and $\frac{3\pi}{2\nu}$, and the antinodal surfaces are at $\theta = 0$ and $\frac{\pi}{\nu}$. Then according to equation (3.24), if combustion is concentrated at a node, the pressure coefficient is zero, so that the interaction index required for neutral oscillations is infinite. Thus the operation in unconditionally stable. On the other hand, if combustion is concentrated at an antinode, the coefficient $A_{\nu h}(\theta_i)$ attains its maximum value of 2. Then the interaction index at a stability limit is just half of that for a uniform combustion distribution. Positions of the combustion zone intermediate between the nodes and antinodes give $A_{\nu h}$ values between zero and two. In particular, injection at $\theta = \frac{\pi}{4\nu}, \frac{3\pi}{4\nu}, \frac{5\pi}{4\nu}$ or $\frac{7\pi}{4\nu}$ results in a pressure sensitivity equivalent to that of uniform injection. These results correspond to those obtained by the analysis of longitudinal modes for combustion concentrated at arbitrary axial stations (1).

When the propellants are injected at more than one discrete angle, the distribution function can be written as

$$\mu(\theta) = \sum_{i=1}^{j} \eta_i\, \delta(\theta_i) \tag{3.26}$$

where η_i is the fraction of the total flow rate injected at $\theta = \theta_i$ and $\delta(\theta_i)$ is the Dirac function, as before. Then

$$A_{\nu h} = 2\sum_{i=1}^{j} \eta_i \cos^2 \nu\theta_i \tag{3.27}$$

For the case in which $\eta_i = \frac{1}{j}$

$$A_{\nu h} = \frac{2}{j}\sum_{i=1}^{j} \cos^2 \nu\theta_i \tag{3.27a}$$

The experimental rocket motors used in this investigation had injection

concentrated at twelve angular positions. It can be checked that $A_{11} = A_{21} = 1$ for this case, so that the experimental motors represented well the pressure sensitivity of combustion uniformly distributed in the tangential direction.

Finally, the case of combustion concentrated both radially and tangentially will be considered. Let

$$\mu(r,\theta) = \sum_{i=1}^{k} \sum_{j=1}^{l} \eta_{ij}\, \delta(r_i)\, \delta(\theta_j) \tag{3.28}$$

This burning rate distribution represents that corresponding to kl discrete injection points (r_i, θ_j). The pressure coefficient for a standing tangential mode is then

$$A_{\nu h} = \frac{\sum_{i=1}^{k} \sum_{j=1}^{l} \eta_{ij} \int_0^1 \delta(r_i) J_\nu^2(s_{\nu h} r)\, r\, dr \int_0^{2\pi} \delta(\theta_j) \cos^2 \nu\theta\, d\theta}{\pi \left[J_\nu^2(s_{\nu h}) - J_{\nu-1}(s_{\nu h}) J_{\nu+1}(s_{\nu h}) \right]}$$

which is equivalent to

$$A_{\nu h} = \sum_{i=1}^{k} \sum_{j=1}^{l} \eta_{ij}\, A_{\nu h}(r_i)\, A_{\nu h}(\theta_i) \tag{3.29}$$

where $A_{\nu h}(r_i)$, $A_{\nu h}(\theta_i)$ are defined in equations (3.19) and (3.25). The remarks made above concerning the location, both radially and tangentially, of the injection points apply to this case also. If the injection rate is the same at each point, then $\eta_{ij} = \frac{1}{kl}$, and equation (3.29) simplifies to

$$A_{\nu h} = \left(\frac{1}{k} \sum_{i=1}^{k} A_{\nu h}(r_i) \right) \left(\frac{1}{l} \sum_{j=1}^{l} A_{\nu h}(\theta_j) \right) \tag{3.29a}$$

which is just the product of the expressions obtained previously, equations (3.22a) and (3.27a), by considering separately the effects of radial and tangential injection concentration.

In order to determine the velocity effects for nonuniform injection distributions, it is convenient to divide equation (3.14) through by $A_{\nu h}$,

after inserting the definitions

$$P = n(1 - e^{-i\omega\tau}), \quad Q = \frac{l_r}{n} P, \quad J = \frac{l_\theta}{n} P.$$

Thus,

$$\left(1 + i\frac{B_{\nu h}}{\gamma\omega A_{\nu h}} \cdot \frac{l_r}{n} + i\frac{C_{\nu h}}{\gamma\omega A_{\nu h}} \cdot \frac{l_\theta}{n}\right) n(1 - e^{-i\omega\tau}) = \frac{h}{A_{\nu h}} = h'$$

The characteristic equation is now of the same form as equation (2.78). Then, once the pressure effect of the nonuniformity has been taken into account, the velocity effects modify the stability limits as discussed for the uniform injection case. That is, if the expansion coefficient $C_{\nu h}$ is of the form $-i\tilde{C}_{\nu h}$, where $\tilde{C}_{\nu h}$ is a positive, real number, the tangential velocity will cause a contraction or expansion in the n direction of the stability limit curves on the n, τ - plane. The effect of the radial velocity, as before, will be a shifting of the curves in the τ direction. The magnitudes of these effects will depend on the values taken by $\frac{B_{\nu h}}{\gamma\omega A_{\nu h}}$ and $\frac{C_{\nu h}}{\gamma\omega A_{\nu h}}$. These coefficients will now be examined for several cases of nonuniform injection distribution.

From equations (3.10), the two velocity coefficients for a general burning rate distribution $\mu(r, \theta)$ are

$$\frac{B_{\nu h}}{\gamma\omega A_{\nu h}} = \frac{1}{\gamma_f} \frac{\int_0^1 \int_0^{2\pi} \mu(r,\theta)\, J_\nu'(s_{\nu h} r)\, J_\nu(s_{\nu h} r)\, \Theta_\nu \Theta_\nu^*\, r\, dr\, d\theta}{\int_0^1 \int_0^{2\pi} \mu(r,\theta)\, J_\nu^2(s_{\nu h} r)\, \Theta_\nu \Theta_\nu^*\, r\, dr\, d\theta} \tag{3.31}$$

$$\frac{C_{\nu h}}{\gamma\omega A_{\nu h}} = \frac{1}{\gamma_f s_{\nu h}} \frac{\int_0^1 \int_0^{2\pi} \mu(r,\theta)\, \frac{1}{r} J_\nu^2(s_{\nu h} r)\, \Theta_\nu' \Theta_\nu^*\, r\, dr\, d\theta}{\int_0^1 \int_0^{2\pi} \mu(r,\theta)\, J_\nu^2(s_{\nu h} r)\, \Theta_\nu \Theta_\nu^*\, r\, dr\, d\theta} \tag{3.32}$$

When the nonuniformity is in the radial direction only, the coefficients

become

$$\frac{B_{\nu h}}{\gamma \omega A_{\nu h}} = \frac{i}{\gamma f} \frac{\int_0^1 \mu(r)\, J_\nu'(s_{\nu h} r)\, J_\nu(s_{\nu h} r)\, r\, dr}{\int_0^1 \mu(r)\, J_\nu^2(s_{\nu h} r)\, r\, dr} \tag{3.33}$$

$$\left.\begin{aligned} \frac{C_{\nu h}}{\gamma \omega A_{\nu h}} &= -i \frac{\nu}{\gamma f s_{\nu h}} \frac{\int_0^1 \mu(r)\, \frac{1}{r} J_\nu^2(s_{\nu h} r)\, r\, dr}{\int_0^1 \mu(r)\, J_\nu^2(s_{\nu h} r)\, r\, dr} = -i \frac{\bar{C}_{\nu h}}{\gamma \omega A_{\nu h}} \\ \frac{C_{\nu h}}{\gamma \omega A_{\nu h}} &= 0 \end{aligned}\right\} \tag{3.34}$$

(spinning mode)

(standing mode)

It is clear that the convergence problems encountered previously* with the tangential velocity effect for a standing mode are present for any combustion distribution which is uniform in the tangential direction. The effects of nonuniformities can be seen by considering the case of combustion concentrated at a single radius. For $\mu(r) = \delta(r_i)$ the coefficients are

$$\frac{B_{\nu h}}{\gamma \omega A_{\nu h}} = \frac{1}{\gamma f} \frac{J_\nu'(s_{\nu h} r_i)}{J_\nu(s_{\nu h} r_i)} \tag{3.35}$$

$$\frac{\bar{C}_{\nu h}}{\gamma \omega A_{\nu h}} = \frac{\nu}{\gamma f s_{\nu h}} \cdot \frac{1}{r_i} \qquad \text{(spinning mode)} \tag{3.36}$$

The magnitudes of these velocity effect coefficients relative to those for uniform injection are shown in Figures 32 and 33.

For the tangential modes, both the radial and tangential velocity effects increase in relation to the pressure effect as the radius of injection approaches zero. However, since the pressure effect coefficient is also decreasing, and at a more rapid rate, the overall result is that of increasing

*vid. pp. 56, 57

stability as the radius of injection is decr ased. In the case of the first radial mode, similar conclusions can be drawn as the injection radius approaches the radius which corresponds to the pressure node, $r = 0.6276$.

When the nonuniformity in the burning rate distribution is entirely in the tangential direction, the velocity effect coefficients differ from the uniform injection coefficients only for the standing mode, for which

$$\frac{B_{\nu h}}{\gamma \omega A_{\nu h}} = \frac{1}{\delta f} \frac{\int_0^1 J_\nu'(s_{\nu h} r)\, J_\nu(s_{\nu h} r)\, r\, dr}{\int_0^1 J_\nu^2(s_{\nu h} r)\, r\, dr}$$

$$\frac{C_{\nu h}}{\gamma \omega A_{\nu h}} = -\frac{\nu}{\gamma f s_{\nu h}} \frac{\int_0^1 J_\nu^2(s_{\nu h} r)\, dr}{\int_0^1 J_\nu^2(s_{\nu h} r)\, r\, dr} \cdot \frac{\int_0^{2\pi} \mu(\theta) \sin \nu\theta \cos \nu\theta\, d\theta}{\int_0^{2\pi} \mu(\theta) \cos^2 \nu\theta\, d\theta}$$

Comparison of these equations with equations (2.56) and (2.58b) yields

$$\frac{B_{\nu h}}{\gamma \omega A_{\nu h}} = \left(\frac{B_{\nu h}}{\gamma \omega A_{\nu h}} \right)_{\text{uniform}} \tag{3.37}$$

$$\frac{C_{\nu h}}{\gamma \omega A_{\nu h}} = -\left(\frac{\tilde{C}_{\nu h}}{\gamma \omega A_{\nu h}} \right)_{\text{uniform}} \cdot \frac{\int_0^{2\pi} \mu(\theta) \sin \nu\theta \cos \nu\theta\, d\theta}{\int_0^{2\pi} \mu(\theta) \cos^2 \nu\theta\, d\theta} \tag{3.38}$$

Thus, the radial velocity effect is insensitive to nonuniformities in the tangential direction, as would be expected. In addition, for certain distributions, tangential velocity effects will be present for the standing mode, whereas there are no such effects for the uniform injection case. If $\mu(\theta)$ is properly continuous and vanishes at $\theta = 0, \pi$, then the convergence problems encountered previously will no longer be present because the function which must be expanded in the eigenfunction series, $\frac{1}{r} J_\nu(s_{\nu h} r)\, \mu(\theta) \sin \nu\theta$, does satisfy the same boundary conditions as the eigenfunctions themselves.

For certain functions $\mu(\theta)$ the coefficient vanishes. In order to determine the nature of such distribution functions, the integral in the

nume ator of equation (3.38) is written as the sum of integrals over subintervals of length $\frac{\pi}{2\nu}$,

$$\int_0^{2\pi} \mu(\theta) \sin\nu\theta \cos\nu\theta\, d\theta = \int_0^{\frac{\pi}{2\nu}} \cdots d\theta + \int_{\frac{\pi}{2\nu}}^{\frac{\pi}{\nu}} \cdots d\theta + \cdots + \int_{2\pi-\frac{\pi}{\nu}}^{2\pi-\frac{\pi}{2\nu}} \cdots d\theta + \int_{2\pi-\frac{\pi}{2\nu}}^{2\pi} \cdots d\theta \qquad (3.39)$$

Since

$$\sin\nu\theta = \sin\nu\left(\tfrac{\pi}{\nu}-\theta\right)$$

$$\cos\nu\theta = -\cos\nu\left(\tfrac{\pi}{\nu}-\theta\right),$$

the second integral on the right side of equation (3.39) becomes

$$\int_{\frac{\pi}{2\nu}}^{\frac{\pi}{\nu}} \mu(\theta) \sin\nu\theta \cos\nu\theta\, d\theta = -\int_0^{\frac{\pi}{2\nu}} \mu\left(\tfrac{\pi}{\nu}-\theta\right) \sin\nu\left(\tfrac{\pi}{\nu}-\theta\right) \cos\nu\left(\tfrac{\pi}{\nu}-\theta\right) d\left(\tfrac{\pi}{\nu}-\theta\right)$$

Thus, if $\mu(\theta) = \mu(\frac{\pi}{\nu}-\theta)$, the first two terms on the right cancel. Moreover, if $\mu(\theta)$ is periodic, with period $\frac{\pi}{\nu}$, all pairs of terms in equation (3.39) cancel. Therefore, in order that the tangential velocity effect vanish for a standing tangential mode, the burning rate distribution must satisfy the conditions

$$\left.\begin{aligned} \mu(\theta) &= \mu\left(\theta+\tfrac{\pi}{\nu}\right) \\ \mu(\theta) &= \mu\left(\tfrac{\pi}{\nu}-\theta\right) \end{aligned}\right\} \qquad (3.40)$$

It is clear that the uniform distribution, $\mu = 1$, is such a function.

For functions $\mu(\theta)$ which do not satisfy the conditions (3.40), the tangential velocity coefficient for the standing mode is real, rather than imaginary as for the spinning mode. Thus, for such injectors the tangential velocity causes a shift of the stability limits in the τ direction for the standing mode, but in the n direction for a spinning mode. If the combustion is concentrated along a single radius, $\mu(\theta) = \delta(\theta_i)$, and

$$\frac{C_{vh}}{\gamma\omega A_{vh}} = -\left(\frac{\tilde{C}_{vh}}{\gamma\omega A_{vh}}\right)_{uniform} \cdot \tan\nu\theta_i \qquad \text{(standing mode)} \qquad (3.41)$$

Although $\tan\nu\theta_i \to \infty$ for $\theta_i = \frac{\pi}{2\nu}\,(1+2K)$, $K = 0, 1, \ldots$, the characteristic equation,

$$\left(A_{yh} + i\,\frac{C_{yh}}{\gamma\omega}\cdot\frac{\ell_g}{\kappa} \right) n\left(1 - e^{-i\omega\tau}\right) = h$$

with $A_{yh} \sim \cos^2\nu\theta_i$, $C_{yh} \sim \sin\nu\theta_i \cos\nu\theta_i$, shows that $n \to \infty$ for injection at this angle. If several injection angles are used, so that $\mu(\theta) = \sum_{i=1}^{k} \eta_i\,\delta(\theta_i)$

$$\frac{C_{yh}}{\gamma\omega A_{yh}} = -\left(\frac{\tilde{C}_{yh}}{\gamma\omega A_{yh}}\right)_{uniform} \frac{\sum_{i=1}^{k} \eta_i \sin\nu\theta_i \cos\nu\theta_i}{\sum_{i=1}^{k} \eta_i \cos^2\nu\theta_i} \qquad (3.42)$$

which can vanish if $\mu(\theta)$ satisfies the periodicity and symmetry conditions of equation (3.40). The tangential velocity effect coefficient for injection at a series of discrete points (η_j, θ_j) can be obtained, in the same manner as used for the pressure coefficient A_{yh}, by combining equations (3.36) and (3.42).

B. Application of the theory to a Variable Angle Sector Motor

In the experimental verification of the theory of longitudinal mode combustion instability, stability limits were determined on the mixture ratio, chamber length plane (16). From such limits, it was possible to derive values of the interaction index and sensitive time lag as functions of the mixture ratio. This experimental technique was made possible by the fact that as long as the length was kept greater than that necessary for substantially complete combustion, changes of length had no effect on the combustion zone, i.e., on n and τ, the parameters characterizing the combustion process. Since the chamber resonance properties were changed with a change in length, it was possible to survey the entire range of stability behavior, from stable operation through several harmonics of oscillatory operation.

A similar approach to the study of purely transverse modes of combustion instability is much more difficult. The reason is that the charac-

teristic length for transverse modes is the chamber radius. Simply changing the radius of the combustion chamber will result also in changes in the recirculation pattern and in the nozzle contraction ratio. If the latter is kept constant, the pressure level will fall, unless the injector hole size is increased or more holes are added to the injector. Maintaining the length to diameter ratio of the combustion chamber carries with it the danger of entering regions of longitudinal mode instability. Although some of these variables, such as the contraction ratio and chamber length, can be accounted for theoretically, the dependence of the combustion parameters on the others is not known at the present time.

For tangential modes, which are by far the most commonly observed, the possibility exists of measuring stability limits by using a variable angle sector motor. Such a motor is shown in Figure 34. Changes in the angle can be made by means of sector shaped inserts which fit the internal contours of the combustion chamber from the injector face to beyond the throat of the nozzle. It is not necessary to extend the inserts very far into the supersonic portion of the nozzle. For such a motor, the characteristic length can be taken to be $r_c \alpha$.

The use of a sector motor is not without difficulties. In the study of longitudinal modes, the chamber length can be varied continuously, i.e., in arbitrarily small increments, so that quite precise measurements of the stability limits can be made, at least in principle. However, it is not physically possible to construct an injector which is absolutely uniform in the tangential direction. Therefore, the sector angle can never be continuously variable. Even accepting such a limitation, which may be of greater or lesser importance in any particular investigation, further restrictions are imposed on an injector to be used for angular stability limit tests.

First, the injection distribution must be periodic in the tangential direction. The smallest increment by which the sector angle can be changed is then equal to the period of the injection pattern. It is reasonable to expect the recirculation pattern to have the same period. However, the further requirement is imposed that the symmetry (or periodicity) of the recirculation be maintained relative to meridianal planes. That is, there must be no swirl, or angular distortion, of the recirculation pattern. Hence, it is required that the net momentum of the injector sprays be directed axially. If this condition is not satisfied, urburned propellants may impinge on the faces of the inserts. The liquid layers thus formed may alter the combustion process to a sufficient degree that the tests become worthless. Wall effects become increasingly significant as the sector angle is decreased. Below a certain angle, the equivalence between the sector and the full chamber motors may no longer be valid. However, it must be said that sector motors of fairly small angle (27^{o}) have been operated with steady state performance very close to that of the corresponding full circular motor (9).

In a sector motor, the boundary conditions in the tangential direction are

$$\left.\begin{aligned} w'(\theta = 0) &= 0 \\ w'(\theta = \alpha) &= 0 \end{aligned}\right\} \qquad (3.-2)$$

Since the proper solution of equation (2.37c) for the standing mode is

$$\textcircled{w}_{\nu} = \cos \nu\theta ,$$

the fundamental component of the tangential velocity perturbation is

$$\omega'_{\nu h} = V_{\nu h}(z)\, \frac{dJ_{\nu}}{dr}(s_{\nu h} r)\, \sin \nu\theta$$

Then the solid wall condition requires that

$$\sin \nu\alpha = 0$$

which implies that

$$\nu = \frac{m\pi}{\alpha} \quad , \qquad m = 1, 2, 3, \cdots \tag{3.44}$$

where $m = 1$ corresponds to the first tangential mode, $m = 2$ to the second, etc. The oscillation pattern in a sector motor of angle $\alpha = \pi$ is thus the same as that of the standing mode in a full chamber. The Bessel functions of the first kind, J_ν, are continuous in the order ν. Therefore, the zeros $s_{\nu h}$ of the derivatives of the Bessel functions are continuous in ν, as shown in Figure 35. Thus for a given tangential mode, with each sector angle α is associated a value of the acoustic oscillation frequency. From Figure 35 and equation (3.44) it can be seen that $s_{\nu h}$ increases for decreasing angle. Both the nozzle admittance and the eigenfunction expansion coefficients are functions of $s_{\nu h}$. The effects of the sector angle on $A_{\nu l}$, $B_{\nu l}$, and $C_{\nu l}$ for radially concentrated combustion are shown in Figures 36, 37, and 38.

The center of the combustion chamber, $r = 0$, is a stagnation point for the transverse velocity components for angles less than π. However, for $\alpha > \pi$, $\nu < 1$ for the first tangential mode, so that $r = 0$ is a point of infinite velocity (for inviscid flow). In the flow of a real fluid around such a corner a vortex pattern is established. For oscillatory flow, vortices will be alternately created and destroyed cyclicly on both sides of the corner. Such a phenomenon constitutes a disturbance to the oscillation pattern; it may have an important, but incalculable effect in the stability behavior.

In considering the influence of the transverse velocities and of the injection distribution nonuniformities in a sector motor, it is convenient to make the change of variable

$$\theta' = \frac{\pi\theta}{\alpha} \tag{3.45}$$

so that θ' ranges between 0 and π for θ between 0 and α. Then the tangential eigenfunctions are

$$\Theta_p = \cos p\theta' \tag{3.46}$$

With this modification, all of the expressions derived previously for the standing mode apply to the sector motor.

The effect of the sector angle on the stability limits for the first tangential mode with no velocity effects is demonstrated by Figures 39, 40, and 41. These curves were calculated for the axially concentrated steady state combustion distribution which was discussed in Chapter II. Figure 39 shows the limits for sector angles of 60°, 90°, and 180° for a uniform transverse combustion distribution. The slight differences in the minimum interaction index values are caused by the changes in the acoustic frequency s_{vh} through the nozzle admittance coefficients. The solution for $\omega\tau$ is affected to only a slight extent by the value of s_{vh}. Therefore, τ is approximately proportional to $\frac{1}{s_{vh}}$. As the sector angle is decreased, the region of instability on the n, τ - plane for any particular mode moves toward smaller τ. For a given value of n, the range of unstable time lag values also decreases with decreasing angle.

The effect of concentrated combustion on the stability limits is shown in Figure 40 for $r_i = 8/9$ and in Figure 41 for $r_i = 5/9$. These injection radii correspond to those used in the experimental 9 inch diameter rocket motor. For injection on the larger circle, the unstable zones extend to lower n as the sector angle decreases. On the other hand, for the smaller injection radius, the sector motor becomes more stable as the angle is decreased. Although there is no radius for which the minimum interaction index is independent of the sector angle, from Figure 36 it can be seen that the smallest variation of n_M with α occurs for $r_i \cong 0.76$.

From Figures 39, 40, and 41, it is apparent that any point (n, τ) which is within an unstable region lies on the intersection of the stability limit curves for two sector angles. Therefore, there is a range of angles for which the rocket motor represented by that n, τ pair is unstable (in the mode considered). Thus, the possibility exists for determining values of the interaction index (for pressure) and the sensitive time lag by measuring angular stability limits. Since the velocity indices ℓ_r and ℓ_θ are not presently calculable, these stability limit tests must be carried out using velocity insensitive injectors, such as a tangentially oriented spud injector (see Figure 7) with a sufficiently large number of spuds. If the pressure index and time lag are known, then it appears possible to determine the radial velocity index ℓ_r by noting the difference between the predicted and actual angular stability limits using the radial spud orientation. Then, if $\ell_r = \ell \sin\beta_i$ and $\ell_\theta = \ell \cos\beta_i$, where β_i is the spud orientation angle, as postulated in Chapter II, the tangential velocity index, which is important in the instability of the full circular motor, is determined at the same time.

C. Generalized Time Lag Formulation

In the previous chapter, an expression for the burning rate perturbation was derived, following (i), on the basis of the following time lag schematization. The actual, gradual evolution of combustion products from the liquid propellants was approximated by an instantaneous conversion, after a certain time interval from injection, called the total time lag (τ_T). It was assumed that the combustion process was not sensitive to fluctuating conditions in the combustion chamber during the first part of the total time lag, called the insensitive time lag (τ_i). During the latter part, the sensitive time lag (τ), the rates of the processes occuring during combustion were assumed to depend on the pressure and on the transverse components of the gas velocity. The degree of sensitivity of the combustion process to the

chamber conditions was represented by the pres ure interaction index n and the velocity indices ℓ_r and ℓ_θ . Thus, considering combustion to occur at time t , the interaction indices were assumed to be zero from $t-\tau_T$ to $t-\tau$, and to have constant values from $t-\tau$ to t . Stability criteria were derived on the basis of this time lag scheme. The effect of alternative time lag formulations on the characteristic equation for neutral oscillations will be considered in this section.

The step function combustion model defining the total time lag will be retained in the following analysis. However, the simple division of τ_T into a sensitive and insensitive part will be replaced by the more general scheme shown in Figure 42 (b). According to this model, the combustion process is sensitive to velocity effects only during the time interval τ_1 to τ_3 and to pressure effects only between τ_2 and τ_4. Therefore $\tau_v=\tau_3-\tau_1$ is the velocity sensitive time lag and $\tau_p=\tau_4-\tau_2$ is the pressure sensitive time lag. A straightforward calculation, following the procedure used in Chapter II., yields an expression for the burning rate perturbation.

The overall rate of the processes involved in the combustion of the liquid bipropellants is specified as follows:

$$\left.\begin{aligned}
&f=\bar{f}, \quad t-\tau_T \le t' \le t-\tau_T+\tau_1 \\
&f=\bar{f}(1+\ell v' e^{st'}), \quad t-\tau_T+\tau_1 \le t' \le t-\tau_T+\tau_2 \\
&f=\bar{f}(1+\ell v' e^{st'}+n p' e^{st'}), \quad t-\tau_T+\tau_2 \le t' \le t-\tau_T+\tau_3 \\
&f=\bar{f}(1+n p' e^{st'}), \quad t-\tau_T+\tau_3 \le t' \le t-\tau_T+\tau_4 \\
&f=\bar{f}, \quad t-\tau_T+\tau_4 \le t' \le t
\end{aligned}\right\} \qquad (3.47)$$

where the index ℓ and the perturbation v' refer either to the radial or to the tangential velocity, or to both. The total time lag is defined by the

following equation

$$\int_{t-\tau_T}^{t} f(t')\,dt' = \bar{E}_a = \int_{t-\bar{\tau}_T}^{t} \bar{f}(t')\,dt' \tag{2.17}$$

which expresses the condition that the transformation from reactants to products takes place when the processes occurring during the time lag have accumulated to a certain level.

Introducing the expressions (3.47) into equation (2.17) gives

$$\int_{t-\tau_T}^{t-\tau_T+\tau_1} \bar{f}\,dt' + \int_{t-\tau_T+\tau_1}^{t-\tau_T+\tau_2} \bar{f}(1+\ell v' e^{st'})\,dt' + \int_{t-\tau_T+\tau_2}^{t-\tau_T+\tau_3} \bar{f}(1+\ell v' e^{st'}+n p' e^{st'})\,dt'$$

$$+ \int_{t-\tau_T+\tau_3}^{t-\tau_T+\tau_4} \bar{f}(1+n p' e^{st'})\,dt' + \int_{t-\tau_T+\tau_4}^{t} \bar{f}\,dt' = \bar{E}_a = \int_{t-\bar{\tau}_T}^{t} \bar{f}\,dt' \tag{3.48}$$

Upon rearrangement equation (3.48) becomes

$$\int_{t-\tau_T}^{t} \bar{f}\,dt' + \int_{t-\tau_T+\tau_1}^{t-\tau_T+\tau_3} \bar{f}\ell v' e^{st'}dt' + \int_{t-\tau_T+\tau_2}^{t-\tau_T+\tau_4} \bar{f} n p' e^{st'}dt' = \int_{t-\bar{\tau}_T}^{t} \bar{f}\,dt'$$

or

$$\int_{t-\tau_T}^{t-\bar{\tau}_T} \bar{f}\,dt' = -\ell \int_{t-\tau_T+\tau_1}^{t-\tau_T+\tau_3} \bar{f} v' e^{st'}dt' - n \int_{t-\tau_T+\tau_2}^{t-\tau_T+\tau_4} \bar{f} p' e^{st'}dt' \tag{3.49}$$

Assuming the spatial nonuniformity of $\bar{f}$ to be negligible, the integral on the left side can be written as

$$\bar{f}(\tau_T - \bar{\tau}_T)$$

so that

$$\tau_T - \bar{\tau}_T = -\ell \int_{t-\bar{\tau}_T+\bar{\tau}_1}^{t-\bar{\tau}_T+\bar{\tau}_3} v' e^{st'}dt' - n \int_{t-\bar{\tau}_T+\bar{\tau}_2}^{t-\bar{\tau}_T+\bar{\tau}_4} p' e^{st'}dt' \tag{3.50}$$

neglecting higher order terms.

The burning rate perturbation was found in Chapter II to be related to the time rate of change of the time lag by the expression

$$Q' e^{st} = -\frac{d\bar{u}}{dz}\frac{d\tau_T}{dt} \tag{2.16}$$

Differentiation of equation (3.50) with respect to time and making use of the definitions of τ_v and τ_p gives

$$\frac{d\tau_T}{dt} = -l v' e^{s(t-\bar{\tau}_T+\bar{\tau}_1)}\left(e^{s\bar{\tau}_v}-1\right) \tag{3.51}$$

$$-n p' e^{s(t-\bar{\tau}_T+\bar{\tau}_2)}\left(e^{s\bar{\tau}_p}-1\right) \quad + \text{higher order terms}$$

Then, since the burning rate perturbation is of the form

$$Q' = \frac{d\bar{u}}{dz}\mathcal{P} p' + \frac{d\bar{u}}{dz}\mathcal{R} v' + \frac{d\bar{u}}{dz}\mathcal{J} w' \tag{3.52}$$

The proportionality factors are, from equation (3.51),

$$\left.\begin{aligned}\mathcal{P} &= n e^{-s(\bar{\tau}_T-\bar{\tau}_2)}\left(e^{s\bar{\tau}_p}-1\right)\\ \mathcal{R} &= l_r e^{-s(\bar{\tau}_T-\bar{\tau}_1)}\left(e^{s\bar{\tau}_v}-1\right)\\ \mathcal{J} &= l_\theta e^{-s(\bar{\tau}_T-\bar{\tau}_1)}\left(e^{s\bar{\tau}_v}-1\right)\end{aligned}\right\} \tag{3.53}$$

These expressions are to be compared with those of equation (2.32).

From equation (3.53) it can be seen that the more general formulation of the combustion process requires the use of eight parameters: the total time lag $\bar{\tau}_T$; the pressure interaction index n and time lags $\bar{\tau}_p$, $\bar{\tau}_2$; the velocity indices l_r , l_θ and time lags $\bar{\tau}_v$, $\bar{\tau}_1$. If a relation exists between l_r and l_θ , as in the case of the unlike impinging doublet spud injector considered in Chapter II , then the number of parameters required is reduced to seven.

The characteristic equation

$$A_{vh}\mathcal{P} + i\frac{B_{vh}}{\gamma\omega}\mathcal{R} + i\frac{C_{vh}}{\gamma\omega}\mathcal{J} = h \tag{3.54}$$

is a complex relation between the combustion parameters which must exist if neutral oscillations of frequency are to occur. A solution can be obtained, as discussed previously, only if all but two of the parameters are known. At the present time, it is not possible to calculate any of the sensitive or insensitive time lags or interaction indices. However, the pressure sensitivity theory has been applied successfully to the analysis of longitudinal modes of instability. According to this formulation,

$$\bar{\tau}_2 = \bar{\tau}_T - \bar{\tau}_p$$

so that

$$\mathcal{P} = n\,(1 - e^{-s\bar{\tau}_p}) \tag{3.55}$$

on the basis of this longitudinal mode theory, a method has been developed for measuring n and $\bar{\tau}_p$ experimentally.

The time lag model used in previous sections of this dissertation constitutes the simplest extension of the pressure sensitivity theory to include velocity effects. Thus, the velocity time lags were assumed to be identical to the pressure time lag. In the preliminary experimental studies, it was observed that the velocity effects were more important in the early combustion region than in the zone of greatest combustion intensity. Therefore, a better approximation to the actual combustion process than the simple, common-time-lag model may be obtained by setting $\bar{\tau}_1 = 0$, so that

$$\left.\begin{aligned} \mathcal{R} &= \ell_r e^{-s\bar{\tau}_T}\,(e^{s\bar{\tau}_v} - 1) \\ \mathcal{J} &= \ell_\theta e^{-s\bar{\tau}_T}\,(e^{s\bar{\tau}_v} - 1) \end{aligned}\right\} \tag{3.56}$$

while retaining equation (3.55) to describe the pressure effect.

It is seen that the total time lag is involved in the separate time lag formulation. The total time lag for a propellant element is defined as

$$\bar{\tau}_T = \bar{\tau}_T(\bar{z}) = \int_0^{\bar{z}} \frac{d\bar{z}'}{\bar{u}_2(\bar{z}')} \tag{3.57}$$

where z is the station at which the element undergoes conversion to combustion products. If combustion is concentrated at a single axial station z_m and all elements have the same velocity, equation (3.56) becomes

$$\bar{\tau}_T = \int_0^{z_m} \frac{dz'}{\bar{u}_L(z')} = \frac{z_m}{\bar{u}_{Lm}}$$

where $\bar{u}_{Lm}$ is a mean liquid velocity. For this case the functions $\mathcal{R}$ and $\mathcal{J}$ are independent of z. If the combustion is distributed axially, then $\mathcal{R}=\mathcal{R}(z)$ and $\mathcal{J}=\mathcal{J}(z)$, so that the form of the characteristic equation is somewhat modified. Equation (2.53b), for $p=\nu$, $q=h$, becomes

$$\frac{d^2}{dz^2}\left(\frac{P_{B\nu h}}{P_{oo}}\right) = \tilde{\mathcal{R}}\, e^{-s\bar{\tau}_T(z)} \frac{d\bar{u}}{dz} \tag{3.58}$$

where $\tilde{\mathcal{R}} = \ell_r(e^{s\bar{\tau}_\nu} - 1)$. Then

$$\frac{d}{dz}\left(\frac{P_{B\nu h}}{P_{oo}}\right) = \tilde{\mathcal{R}} \int_0^z e^{-s\bar{\tau}_T(z')} \frac{du}{dz'} dz' \tag{3.59a}$$

and

$$\frac{P_{B\nu h}}{P_{oo}} = \tilde{\mathcal{R}} \int_0^z dz' \int_0^z e^{-s\bar{\tau}_T(z'')} \frac{d\bar{u}}{dz''} dz'' + K_{B\nu h} \tag{3.59b}$$

Similar results are obtained for $P_{C\nu h}$. If a function $\tilde{h}_1$, is defined as

$$\tilde{h}_1 = \gamma \int_0^{z_e} e^{-s\bar{\tau}_T(z)} \frac{d\bar{u}}{dz} dz - i\gamma s_{\nu h} \mathcal{E} \int_0^{z_e} dz \int_0^z e^{-s\bar{\tau}_T(z')} \frac{d\bar{u}}{dz} dz' \tag{3.60}$$

then the characteristic equation for the case of distributed combustion takes the form

$$A_{\nu h}\,\mathcal{P} + i\left(\frac{B_{\nu h}}{\gamma\omega}\right)\left(\frac{\tilde{h}_1}{h_1}\right)\tilde{\mathcal{R}} + i\left(\frac{C_{\nu h}}{\gamma\omega}\right)\left(\frac{\tilde{h}_1}{h_1}\right)\tilde{\mathcal{J}} = h \tag{3.61}$$

and solutions are obtained in the same manner as for the concentrated case.

An important application of either equation (3.54) or (3.61) is the determination of the velocity effect parameters once the pressure interaction index n and time lag $\bar{\tau}_p$ are known. It is clear that a value of one of the velocity indices ℓ_r, ℓ_θ, or a relation between the two, must be known in order to find solutions of the characteristic equation. Since both the radial and the tangential velocity effects are of the same form, it is necessary to discuss the solution for only one of them. Thus, let $\ell_\theta = 0$ in the following. For simplicity, the solution of equation (3.54) will be considered.

For this case, the characteristic equation can be written in the form

$$\ell_r \left(1 - e^{i\omega\bar{\tau}_v}\right) = g(\omega) \tag{3.62}$$

where

$$g = g_r + i g_i = \frac{i\gamma\omega\, e^{i\omega\bar{\tau}_T}}{B_{\gamma h}} \left[h(\omega) - A_{\gamma h}\, n \left(1 - e^{-i\omega\bar{\tau}_p}\right) \right]$$

Since equation (3.62) is complex, it is equivalent to the two real equations

$$\begin{aligned} \ell_r - \ell_r \cos\ \omega\bar{\tau}_v &= g_r \\ -\ell_r \sin\ \omega\bar{\tau}_v &= g_i \end{aligned} \tag{3.63}$$

The solution of this simultaneous pair is

$$\begin{aligned} \ell_r(\omega) &= \frac{g_r^2 + g_i^2}{2 g_r} \\ \bar{\tau}_v(\omega) &= \frac{1}{\omega} \sin^{-1}\left(\frac{g_i}{\ell_r}\right) = \frac{1}{\omega} \cos^{-1}\left(1 - \frac{g_r}{\ell_r}\right) \end{aligned} \tag{3.64}$$

The most important difference between the "common" and "separate" time lag formulations is the presence of the total time lag as a parameter in the latter model. Since $\bar{u}_L$ is $O(\bar{u}_e)$ and z_m is $O(1)$, the total time lag $\bar{\tau}_T$ is $O\left(\frac{1}{\bar{u}_e}\right)$. Thus, small variations in the frequency ω, which in the method of solution is regarded as the independent variable, cause large changes in the function $g(\omega)$ Therefore, it is important that the combustion

distribution $\bar{\alpha}$ (z) and the liquid velocity $\bar{u}_L(z)$ be accurately known if a valid solution for the combustion parameters is to be obtained from the separate time lag formulation. It can be concluded, then, that further study of the details of the combustion process is needed in order to refine the time lag model properly.

CHAPTER IV

Experimental Results and Conclusions

A. General Considerations

The stability limit relations for transverse modes of instability in the two preceding chapters were based on the concept of a sensitive combustion time lag. The validity of this model as applied to longitudinal modes has been demonstrated experimentally. However, the extension to transverse modes involved more than just a geometric change in the number of dimensions. It was necessary also to include in the combustion model a sensitivity to velocity as well as pressure oscillations, to treat nonuniform injection distributions, and to develop a method of measuring stability limits at which the linearized theory could be applied. None of the effects considered had been studied systematically by any previous worker. Therefore, the final phase of the present investigation consisted of a series of experiments designed to test the theoretical predictions.

The experimental apparatus used in these tests was the same as that used in the exploratory tests described in Chapter I. All tests were made at a mean chamber pressure of 150 psia and at a thrust level of 1000 pounds based on operation of the full circular chamber. The injector spuds were designed to give equal propellant velocities and axially directed spray fans at a mixture ratio of 1.4. Most of the effort was devoted to the measurement of angular stability limits, using the variable angle sector motor. A limited number of full motor tests were made in order to observe the wave patterns of the spinning forms of tangential modes. In some of these tests, destructible barriers were used to determine the role of starting transients in the stability problem. The number of full motor tests was necessarily restricted by the extremely destructive nature of the spinning tangential modes. Tests

were also conducted with a variable length motor in order to use the well-developed longitudinal mode stability limit method to measure the pressure interaction index and sensitive time lag. Correspondence between the longitudinal and transverse motors was achieved by making the cross section of the variable length motor in the shape of a 30° sector, as shown in Figure 43. In this way the nature of the recirculation pattern is maintained the same in the longitudinal tests as in the transverse, provided that the injector satisfies the conditions required by the sector motor concept, which were discussed in Chapter III.

In the experimental program the propellant combination and injector type were held constant. The combination of liquid oxygen and ethyl alcohol was chosen on the basis of the large amount of experience gained in the use of this combination in the previous investigation of longitudinal modes of instability. The unlike impinging doublet injector was selected because of the nature of its symmetry. The spray formed by this type of injector can be expected to be sensitive to mixing effects of the velocity component parallel to the line of centers of the unlike propellant orifices but not of the component normal to the line of centers. The use of the spud injector, with the spud orientation variable, facilitated the separate study of the effects of the radial and tangential velocity components. However, the spray angle with respect to the combustion chamber axis is a function of the mixture ratio. Only at the design mixture ratio is the net spray momentum of the tangential spud orientation directed axially. Thus, a swirl component is introduced into the recirculation pattern for off-design operation, and serious trouble may be encountered from wall effects, especially for small sector angles. Therefore, this type of injector is not suitable for sector tests over a wide range of mixture ratios, so that the results of the stability limit tests can be regarded as valid only near the design point.

The determination of the variable angle stability limits was effected by means of a large number of rocket test runs. Individual tests were quite simple. The motor was operated at preselected values of the mixture ratio and chamber pressure, which were monitored by steady state gages and flowmeters. The primary measurement was the oscillatory component of the chamber pressure. Both amplitude and frequency data were recorded. The determination of the mode of instability was made on the basis of the frequency of the oscillations. It has been observed by many investigators that the frequency of purely transverse modes is always within ten percent of the frequency of the acoustic modes in a closed cylinder. This result is obtained even in the case of very large amplitude oscillations.

The exact amplitude level of the oscillation in an unstable motor is of little significance to a linear theory. However, the variation of the amplitude as a stability limit is approached can be an indication of the location of the limit. This fact is of particular importance in view of the rather large sector angle increment required by the experimental apparatus. Figure 44 shows the typical variation of the oscillation amplitude with sector angle for a constant value of mixture ratio. The transition from the first to the second tangential modes was generally quite sharp. In the case shown in Figure 44, a very small mixture ratio shift at an angle of 180° caused a change in the mode with little variation of amplitude. However, the limits between stable operation and the first tangential mode of instability were less clearly defined. Many cases of organized oscillations alternating irregularly with random combustion noise were observed. At the small angles associated with these limits, the combustion noise level was quite high, often exceeding 10 psi (rms).

In most of the stability limit tests a single pressure transducer was used. The amplitude of a standing mode oscillation varies approximately

as $\cos \frac{m\pi}{\alpha}\theta$, where $\theta=0$ and $\theta=\alpha$ correspond to the flat walls formed by the sector inserts. For large scale oscillations, the wave shape departs from the sinusoidal, so that the amplitude does not vanish at the nodes ($\theta=\frac{\alpha}{2m}$), as shown in Figure 45. In order to obtain the maximum amplitude, the pressure transducer was placed as near as practicable to one of the flat walls. For full motor tests, and in some sector tests, two or three pressure pickups were inserted at 90° intervals around the chamber circumference. In this manner it was possible to detect whether a particular oscillation was of the spinning or standing type. By means of observations of the relative phases of the pressure traces the direction of travel of a spinning wave, which was of great significance in the velocity effect studies, could be determined.

The experiments were organized into three series. First, sector motor stability limit tests using the tangential orientation of the injector spuds were made in order to verify theoretical predictions concerning the effects of chamber diameter and injection diameter in the absence of velocity effects. The bases for this series were the theoretical demonstration of the absence of tangential velocity effects in standing modes and the nature of the symmetry of the unlike doublet type of injector. The second series of experiments utilized full circular chambers in order to study the tangential velocity effects. In particular, these tests sought to determine the positive velocity direction with respect to the injector doublet. Using the information obtained from the second series, the sign of the radial velocity index could be determined. The third series of experiments was then devoted to measuring the angular stability limits using the radial spud orientation. These tests were designed to ascertain the validity of the theoretical prediction that the radial velocity causes a shift of the angular stability limits in a direction which depends on the sign of the velocity index. The results of the experimental program will be discussed in connection with the corresponding

theoretical calculations in the following sections.

B. Sector Motor Tests with Tangential Spud Orientation

The angular stability limits shown in Figure 46 are typical of the results obtained from the sector motor tests. A point representing each test has been plotted on the mixture ratio, sector angle plane with a symbol which describes the nature of the operation, e. g. , stable, first tangential mode, etc. At small angles, the rocket motors operate stably. As the angle is increased, a region of first tangential mode stability is found. The second tangential mode is observed at angles greater than 180°. No other modes have been observed in these tests. Although the transition from the first to the second mode is sharp in general, there is some difficulty in obtaining reproducibility. Possibly this effect is a result of overlapping of the unstable regions for the two modes (see Figure 21). At the lower limit of the first tangential mode the 30° increment in sector angle restricts the accuracy obtainable in the definition of the stability limit.

The variation of the propellant spray angle with mixture ratio results in the possibility of effects caused by distortion of the recirculation pattern and liquid impingement on the walls. Therefore one is advised to draw conclusions only from the tests made in the vicinity of the design mixture ratio. However, it has been found that by surveying a rather wide mixture ratio range, it is possible to compensate somewhat for the coarseness of the sector angle variation. As an example, in Figure 46 it is apparent that the limit between the first and second modes at a mixture ratio of 1.4 lies close to 180°. If testing had been confined only to that one mixture ratio, the limit could only have been described as being somewhere between 180° and 210°. For the most part, however, the variation of the stability limits with mixture ratio is very small, unlike the results obtained for longitudinal mode stability limits (16).

The tests shown in Figure 46 correspond to a rocket motor with a 9 inch combustion chamber diameter, for which the chamber exit Mach number was approximately 0.05. The propellants were injected near the outer periphery, on an 8 inch diameter circle. The theoretical angular stability limits corresponding to this configuration are shown in Figure 47. Because of the theoretical result that tangential velocity effects are absent in standing modes, and the fact that radial velocity effects on the spray produced by a tangentially oriented doublet can be expected to be quite small, the limit curves of Figure 47 were calculated assuming only pressure sensitivity of the combustion process.

Considering the stability limits at the design mixture ratio (1.4), it is seen that the (n, τ) point representing this particular motor must fall within the small oval shaded area. Thus the interaction index must lie between 0.60 and 0.75 and the time lag between 0.11 and 0.14 millisecond. In previous stability limit tests using an unlike impinging doublet injector with a design mixture ratio of 1.4, the values obtained for the combustion parameters were: n = 1.7, τ^* =0.15 millisecond. The most striking difference between these results is the greatly reduced interaction index as determined from the transverse mode stability limit tests. However, the longitudinal mode tests were made with a 3-inch diameter chamber, at a thrust level of 250 pounds and a chamber pressure of 300 psia. Therefore, the comparison is not really valid.

In order to determine whether the combustion parameters determined from the tangential orientation sector tests agree with those which can be obtained from longitudinal tests, it was necessary to construct and operate a variable length, 30° sector motor tests. The use of the sector-shaped cross section assured the matching of the recirculation pattern in the variable angle and variable length motors. However, comparison of the values of the

combustion parameters with the theoretical longitudinal mode stability pattern, as shown in Figure 48, indicated that no instability could be expected with the variable length motor because of the low interaction index and sensitive time lag values. The longitudinal mode tests are presented in Figure 49. It can be seen that the theoretical prediction of stability was indeed verified. However, this result cannot be considered as a positive demonstration of the identity of the pressure effect combustion parameters in both longitudinal and transverse modes.

The same injector spuds were also used in a 6 inch diameter combustion chamber at the same levels of pressure and thrust, so that the exit Mach number was increased to 0.10. Propellant injection was on a 5 inch diameter circle, slightly smaller in relation to the chamber diameter than that of the preceding case. Figure 50 shows the theoretical stability limit curves corresponding to this motor configuration. It should be noted that, if the dimensional time lags are the same for the 6 and 9 inch motors, the nondimensional time lags are in the inverse ratio of the diameters, i.e., $\tau_6 = \frac{3}{2}\tau_9$. However, the experimental stability limits tests resulted in a quite different range of possible n, τ values. From Figure 51 it can be seen that the lower limit remained between 60° and 90° and the upper limit was located between 150° and 180°. Therefore, the values of the combustion parameters for the 6 inch motor differ from those obtained with the 9 inch motor. The interaction index and sensitive time lag values corresponding to the stability limits of the smaller motor are: $.65 < n < .90$; $.73 < \tau^* < .93$ (milliseconds). The primary difference between the two cases is seen to be in the time lag value.

Very little is known concerning the dependence of the parameters n and τ on the physical conditions in the combustion chamber. Since the chamber pressure, propellant flow rates, and injector spud geometry were the same for the 9 inch and 6 inch motors, the conclusion can be drawn that the

decrease in the sensitive time lag was brought about by the lateral contraction of the recirculation zone. It should be pointed out that the theoretical curves were calculated on the basis of combustion infinitely concentrated in the radial direction. However, it was shown in Chapter III that the amount of spreading expected for these injectors would contribute an error of less than two percent, which is much less than the uncertainty in the experimental stability limits.

The third series of tangential spud orientation angular stability limit tests was designed to investigate the effect of the injection diameter on stability. For these experiments the 9 inch combustion chamber was utilized, with the same injector spuds as used previously arranged on a 5 inch diameter circle. According to the distribution function treatment of nonuniform injection, the unstable regions on the n, τ plane shift toward higher interaction index values as the injection diameter is decreased relative to the combustion chamber diameter. As shown in Figure 52, an interaction index greater than unity is required for instability when injection is concentrated at 5/9 of the chamber diameter. Assuming that the combustion parameters are not greatly affected by the change in the recirculation pattern, the prediction is made that the rocket motor will operate stably. The experimental results shown in Figure 53 are seen to be mostly stable. The combustion noise level on these tests was higher than that observed in the two previous series, averaging 15 psi (rms). For some tests at angles greater than 180°, oscillations at frequencies corresponding to one or another of the transverse modes dominated the pressure fluctuations intermittently. Although these tests are shown in Figure 53 as "intermittent instability" they are not an indication of instability but rather due to the preferential amplification associated with the resonance properties of the combustion chamber.

Although this test series established qualitatively the validity

of the theoretical approach to nonuniform injection distributions, it was not the quantitative proof one would desire. In order to accomplish a more positive verification an injection diameter intermediate between 5 and 8 inches should be used, in order that there be a region of instability, from the limits of which values of the combustion parameters could be obtained. However, the results of the 6 inch diameter motor tests have demonstrated that the time lag and interaction index are not insensitive to changes in the injection geometry. Therefore, quantitative verification of the theory for the injection distribution effect may not be possible.

C. Full Motor Tests with Tangential Spud Orientation

From the linearized velocity effect theory the result is obtained that the tangential velocity effects are absent in standing modes and present in spinning modes. The tangential velocity perturbation acts to shift the stability limits on the n, τ -plane to smaller values of the interaction index. The effect of the radial velocity perturbation is to shift the stability limits to larger or smaller time lag values, depending on the sign of the velocity index. A positive velocity index is associated with the tangential velocity effect. However, the positive tangential direction is not defined in terms of the combustion chamber geormetry, as in the case of the radial velocity. The positive tangential direction is defined as the direction in which a spinning wave travels.

The sign of the velocity index depends on the characteristics of the spray formed by the injector. According to the theoretical model, a positive velocity index implies that the burning rate is increased when the velocity perturbation is in the positive direction. The symmetry of the unlike impinging doublet injector is such that the radial and tangential velocity effects can be separated, as discussed previously. For the radial spud orientation, the velocity effect, due solely to the radial velocity

component, cannot be calculated unles the sign of the velocity index is known for a particular injector arrangement. At the present time knowledge of the details of the combustion process is insufficient to allow the prediction of the velocity index sign. Therefore, one must resort to experimental means, based on spinning mode tests with the tangential spud orientation. By observing the direction of wave travel with respect to the injector spuds, it is possible to determine the direction of the velocity perturbation which increases the burning rate. From this information the sign of the radial velocity index for a given radial injector arrangement can be found.

Several full motor tests were made with the tangential spud orientation. Three pressure transducers were used to determine the direction of the wave travel with respect to the injector spuds. The results of four typical tests are shown in the following table:

Test No.	Chamber Diameter	Injection Diameter	$\bar{n}_{design}$	$\frac{\bar{n}}{\bar{n}_{design}}$	Mode	Direction
1	9	8	1.4	.90	1T	F → O
2	9	8	1.4	.87	2T	F → O
3	6	5	2.2	.43	1T	F → O
4	9	8	1.0	1.39	1T	F → O

The wave travel direction was determined as follows. The injector was so constructed that looking from the nozzle, the fuel injection hole on each spud lay on the clockwise side of the oxidizer hole. The transducer signals showed that the wave traveled in the counterclockwise direction. Therefore, the wave crossed each spud from the fuel side to the oxidizer side, or F → O, as shown in the table. For the first tangential mode oscillations, the pressure transducers were arranged at 90° intervals, as are No. 1 and No. 2 in Figure 10. In the case of the second mode, the wave direction was determined by placing a third transducer at the downstream location, but angularly midway between

the other two. The resulting phase error was not large enough to affect the test results.

The angle of the injection spray with respect to the combustion chamber axis is a function of the ratio of the test mixture ratio to the design mixture ratio, $\bar{r}/\bar{r}$ design. If this ratio is less than one, the net lateral spray momentum is in the direction F → O, and if it is greater than one , the spray momentum direction is O → F. It is clear from the test results that the wave travel direction is not affected by any rotation caused by off-design operation of the injector.

It should be noted that although the operating conditions for tests 1 and 2 were very nearly the same the resulting oscillations were of different modes. Moreover, from Figure 46 it can be seen that the unstable mode of the standing type is the second tangential. The velocity effects for this configuration are illustrated by Figure 54. Although point "A," representing the test motor, is within only the second mode unstable zone for the standing mode, it lies within both the first and second mode zones for the spinning mode. The difference between test 1 and 2 was in the starting period. That is, test 1 utilized the normal starting procedures, whereas an aluminum barrier was used in test 2. The effect of the barrier was to stabilize the first tangential mode during the first second of operation by constraining a standing mode oscillation pattern in the chamber. Upon burnout of the barrier, the oscillation changed to the spinning type without changing the mode. This result is an example of nonlinear effects. Although for very small oscillations both modes could co-exist, if the amplitudes are large, one mode will dominate to the exclusion of the other. In this case the dominant mode will be the first tangential, unless the second tangential mode is allowed to grow to large amplitudes, as in test number 2.

D. Sector Motor Tests with Radial Spud Orientation

The full motor tangential orientation tests demonstrated that for the injector used in this investigation the burning rate is increased by a velocity perturbation in the direction F → O. For the radial orientation angular stability limit tests, the arrangement of the injector was such that the direction O → F was positive (outward). Therefore, a negative radial velocity was required to increase the burning rate; that is, the radial velocity index ℓ_r was negative. According to the velocity effect theory, as discussed in Chapter II, for $\ell_r < 0$, the stability limits on the n,τ -plane are shifted toward smaller τ. It has also been shown that the stability limits are moved in the direction of larger τ as the sector angle is increased. Thus, if the pressure interaction index and sensitive time lag are to be independent of the orientation of the injector spuds, the effect of the radial velocity must be counteracted by an increase in the sector angle. That is, the stability limits for the radial orientation should be at larger angles than those of the tangential orientation (no velocity effects).

This prediction was borne out by all of the radial orientation tests. Figure 55 shows the results for the 9 inch chamber and 8 inch injection diameters. The lower limit of the first tangential mode was located (at $\bar{n}$ = 1.4) at approximately 90°, and the upper limit between 180° and 210°, rather than the 60°-90° and 180° results of the previous tangential orientation series (Figure 46). From Figure 55 it can be seen that off-design operation caused significant variation of the stability limits with mixture ratio, which may be due to distortion of the recirculation pattern.

Similar results were obtained for the 6 inch chamber, 5 inch injector (Figure 56). For this case the shift of the upper limit from 150°-180° to 210° is greater than the shift observed for the 9 inch chamber. However, one hesitates to trust the test results which show the first tangential mode

at angles greater than 180° because of the unknown influence of the unsteady vortex pattern resulting from the flow past the sharp corner.

The experimental results for the 9 inch motor with injection on a 5 inch diameter circle are shown in Figure 57. As in the case of the corresponding tangential orientation tests, the pattern is one of stability. This result is in agreement with the theoretical prediction that the effect of the radius of injection is essentially to change the interaction index required for instability.

It is possible in principle to determine the magnitude of the velocity index by comparing the stability limits obtained for the radial and tangential spud orientations. Since in the latter case the velocity effects are absent, the difference in the limits is a measure of the velocity index. However, the rate of change of the time lag with respect to the radial velocity index for a constant value of the pressure interaction index is very small. Therefore, because of the large uncertainty in the stability limits, which is due to the 30° increment in sector angle obtainable with the available experimental apparatus, it was not possible to determine the value of the velocity index from these radial orientation tests with any meaningful accuracy.

E. Conclusions

The primary goal of this investigation was to evaluate the validity of applying to the transverse modes of instability the sensitive time lag theory which had been used successfully to explain the longitudinal modes. In that theory the combustion process was characterized by two parameters, the sensitive time lag τ and the interaction index n. It was assumed that all physico-chemical conditions which affected the combustion process rates could be correlated to the local pressure. The degree of sensitivity was measured by the interaction index. The longitudinal mode analysis

showed that if the interaction index for a given rocket motor system was sufficiently large, there existed ranges of the dimensionless time lag $\tau^* \bar{c}_o^* / L_c^*$ in which the rocket operation would be oscillatory. The predictions of this theory were verified for a variety of injector types and propellant combinations by means of stability limit measurements using a variable length (L_c^*) rocket motor.

When the sensitive time lag theory was applied to purely transverse modes of instability, similar results were obtained as for the longitudinal case with the combustion chamber radius r_c^* replacing the chamber length L_c^* in the nondimensionalized time lag, $\tau^* \bar{c}_o / r_c^*$. However, a preliminary series of exploratory tests showed that the pressure sensitivity theory was not sufficient to explain two experimental observations: (1) the stability behavior of the standing forms of tangential modes was quite different from that of the spinning form, and (2) the orientation of the doublet injection pattern with respect to the radial and tangential coordinate directions had a significant effect on stability.

Based on the findings of the preliminary tests a velocity sensitivity theory was developed. The radial and tangential velocity perturbations were assumed to influence the rates of the processes involved in the combustion of the liquid propellants in a manner analogous to the pressure perturbation in the original theory. A physical mechanism was suggested to lie in the enhancement of the mixing of the vapors of the two propellants which could be effected by the transverse components of the gas velocity. The analysis based on these considerations predicted that the tangential velocity perturbation would have a strong destabilizing effect on spinning tangential modes but would have no effect on standing modes. The radial velocity was shown to cause a shifting of the unstable time lag ranges for a given interaction index. The orientation effects noted in the preliminary experiments

were seen to be the results of the uni-directional sensitivity of the doublet type of injector

Previous instability analyses had assumed that the steady state flow in the combustion chamber was one-dimensional, implying that the propellants were injected uniformly across the face of the injector. However, practical considerations dictated the use of rocket motors in which the propellants were injected around the circumference of a single circle. Another result of the preliminary test phase was that the radius of the injection circle in relation to the combustion chamber radius was an important factor in the stability behavior of a rocket motor. The effect of the nonuniform injection distribution was treated in the present analysis by means of a transverse distribution function. For injection concentrated at a single radius, it was demonstrated that there is a greater tendency to instability as the injection radius is increased.

In order to evaluate the instability theory in a systematic manner, it was necessary to find a method of measuring stability limits, as was done for the longitudinal mode case. For tangential modes of oscillation, the sector motor method of measuring angular limits was developed. In this method, the sector angle replaces the chamber length as the variable which governs the resonance properties of the combustion chamber. The requirement imposed on a stability limit motor is that the recirculation pattern be preserved. In the case of the sector motor this implies that the injection distribtuion must be periodic in the tangential direction and that the propellants sprays must be directed axially in order to achieve proper simulation of the full circular chamber. A limitation of this method was seen to be present in the case that the time lag of the rocket system is such that the first tangential mode is unstable for sector angles greater than 180°. For such angles, the oscillating flow past

the corner would set up an unsteady vortex pattern with unknown effects on the stability limits.

From the measurements of angular stability limits made for several combustion chamber configurations, a qualitative, but not quantitative, confirmation of the theoretical predictions concerning velocity and injection distribution effects was obtained. The interaction index values derived from the angular stability limits were so low that longitudinal mode instability was not possible. Tests made with a variable length 30° sector motor did show no longitudinal mode instability, precluding a quantitative comparison of combustion parameters derived from the two different methods. Because of the rather large sector angle increment (30°) it was impossible to derive values of the velocity interactions indices.

The experimental phase of the investigation was not intended to be exhaustive. Tests were confined to a single injector type and one propellant combination. However, with the limited number of configurations explored it was seen that the combustion parameters were strongly dependent on the injector spray characteristics and on the nature of the recirculation pattern. Therefore, there is a clear need for systematic investigations into the factors which influence the sensitive time lag and interaction indices (both pressure and velocity). A possible method for measuring the velocity parameters is illustrated by Figure 58. The propellants are injected radially inward from the chamber wall in a variable length rocket motor. For this manner of injection, the velocity fluctuations associated with longitudinal modes will act transversely to the propellant sprays. If the injector section is placed near the closed end of the chamber, the pressure effects will dominate, whereas location of the injection near the center will maximize the velocity effect. By measuring stability limits for several injector positions, it should be possible to deduce values of the velocity parameters.

A factor which has not been considered in this investigation is the possibility of an oscillating injection flow rate. For chambers of the sizes used in the experimental tests the oscillation frequency is sufficiently high that the feed system will not respond appreciably to the pressure fluctuations in the combustion chamber. However, as the diameter is increased the frequency is reduced, with the result that for large rocket motors the interaction of the feed system with the combustion chamber can no longer be neglected in the analysis of high frequency instability. In such problems the analyses of Scala (5) and Crocco (29) should prove helpful. However, neither investigator considered wave effects in the feed lines, which have often been observed to be of considerable importance. Thus, additional complications due to adding injection rate fluctuations will be involved in the application of the instability theory to large liquid rockets.

In the theoretical developments, the through velocity in the combustion chamber was restricted to values sufficiently small that the square of the Mach number could be neglected compared to unity. The present theory might be carried to $\bar{u}_e \cong 0.3$, corresponding to the Redstone engine, but at this point terms of the order of ten percent are being neglected. In order to apply the analysis to more recent engines, the restriction on the velocity will have to be removed, thus adding a great deal of complexity to the problem.

The next major step in the investigation of combustion instability must be the consideration of nonlinear effects. All of the systematic, quantitative work to date has been concerned with linear instability, that is, with oscillations which are spontaneously initiated. However, even some of the experiments made in this investigation indicated the presence of nonlinear phenomena, particularly in the starting transients. Some types of injectors (for example, the showerhead and like-on-like) are clearly

susceptible to nonlinear velocity effects. Also the shattering of liquid propellant droplets by high amplitude waves has been shown to exert an important effect on the combustion process. At the present time the theoretical approach to nonlinear instability has barely begun. In addition to more sophisticated theoretical techniques, much more refined instrumentation and experimental methods will be required. However, the linearized solution of the instability problem has yielded much valuable insight into the combustion process in liquid propellant rockets and should provide a firm foundation for the future studies.

REFERENCES

1. Crocco, L., and Cheng, S. I., "Theory of Combustion Instability in Liquid Propellant Rocket Motors," AGARDograph No. 8, Butterworths Scientific Pub., Ltd., London, 1956.

2. Gunder, D. F., and Friant, D. R., "Stability of Flow in a Rocket Motor," Journ. Appl. Mech., vol. 17, p. 327, (1950).

3. Yachter, M., "Discussion of the Paper of Ref. 2," Journ. Appl. Mech., vol. 18, p. 114 (1951).

4. Summerfield, M., "A Theory of Unstable Combustion in Liquid Propellant Rocket Systems," Jour. Amer. Rocket Soc., vol. 21, p. 108 (1951).

5. Scala, S. M., "Transverse Wave and Entropy Wave Combustion Instability in Liquid Propellant Rockets," Princeton University (Ph.D. Thesis), Aero. Engng. Rep. no. 380, April 1, 1957.

6. Crocco, L., Harrje, D. T., and Condomines, A., "Combustion Instability in Liquid Propellant Rocket Motors," 29th Quarterly Progress Report, 1 May 1959 to 31 July 1959, Princeton University Aero. Engng. Rep. no. 216cc.

7. Berman, K., and Cheney, S. H., "Combustion Studies in Rocket Motors," Journ. Amer. Rocket Soc., vol. 23, no. 2 p. 89 (1953).

8. Ellis, H., Odgers, I., Stosick, A. J., Van de Verg, N., and Wick, R. S., "Experimental Investigation of Combustion Instability in Rocket Motors," Fourth Symposium on Combustion, Williams and Wilkins Co., 1953.

9. Ellis, H., "Liquid Propellant Rocket Combustion Research," Edwin G. Baetger, II Colloquium, Princeton University, February 9, 1960

10. Male, T., and Kerslake, W. R., and Tischler, A. O. "Photographic Study of Rotary Screaming and Other Oscillations in a Rocket Engine," NACA RM E54A29, May 25, 1954.

11. Male, T., and Kerslake, W. R., "A Method for Prevention of Screaming in Rocket Engines," NACA RM E54F28a, August, 1954 (Confidential).

12. Osborn, J. R., and Bonnell, J. M., "On the Importance of Combustion Chamber Geometry in High Frequency Oscillations in Rocket Motors," paper presented at the ARS Semi-Annual Meeting, Los Angeles, California, May 9-12, 1960.

13. Osborn, J. R., and Bonnell, J. M., "On the Effect of Fuel Composition on High Frequency Oscillations in Rocket Motors Burning Premixed Hydrocarbon Gases and Air," paper presented at ARS 15th Annual Meeting, Washington, D. C., December 5-8, 1960.

14. Rayleigh, "The Theory of Sound," Vol. II, Dover Pub., 1955, p. 232.

15. Crocco, L., "Aspects of Combustion Instability in Liquid Propellant Rockets," Journ. Amer. Rocket Soc., Part I: vol. 21, November, 1951, Part II: vol. 22, January, 1952.

16. Crocco, L., Grey, J., and Harrje, D. T., "Theory of Liquid Propellant Rocket Combustion Instability and Its Experimental Verification," ARS Journal, vol. 30, no. 2, February, 1960.

17. Maslen, S. J., and Moore, F. K., "On Strong Transverse Waves Without Shocks in a Circular Cylinder," Journ. Aero Sci., vol. 23, no. 6 (1956).

18. Pickford, R., and Peoples, R. G. "The Inherent Stability of the Combustion Processes," paper presented at the ARS 15th Annual Meeting, Washington, D. C., December 5-8, 1960

19. Li, Y. T., "Dynamic Pressure Measuring System for Jet Propulsion Research," Journ. Amer. Rocket Soc., vol. 23, no. 3, p. 124 (1953).

20. Jones, H. B., Jr., and Harrje, D. T., "An Integrated Combustion Instability Recording and Analysis Installation," in "Progress in Astronautics and Rocketry," vol. 2, New York Academic Press, pp. 175-188 (1960).

21. Wieber, Paul R., and Mickelsen, William, "Effect of Transverse Acoustic Oscillations on the Vaporization of a Liquid-Fuel Droplet," NASA TN D-287, May, 1960.

22. Wise, H., Lorell, J., and Wood, B. J., "The Effects of Chemical and Physical Parameters on the Burning of a Liquid Droplet," Fifth Symposium (International) on Combustion, Reinhold Publishing Co., New York, 1955, pp. 132-141.

23. Priem, Richard J., and Heidmann, Marcus F. "Propellant Vaporization as a Design Criterion for Rocket-Engine Combustion Chambers," NASA TR R-67, 1960

24. Pass, Isaac, and Tischler, Adelbert O., "Effect of Fuels on Screaming in 200-Pound-Thrust Liquid-Oxygen-Fuel Rocket Engine," NACA RM E56 C 10, June 22, 1956.

25. Crocco, L., Harrje, D. T., and Reardon, F. H., "Combustion Instability in Liquid Propellant Rocket Motors," 30th Quarterly Progress Report, 1 August, 1959 to 31 October, 1959, Princeton University Aero. Engng. Rep. no. 216dd.

26. Bellman, D. R. Humphrey, J. C., and Male, T., "Photographic Investigation of Combustion in a Two-Dimensional Transparent Rocket Engine," NACA Report no. 1134.

27. Courant, R., and Hilbert, D., "Methods of Mathematical Physics." Vol. I Interscience Publishers Inc., New York, 1953.

28. Kantorovish, L. V., and Krylov, V. I., "Approximate Methods of Higher Analysis," P. Noordhoff, Ltd.,Groningen, The Netherlands, 1958.

29. Croke, E. J., "Measurement of the Inertial Flow Phase Lag in and Orifice system by Means of a Momentum-Sensitive Transient Flowmeter," M. S. E. Thesis, Princeton University, 1958.

TABLE I

Results of Preliminary Barrier Tests

Test No.	Configuration	Stability Behavior
1	Full, 6" chamber, 9" injector, spuds tangential	185 psi peak-to-peak oscillations
2	180° sector (insert)	Stable
3	Barrier extending from injector face to nozzle throat	Stable
4	Barrier, from injector to 1-3/8" downstream	Stable
5	Barrier, from injector to 3/4" downstream	Stable
6	Barrier, from injector to 5/8" downstream	Stable
7	Barrier, from injector to 1/2" downstream	40 psi peak-to-peak oscillations.
8	Barrier, from injector to 1/2" downstream	90 psi peak-to-peak oscillations
9	Barrier, from injector to 1/2" downstream	Stable
10	Barrier, from 1/4" from injector to 1-5/8" downstream	17 psi peak-to-peak oscillations

Notes. 1. The same injector and chamber were used on all tests.

2. All instabilities were of the first tangential mode.

3. The barriers showed evidence of burning on tests 7 & 8.

TABLE II

Velocity Effect Coefficients for Uniform Injection, Full Circular Chamber

Mode	ν	h	$\frac{B_{\nu h}}{S_{\nu h}}$	$\frac{\tilde{C}_{\nu h}}{S_{\nu h}}$ (Spinning mode)
First tangential	1	1	0.19116	0.77402
Second tangential	2	1	0.18124	0.85258
First radial	0	2	-0.13320	0.00000
First combined	1	2	0.02884	0.22197

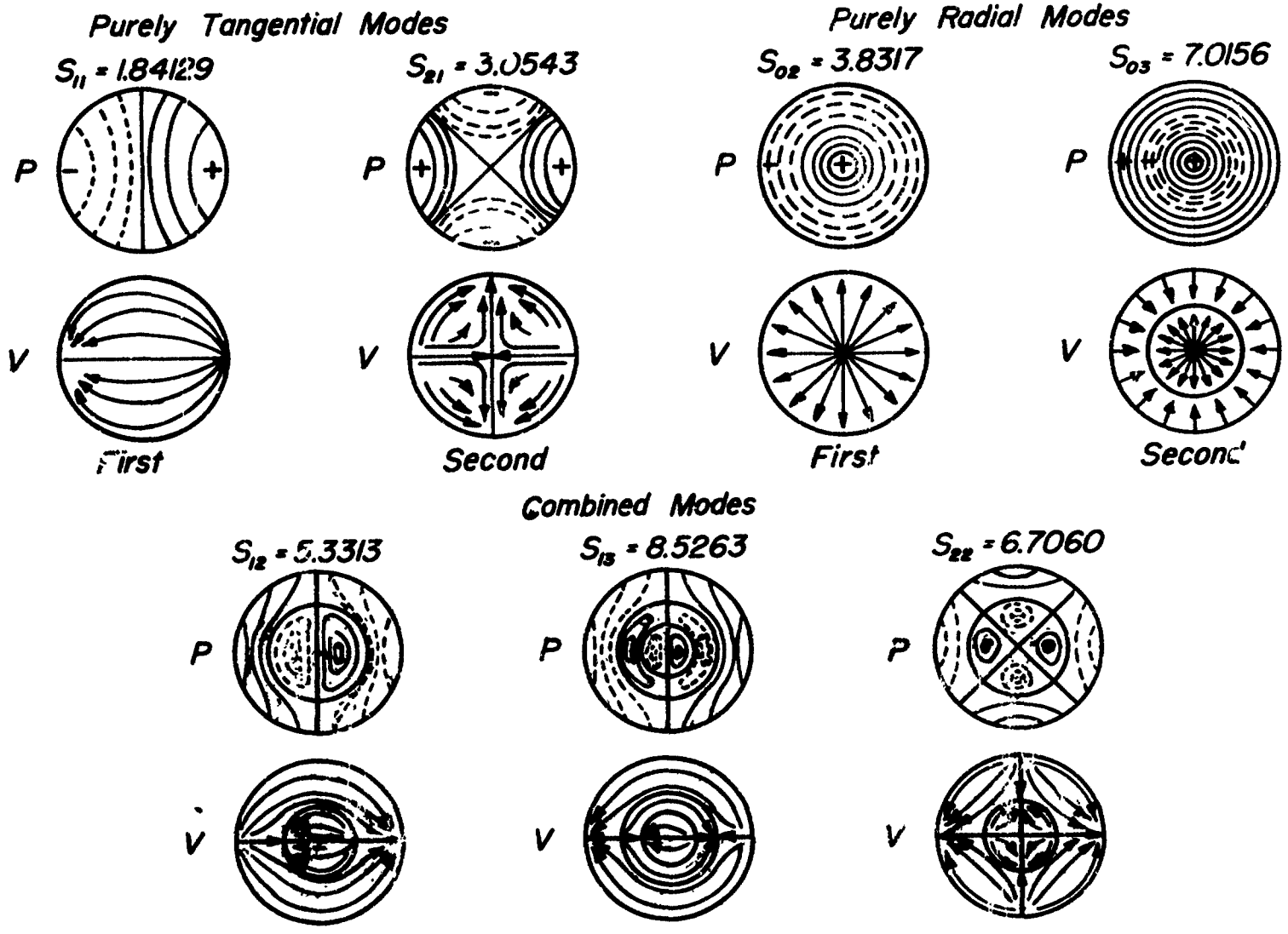
Purely Tangential Modes
Purely Radial Modes
S_{11} = 1.84129
S_{21} = 3.0543
S_{02} = 3.8317
S_{03} = 7.0156
P
V
First
Second
First
Second
Combined Modes
S_{12} = 5.3313
S_{13} = 8.5263
S_{22} = 6.7060

Figure 1

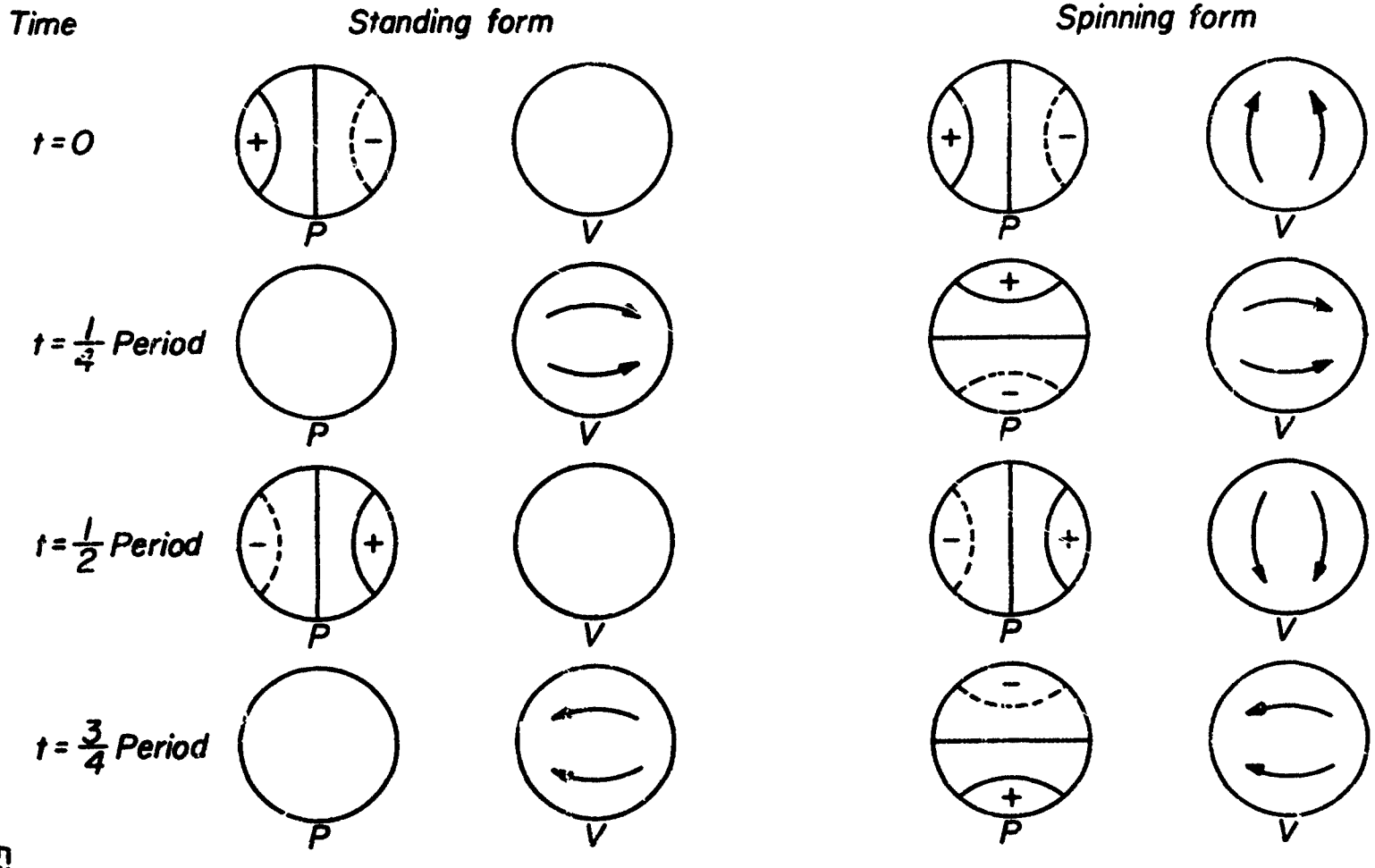

Figure 2

Standing and spinning forms of the first tangential mode

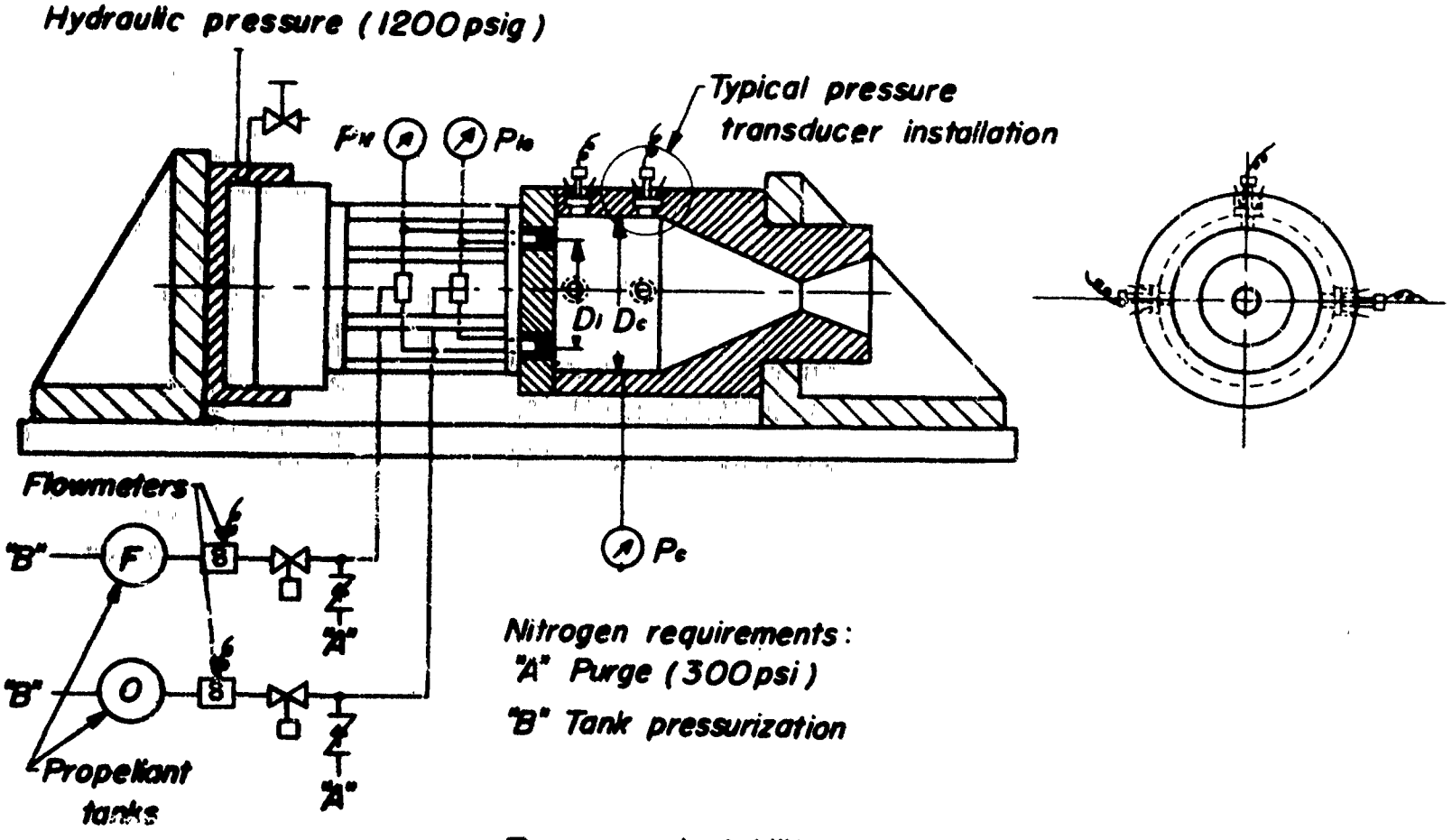

Figure 3

Transverse instability motor schematic

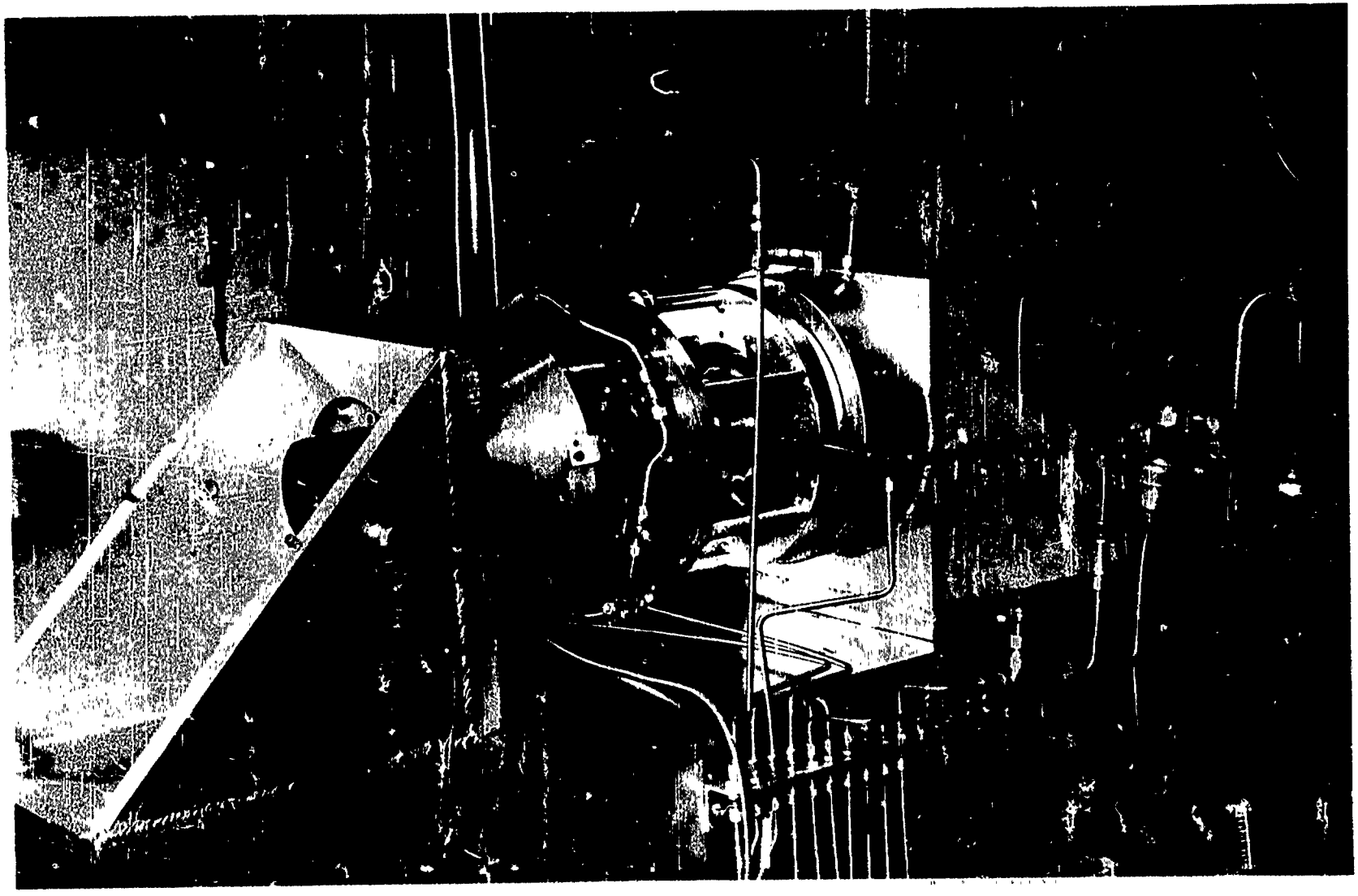

Experimental rocket motor used in transverse mode combustion instability studies

Figure 4

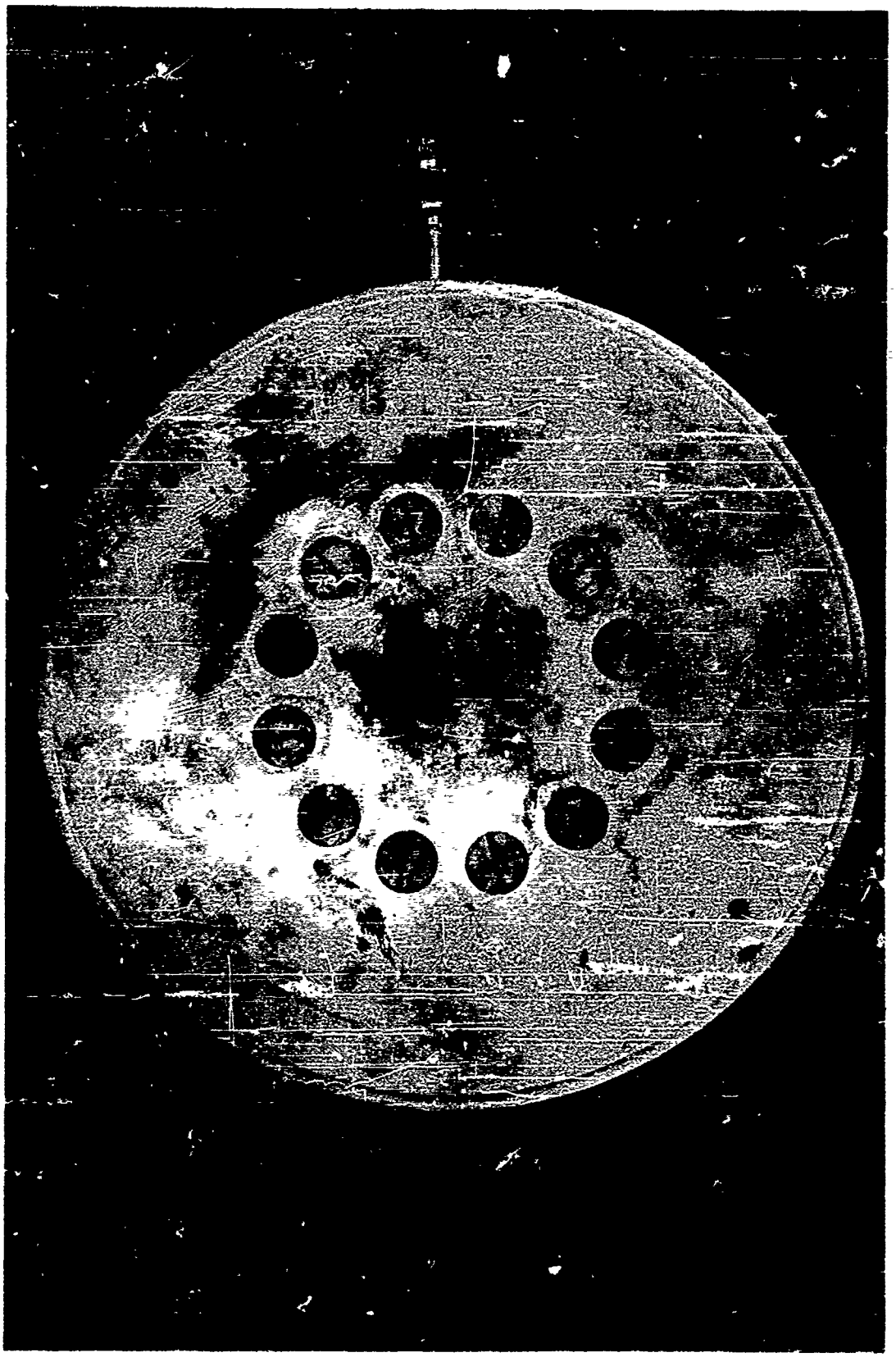

Face of spud injector

Figure 5

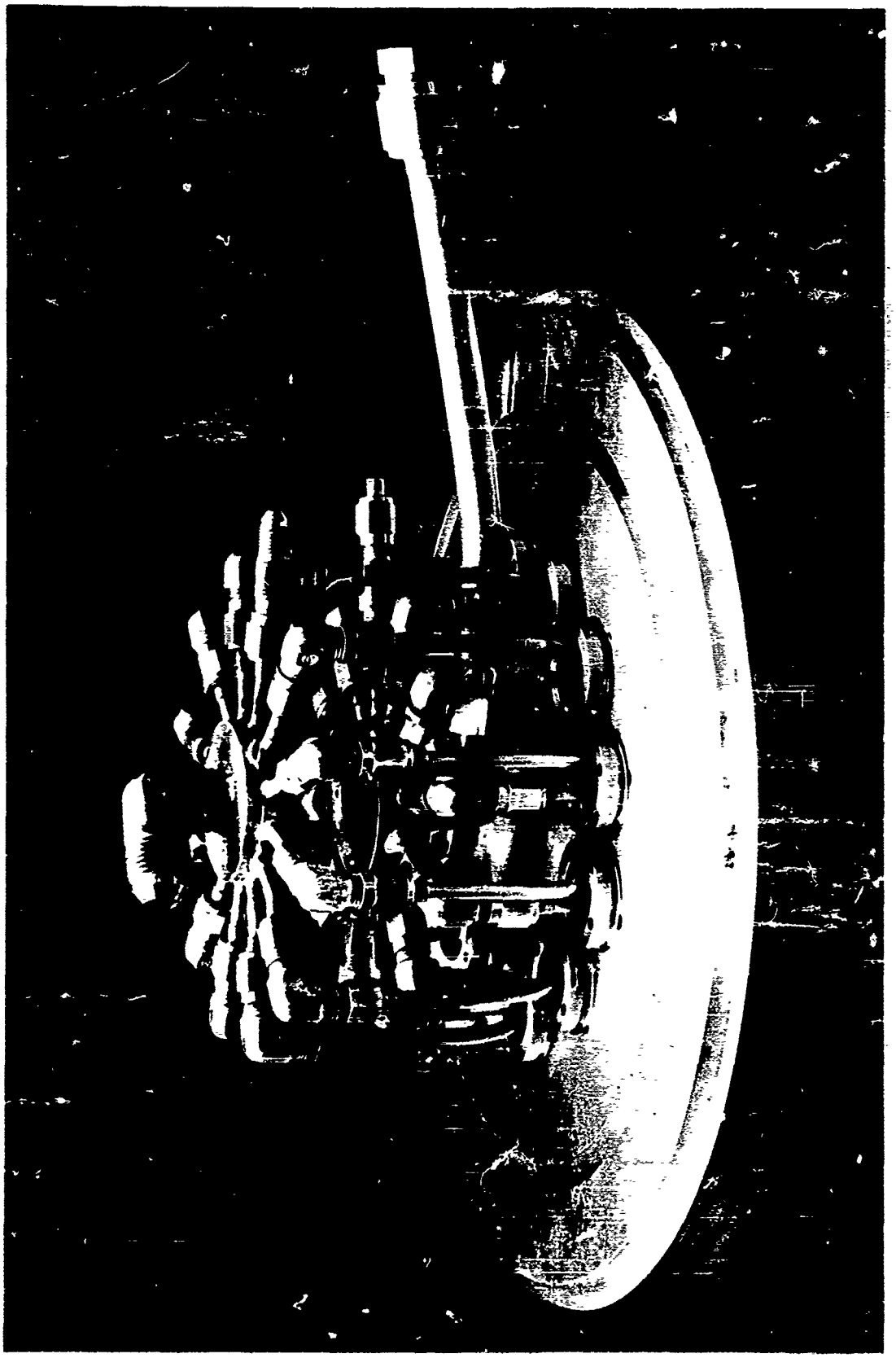

Back of spud injector

Figure (

Doublet spud orientation

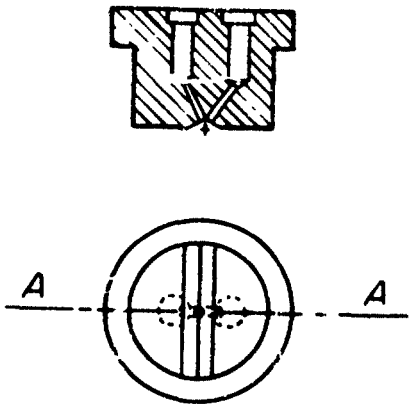

A-A = Line of centers of injection holes

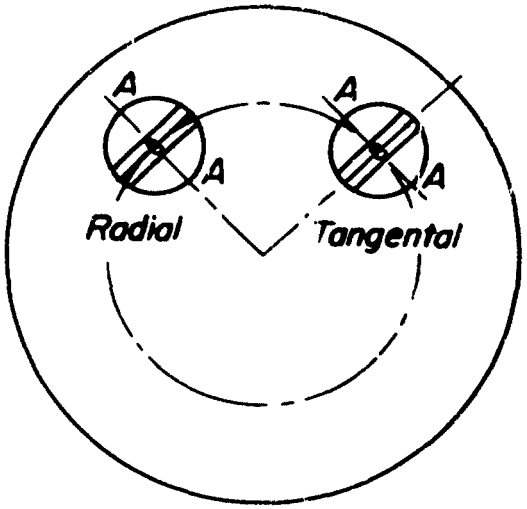

Spud orientation

Figure 7

Transverse instability tests
tangential spud orientation

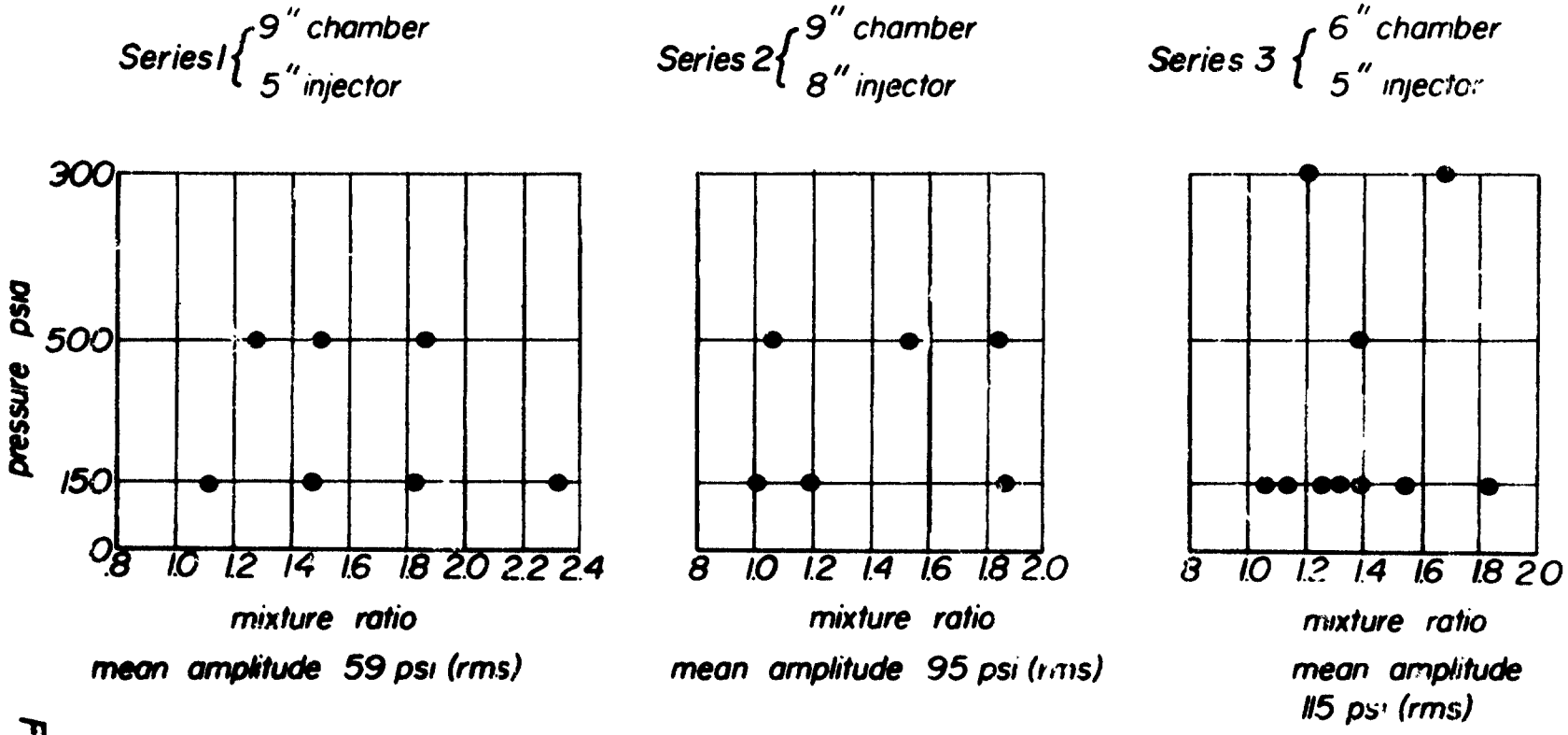

Key : × stable ● first tangential mode

Figure 8

Transverse instability tests
radial spud orientation

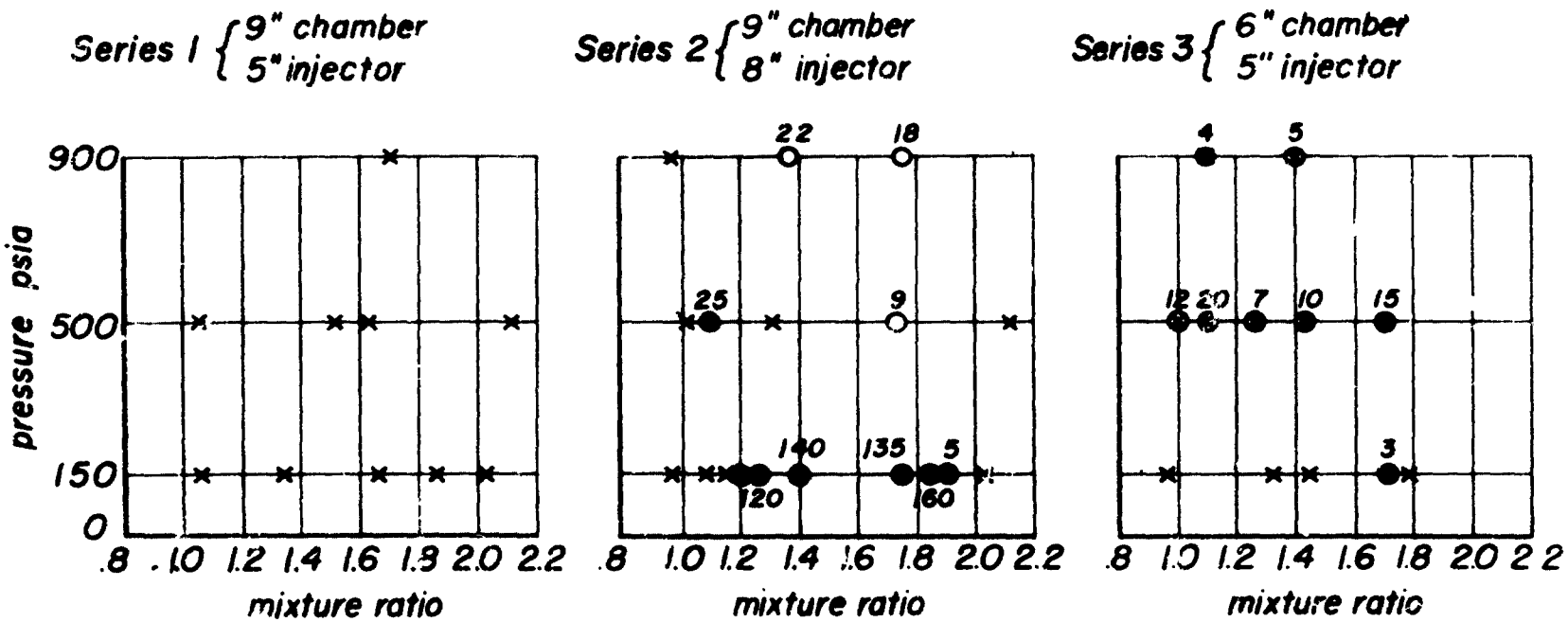

Figure 9

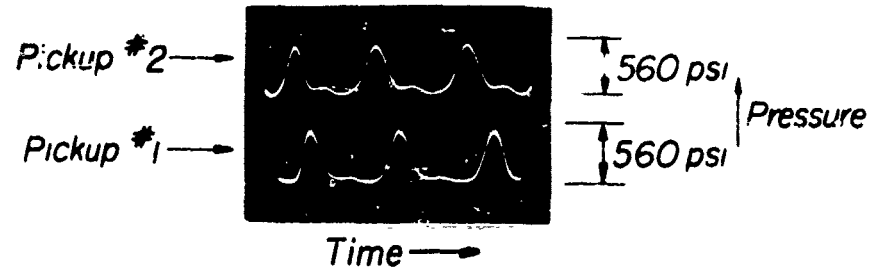

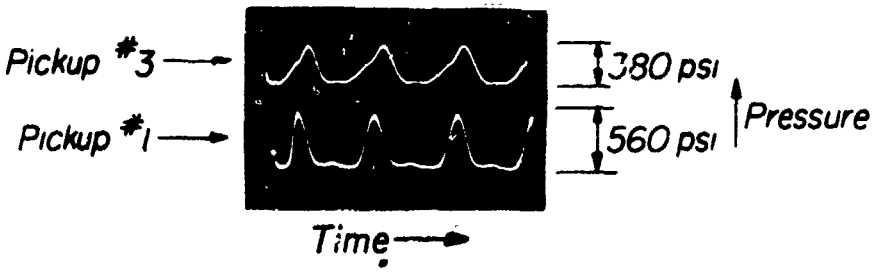

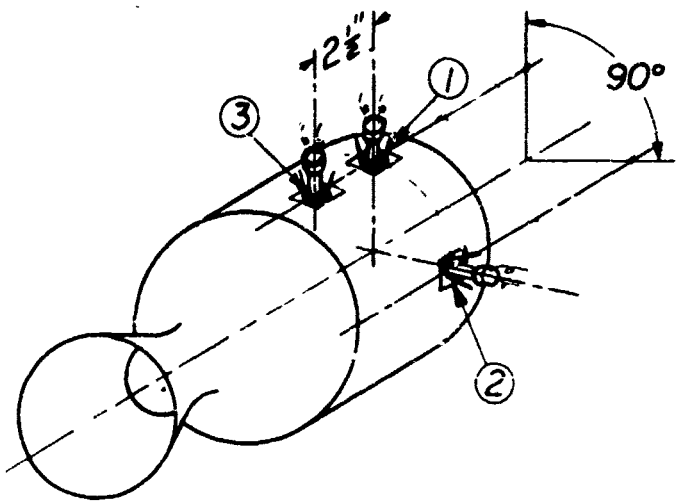

JPR 444

Figure 10

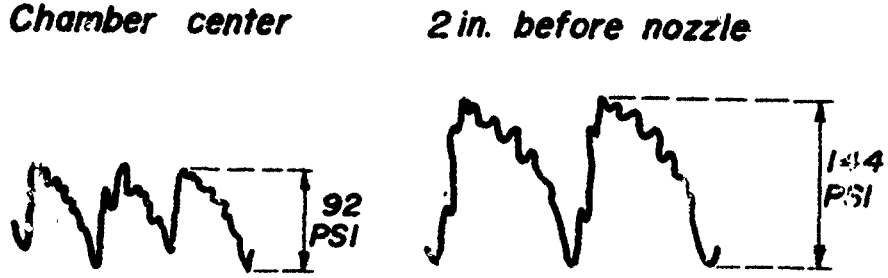

Departure of the pressure oscillation shape from the sinusoidal in a typical test (longitudinal mode instability)

Figure 11

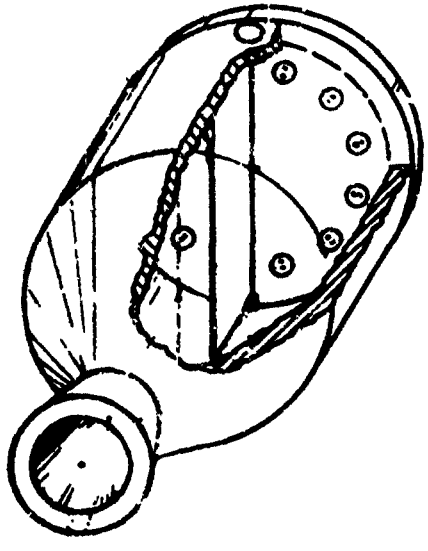

(a) Barrier tests
(temporary and permanent)

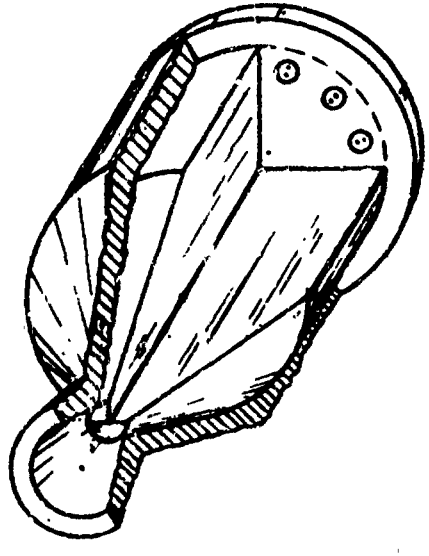

(b) Sector tests
(0 to 360°, 30° increments)

Two methods of transverse instability testing

Figure 12

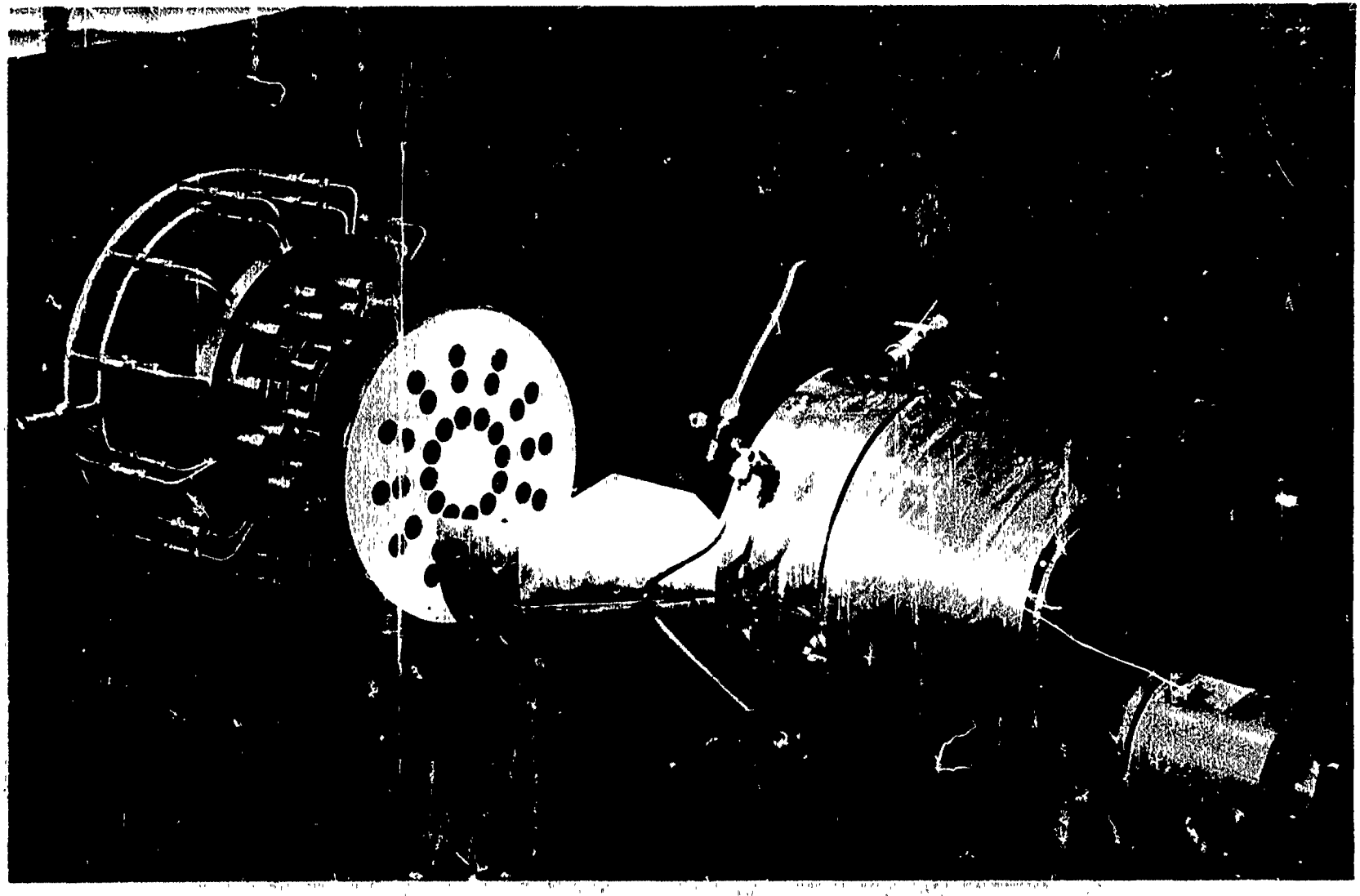

Exploded view of sector motor using distributed injector

Figure 1.

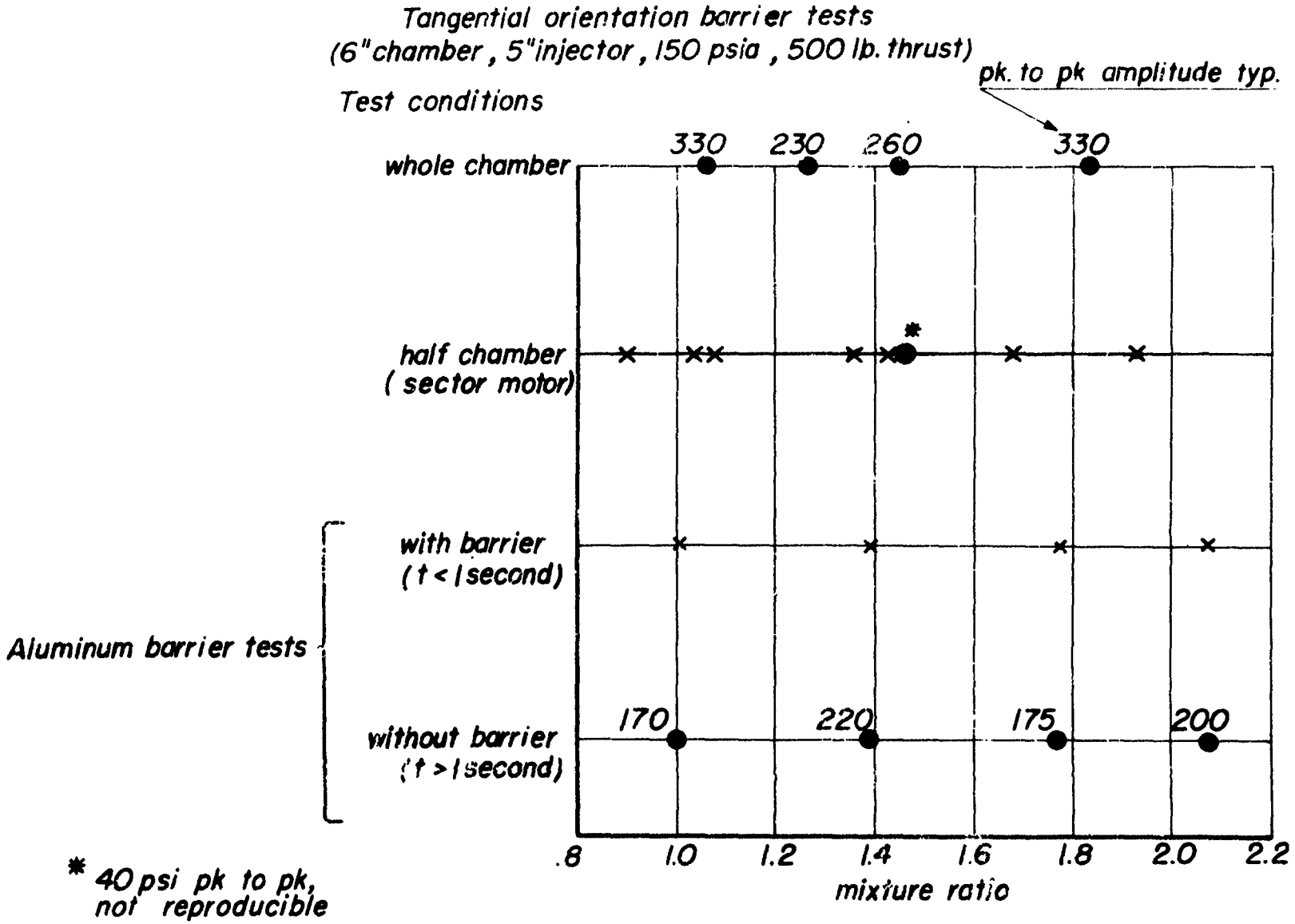

* 40 psi pk to pk, not reproducible

Figure 14

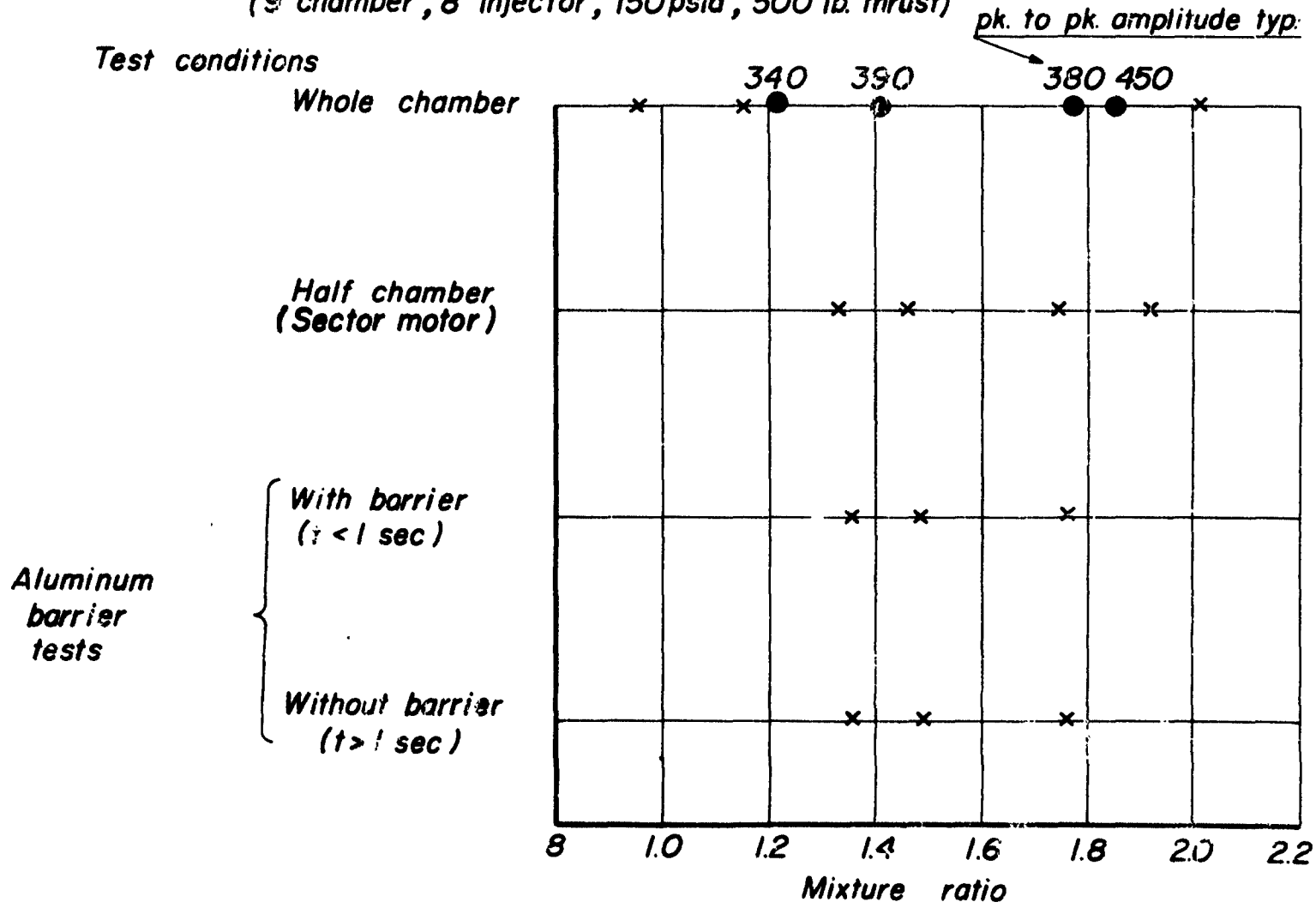
Radial orientation barrier tests
(9"chamber, 8"injector, 150psia, 500 lb. thrust)
pk. to pk. amplitude typ.
Test conditions
Whole chamber
Half chamber
(Sector motor)
Aluminum barrier tests
With barrier
(t < 1 sec)
Without barrier
(t > 1 sec)
340
390
380
450
8
1.0
1.2
1.4
1.6
1.8
2.0
2.2
Mixture ratio

Figure 15

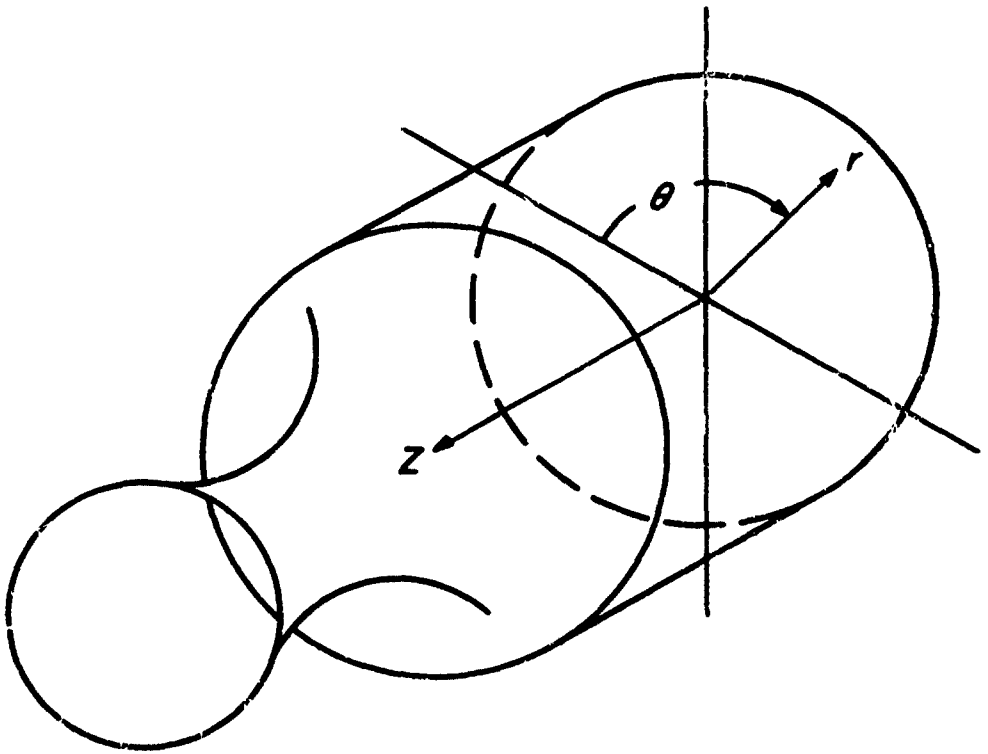

Figure 16

Combustion chamber coordinate system

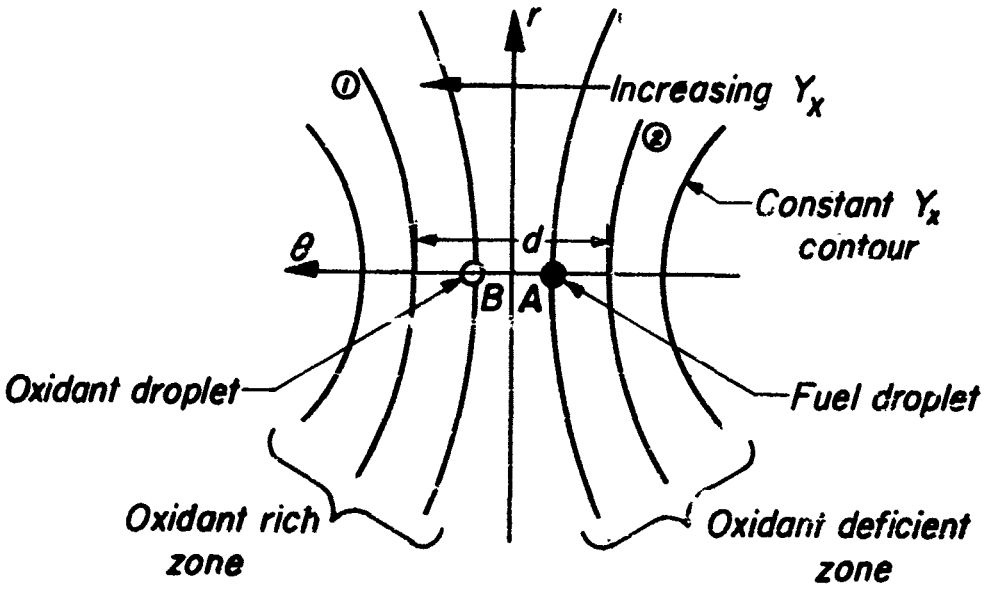

(a) Spray produced by tangentially oriented injector spud

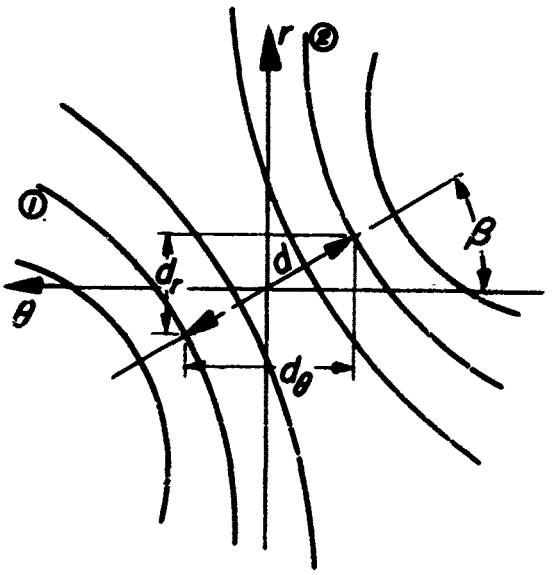

(b) Spray produced by rotated spud

JPR 838

Figure 17

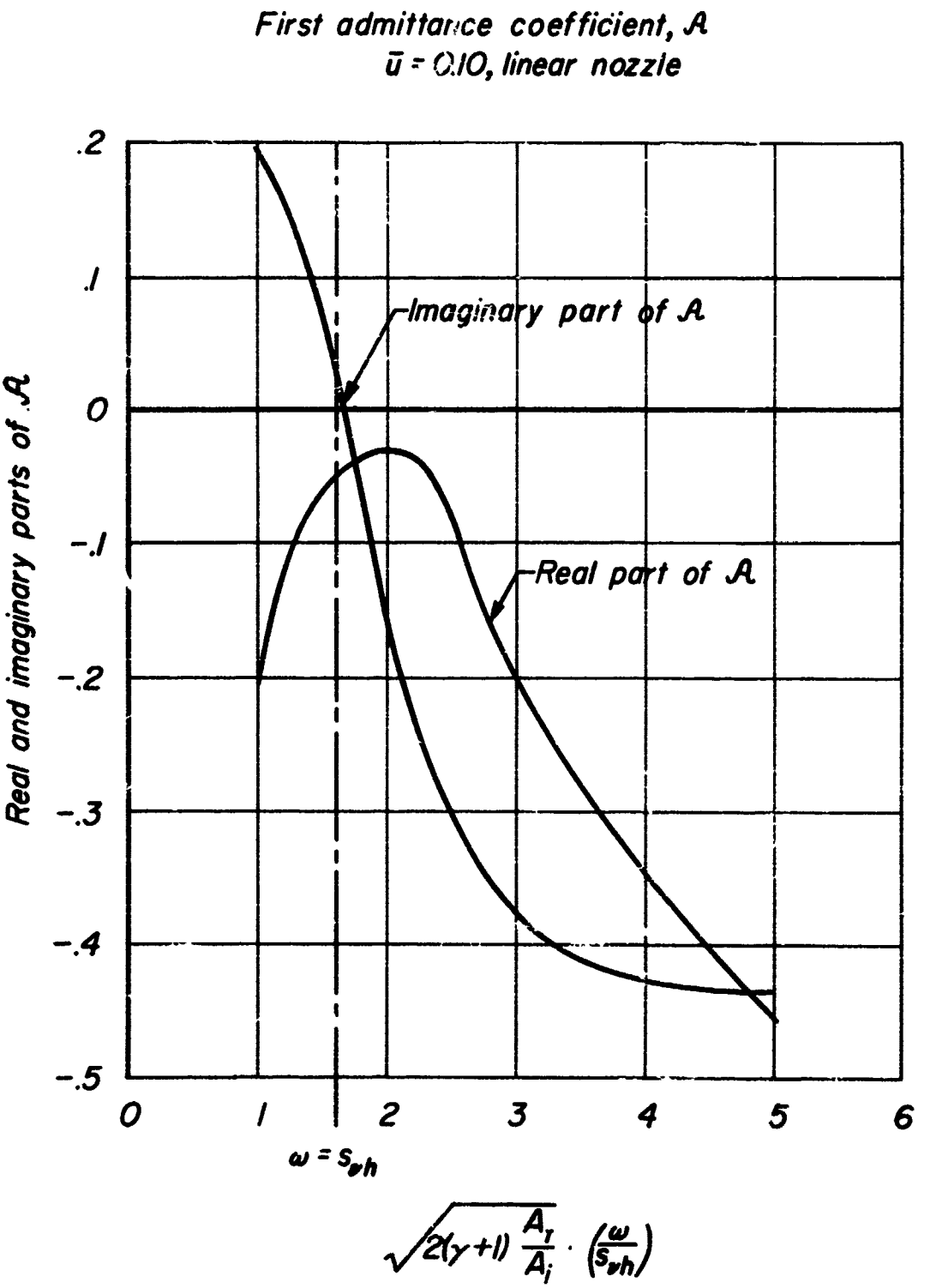
First admittance coefficient, A
$\bar{u}$ = 0.10, linear nozzle
Real and imaginary parts of A
.2
.1
0
-.1
-.2
-.3
-.4
-.5
Imaginary part of A
Real part of A
0
1
2
3
4
5
6
$\omega = s_{vh}$
$\sqrt{2(\gamma+1)\frac{A_r}{A_i}} \cdot \left(\frac{\omega}{s_{vh}}\right)$

Figure 18

Typical solution for $m(\omega)$ and $\tau(\omega)$

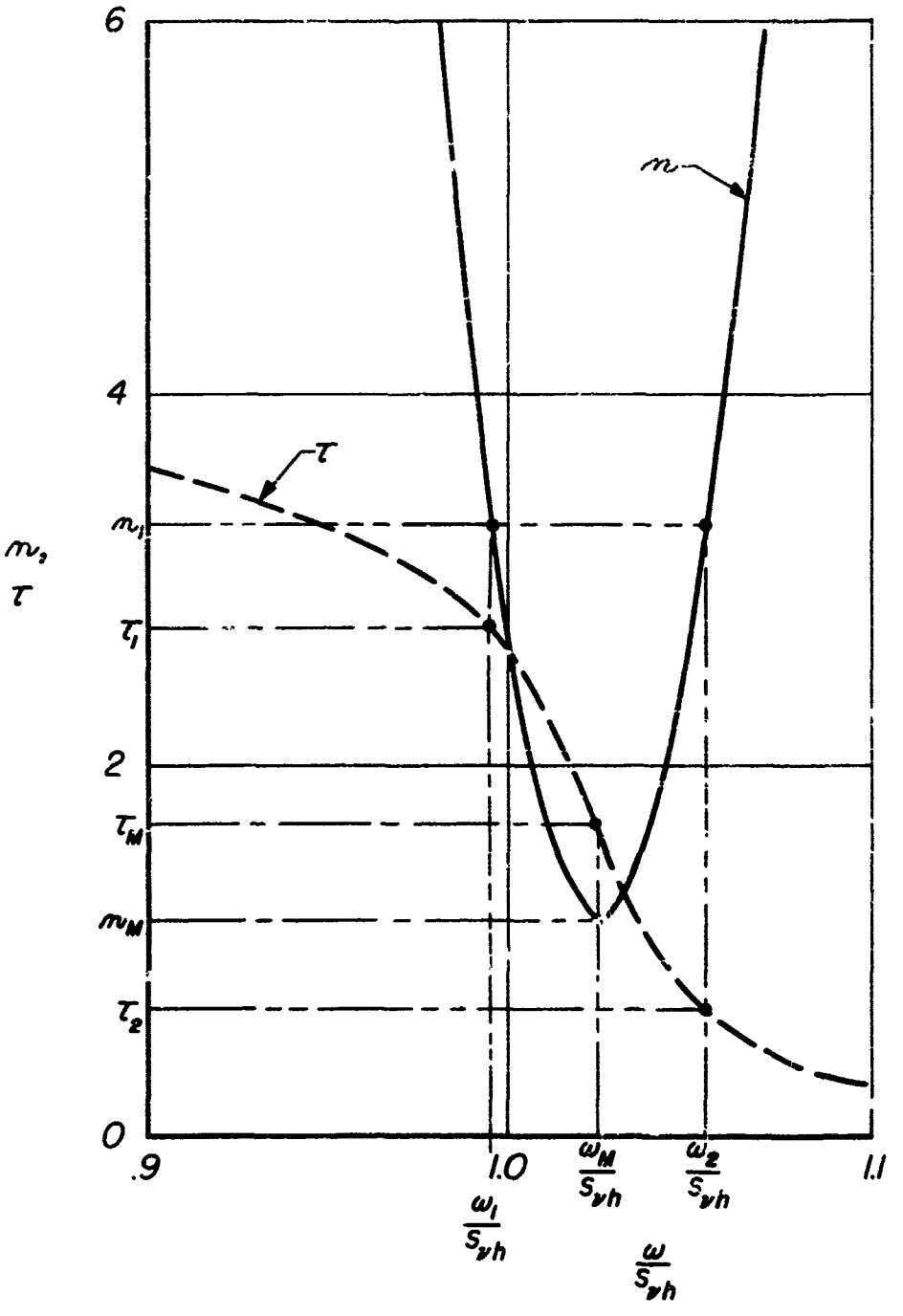

JPR 843

Figure 19

JPR 844

Stable and unstable regions on the n, τ-plane

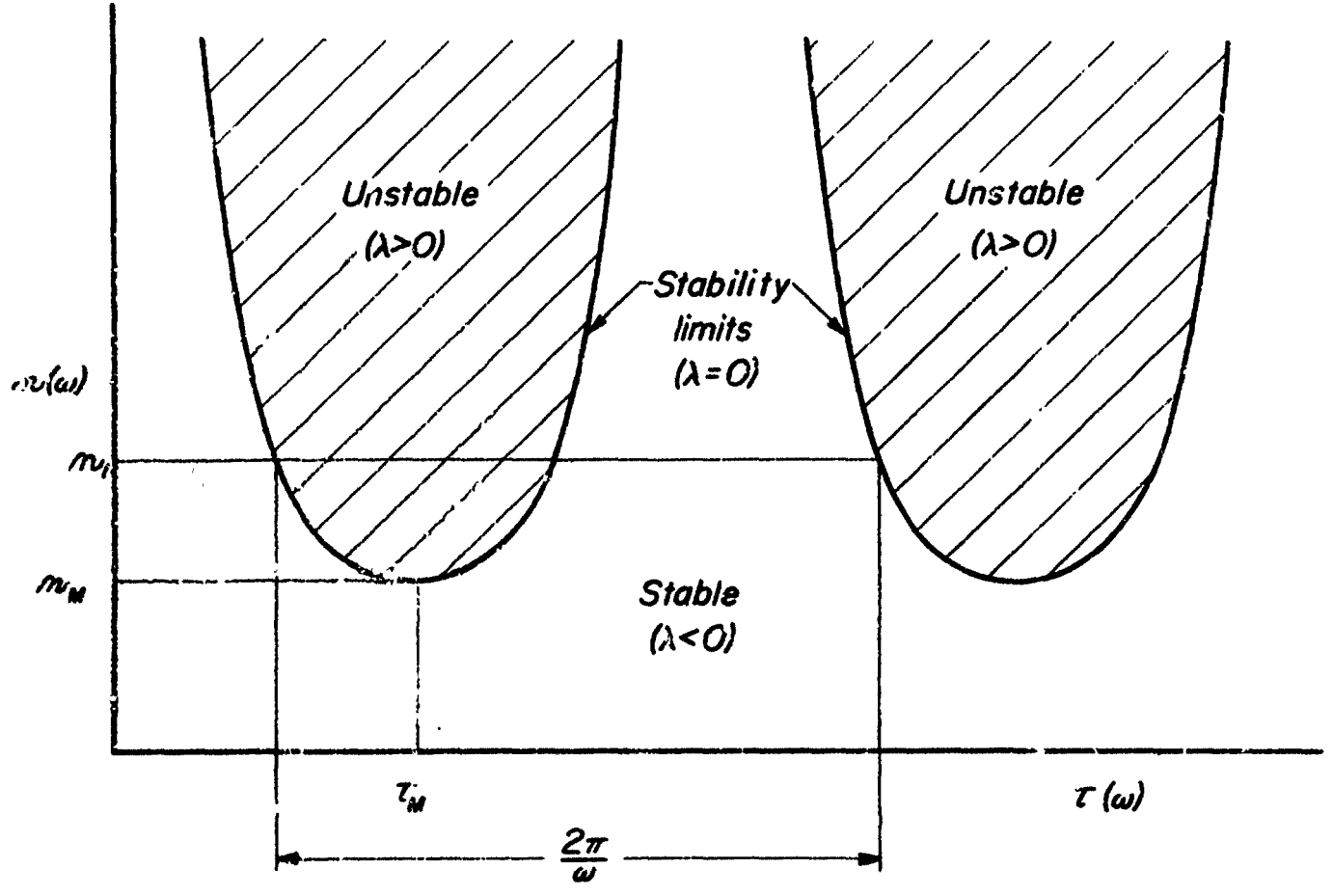

Figure 20

Theoretical stability limits for several purely transverse modes, uniformly distributed combustion, $\bar{u}_e = 0.10$

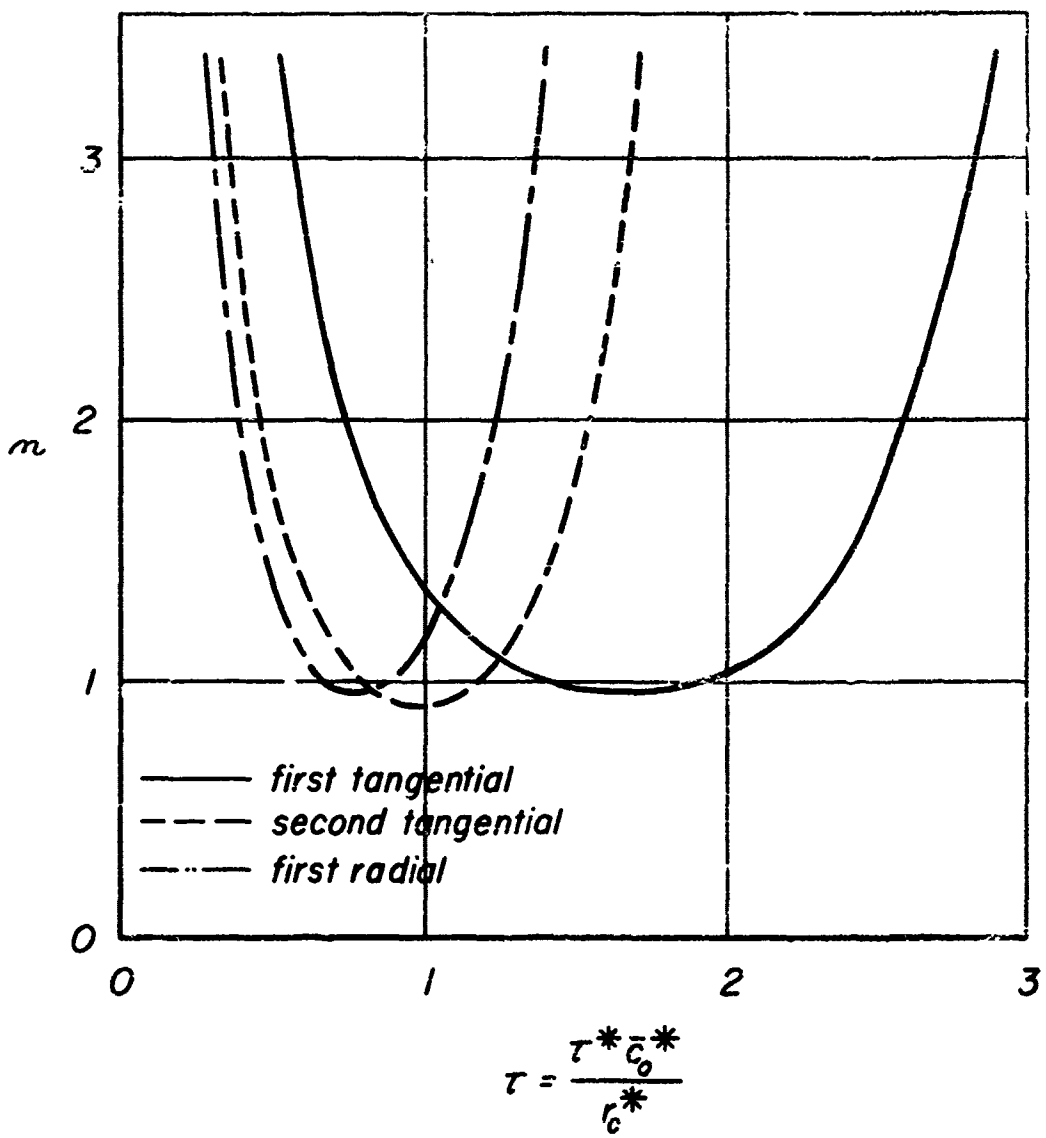

JPR 845

Figure 21

Typical nozzle admittance cofficients

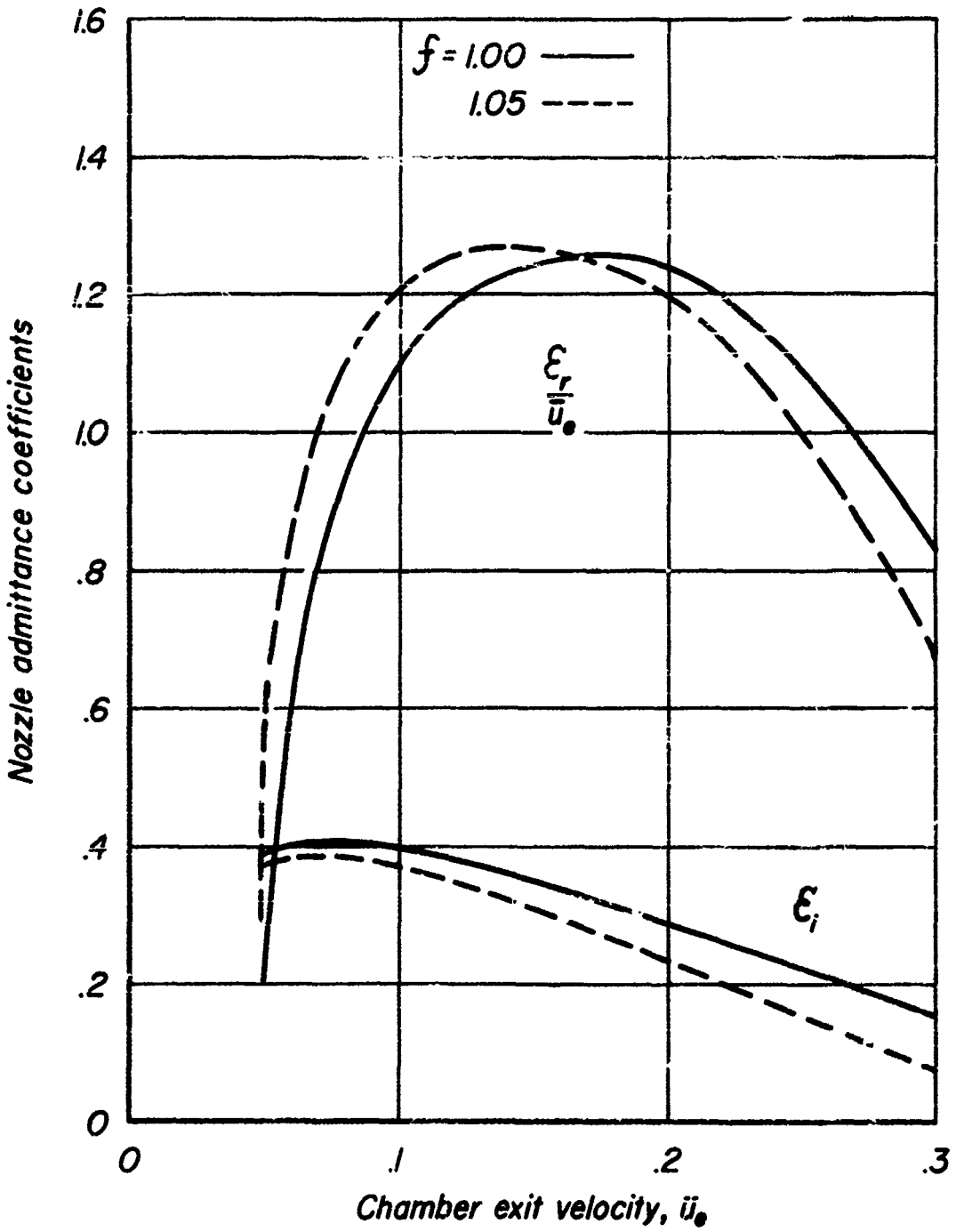

Figure 22

Theoretical effect of chamber exit velocity on stability limits, first tangential mode, uniformly distributed combustion

$\beta = 0.70,\ \kappa = 0.92,\ \zeta = 1.84$

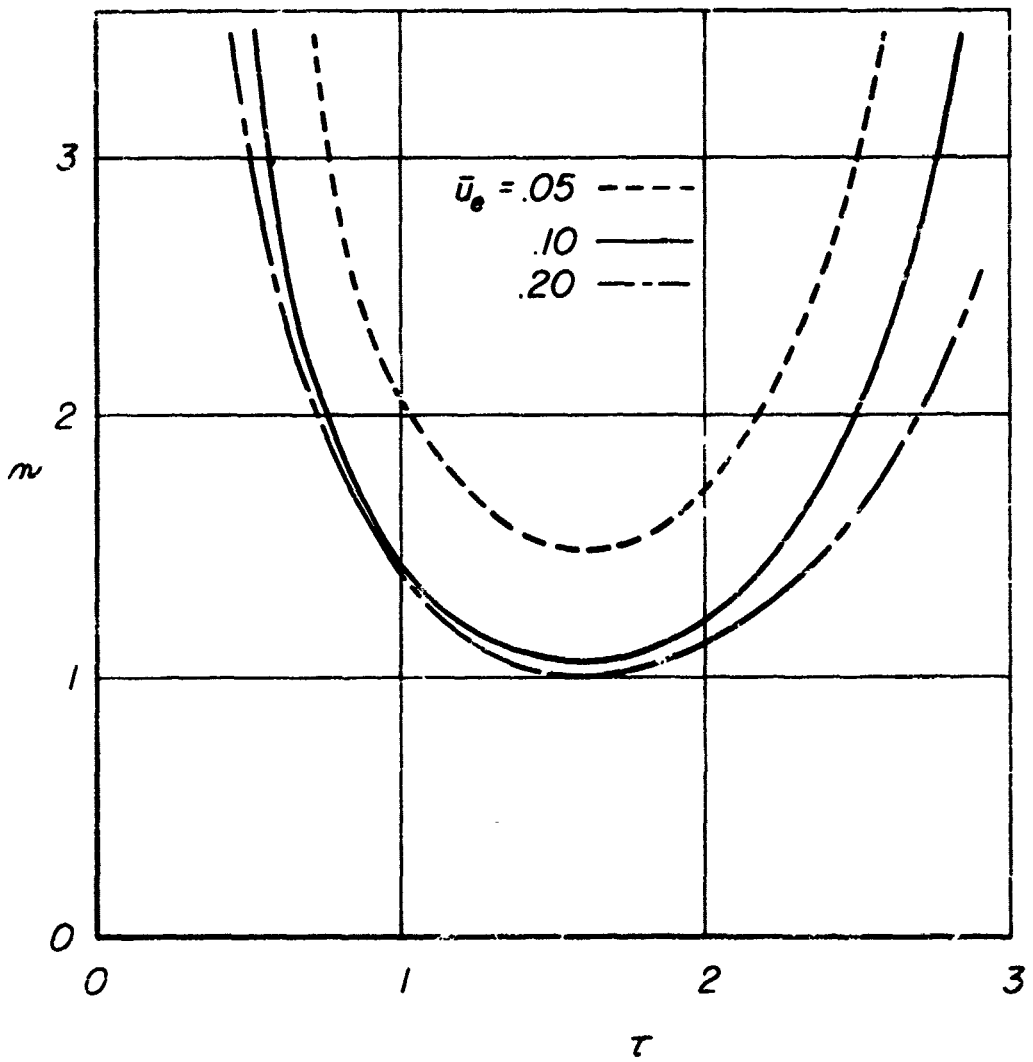

JPR 847

Figure 23

Comparison of theoretical stability limits for linear and conical nozzles, first tangential mode, $\bar{u}_e = 0.05$

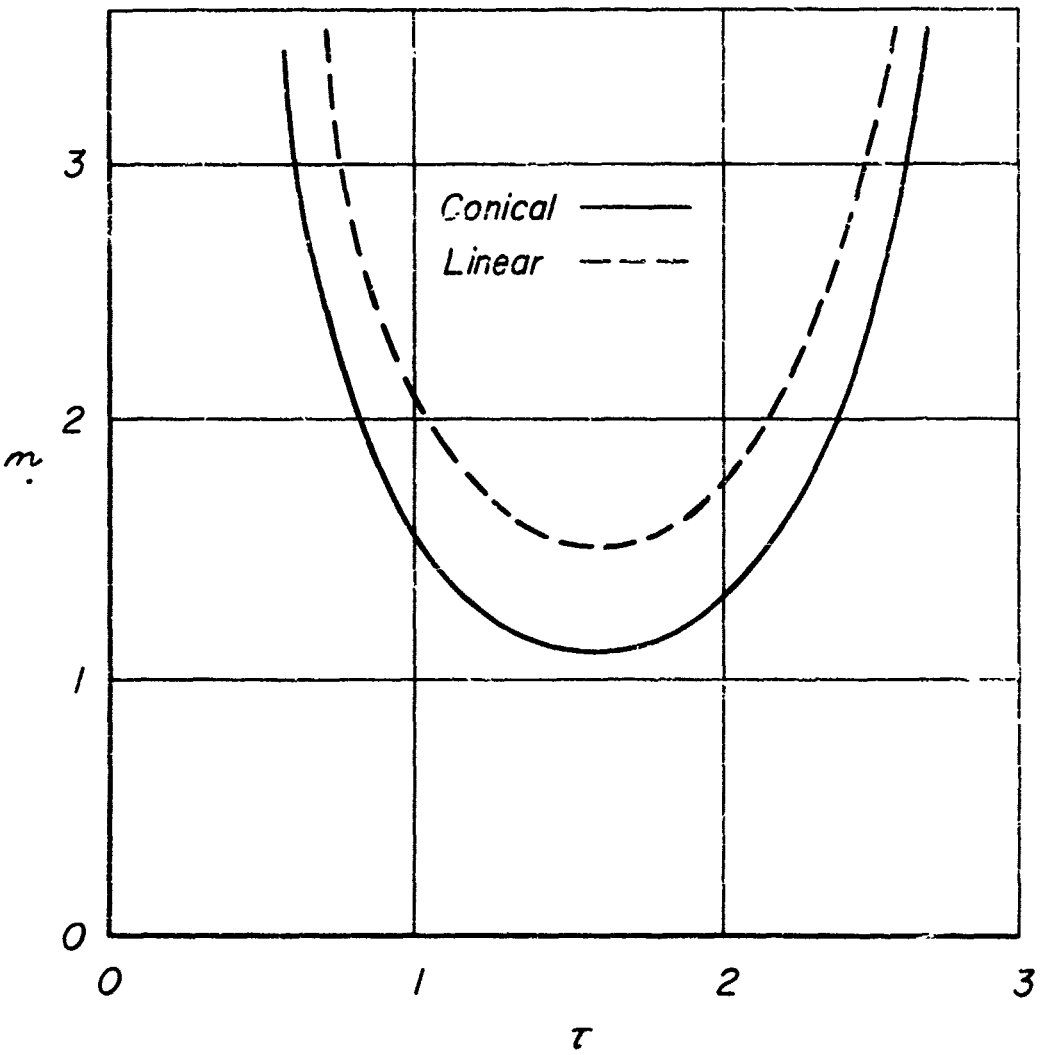

JPR 848

Figure 24

Theoretical effect of β on stability limits, first tangential mode, uniformly distributed combustion

$\bar{u}_e = 0.10$, $c = 0.92$, $\vartheta = 1.84$

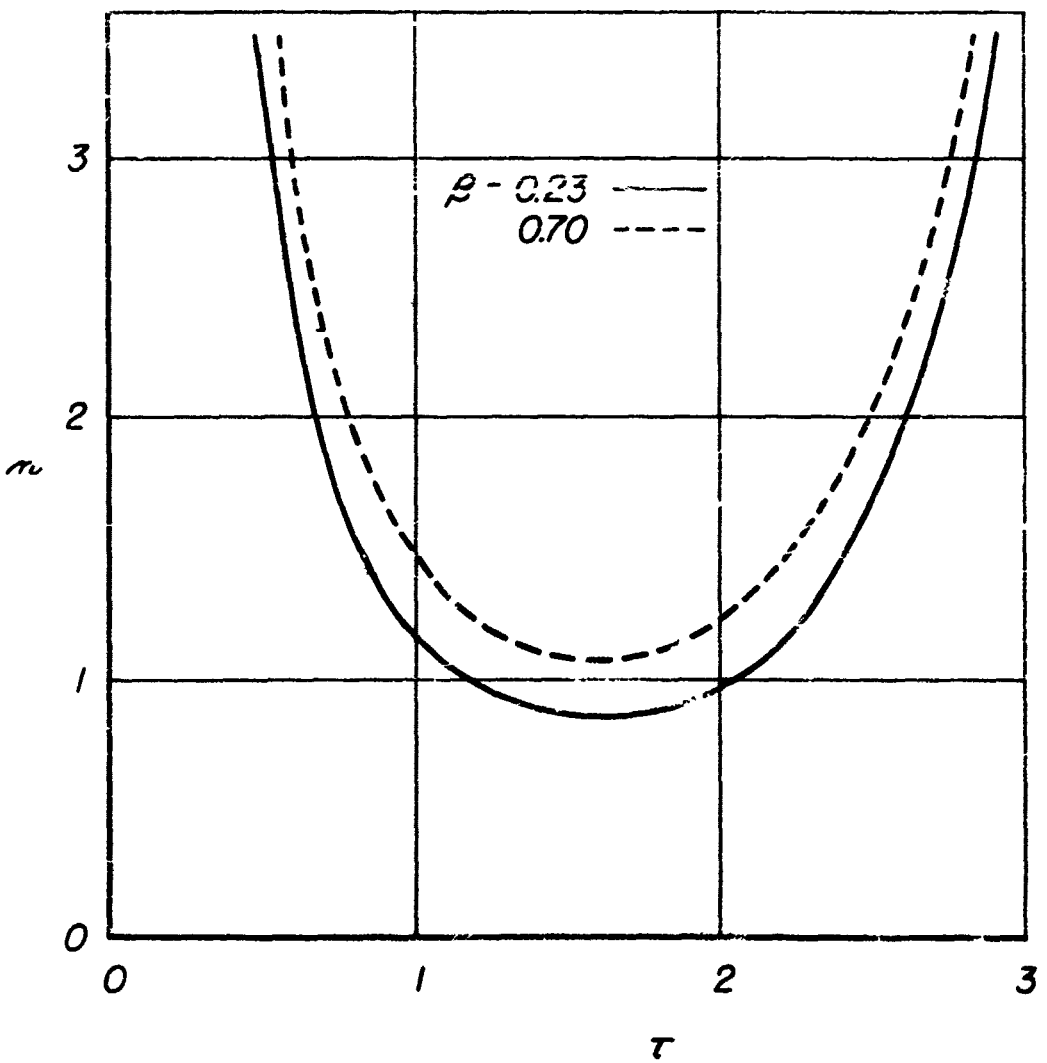

JPR 849

Figure 25

Theoretical effect of $\mathfrak{z}$ on stability limits, first tangential mode, uniformly distributed combustion

$\bar{u}_e = 0.10,\ \kappa = 1.80,\ \beta = 0.35$

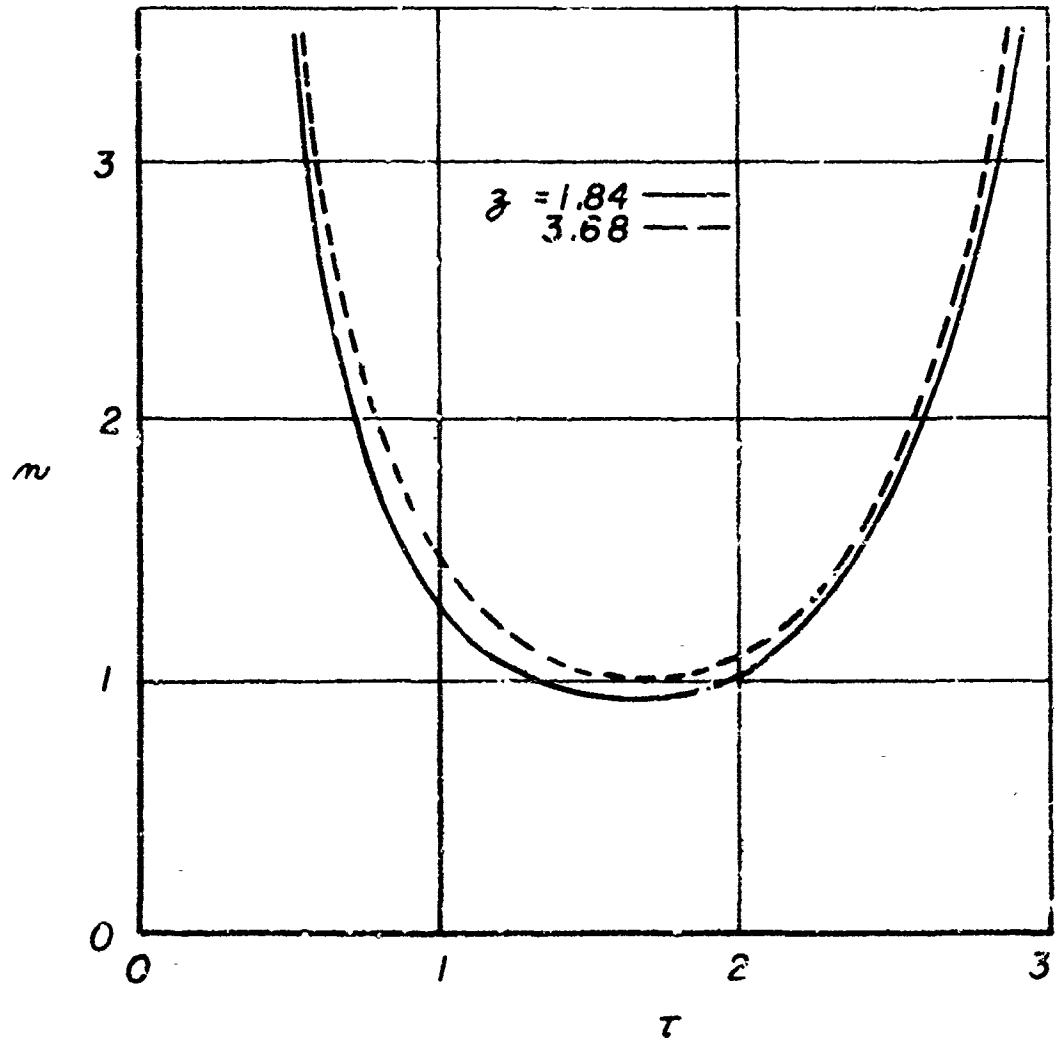

Figure 26

Theoretical tangential velocity effect on stability limits, first tangential mode, uniformly distributed combustion, $\bar{u}_e = 0.10$

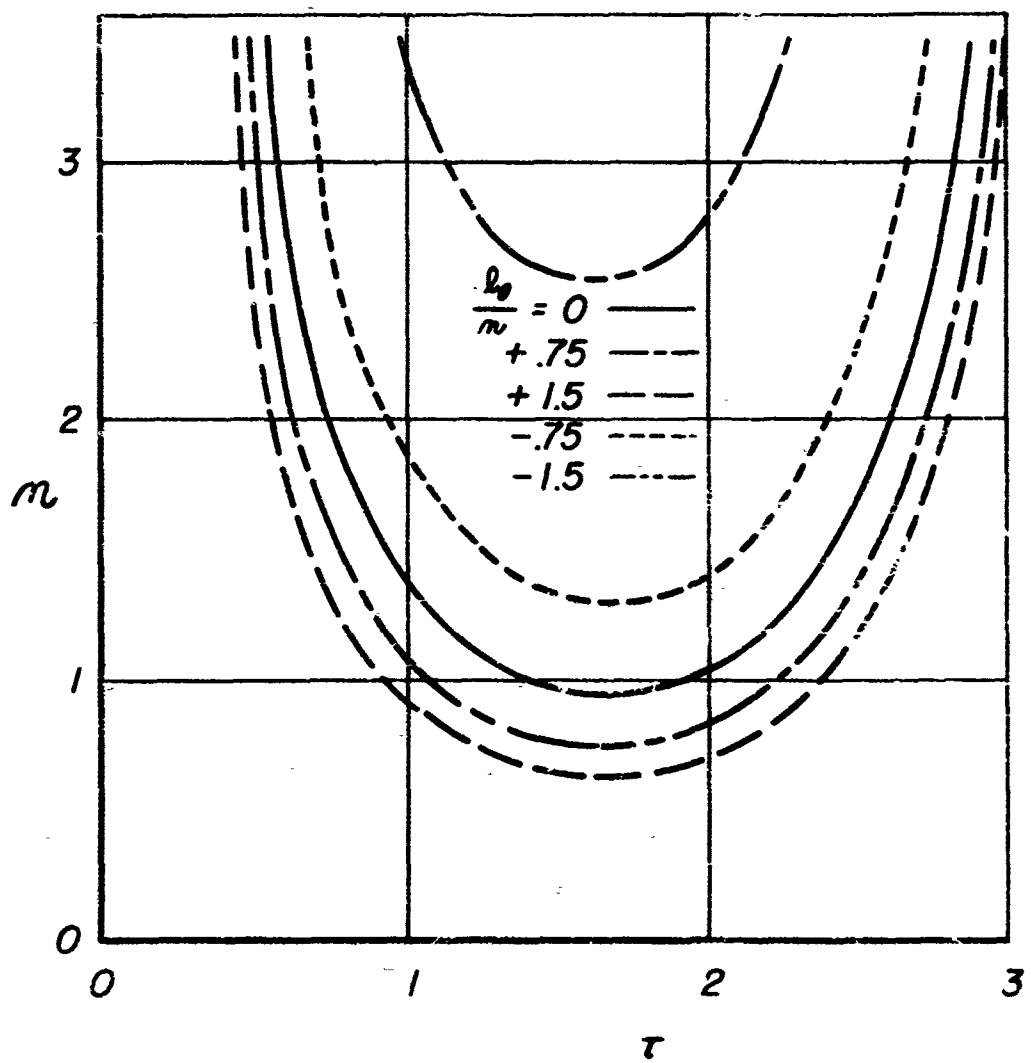

JPR 851

Figure 27

Right side of equation (2.74)
for $\bar{u}_e = 0.10$, $\beta = 0.4$, $c = 1.54$, $\zeta = 2.45$

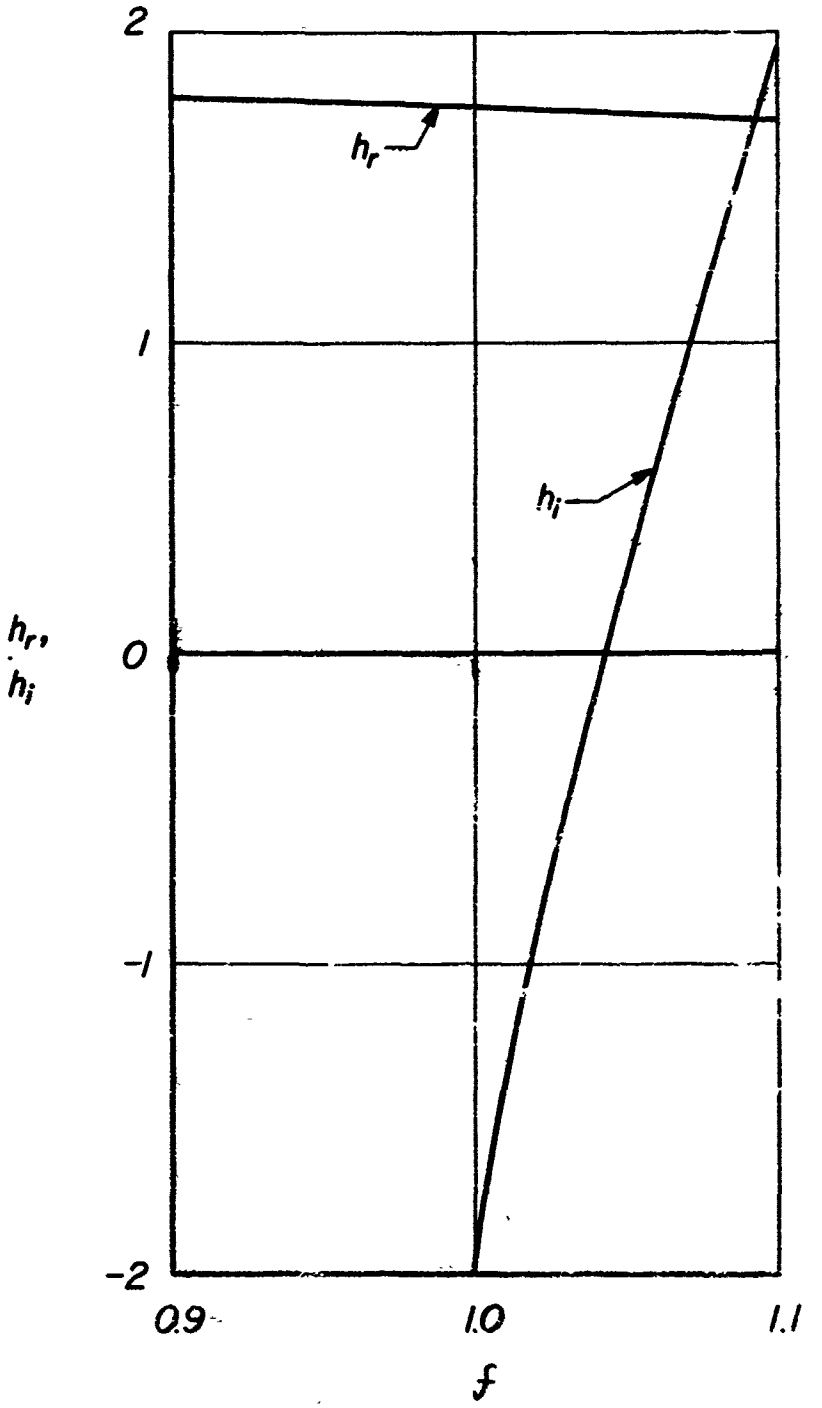

JPR 852

Figure 28

Theoretical radial velocity effect on stability limits, first tangential mode, uniformly distributed combustion

$\bar{u}_e = 0.10$

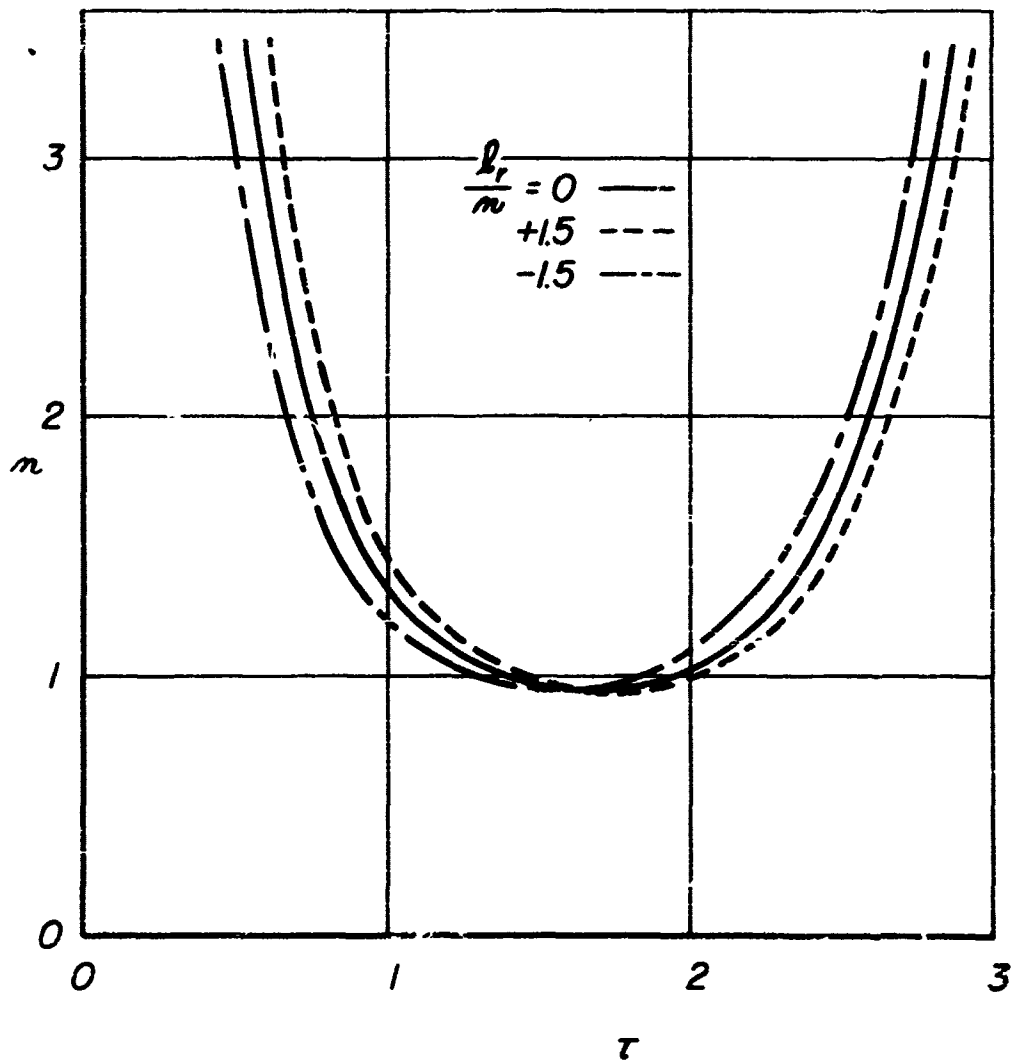

JPR 853

Figure 29

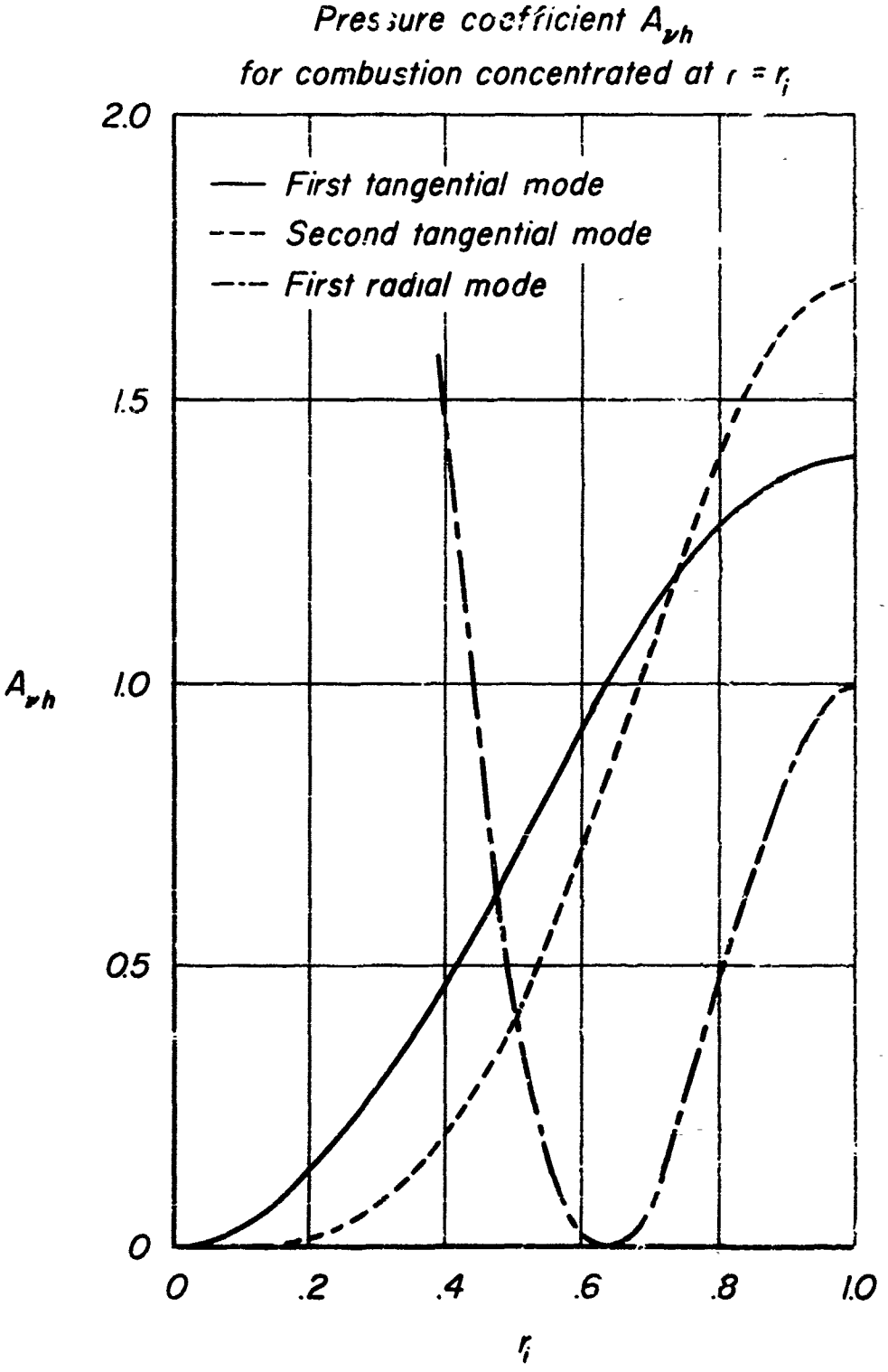

JPR 869

Figure 30

Expansion coefficient A_{11} for rectangular injection distribution

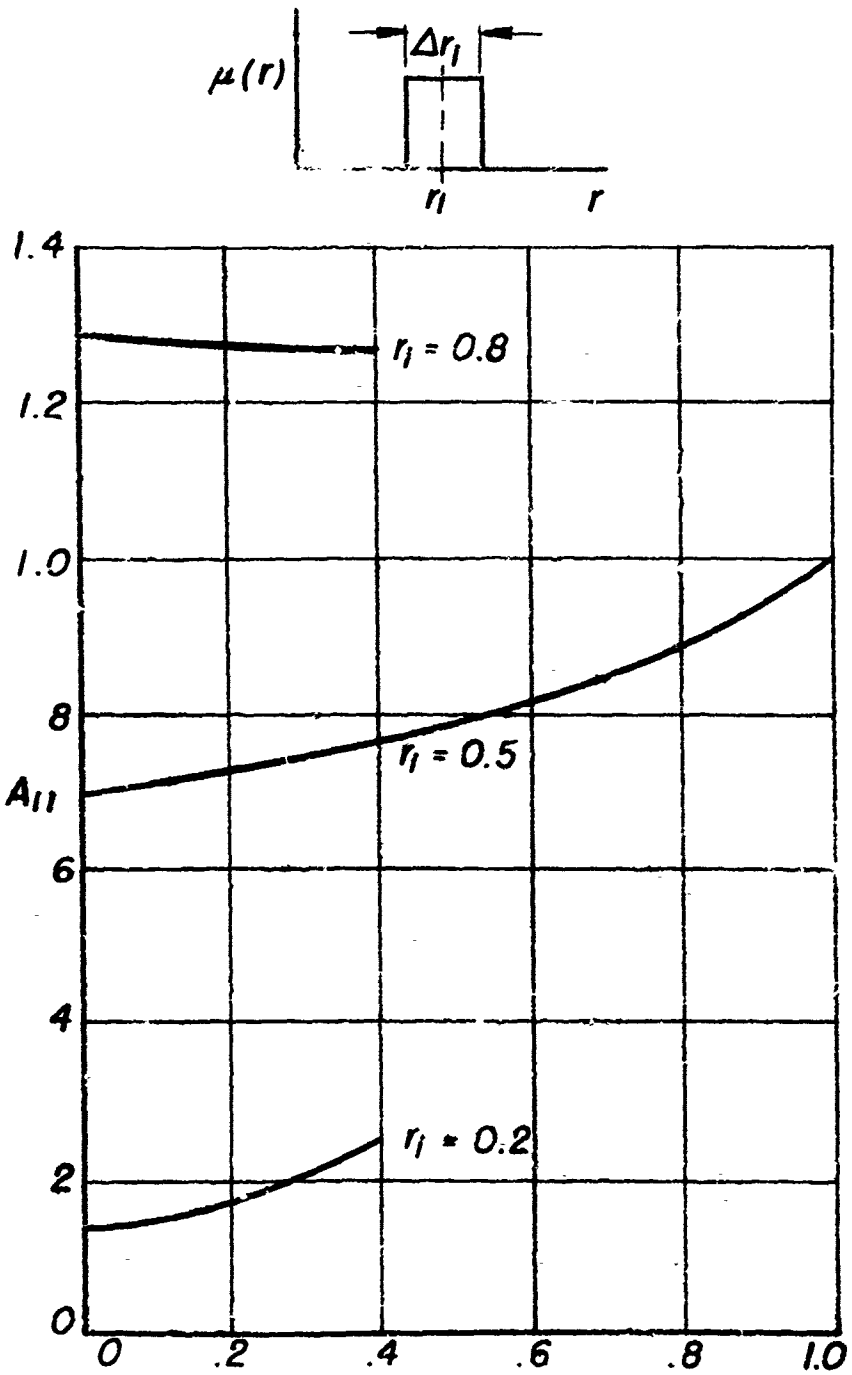

Figure 31

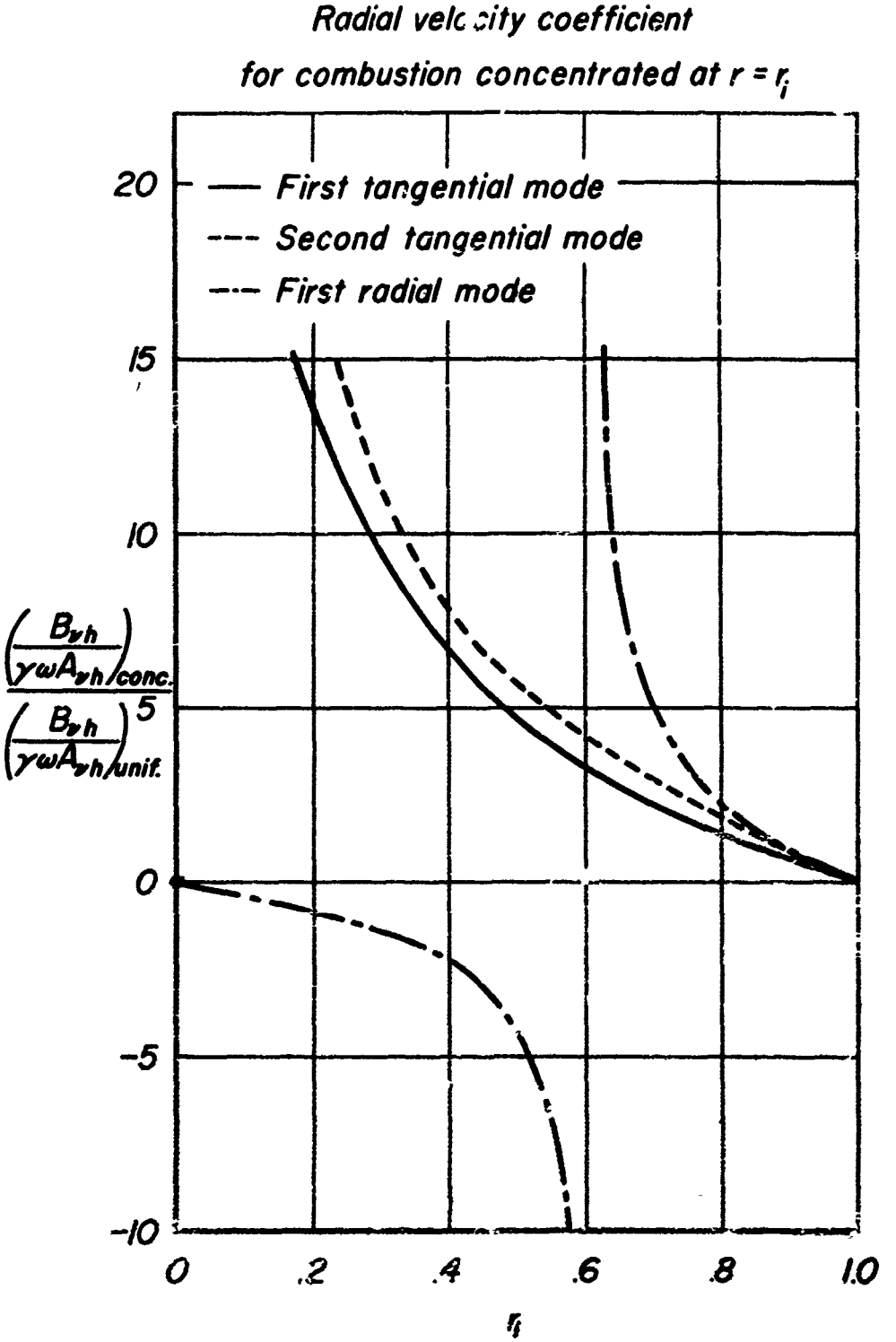

JPR 670

Figure 32

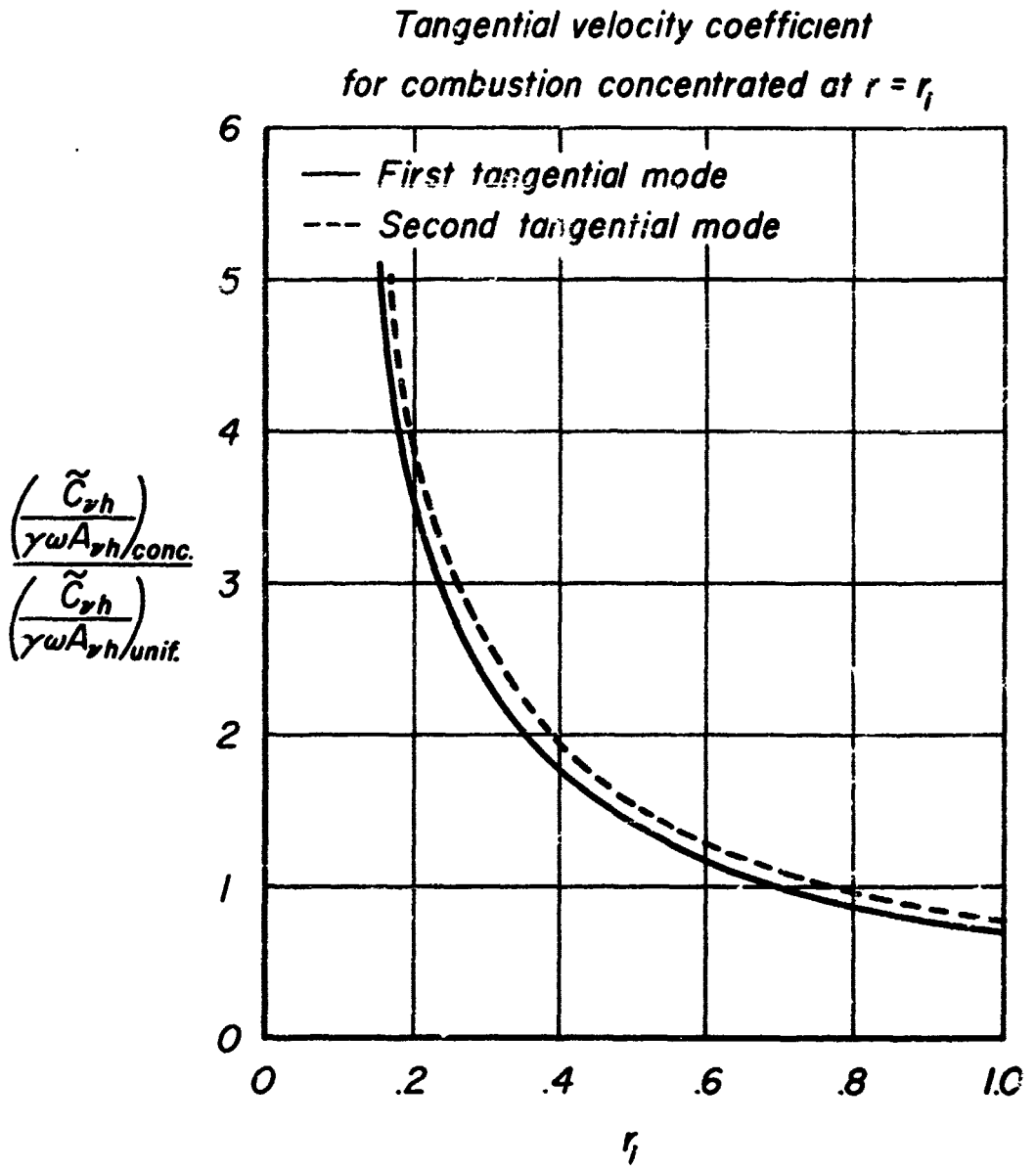

JPR 871

Figure 33

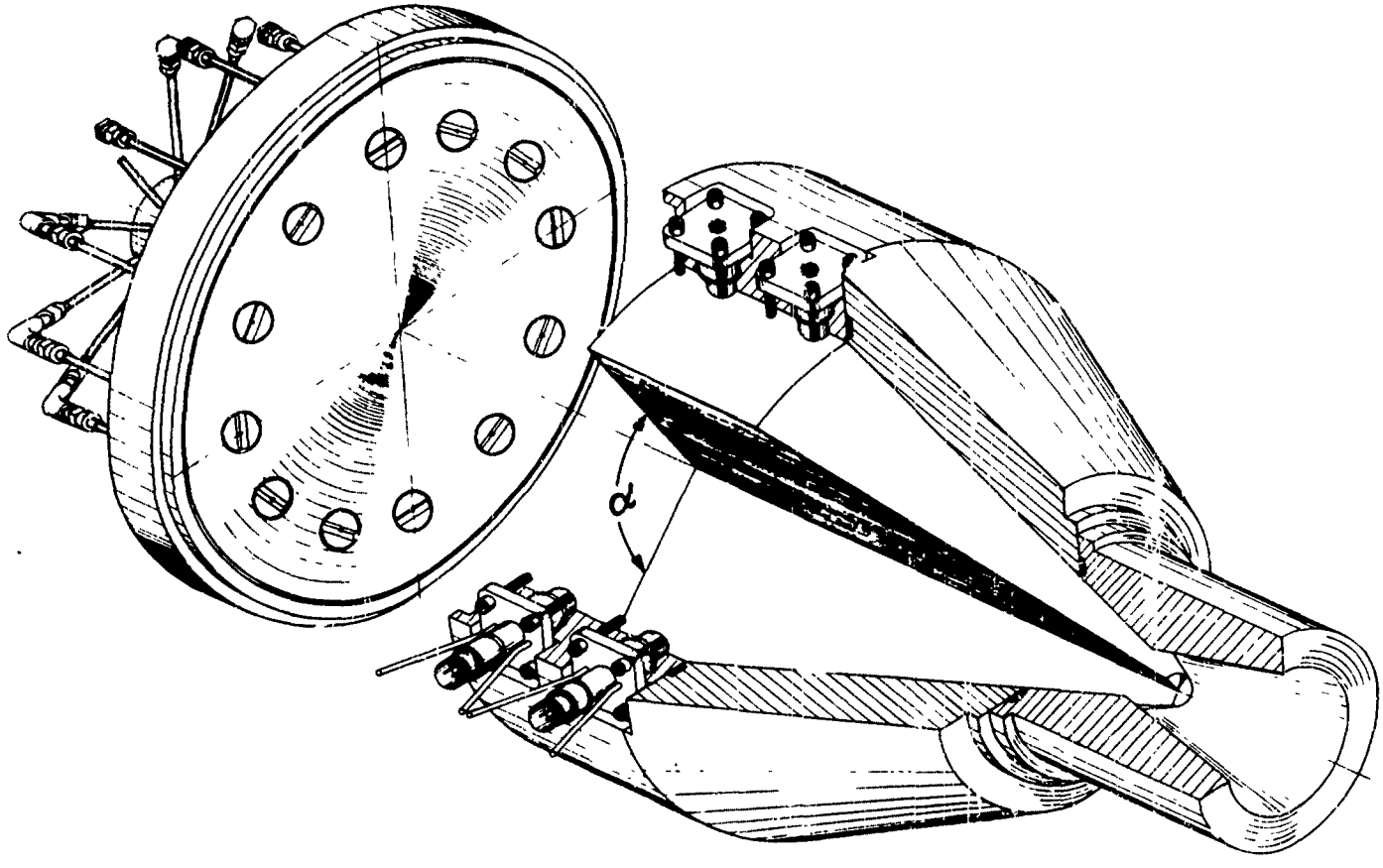

Variable angle sector motor with radially concentrated injection

Figure 34

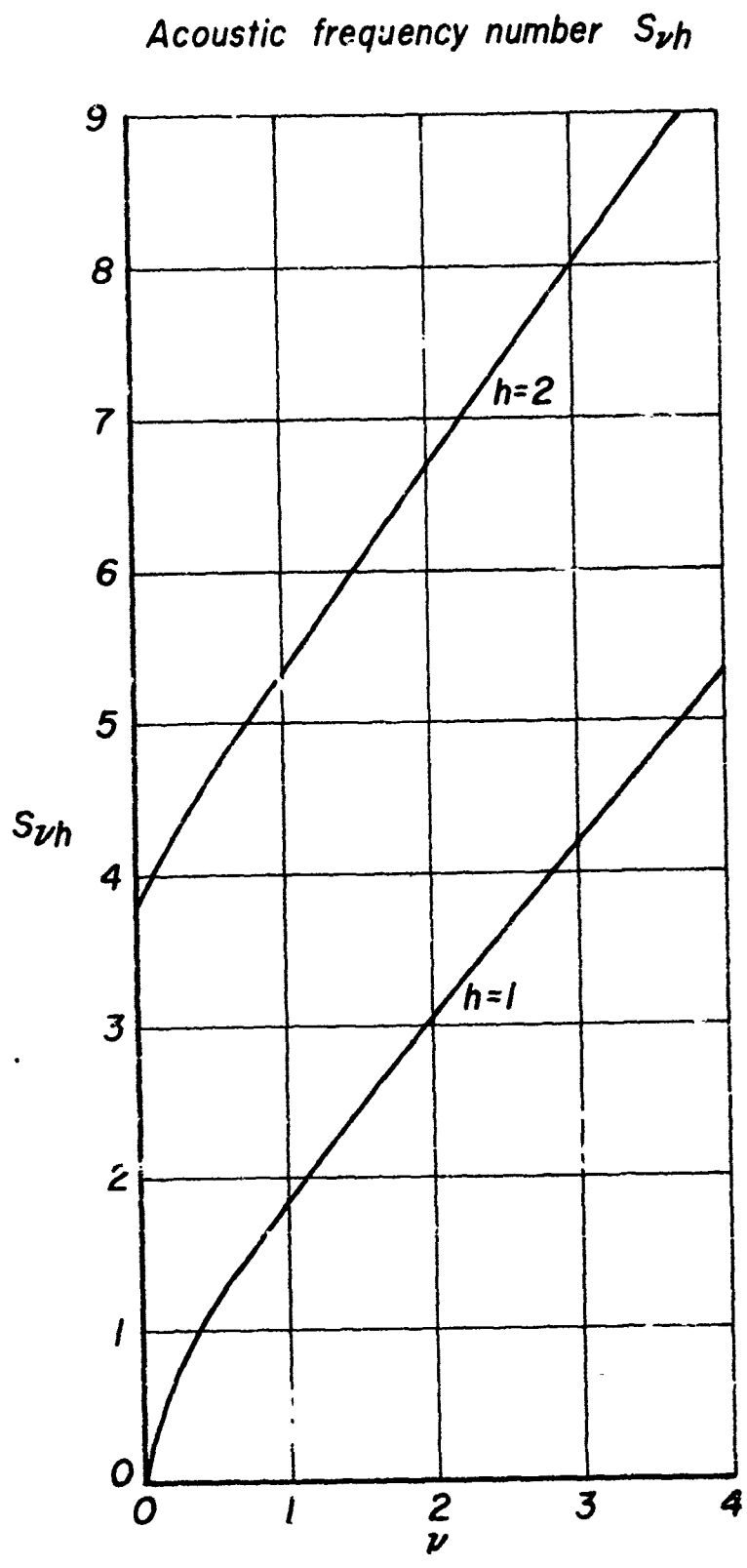

Figure 35

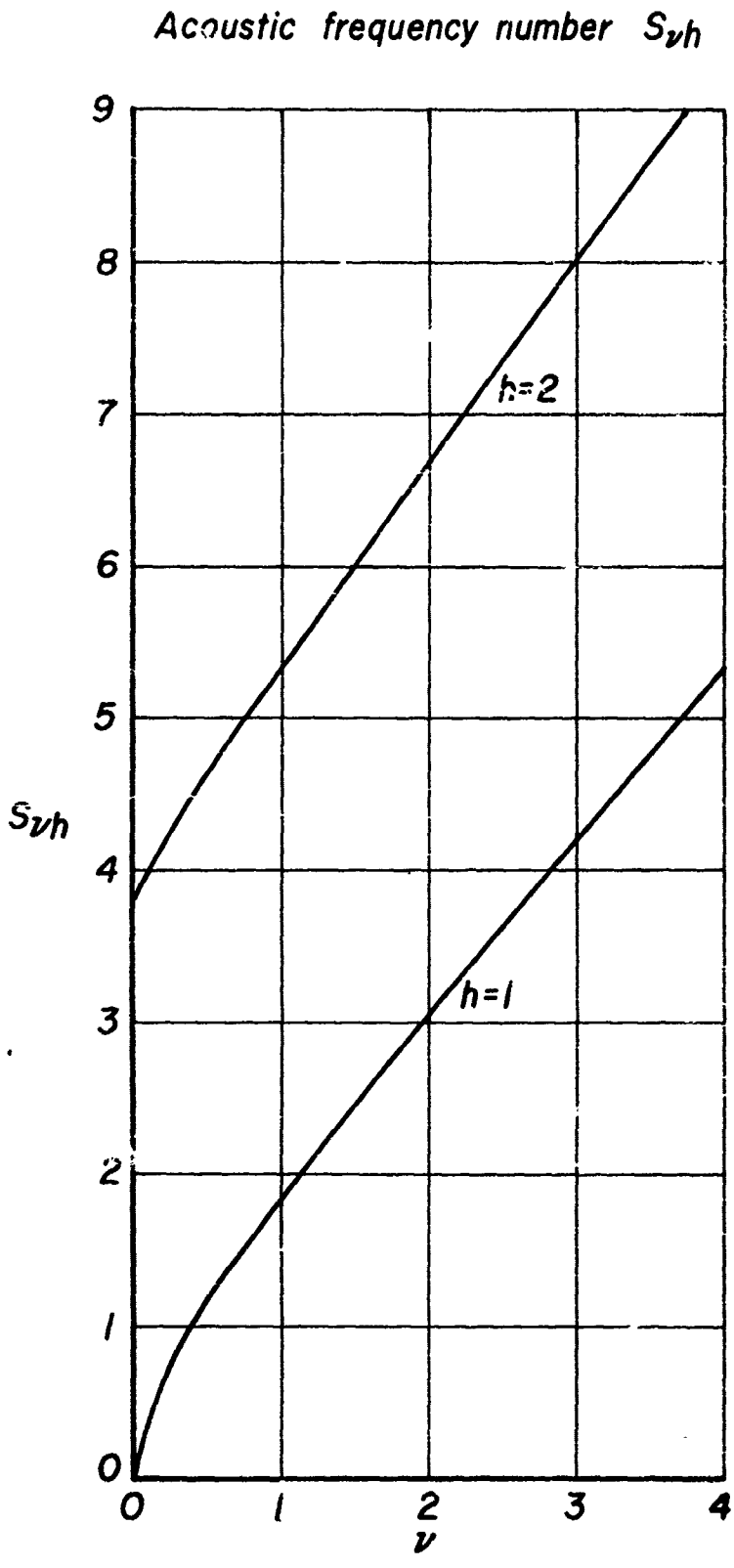
Acoustic frequency number $S_{\nu h}$
9
8
7
6
5
4
3
2
1
0
$S_{\nu h}$
h=2
h=1
0
1
2
3
4
ν

Figure 35

Expansion coefficient $A_{\nu l}$
for combustion concentrated at $r = r_i$

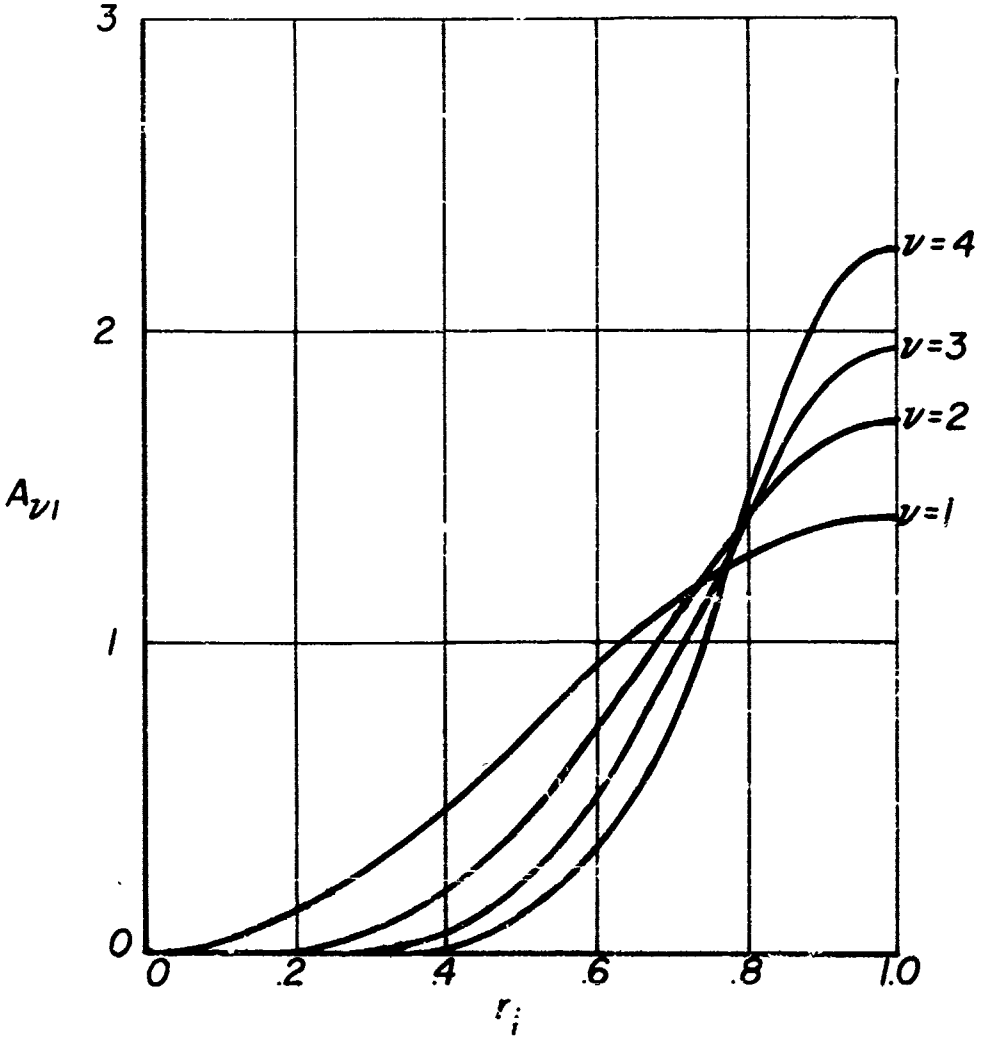

JFR 733

Figure 36

Expansion coefficient $B_{\nu 1}$
for combustion concentrated at $r = r_i$

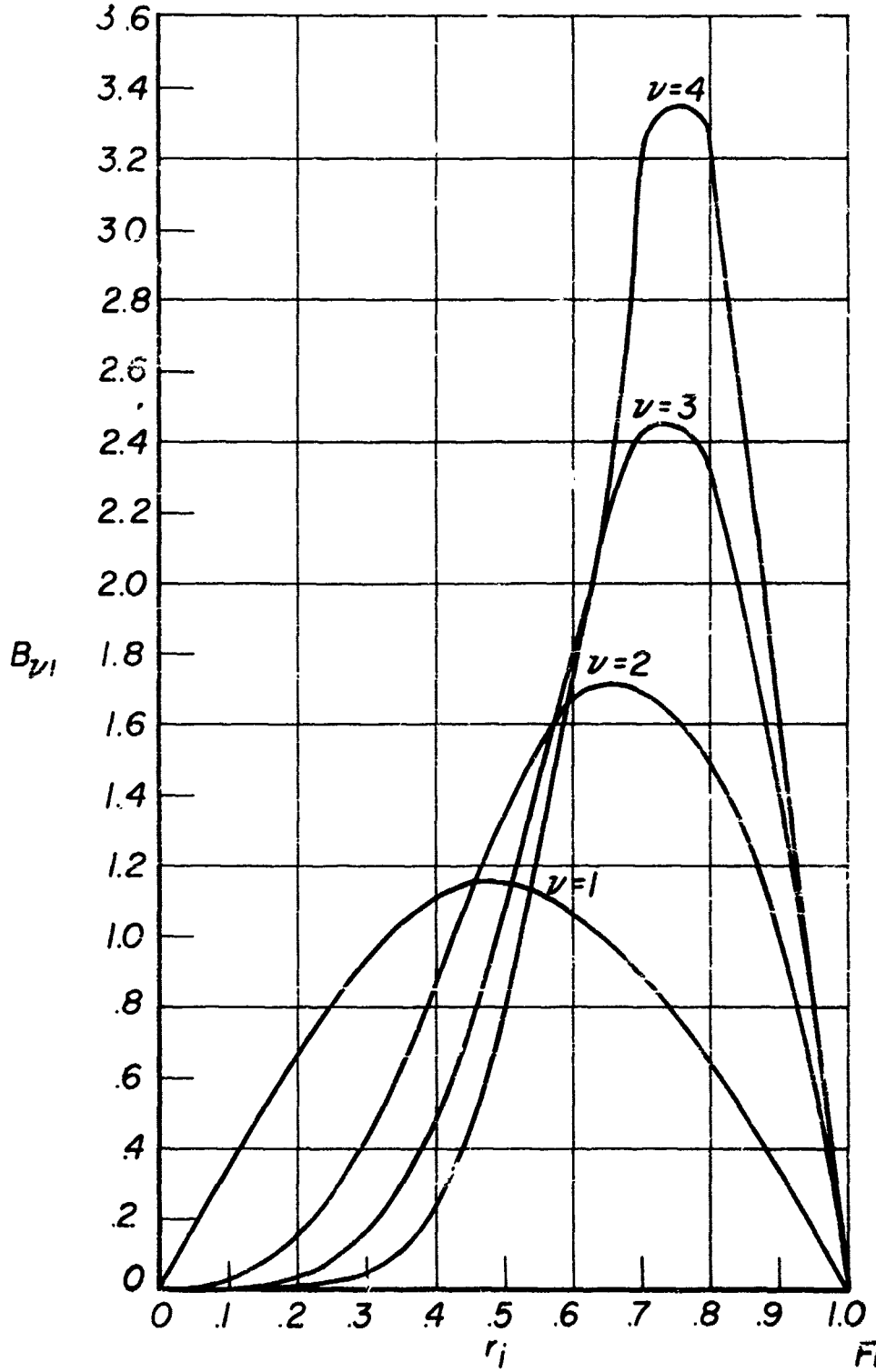

Figure 37

Expansion coefficient $C_{\nu 1}$
for combustion concentrated at $r = r_i$

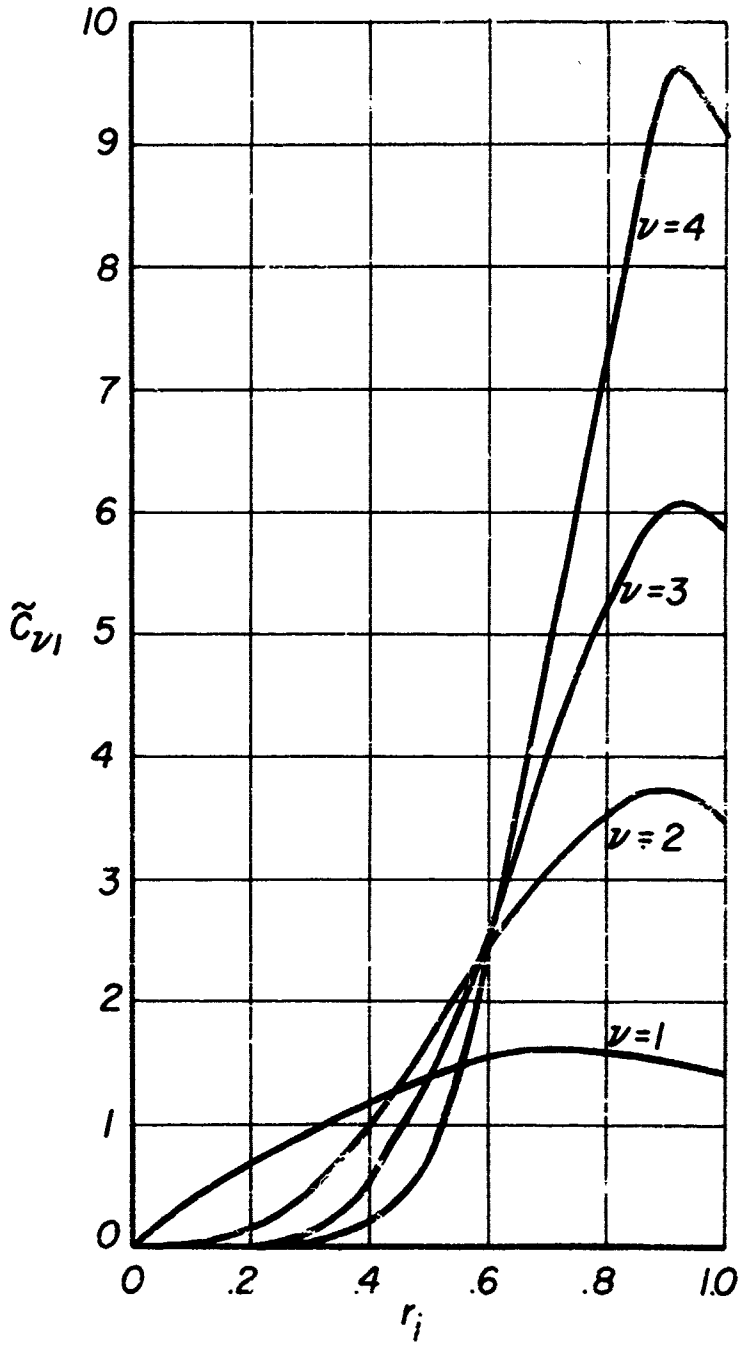

JPR 735

Figure 38

Theoretical stability limits for several sector angles, first tangential mode, uniformly distributed combustion, $\bar{u}_\theta = 0.10$

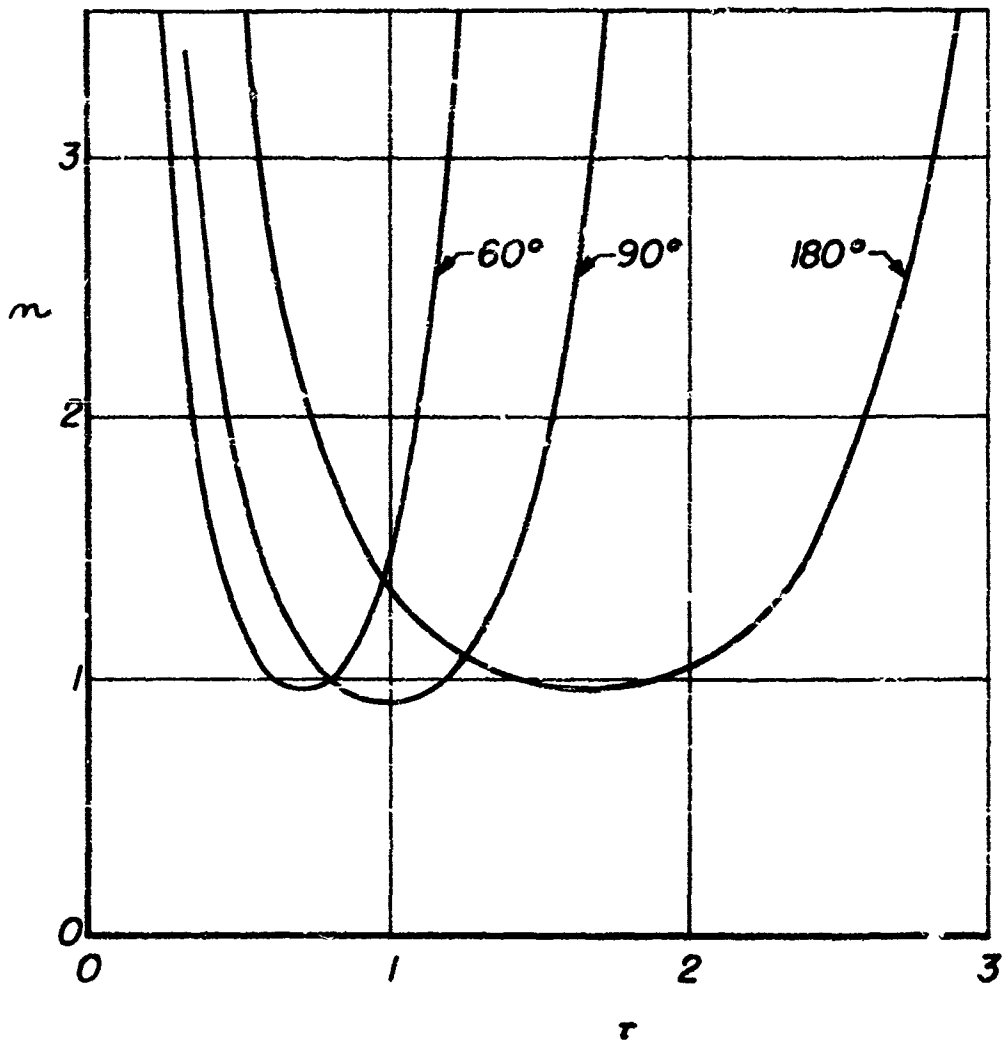

JPR 814

Figure 39

Theoretical stability limits for several sector angles, first tangential mode, combustion concentrated at $r_i = 8/9$ $\bar{u}_\theta = 0.10$

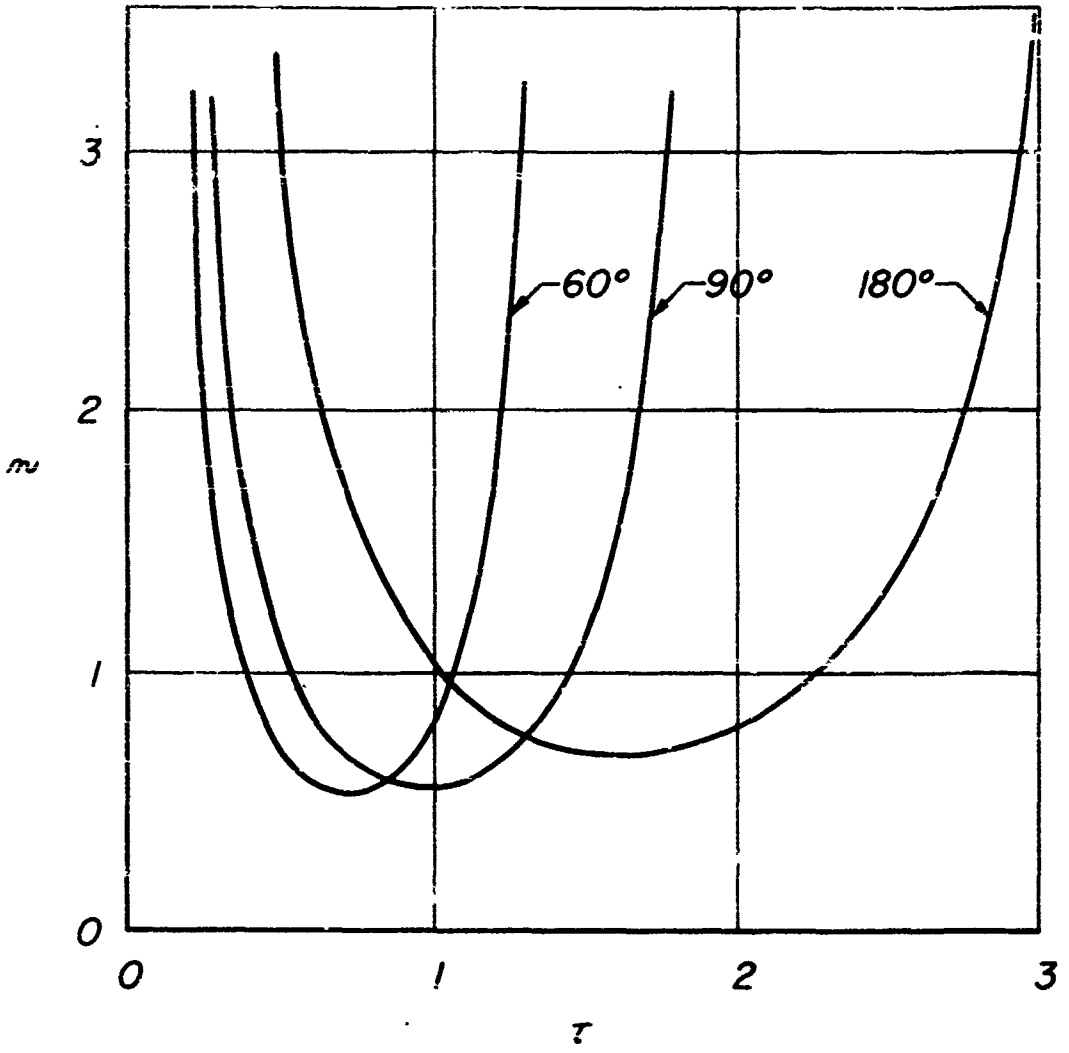

Figure 40

Theoretical stability limits for several sector angles first tangential mode, combustion concentrated at r_i=5/9

$\bar{u}_\theta = 0.10$

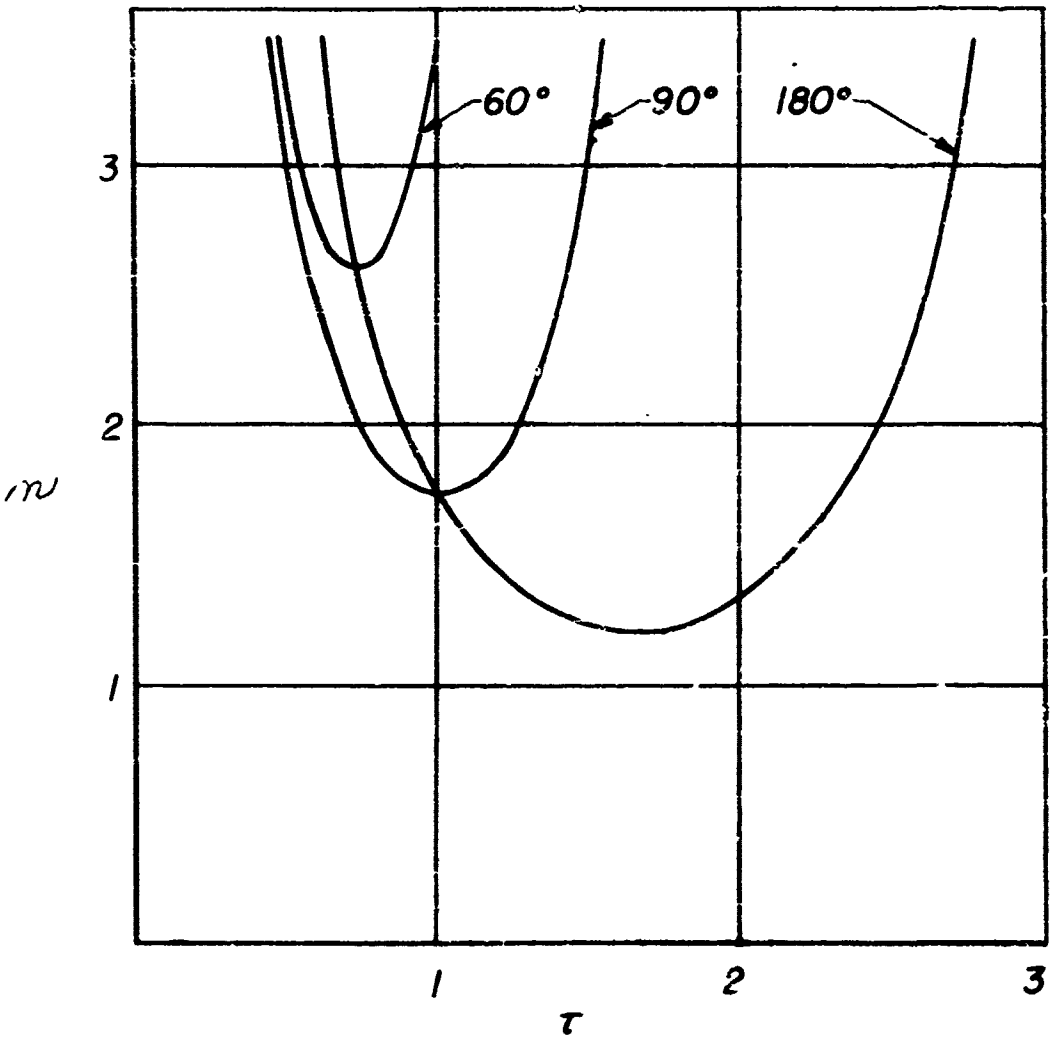

JPR 872

Figure 41

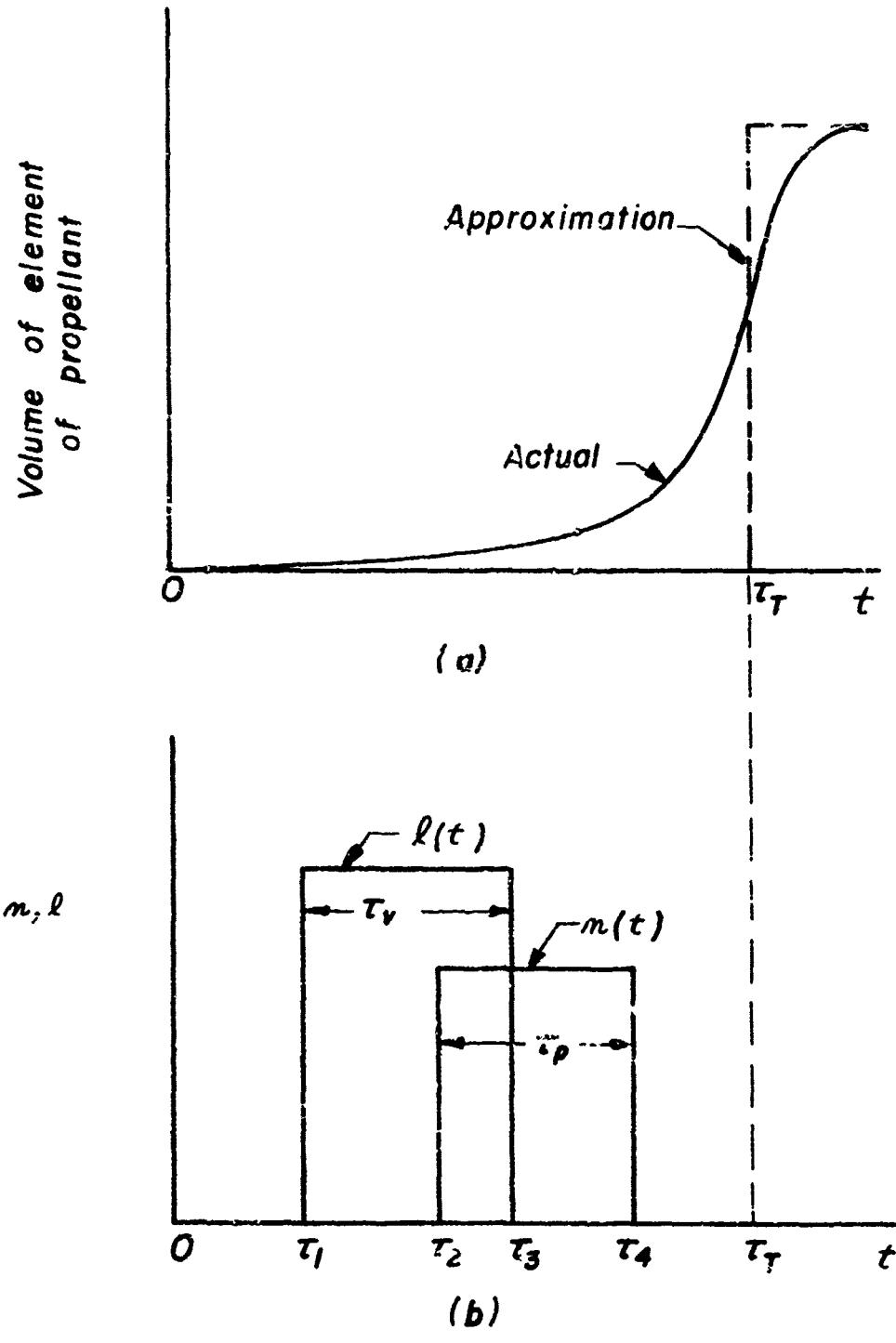

Time lag schematization

Figure 42

JPR 877

JPR 454

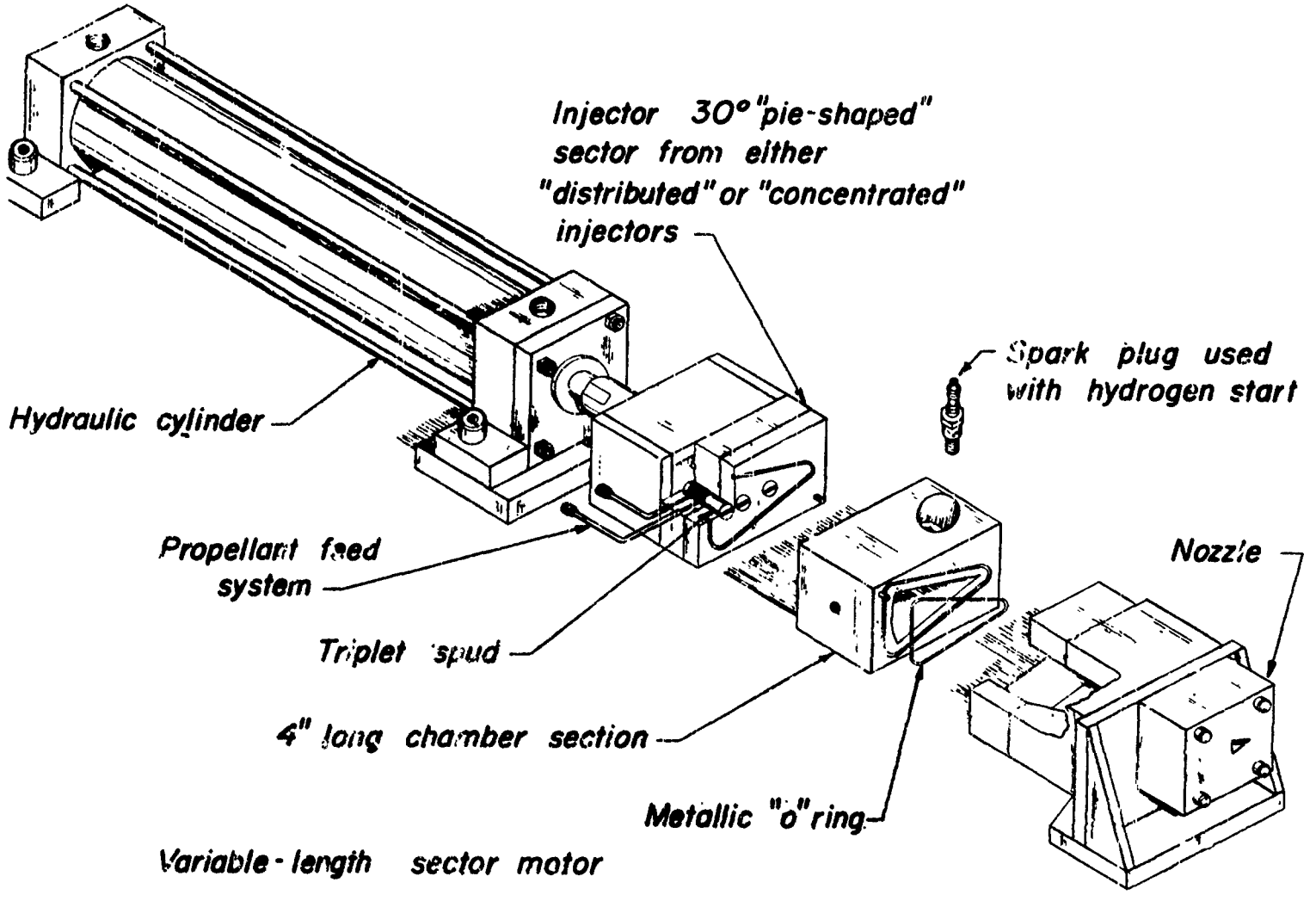

Variable - length sector motor

Figure 43

Typical oscillation amplitudes in a sector motor

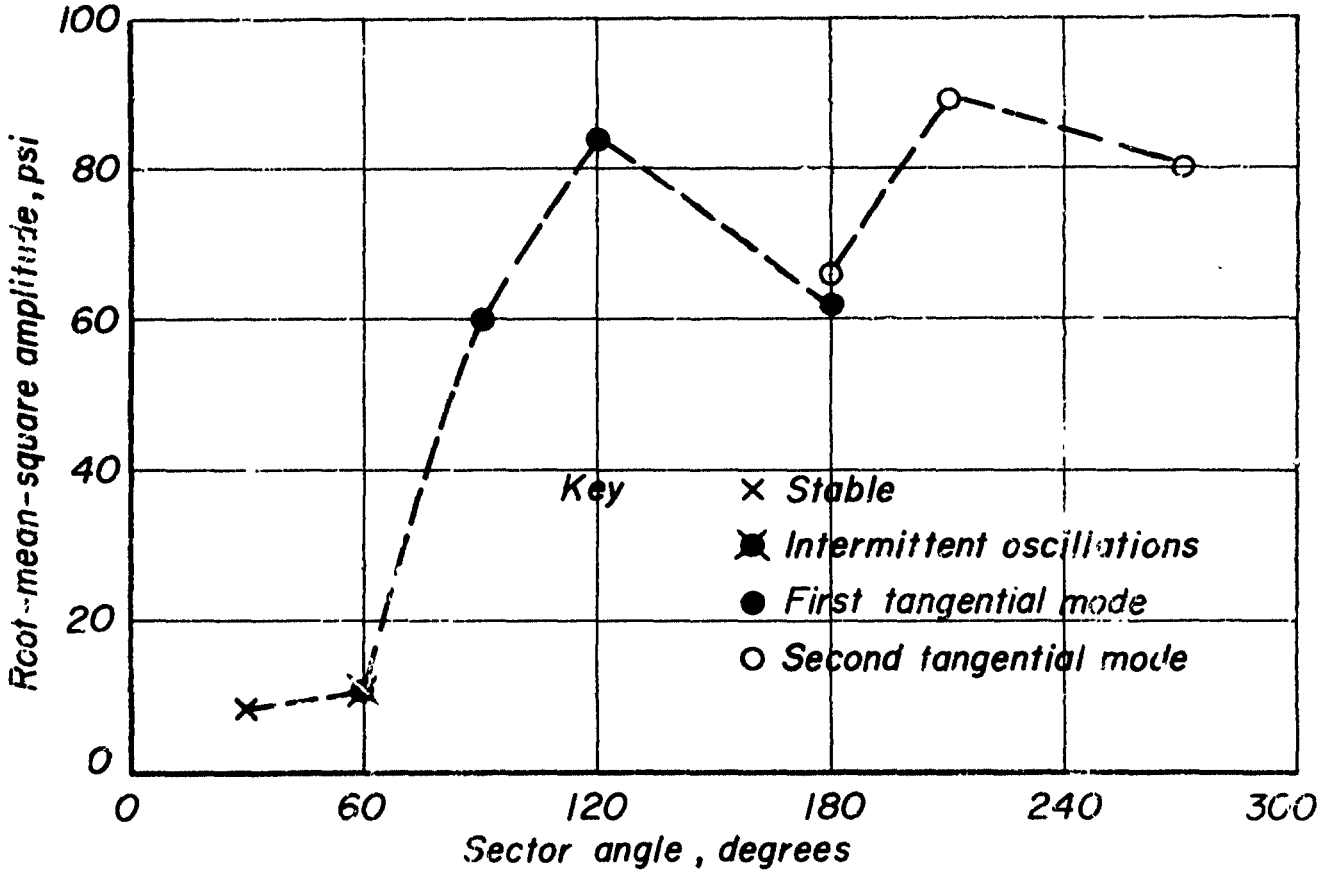

Figure 44

Standing mode wave shapes,
first tangential mode,
180° sector motor

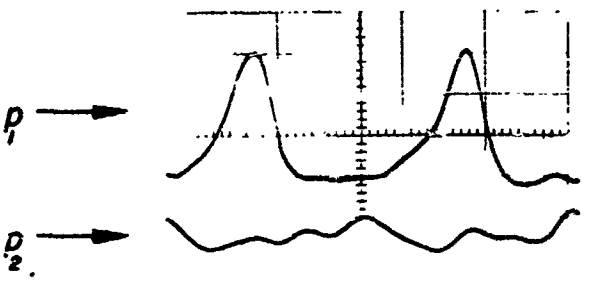

(a) Pressure traces

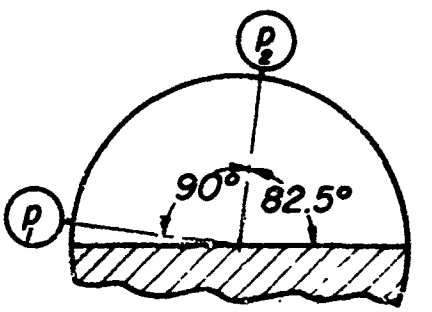

(b) Location of pressure transducers

Figure 45

Tangential orientation sector tests
9" chamber, 8" injector, $\overline{R}_{design}$ = 1.4,
p_c (nominal) = 150 psia, F (nominal) = 1000 lb

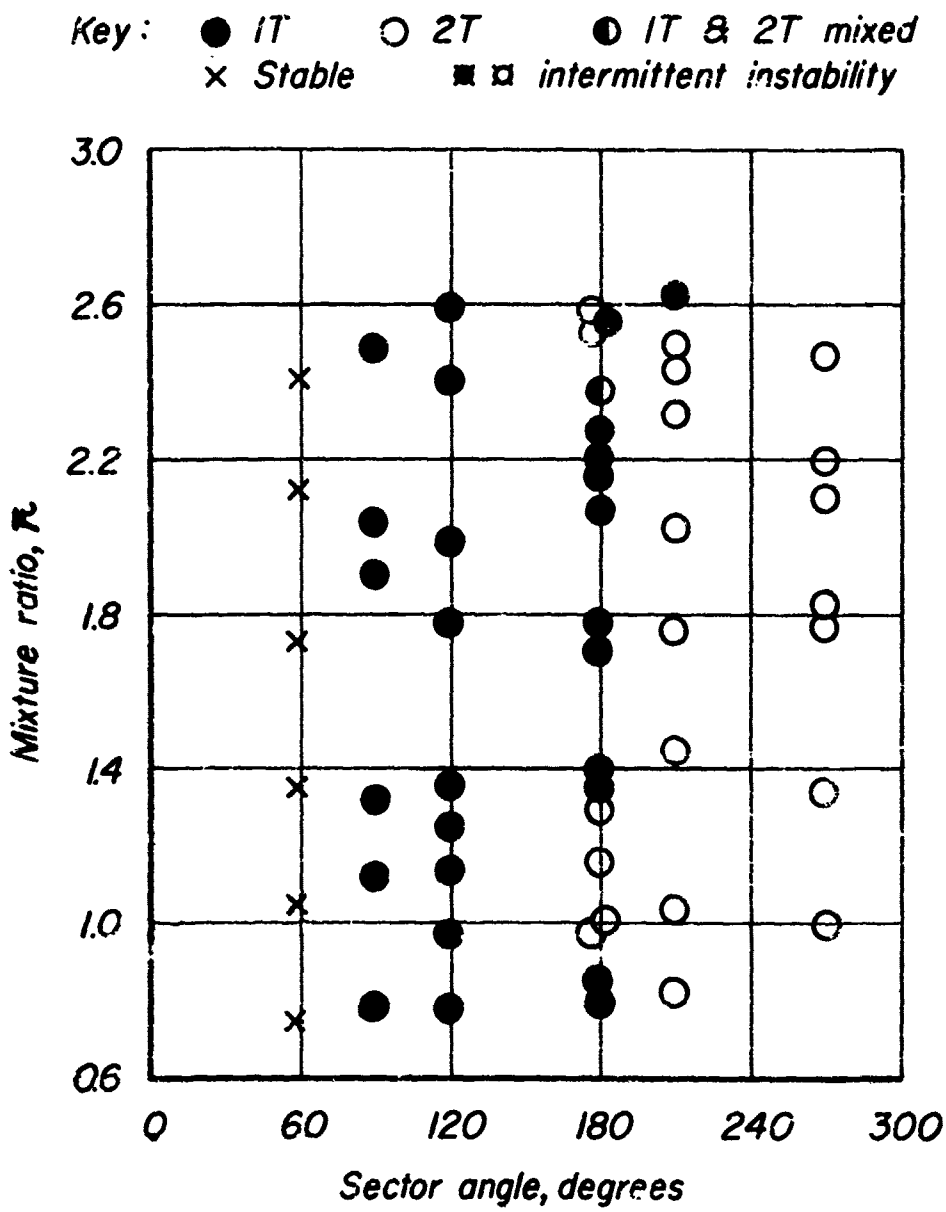

JPR 861

Figure 46

Theoretical sector motor stability limits,
first tangential mode, 9" chamber diameter,
8" injection diameter, p_c = 150 psia, F = 1000 lb
no velocity effects

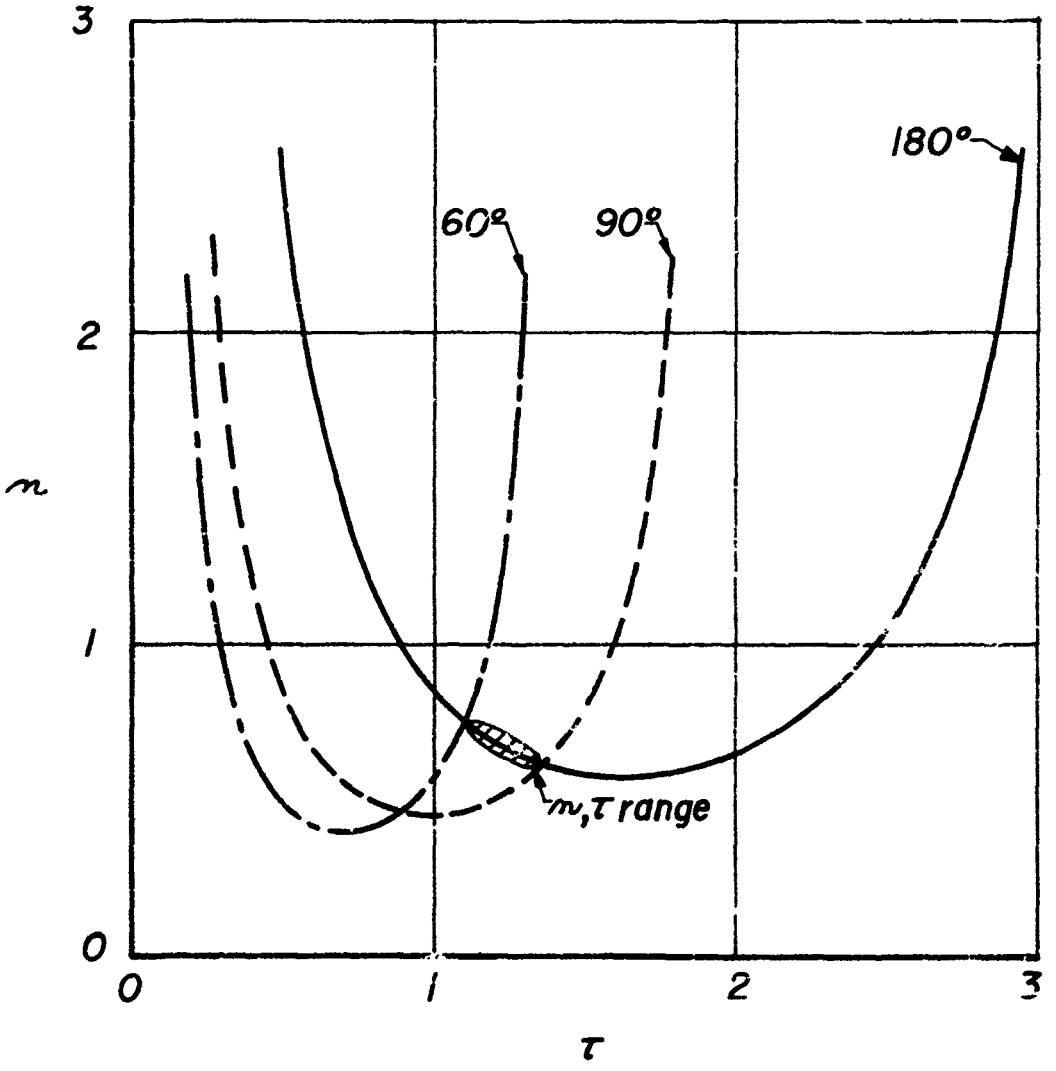

JPR 879

Figure 47

Theoretical stability limits
for variable length sector motor,
first longitudinal mode

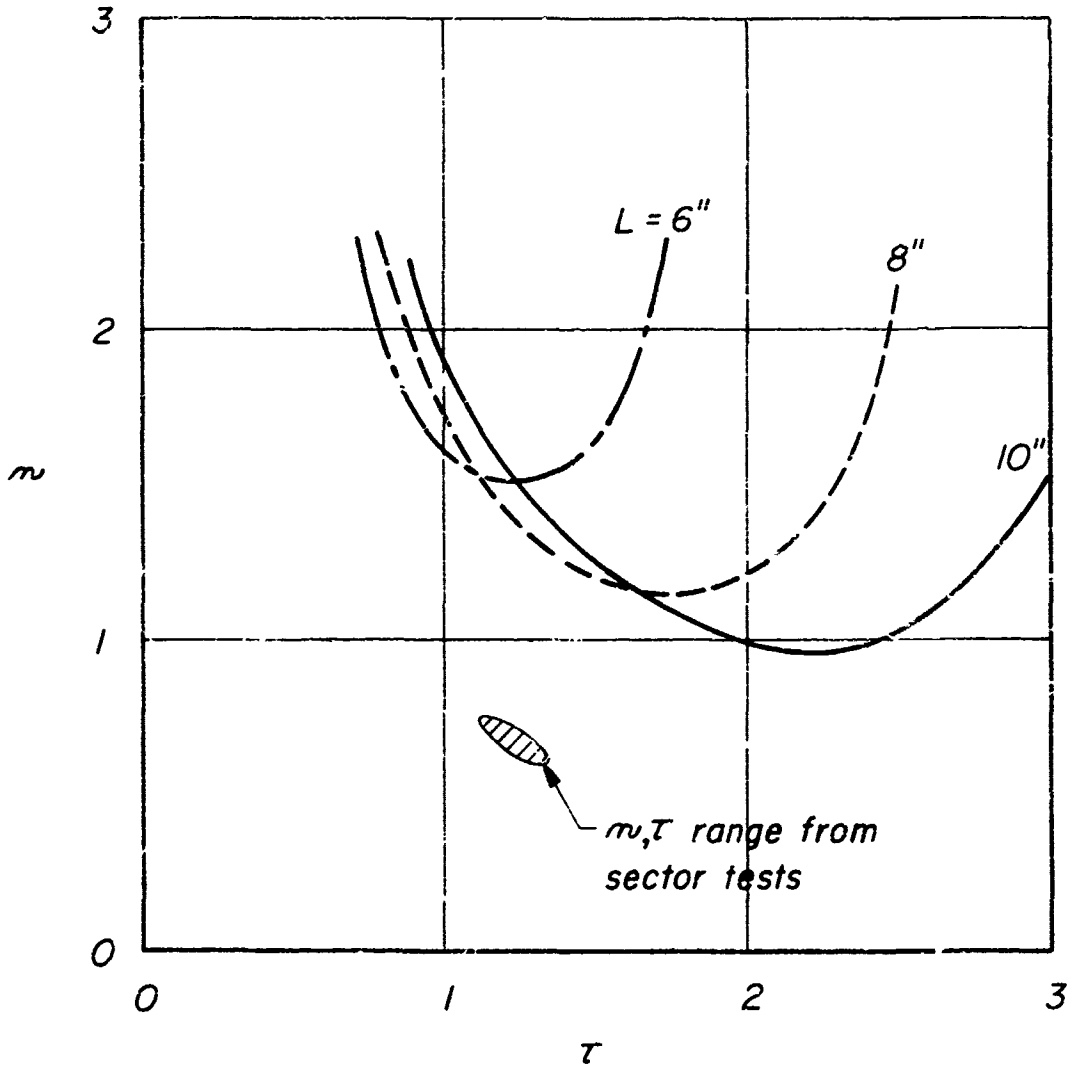

JPR 880

Figure 48

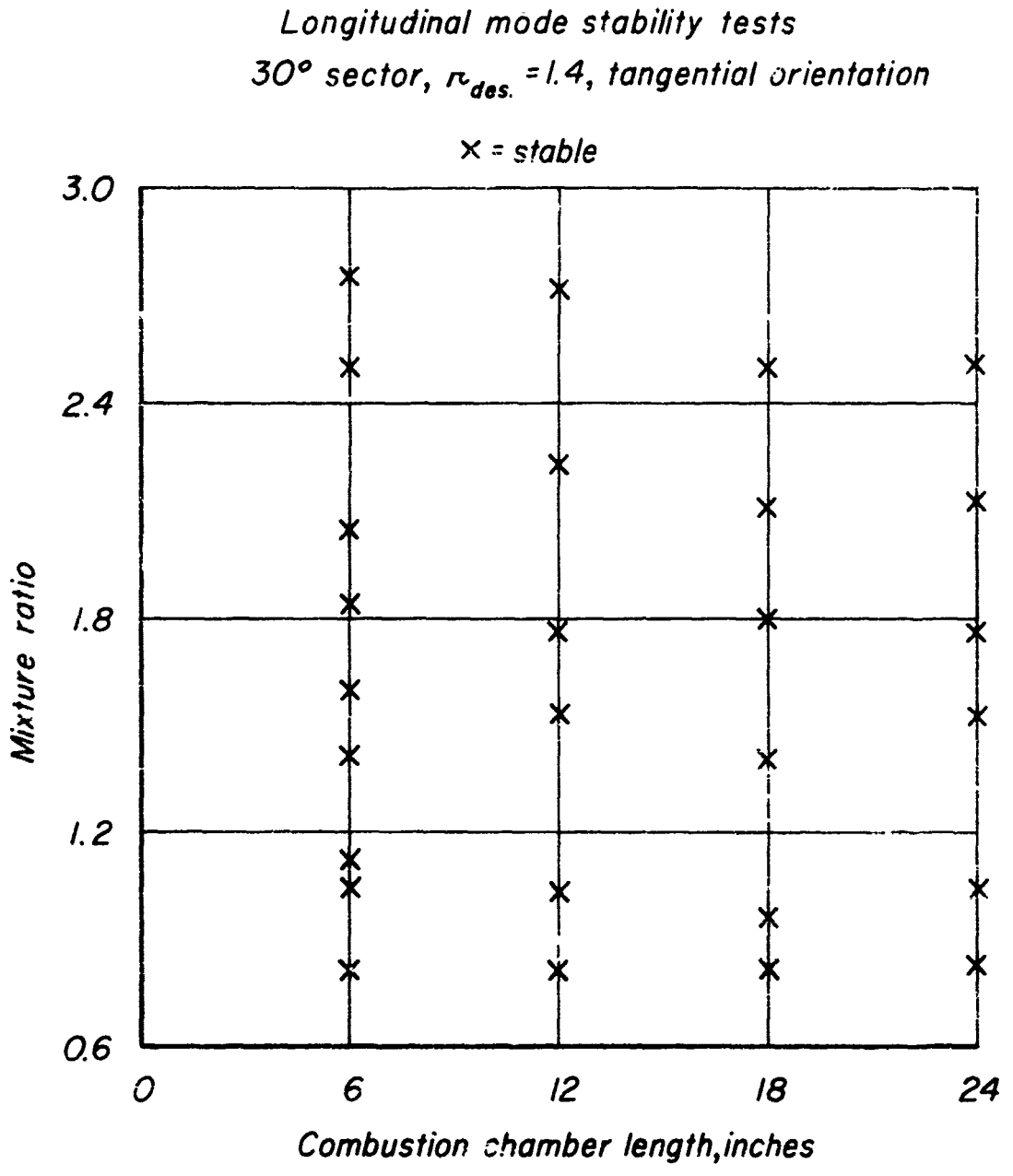

JPR 881

Figure 49

Theoretical sector motor stability limits,
first tangential mode, 6" chamber diameter
5" injection diameter, p_c = 150 psia, F = 1000 lb
no velocity effects

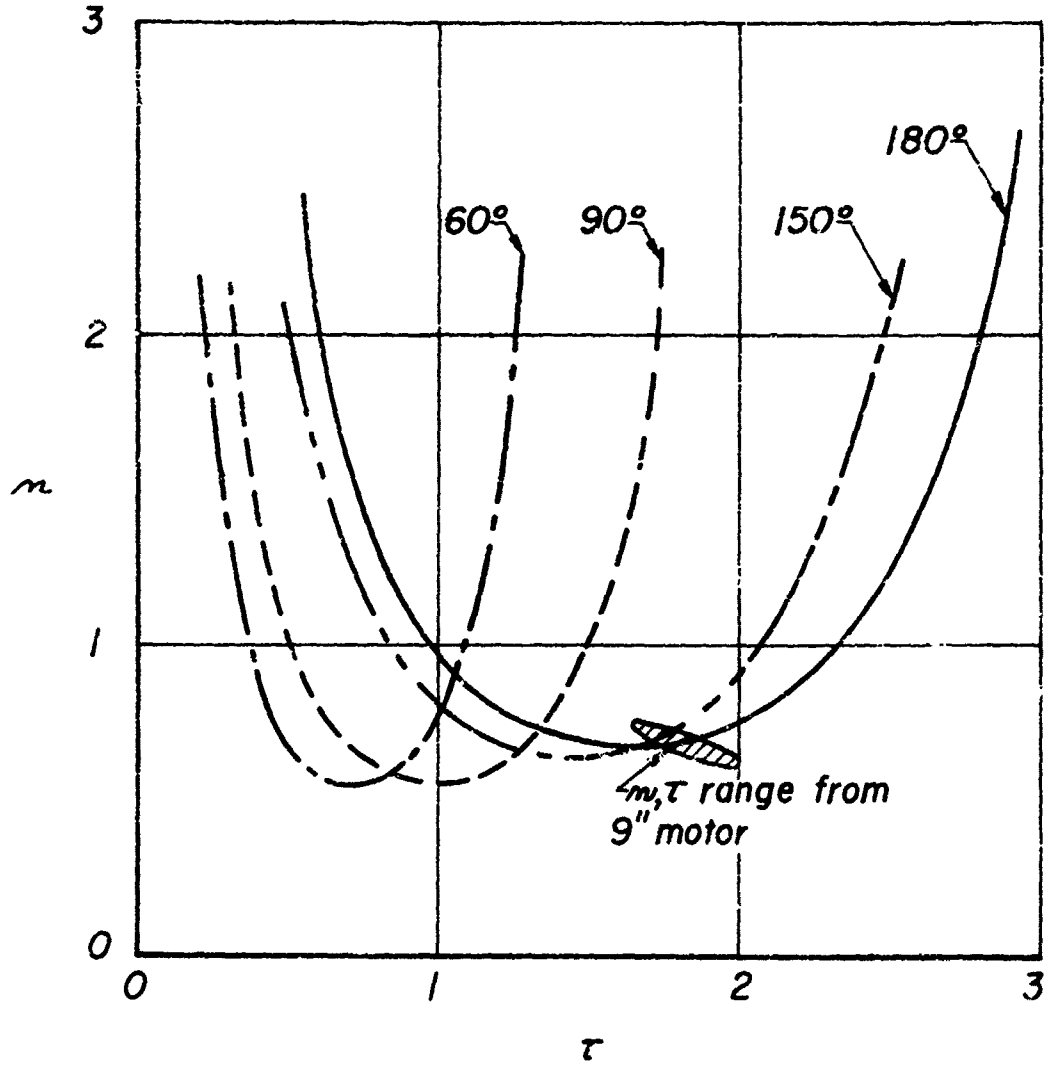

JPR 882

Figure 50

Tangential orientation sector tests
6" chamber, 5" injector, π_{design} = 1.4,
p_c (nominal) = 150 psia, F (nominal) = 1000 lb

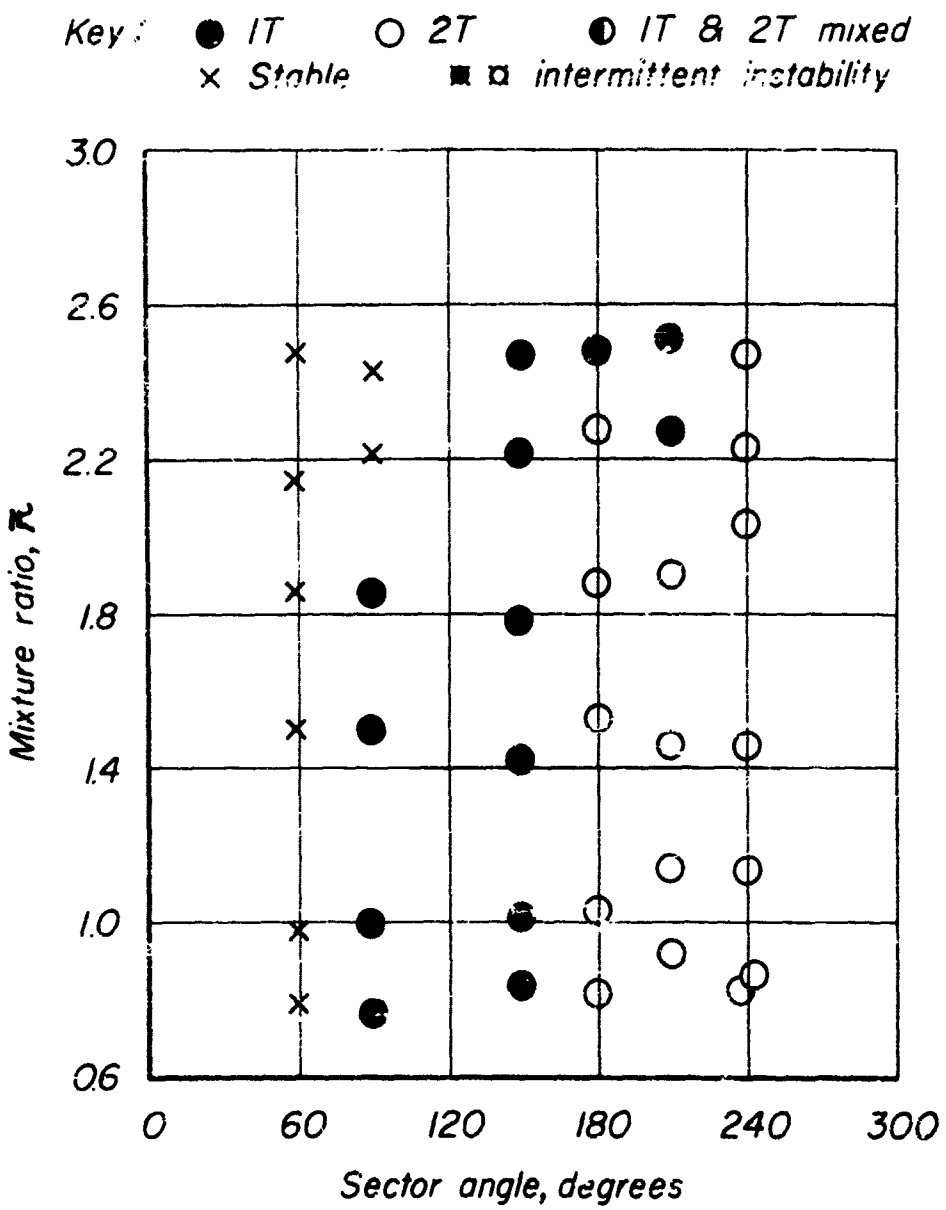

JPR 855

Figure 51

Theoretical sector motor stability limits,
first tangential mode, 9" chamber diameter
5" injection diameter, p_c = 150 psia, F = 1000 lb
no velocity effects

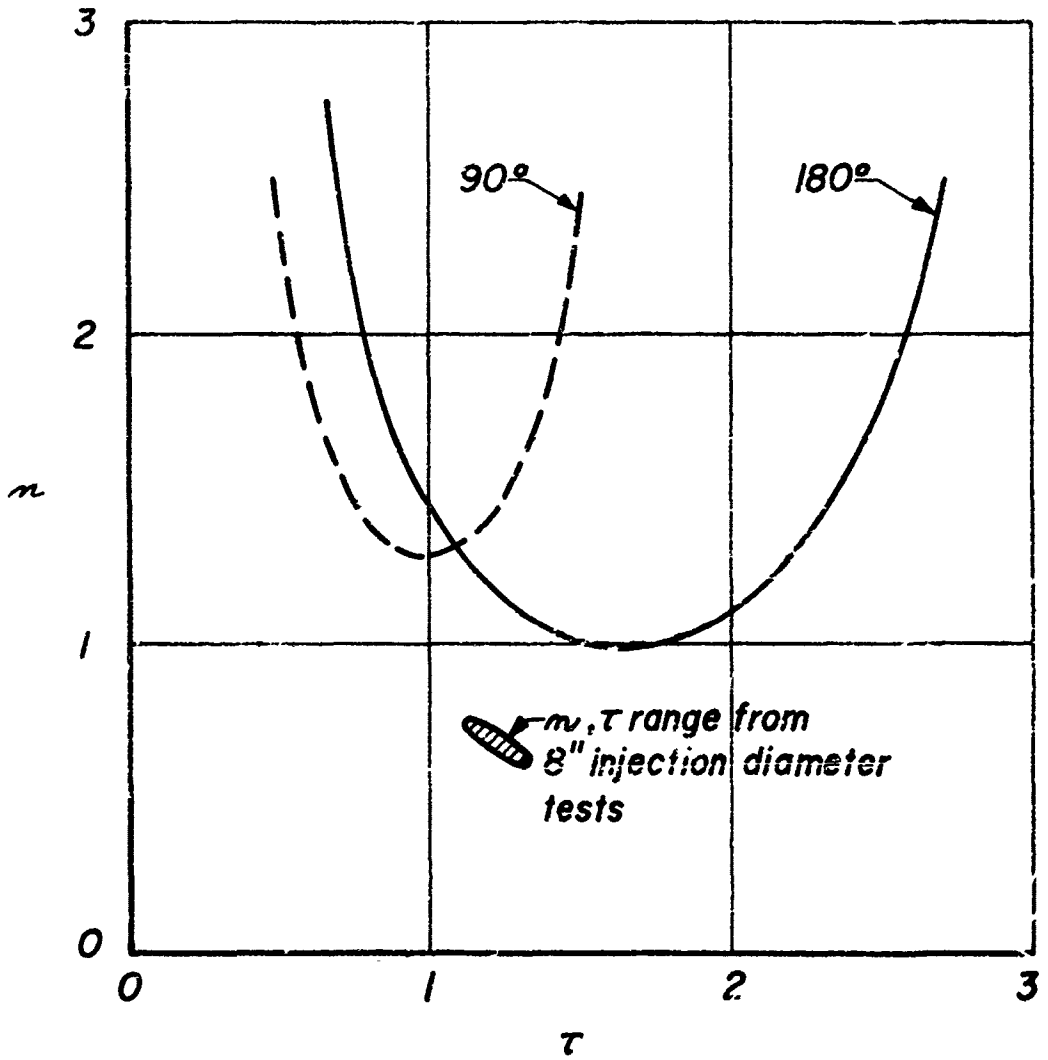

JPR 883

Figure 52

Tangential orientation sector tests
9" chamber, 5" injector, π_{design} = 1.4,
p_c (nominal) = 150 psia, F (nominal) = 1000 lb

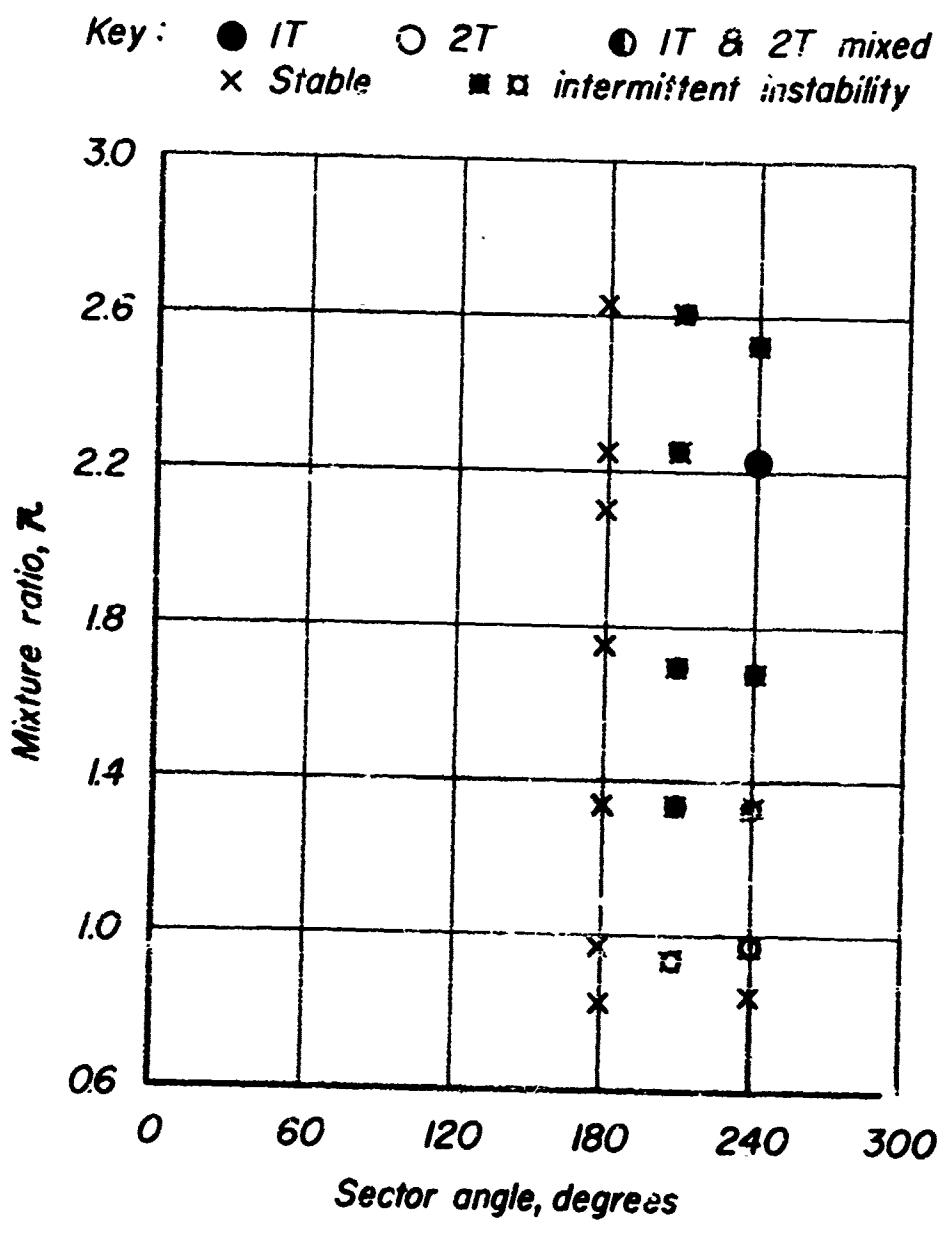

JPR 859

Figure 53

Theoretical tangential velocity effect,
combustion concentrated at $r_f = 8/9$,
$\bar{u}_e = 0.05$

——— no velocity effect

– – – velocity effect included

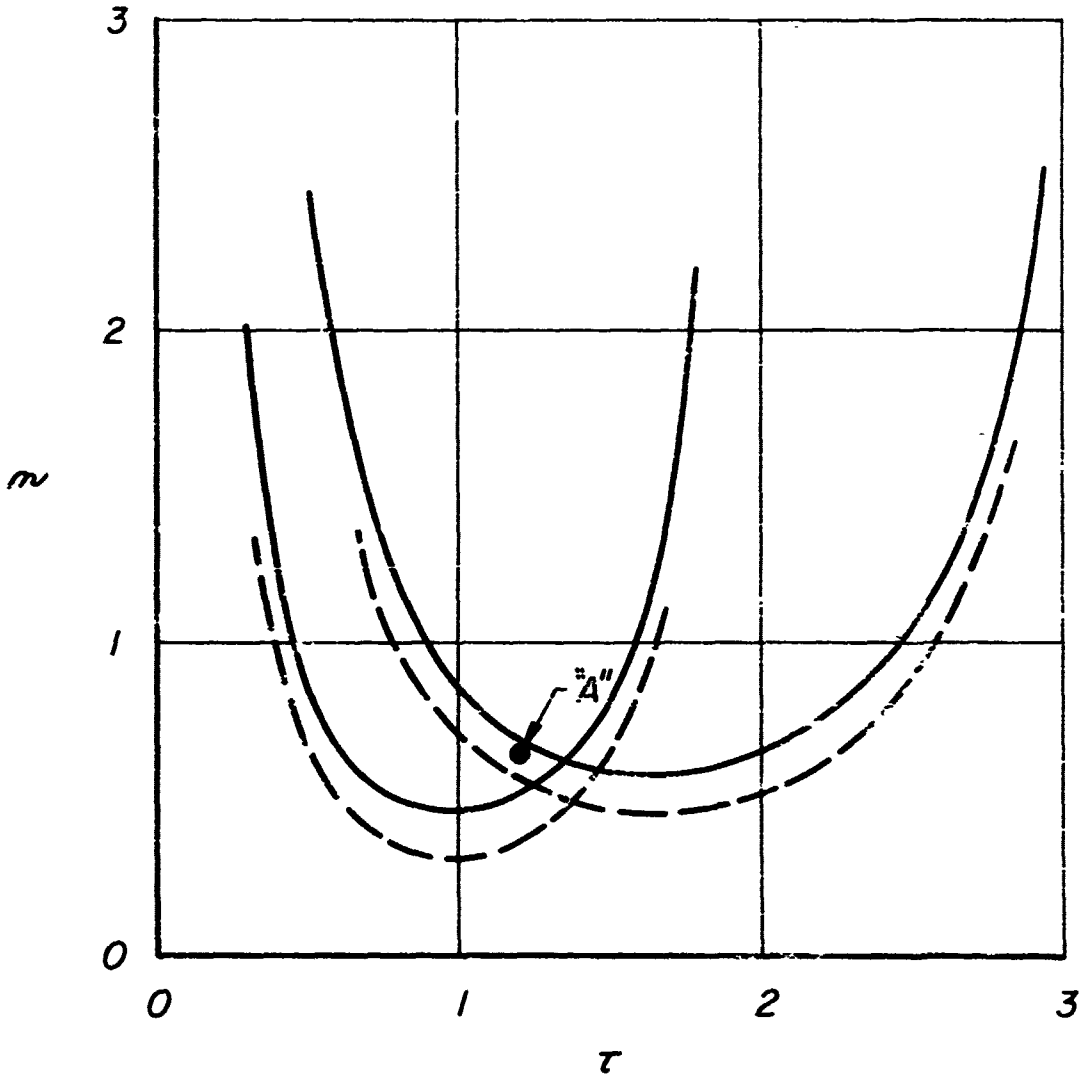

Figure 54

Radial orientation sector tests
9" chamber, 8" injector, π_{design} = 1.4,
p_c (nominal) = 150 psia, F (nominal) = 1000 lb

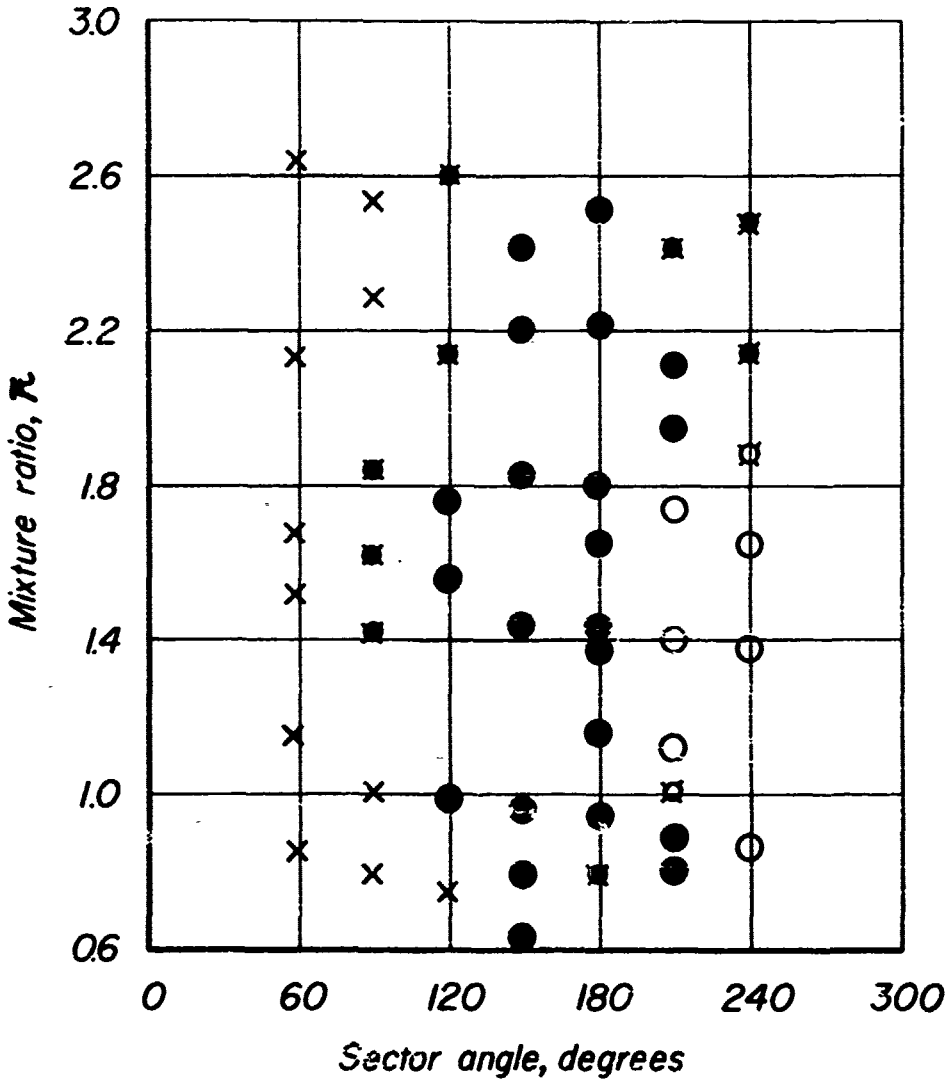

JPR 860

Figure 55

Radial orientation sector tests
6" chamber, 5" injector, π_{design} = 1.4,
p_c (nominal) = 150 psia, F (nominal) = 1000 lb

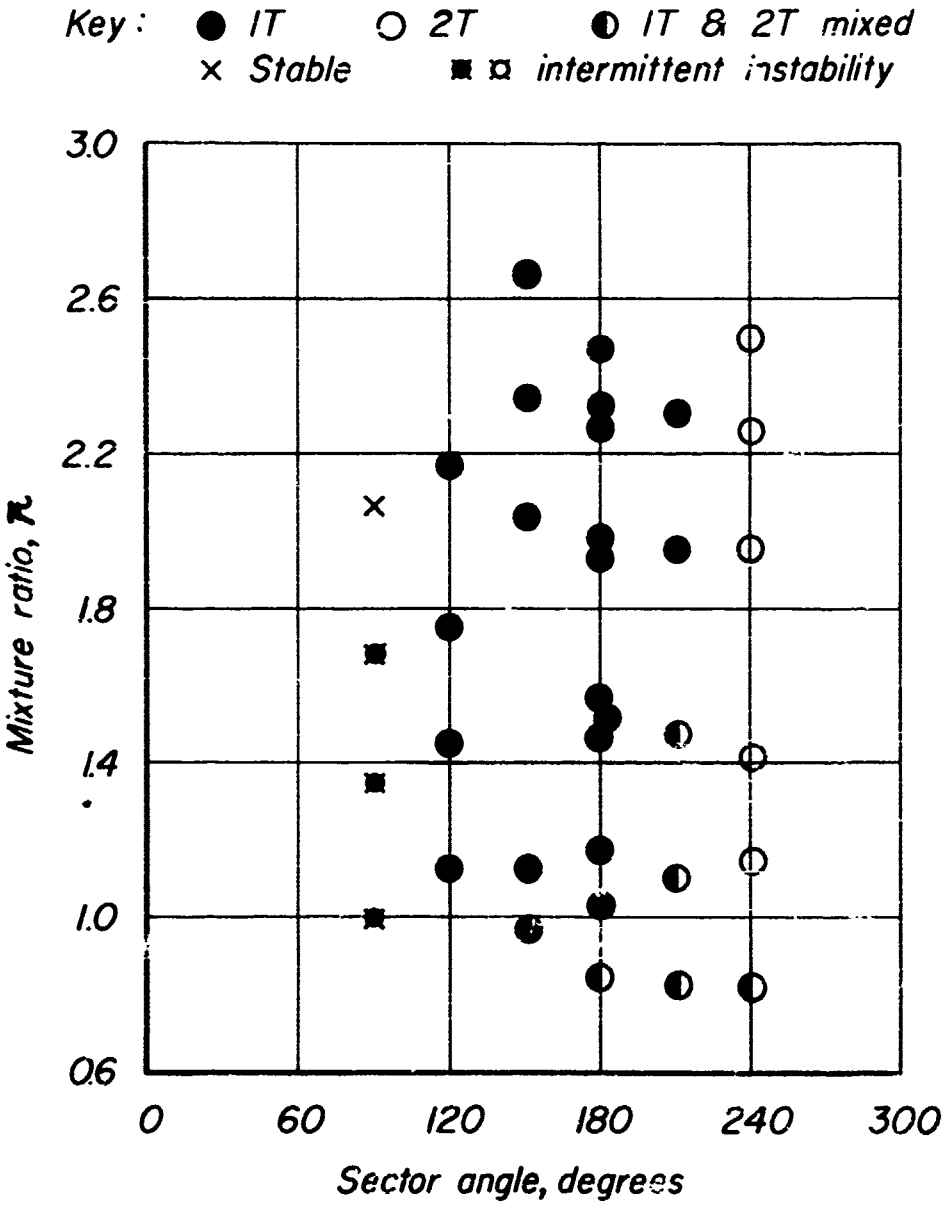

JPR 854

Figure 56

Radial orientation sector tests
9" chamber, 5" injector, π_{design} = 14,
p_c (nominal) = 150 psia, F (nominal) = 1000 lb

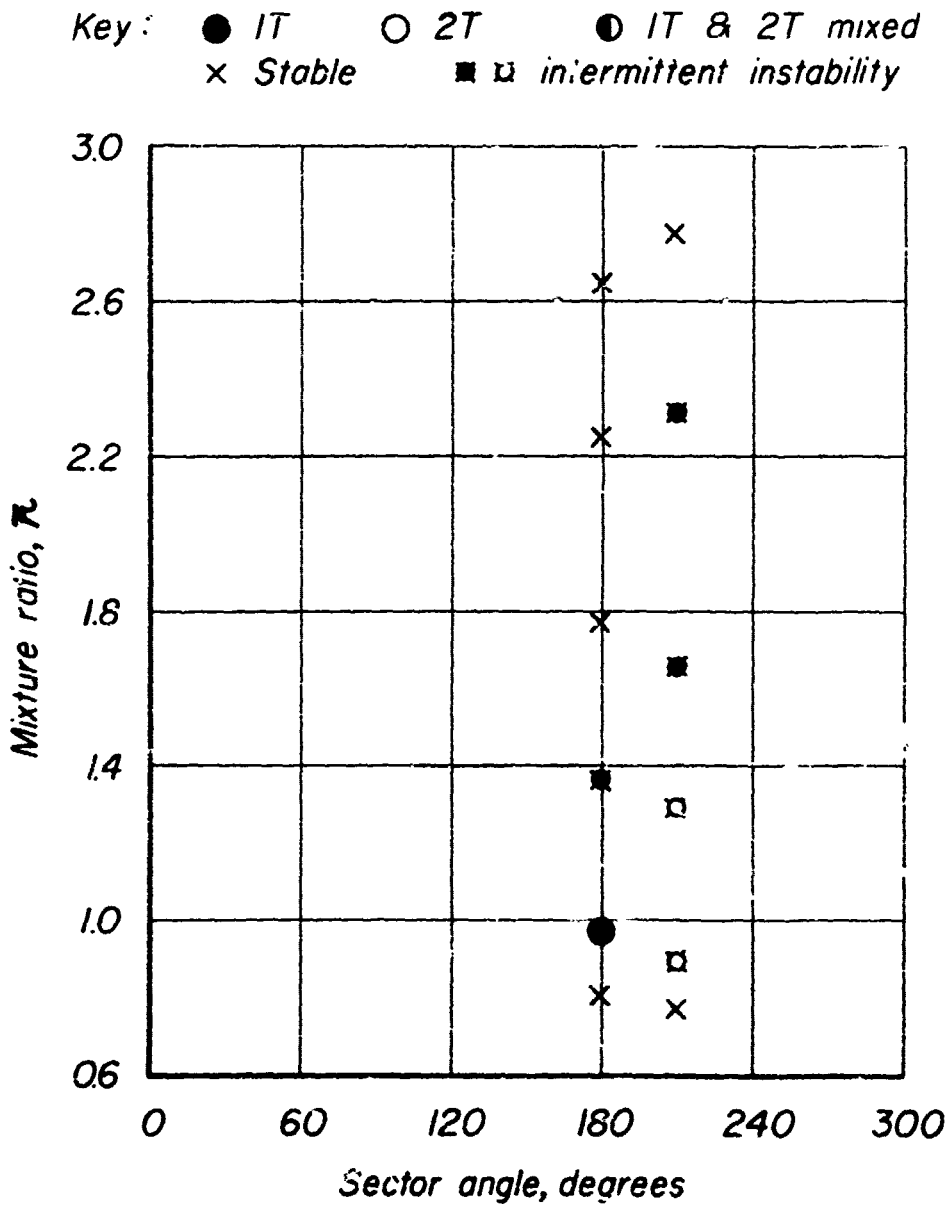

JPR 858

Figure 57

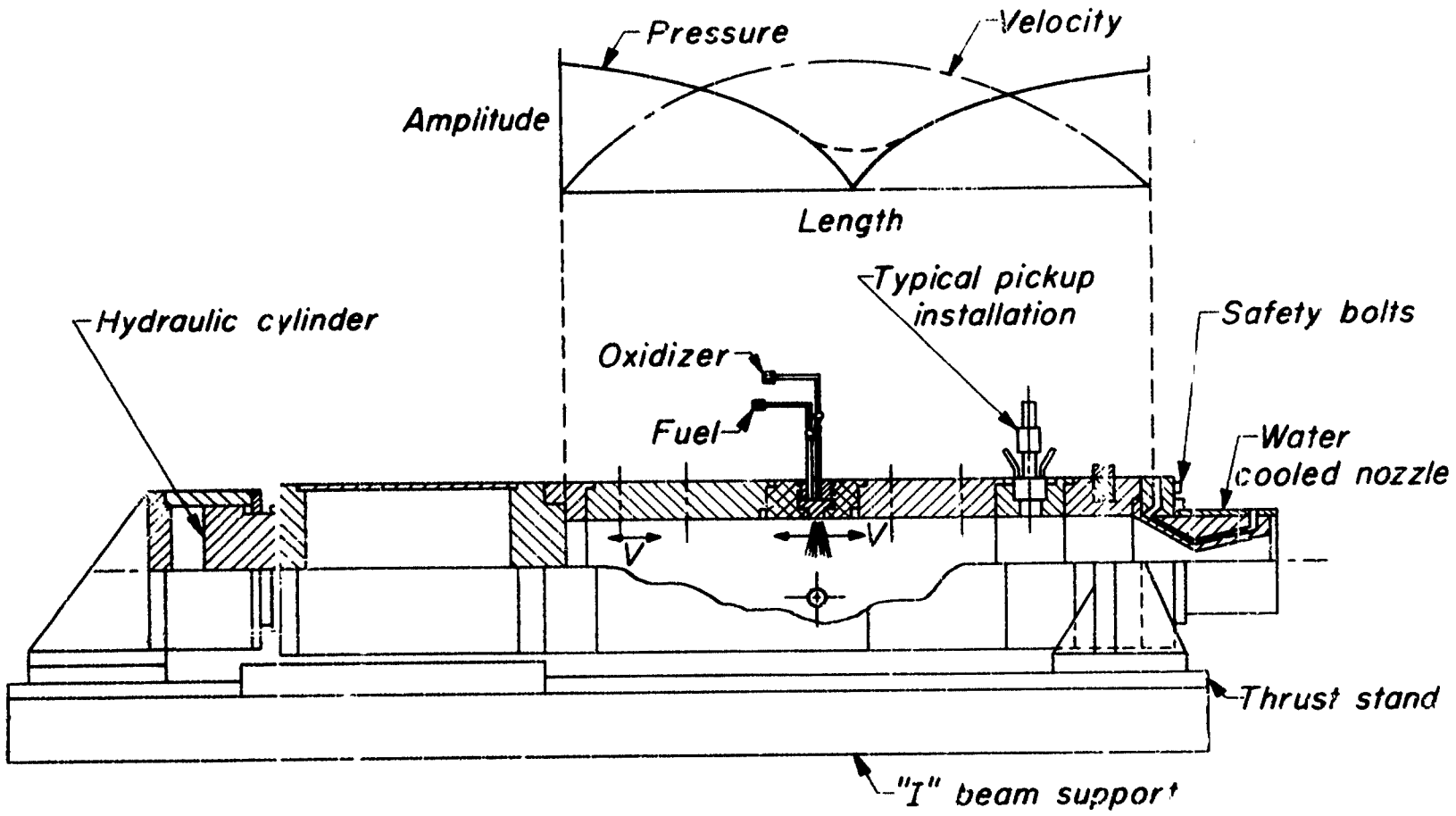

Figure 58

Velocity Effects Motor

Variable length liquid rocket motor, radial injection

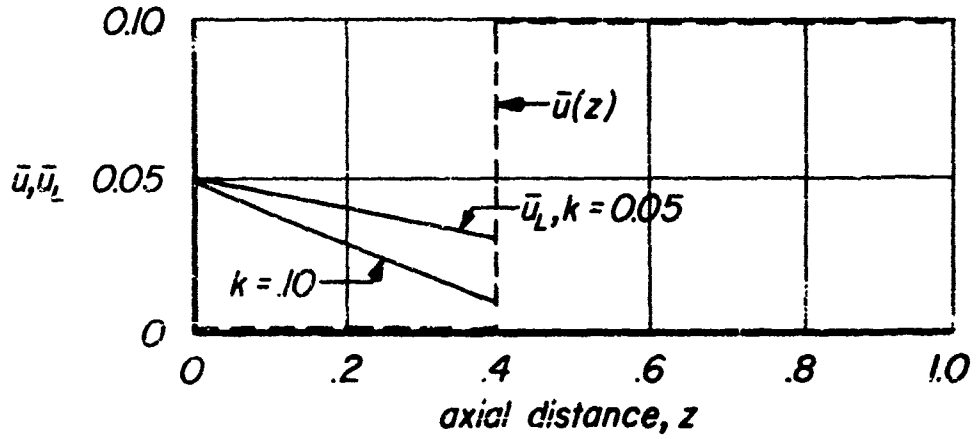

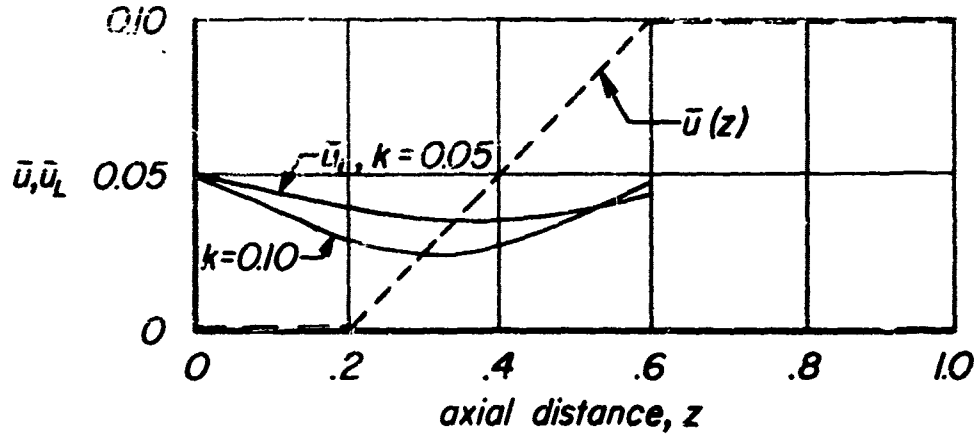

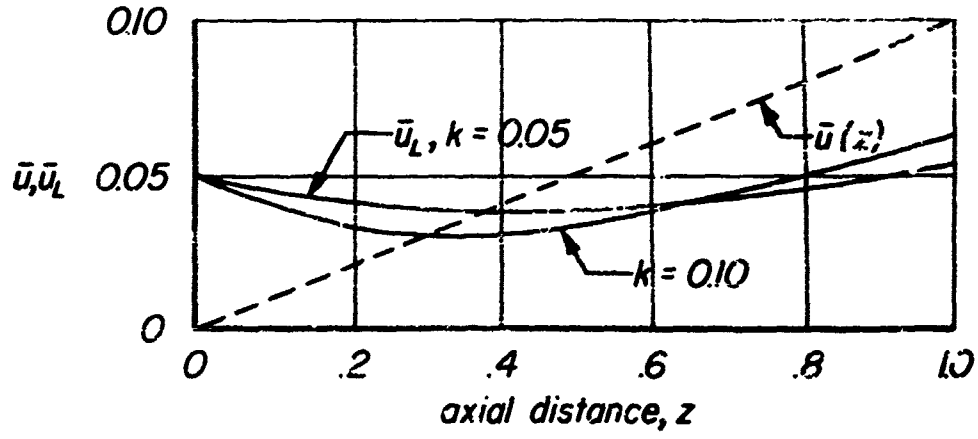

Steady state liquid droplet velocity profiles

JPF 836

Figure A1

$$\frac{k'(z)}{k} = 1 - e^{-(k+i\omega)\int_0^z \frac{dz'}{\bar{u}_L}}$$

$\omega = 1.84129$

$k = 0.05$

$\bar{u}_L \cong \bar{u}_{L_0} = 0.05$

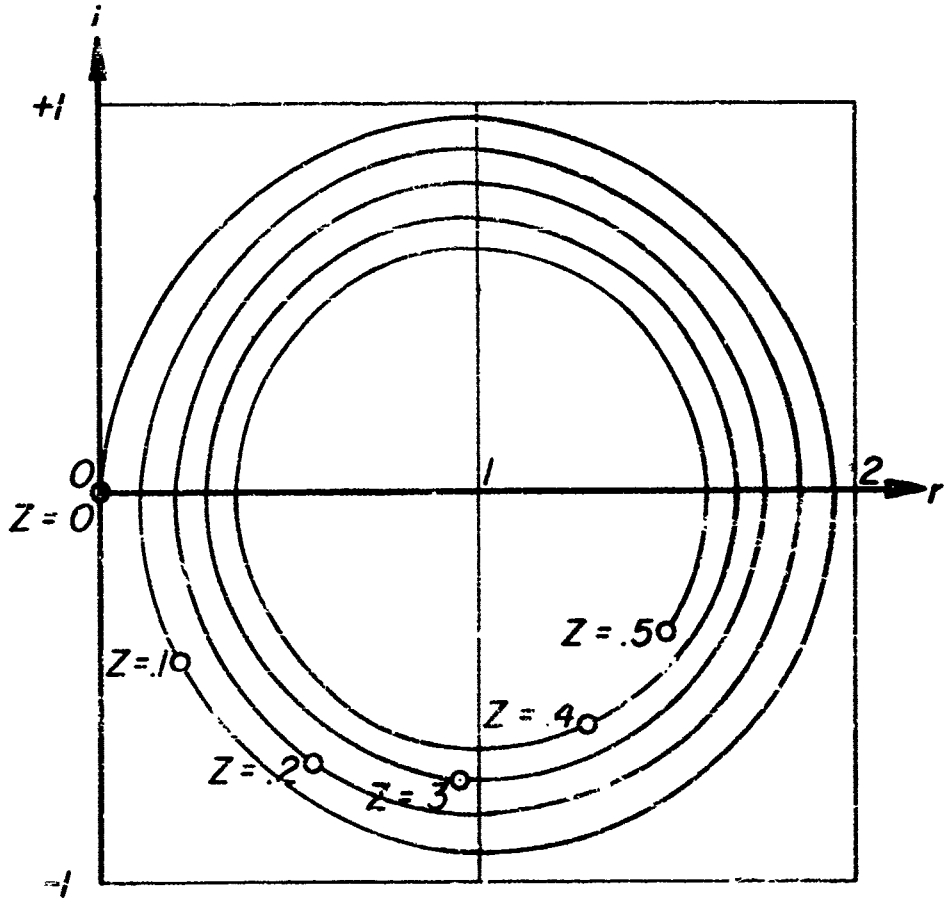

JPR 939

Figure A2

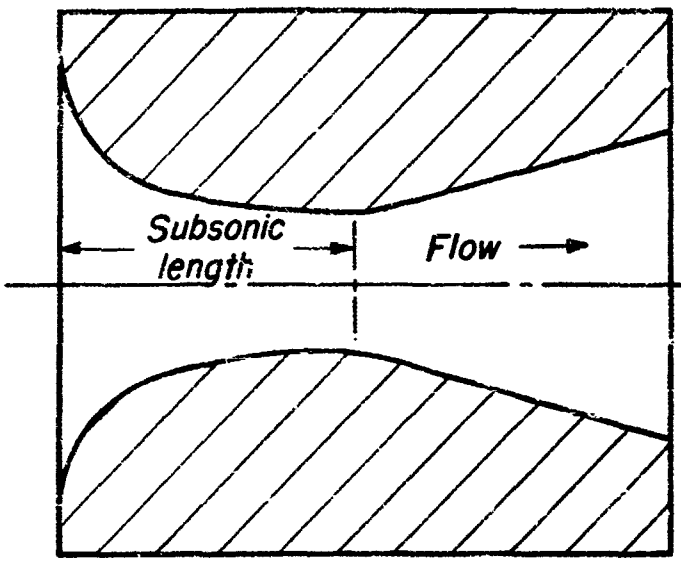

Linear nozzle

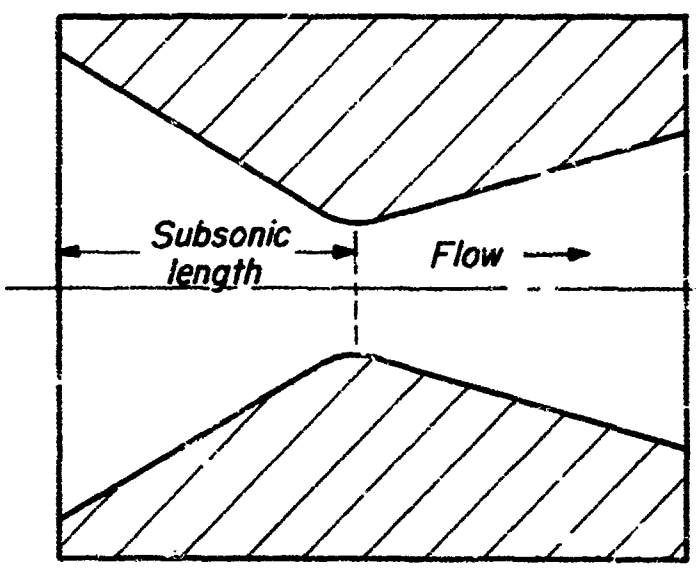

Conical nozzle

Comparison of nozzle profiles

IPR 794

Figure C1

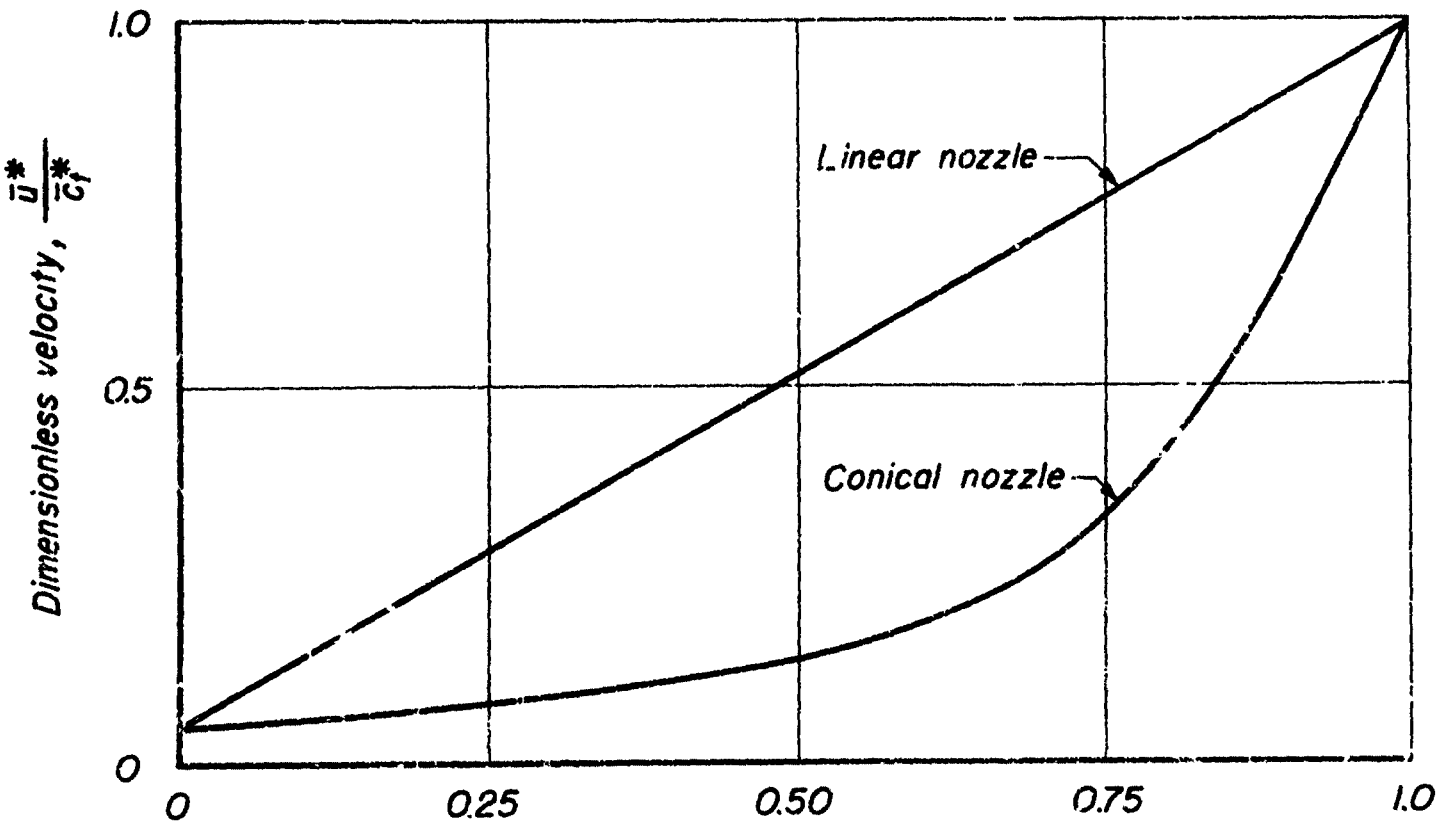

Figure C2

Comparison of subsonic velocity profiles

Admittance coefficient $\mathcal{E}_r$ for conical nozzle

$\bar{u}_e = 0.05$

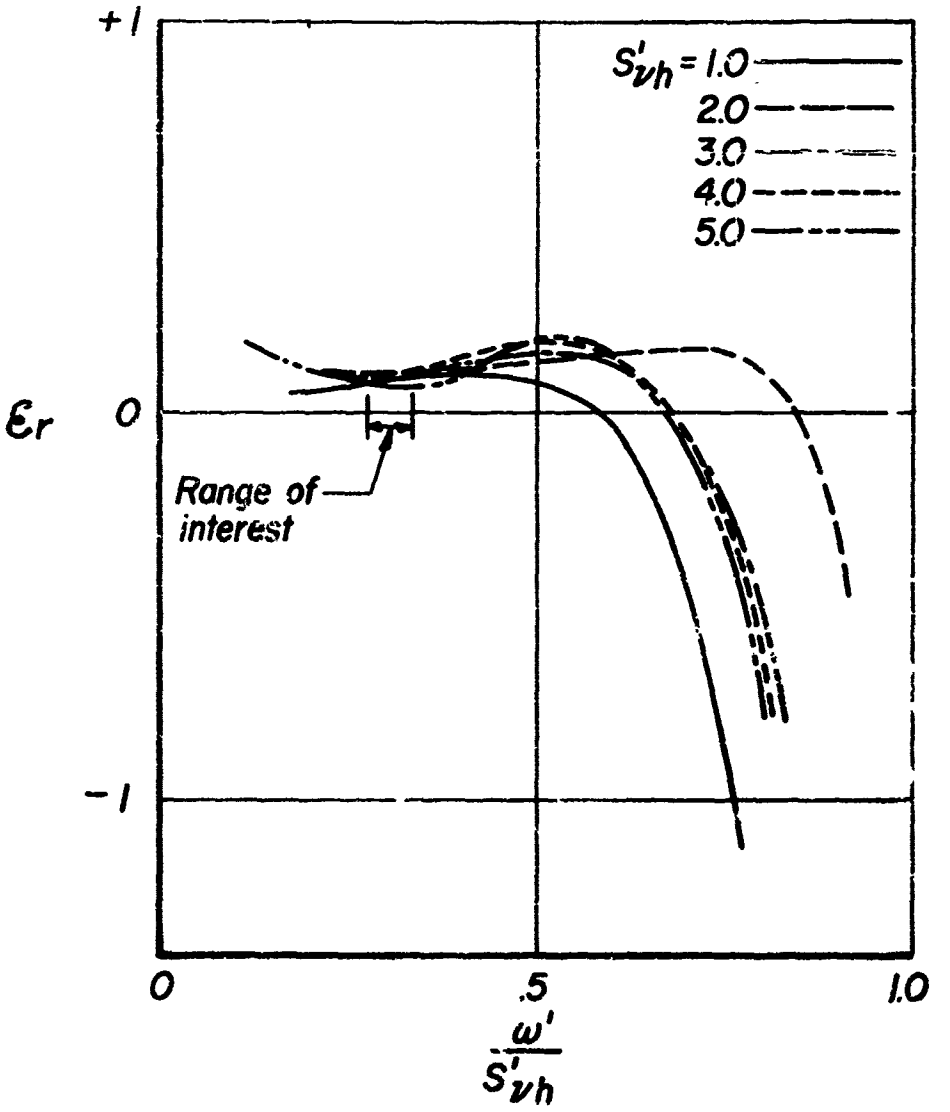

JPR 737

Figure C3

Admittance coefficient ε_i for conical nozzle
$\overline{u}_e = 0.05$

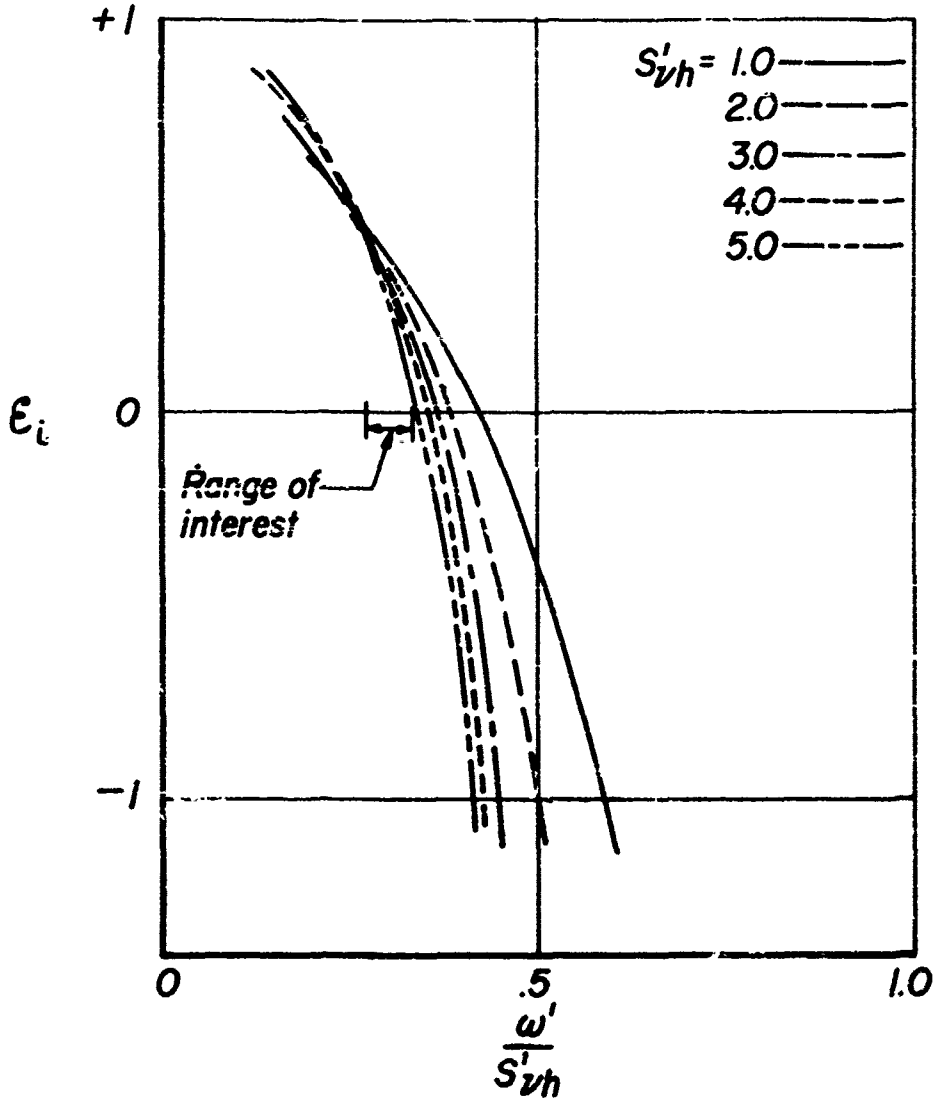

JPR 738

Figure C4

Admittance coefficient ε_r for conical nozzle

$\bar{u}_e = 0.10$

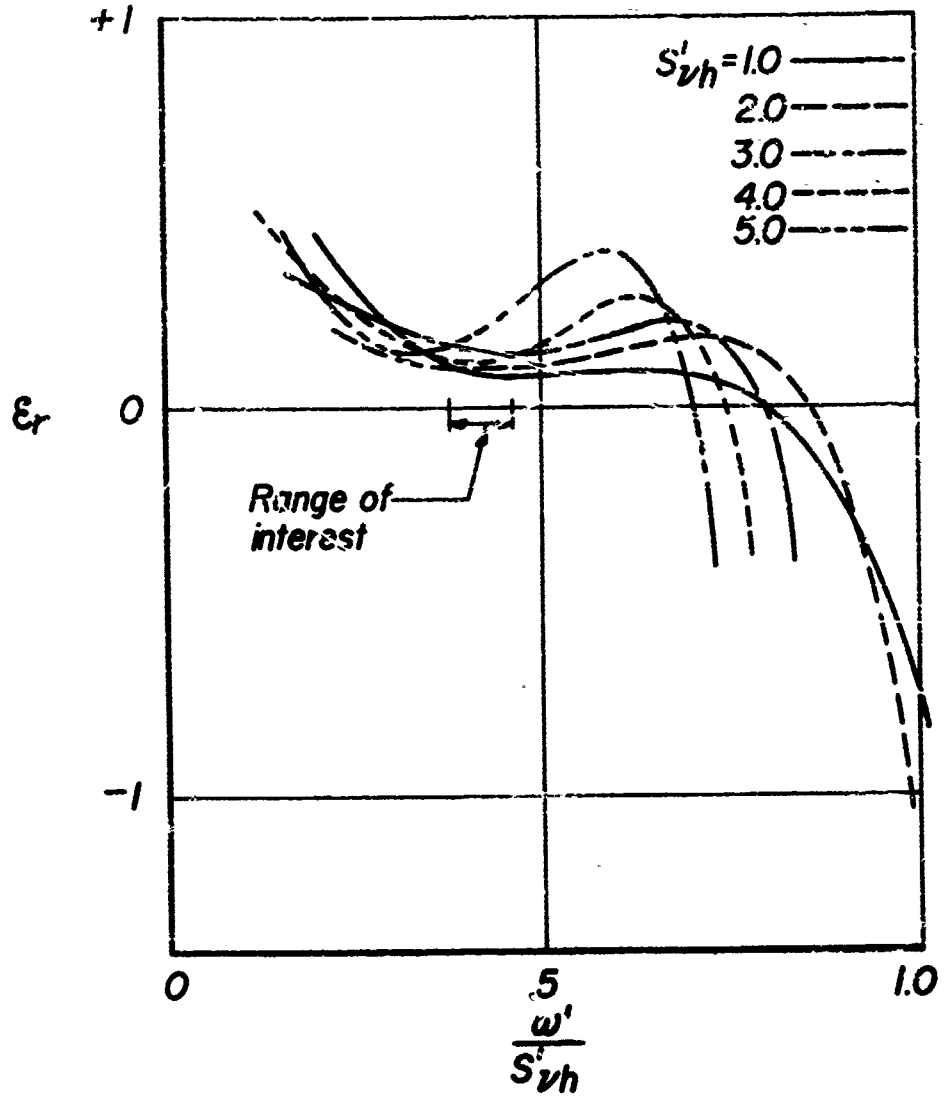

JPR 739

Figure C5

Admittance coefficient ε_i for conical nozzle

$\bar{u}_e = 0.10$

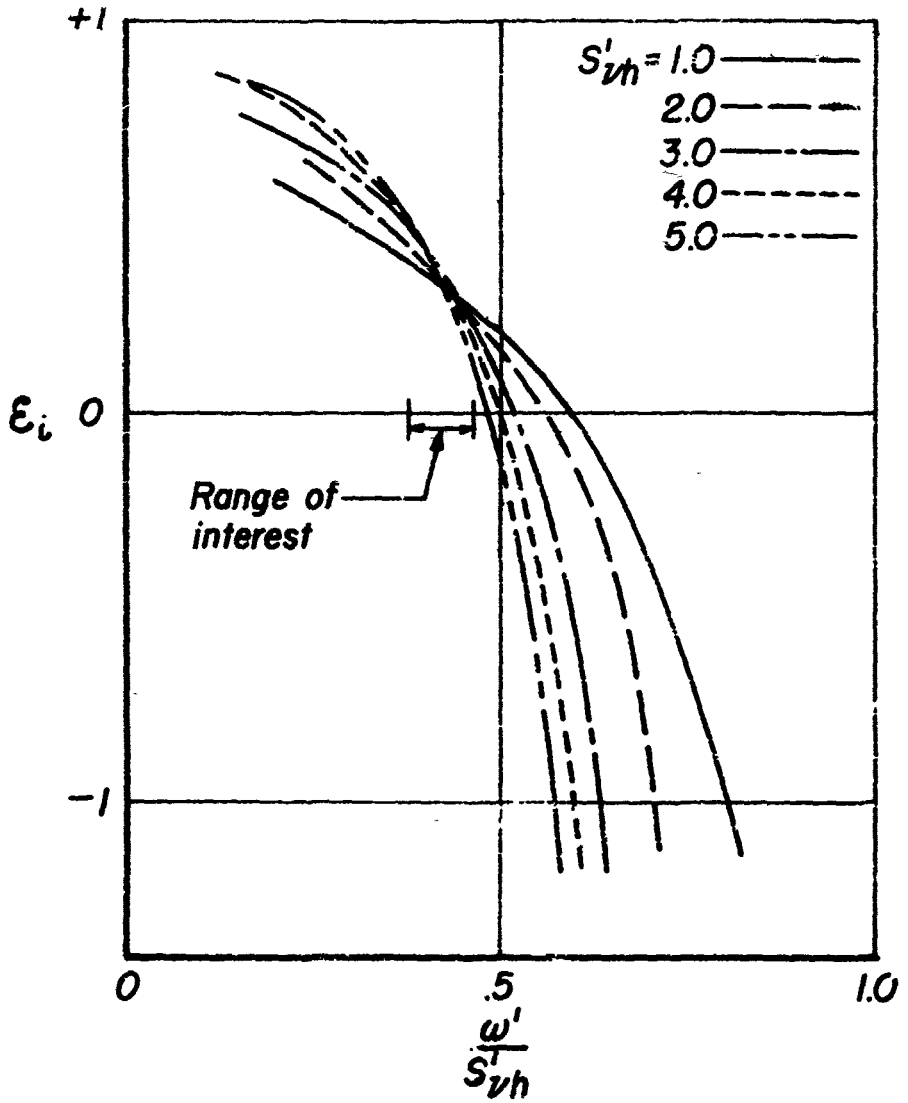

JPR 740

Figure C6

Admittance coefficient $\mathcal{E}_r$ for linear nozzle
$\bar{u}_e = 0.05$

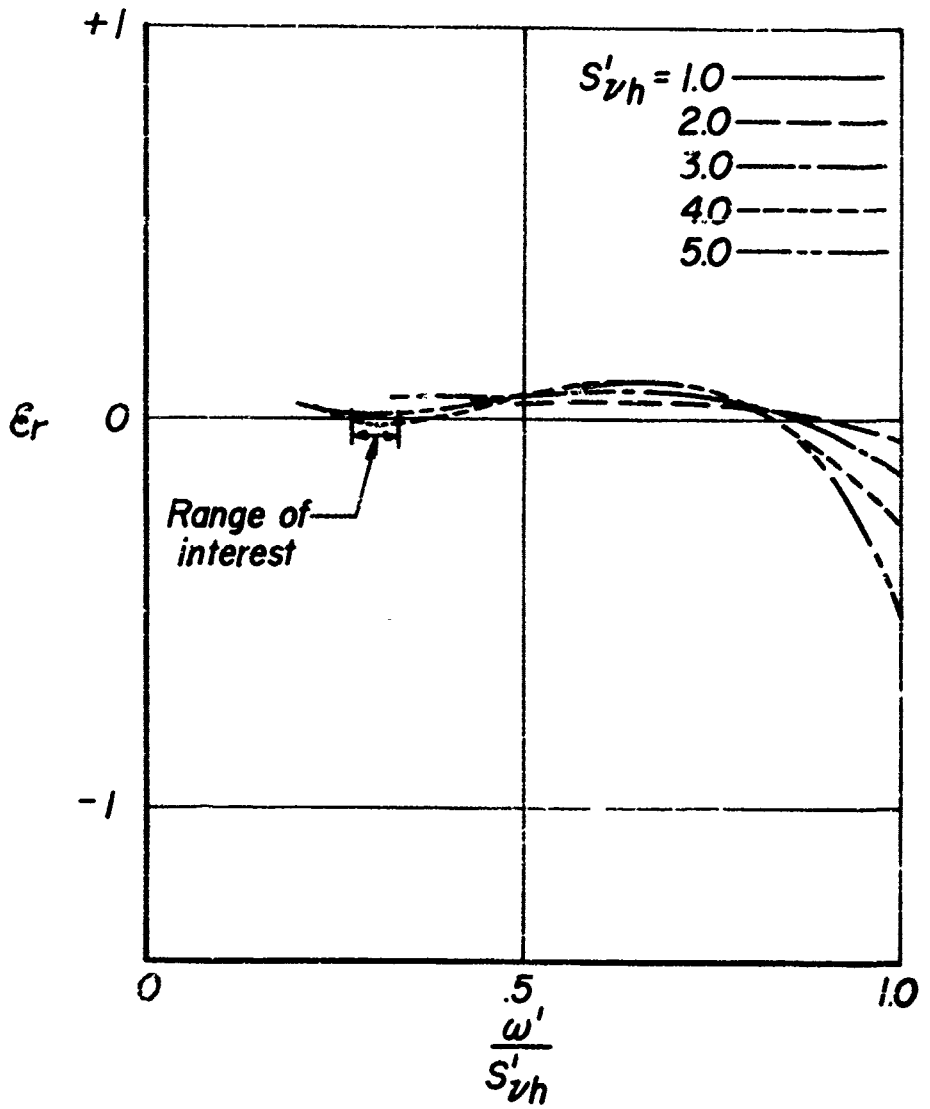

JPR 741

Figure C7

Admittance coefficient ε_i for linear nozzle
$\bar{u}_e = 0.05$

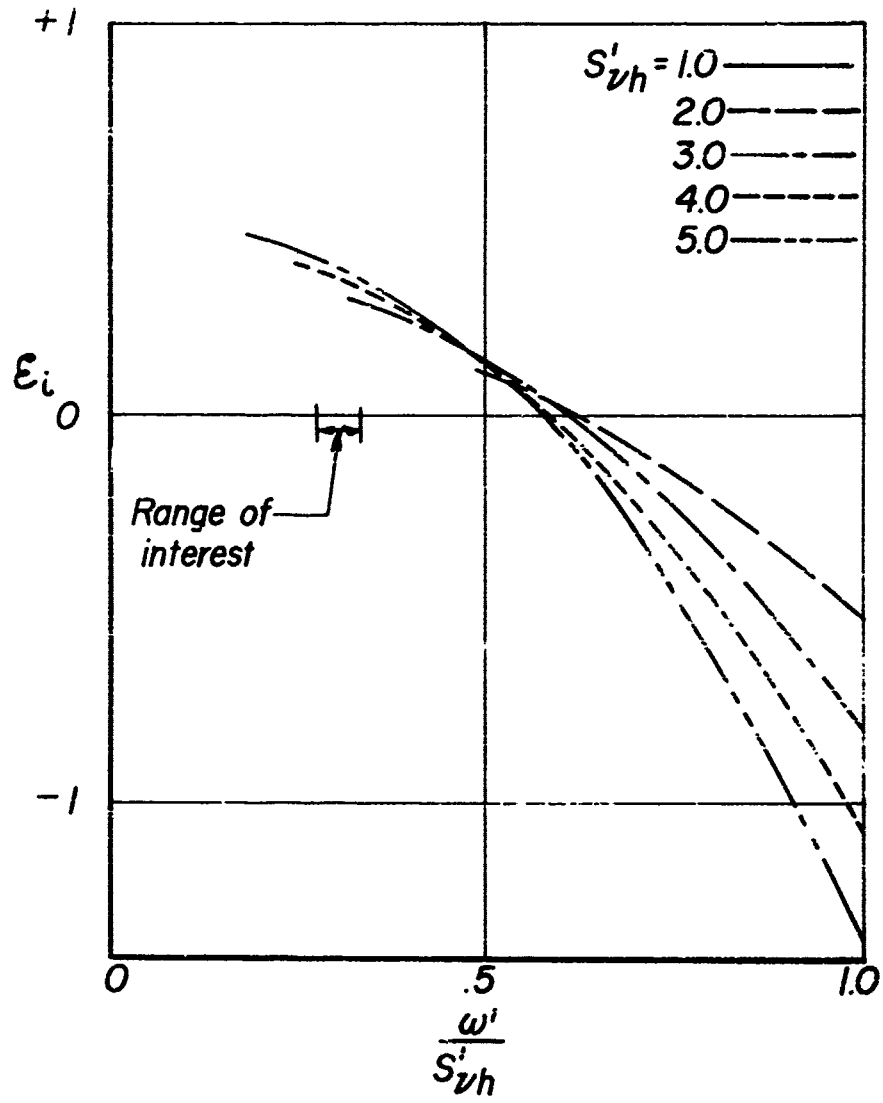

JPR 742

Figure C8

Admittance coefficient ε_r for linear nozzle

$\bar{u}_e = 0.10$

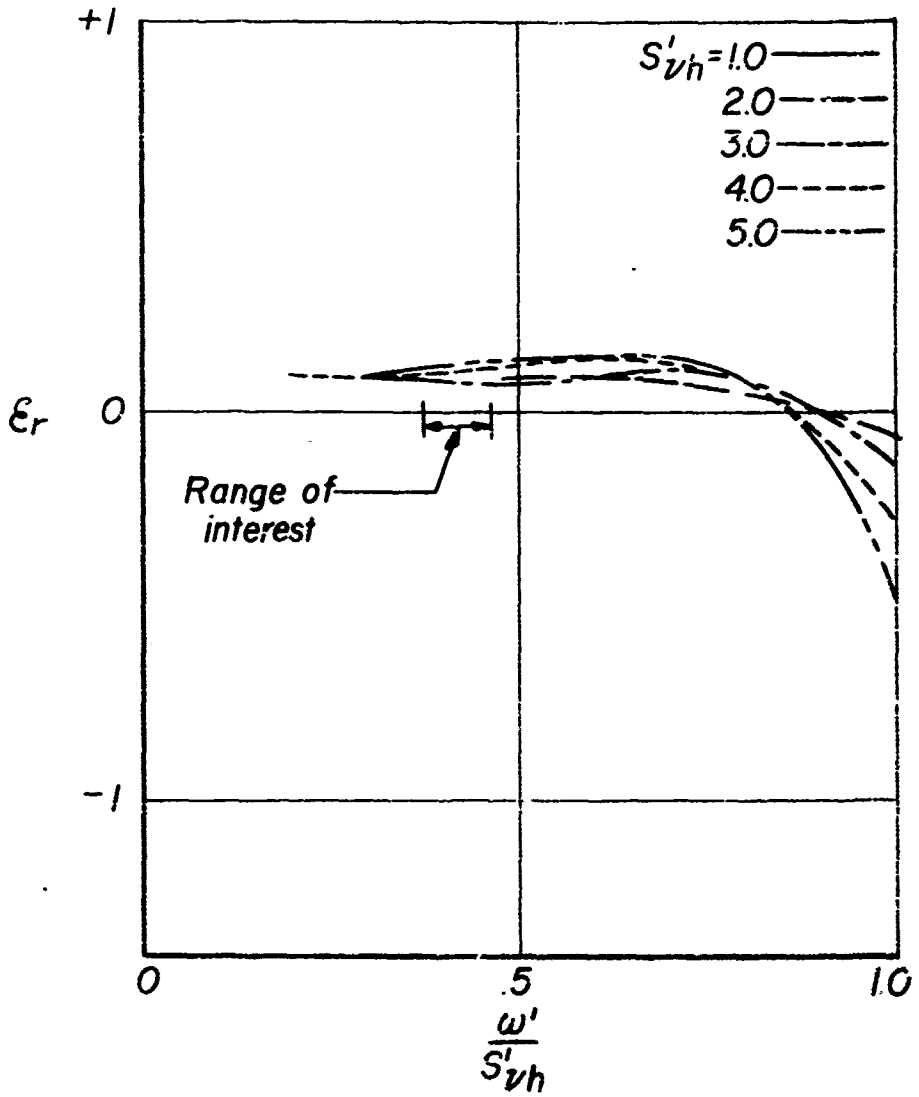

JPR 743

Figure C 9

Admittance coefficient ε_i for linear nozzle

$\bar{u}_e = 0.10$

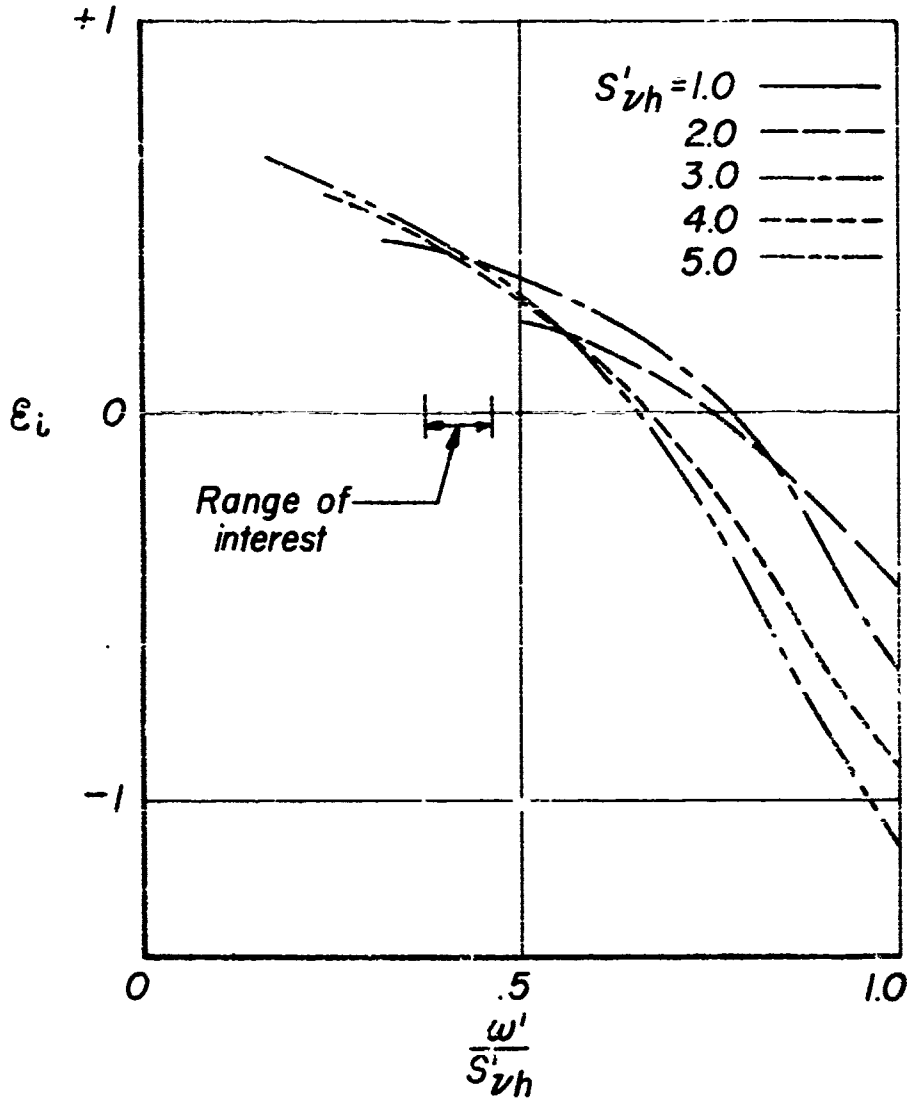

JPR 744

Figure C10

APPENDIX A

Liquid Droplet Dynamics

The steady state droplet dynamics equation describing the interchange of momentum between the liquid and gaseous phases has been written as

$$\bar{u}_L \frac{d\bar{u}_L}{dz} = k(\bar{u} - \bar{u}_L) \tag{2.5e}$$

where k is the momentum interchange coefficient. An approximate expression for k can be obtained by considering a non-burning spherical droplet. The principle of conservation of momentum yields

$$\bar{u}_L^* \frac{d\bar{u}_L^*}{dz^*} \bar{\rho}_L^* \frac{\pi}{6} d_L^{*3} = C_D \frac{\pi}{4} d_L^{*2} \cdot \frac{1}{2} \bar{\rho}^* |\bar{u}^* - \bar{u}_L^*| \cdot (\bar{u}^* - \bar{u}_L^*) \tag{A-1}$$

where $\bar{\rho}_L^*$ is the liquid density (dimensional), d_L^* the droplet diameter, C_D the drag coefficient, $\bar{u}^*$ and $\bar{u}_L^*$ the gas and liquid velocities. Thus

$$k^* = \frac{3}{4} \frac{C_D}{d_L^*} \frac{\bar{\rho}^*}{\bar{\rho}_L^*} |\bar{u}^* - \bar{u}_L^*| \tag{A-2}$$

which can be written in terms of the Reynolds number,

$$Re = \frac{\bar{\rho}^* |\bar{u}^* - \bar{u}_L^*|}{\bar{\mu}^*}$$

as

$$k^* = \frac{3}{4} \frac{\bar{\mu}^*}{d_L^{*2} \bar{\rho}_L^*} C_D Re \tag{A-3}$$

For Reynolds numbers in the range of rocket motor interest ($20 < Re < 100$), $C_D Re$ is nearly constant. In view of the complexity of the motion of burning propellant droplets under turbulent conditions, it is probably best to regard the coefficient k^* as an empirical factor correlating the liquid and gas velocity variations. In dimensionless form

$$k = \frac{k^* r_c^*}{\bar{c}_0^*}$$

A solution of equation (2.5e) can be obtained analytically by making the substitution

$$\bar{u}_L = y\, z$$

which for a linear variation of $\bar{u}$ with z (i.e., $\bar{u} = c_1 z$) gives the integrable equation

$$\frac{y\, dy}{y^2 + k y - c_1 k} + \frac{dz}{z} = 0 \tag{A-4}$$

The result is the cumbersome expression

$$\sqrt{\bar{u}_L^2 + k z \bar{u}_L - k c_1 z^2} = c_2 \left(\frac{2\bar{u}_L + kz - z\sqrt{k^2 + 4kc_1}}{2\bar{u}_L + kz + z\sqrt{k^2 + 4kc_1}} \right)^{\frac{k}{2\sqrt{k^2+4kc_1}}} \tag{A-5}$$

A more convenient procedure is to solve equation (2.5e) numerically. For most purposes the simple difference equation

$$\bar{u}_{L_{j+1}} = \bar{u}_{L_j} + k \Delta z \left(\frac{\bar{u}_j - \bar{u}_{L_j}}{\bar{u}_{L_j}} \right), \quad \Delta z = z_{j+1} - z_j \tag{A-6}$$

with the boundary condition

$$\bar{u}_{L_j} = u_{L0}, \quad z_j = 0$$

yields sufficiently good results. Figure A1 shows typical solutions for different $\bar{u}(z)$ profiles and k values.

The equation for the perturbation axial liquid velocity is the first of equations (2.14f),

$$s u_L' + \bar{u}_L \frac{\partial u_L'}{\partial z} + \frac{d\bar{u}_L}{dz} u_L' = k(u' - u_L') \tag{A-7}$$

and the boundary condition is $u_L'(z=0) = 0$. Scala (5) has considered the solution of this equation in detail. His result can be obtained by making

an order of magnitude analysis. Assuming that the droplet momentum coefficient k and the liquid droplet velocity $\bar{u}_L$ are $O(\bar{u}_e)$, as discussed above in Chapter II, consideration of the steady state droplet equation (2.5e) shows that $\frac{d\bar{u}_L}{dz}$ is also $O(\bar{u}_e)$. From equation (A-7) it can be seen that u_L' is at most $O(\bar{u}_e)$. Then, assuming that differentiation does not change the order of magnitude, the terms $\bar{u}_L \frac{\partial u_L'}{\partial z}$ and $\frac{d\bar{u}_L}{dz} u_L'$ of equation (A-7) are $O(\bar{u}_e^2)$ while the other terms are $O(\bar{u}_e)$. Therefore, the solution good to terms of $O(\bar{u}_e)$ is

$$u_L' = \frac{k}{k+s} u' = \frac{k}{s} u' + O(\bar{u}_e^2) \qquad \text{(A-8)}$$

However, this order of magnitude procedure cannot be used in general, since it may not be possible to satisfy the boundary conditions when the term containing the highest derivative is neglected. Thus, for the transverse velocities the relations

$$v_L' = \frac{k}{s} v' \quad , \quad w_L' = \frac{k}{s} w'$$

cannot satisfy the boundary conditions at the injector face, where

$$v_{L0}' = w_{L0}' = 0$$

but

$$v_0' \neq 0 \quad , \quad w_0' \neq 0$$

For either the radial or tangential liquid velocity perturbations, the governing equation is

$$s v_L' + \bar{u}_L \frac{\partial v_L'}{\partial z} = k (v' - v_L')$$

which can be written as

$$\frac{\partial v_L'}{\partial z} + \frac{k+s}{\bar{u}_L} v_L' = \frac{k}{\bar{u}_L} v' \tag{A-9}$$

An integrating factor for this equation is

$$e^{(k+s)\int_0^z \frac{dz'}{\bar{u}_L(z')}}$$

Multiplying through by this factor gives

$$e^{(k+s)\int_0^z \frac{dz'}{\bar{u}_L}} \frac{\partial v_L'}{\partial z} + \frac{(k+s)}{\bar{u}_L} e^{(k+s)\int_0^z \frac{dz'}{\bar{u}_L}} v_L' = \frac{k}{\bar{u}_L} v' e^{(k+s)\int_0^z \frac{dz'}{\bar{u}_L}}$$

It can be seen that the left side is equivalent to

$$\frac{\partial}{\partial z}\left[v_L' \, e^{(k+s)\int_0^z \frac{dz'}{\bar{u}_L}} \right]$$

Thus integrating both sides with respect to Z yields

$$v_L' e^{(k+s)\int_0^z \frac{dz'}{\bar{u}_L}} = k \int_0^z \frac{v'(z', r, \theta)}{\bar{u}_L(z')} e^{(k+s)\int_0^{z'} \frac{dz''}{\bar{u}_L}} dz' \tag{A-10}$$

The right side of this equation can be evaluated by integrating by parts, so that equation (A-10) becomes

$$v_L' e^{(k+s)\int_0^z \frac{dz'}{\bar{u}_L}} = \frac{k}{k+s}\left[v'(z, r, \theta) e^{(k+s)\int_0^z \frac{dz'}{\bar{u}_L}} v'(0, r, \theta) - \int_0^z \frac{\partial v'}{\partial z} e^{(k+s)\int_0^{z'} \frac{dz''}{\bar{u}_L}} dz' \right] \tag{A-11}$$

It is shown in Chapter II that $\frac{\partial v'}{\partial z}$ is $O(\bar{u}_e \cdot v')$. Neglecting the integral term on the right side gives an expression for the liquid velocity perturbation which is good to $O(\bar{u}_e \cdot v')$ but not to $O(\bar{u}_e^2 \cdot v')$:

$$v_L' = \frac{k}{k+s}\left[v'(z, r, \theta) - v'(0, r, \theta) e^{-(k+s)\int_0^z \frac{dz'}{\bar{u}_L}} \right] \tag{A-12}$$

Since $\frac{\partial v'}{\partial z}$ is $O(\bar{u}_e \cdot v')$ and z is $O(1)$, then $v'(z) - v'(0)$ is $O(\bar{u}_e \cdot v')$, or $v'(0) = v'(z) + O(\bar{u}_e v')$. Also $\frac{k}{\bar{u}_{Lm}} = \frac{k_r}{\bar{u}_{Lm}} + O(\bar{u}_e^2)$. Therefore, the final expression for v_L' can be written as

$$v_L' = \frac{k'(z)}{s} v' \tag{A-13}$$

where

$$k'(z) = k\left(1 - e^{-(k+s)\int_0^z \frac{dz'}{\bar{u}_L}}\right) \tag{A-14}$$

For neutral oscillations, $s = i\omega$, and for small values of the droplet momentum coefficient, $\bar{u}_L \cong \bar{u}_{Lm}$. Then

$$\frac{k'(z)}{k} \cong 1 - e^{-\frac{k_r z}{\bar{u}_{Lm}} - i\frac{\omega z}{\bar{u}_{Lm}}}$$

This function is represented by a curve on the complex plane which for increasing axial distance z spirals inward around the point (1,0). As an example, the function k'/k is shown in Figure A2 for $k = 0.05$, $\bar{u}_{Lm} = 0.05$, $\omega = 1.84129$. (the dimensionless frequency of the first tangential acoustic mode), and $0 \le z \le 0.5$.

APPE DIX B

Perturbation Solution with Axially Concentrated Combustion

When combustion is concentrated near a single axial station, as in the case of well mixed propellants, the steady state velocity gradient $\frac{d\bar{u}}{dz}$ is locally O(1). The analysis presented in Chapter II assumes that the velocity gradient never exceeds O($\frac{1}{\varepsilon}$). The case of axially concentrated combustion requires a somewhat different and more complicated procedure than that used previously.

The first order perturbation equations, with $\frac{d\bar{u}}{dz} = O(1)$, are

$$s\rho_1 + \frac{\partial u_1}{\partial z} + \frac{\partial v_1}{\partial r} + \frac{v_1}{r} + \frac{1}{r}\frac{\partial w_1}{\partial \theta} + \frac{d\bar{u}}{dz}\rho_1 + \frac{d\bar{\rho}}{dz}u_0 = Q_1 \tag{B-1}$$

$$s u_1 + 2\frac{d\bar{u}}{dz}u_1 + \bar{\rho}\bar{u}\frac{d\bar{u}}{dz}\rho_0 = -\frac{1}{\gamma}\frac{\partial p_1}{\partial z} \tag{B-2}$$

$$s\left(v_1 + \bar{\rho}_L \frac{k'}{s} v_0\right) + \frac{d\bar{u}}{dz}v_1 + \frac{d\bar{\rho}}{dz}v_0 = -\frac{1}{\gamma}\frac{\partial p_1}{\partial r} \tag{B-3}$$

$$s\left(w_1 + \bar{\rho}_L \frac{k'}{s} w_0\right) + \frac{d\bar{u}}{dz}w_1 + \frac{d\bar{\rho}}{dz}w_0 = -\frac{1}{\gamma r}\frac{\partial p_1}{\partial \theta} \tag{B-4}$$

$$s(p_1 - \rho_1) + \frac{d\bar{u}}{dz}\left(\frac{\gamma-1}{\gamma}p_0\right) + \frac{d\bar{\rho}}{dz}(p_1 - \rho_1) = \frac{\gamma-1}{\gamma}s p_1 \tag{B-5}$$

The entropy perturbation is given by

$$\mathcal{S}_1 = \frac{p_1}{\gamma} - \rho_1 = \frac{\gamma-1}{\gamma}\cdot\frac{\frac{d\bar{\rho}}{dz}}{s + \frac{d\bar{u}}{dz}}\cdot(p_0 + p_1) \tag{B-6}$$

At the chamber exit, where $\frac{d\bar{u}}{dz} = 0$, $s_1 = 0$, as before.

The energy and continuity equations are combined to eliminate the density ρ_1 . Then the set of linear partial differential equations to be solved is

$$\frac{\partial u_1}{\partial z} + s\frac{p_1}{\gamma} + \frac{\partial v_1}{\partial r} + \frac{v_1}{r} + \frac{1}{r}\frac{\partial w_1}{\partial \theta} = Q_1 - \frac{d\bar{u}}{dz} p_1 - \frac{d\bar{u}}{dz} p_0 \tag{B-7}$$

$$\frac{\partial}{\partial z}\left(\frac{p_1}{\gamma}\right) + s u_1 = -2\frac{d\bar{u}}{dz} u_1 - 2\bar{u}\frac{d\bar{u}}{dz}\left(\frac{p_0}{\gamma}\right) \tag{B-8}$$

$$s v_1 + \frac{\partial}{\partial r}\left(\frac{p_1}{\gamma}\right) = -\frac{d\bar{u}}{dz} v_0 - \frac{d\bar{u}}{dz} v_1 - \bar{\rho}_L k' v_0 \tag{B-9}$$

$$s w_1 + \frac{1}{r}\frac{\partial}{\partial \theta}\left(\frac{p_1}{\gamma}\right) = -\frac{d\bar{u}}{dz} w_0 - \frac{d\bar{u}}{dz} w_1 - \bar{\rho}_L k' w_0 \tag{B-10}$$

As was done previously, the solutions are represented as sums of partial solutions,

$$\left.\begin{aligned} p_1 &= p_A + p_B + p_C + p_D \\ u_1 &= u_A + u_B + u_C + u_D \\ Q_1 &= Q_A + Q_B + Q_C \\ &\vdots \end{aligned}\right\} \tag{B-11}$$

where Q_A is to be identified with the pressure dependence, Q_B with the radial, and Q_C with the tangential, velocity dependence.

The right hand side of equation (B7) can be simplified by noting that

$$\frac{d\bar{u}}{dz} p_1 = \frac{\partial}{\partial z}(\bar{u} p_1) - \bar{u}\frac{\partial p_1}{\partial z} = \frac{\partial}{\partial z}(\bar{u} p_1) + O(\bar{u}^2)$$

The other equations can be treated similarly.

The equations for the partial solution "A" are

$$\left.\begin{aligned}
&\frac{\partial u_A}{\partial z} + s\left(\frac{p_A}{\gamma}\right) + \frac{\partial v_A}{\partial r} + \frac{v_A}{r} + \frac{1}{r}\frac{\partial w_A}{\partial \theta} = Q_A - \frac{\partial}{\partial z}(p_A \bar{u}) \\
&\frac{\partial}{\partial z}\left(\frac{p_A}{\gamma}\right) + s u_A = -2\frac{\partial}{\partial z}(\bar{u} u_A) \\
&s v_A + \frac{\partial}{\partial r}\left(\frac{p_A}{\gamma}\right) = -\frac{\partial}{\partial z}(\bar{u} v_A) \\
&s w_A + \frac{1}{r}\frac{\partial}{\partial \theta}\left(\frac{p_A}{\gamma}\right) = -\frac{\partial}{\partial z}(\bar{u} w_A)
\end{aligned}\right\} \qquad (B\text{-}12)$$

The equations for the "B" and "C" partial solutions are of the same form.

For the "D" solution, the equations are

$$\left.\begin{aligned}
&\frac{\partial u_D}{\partial z} + s\left(\frac{p_D}{\gamma}\right) + \frac{\partial v_D}{\partial r} + \frac{v_D}{r} + \frac{1}{r}\frac{\partial w_D}{\partial \theta} = -\gamma\frac{\partial}{\partial z}\left(\bar{u}\frac{p_o}{\gamma}\right) \\
&\frac{\partial}{\partial z}\left(\frac{p_D}{\gamma}\right) + s u_D = -2\frac{\partial}{\partial z}\left(\bar{u}^2\frac{p_o}{\gamma}\right) \\
&s v_D + \frac{\partial}{\partial r}\left(\frac{p_D}{\gamma}\right) = -\frac{d\bar{u}}{dz} v_o - k'\bar{\rho} v_o \\
&s w_D + \frac{1}{r}\frac{\partial}{\partial \theta}\left(\frac{p_D}{\gamma}\right) = -\frac{d\bar{u}}{dz} w_o - k'\bar{\rho}_L w_o
\end{aligned}\right\} \qquad (B13)$$

Consider first the set (B13). Since the right side of each equation contains only zeroth order terms, the "D" solutions take the form

$$\left.\begin{aligned}
p_D &= P_D(z)\,\Psi_{\nu h}(r)\,\Theta_\nu(\theta) \\
u_D &= U_D(z)\,\Psi_{\nu h}(r)\,\Theta_\nu(\theta) \\
v_D &= V_D(z)\,\frac{d\Psi_{\nu h}}{dr}(r)\,\Theta_\nu(\theta) \\
w_D &= V_D(z)\,\frac{1}{r}\Psi_{\nu h}(r)\,\frac{d\Theta_\nu}{d\theta}(\theta)
\end{aligned}\right\} \qquad (B\text{-}14)$$

Substitution of these expressions into (B13) gives

$$\left.\begin{aligned}
&\frac{d}{dz}\left(U_D + \gamma\bar{u}\frac{P_o}{\gamma}\right) + s\frac{P_D}{\gamma} - s^2_{\nu h} V_D = 0 \\
&\frac{d}{dz}\left(\frac{P_D}{\gamma} + 2\bar{u}^2\frac{P_o}{\gamma}\right) + s U_D = 0 \\
&s V_D + \frac{P_D}{\gamma} - \frac{d}{dz}\left(\frac{\bar{u} P_o}{\gamma s}\right) - k'\bar{\rho}_L\frac{P_o}{\gamma s}
\end{aligned}\right\} \qquad (B\text{-}15)$$

Eliminating V_D between the first and third of equations (B-15) yields the pair

$$\left.\begin{aligned} &\frac{d}{dz}\left(U_D + \gamma\bar{u}\frac{P_0}{\gamma} - \frac{s_{vh}^2}{s^2}\bar{u}\frac{P_0}{\gamma}\right) - \frac{s_{vh}^2}{s^2}\frac{d}{dz}\bar{u}\frac{P_0}{\gamma} + s\left(1+\frac{s_{vh}^2}{s^2}\right)\frac{P_D}{\gamma} = 0 \\ &\frac{d}{dz}\left(\frac{P_0}{\gamma} + 2\bar{u}^2\frac{P_0}{\gamma}\right) + s\,U_D = 0 \end{aligned}\right\} \quad \text{(B-16)}$$

As new dependent variables, define

$$D = U_D + \left(\gamma\bar{u} - \frac{s_{vh}^2}{s^2}\bar{u}\right)\frac{P_0}{\gamma} \quad \text{(B-17)}$$

$$B = \frac{P_0}{\gamma} + 2\bar{u}^2\frac{P_0}{\gamma} \quad \text{(B-18)}$$

Then

$$\left.\begin{aligned} &\frac{dD}{dz} + s\left(1+\frac{s_{vh}^2}{s^2}\right)B = -sE' \\ &\frac{dB}{dz} + sD = sF' \end{aligned}\right\} \quad \text{(B-19)}$$

where

$$E' = -2\bar{u}^2\frac{P_0}{\gamma}\left(1+\frac{s_{vh}^2}{s^2}\right) - \frac{s_{vh}^2}{s^3}\frac{d}{dz}\bar{u}\frac{P_0}{\gamma} = \frac{\rho_k'}{\rho_k}\frac{P_{00}}{\gamma} + O(\bar{u}_e^2)$$

and

$$F' = \left(\gamma\bar{u} - \frac{s_{vh}^2}{s^2}\bar{u}\right)\frac{P_0}{\gamma} = (\gamma+1)\bar{u}\frac{P_{00}}{\gamma} + O(\bar{u}_e^2) \quad \text{(B-20)}$$

Eliminating D from (B-19) gives the second order equation for B( )

$$\frac{d^2B}{dz^2} - (s^2+s_{vh}^2)B = s\frac{dF'}{dz} + s^2E' \quad \text{(B-21)}$$

Now B is $O(\bar{u}_e \cdot P_{00})$ and $s^2 + s_{vh}^2$ is $O(\bar{u}_e)$.

Therefore, (B-21) simplifies to

$$\frac{d^2B}{dz^2} = s\frac{dF'}{dz} + s^2E'$$

or

$$B = s\int_0^z F'(z')dz' + s^2\int_0^z dz'\int_0^{z'} E'(z'')dz'' + \frac{P_D(0)}{\gamma} \tag{B-22}$$

since $\frac{d}{dz}B(0)=0$, $B(0)=\frac{P_D(0)}{\gamma}$. Thus, the result, good to $O(\bar{u}_e)$, is

$$\frac{P_D}{P_{oo}} = s(\gamma+1)\int_0^z \bar{u}(z')dz' + s\int_0^z dz'\int_0^{z'} k'\rho_L\, dz'' + \frac{P_D(0)}{\gamma} \tag{B-23}$$

which is identical to (2.50).

The partial solutions "A", "B", and "C" are slightly more complicated because the terms on the right-hand side of the equations are first order quantities rather than zeroth order.

All three solutions follow the same procedure; the "A" solution will be shown in detail.

The equations to be satisfied are the set of linear, non-homogeneous, simultaneous partial differential equations (B-12). The pressure, velocities, and burning rate are expanded in the transverse eigenfunctions

$$\left.\begin{aligned}
P_A &= \sum_{p=0}^{\infty}\sum_{q=1}^{\infty} A_{pq}\, P_{Apq}(z)\, \Psi_{pq}(r)\, \Theta_p(\theta)\\
u_A &= \sum_{p=0}^{\infty}\sum_{q=1}^{\infty} A_{pq}\, U_{Apq}(z)\, \Psi_{pq}(r)\, \Theta_p(\theta)\\
v_A &= \sum_{p=0}^{\infty}\sum_{q=1}^{\infty} A_{pq}\, V_{Apq}(z)\, \Psi'_{pq}(r)\, \Theta_p(\theta)\\
Q_A &= \sum_{p=0}^{\infty}\sum_{q=1}^{\infty} A_{pq}\, \frac{dH_{Apq}}{dz}(z)\, \Psi_{pq}(r)\, \Theta_p(\theta)
\end{aligned}\right\} \tag{B-24}$$

Then, for each p, q pair, the equations to be solved are

$$\left.\begin{aligned}
&\frac{d}{dz}\left(U_{Apq} + \bar{u}\gamma\frac{P_{Apq}}{\gamma} - H_{Apq}\right) + s\frac{P_{Apq}}{\gamma} - s^2_{pq}V_{Apq} = 0\\
&\frac{d}{dz}\left(\frac{P_{Apq}}{\gamma} + 2\bar{u}U_{Apq}\right) + sU_{Apq} = 0\\
&sV_{Apq} + \frac{P_{Apq}}{\gamma} + \frac{d}{dz}(\bar{u}V_{Apq}) = 0
\end{aligned}\right\} \tag{B-25}$$

Eliminating $s_{pq}^2 V_{Apq}$ from the first equation by means of the third of equations (B-25) gives

$$\left.\begin{aligned} &\frac{d}{dz}\left(U_{Apq} + \bar{u}\gamma\frac{P_{Apq}}{\gamma} - H_{Apq} + \frac{s_{pq}^2}{s}\bar{u}V_{Apq}\right) + \left(s + \frac{s_{pq}^2}{s}\right)\frac{P_{Apq}}{\gamma} = 0 \\ &\frac{d}{dz}\left(\frac{P_{Apq}}{\gamma} + 2\bar{u}U_{Apq}\right) + s\,U_{Apq} = 0 \end{aligned}\right\} \quad (B\text{-}26)$$

By analogy with the "D" solution, new dependent variables are defined:

$$\left.\begin{aligned} \tilde{D}_{pq} &= U_{Apq} + \bar{u}\gamma\frac{P_{Apq}}{\gamma} - H_{Apq} + \frac{s_{pq}^2}{s}\bar{u}V_{Apq} \\ \tilde{B}_{pq} &= \frac{P_{Apq}}{\gamma} + 2\bar{u}U_{Apq} \end{aligned}\right\} \quad (B\text{-}27)$$

In terms of these variables, equations (B-26) can be written as before,

$$\left.\begin{aligned} &\frac{d\tilde{D}_{pq}}{dz} + s\left(1 + \frac{s_{pq}^2}{s^2}\right)\tilde{B}_{pq} = -s\,E'_{pq} \\ &\frac{d\tilde{B}_{pq}}{dz} + s\,\tilde{D}_{pq} = s\,F'_{pq} \end{aligned}\right\} \quad (B\text{-}28)$$

where

$$\left.\begin{aligned} E'_{pq} &= -\left(1 + \frac{s_{pq}^2}{s^2}\right)2\bar{u}U_{Apq} \\ F'_{pq} &= \bar{u}P_{Apq} - H_{Apq} + \frac{s_{pq}^2}{s}\bar{u}V_{Apq} \end{aligned}\right\} \quad (B\text{-}29)$$

Solving for $\tilde{B}_{pq}$ in equations (B-28) gives

$$\frac{d^2\tilde{B}_{pq}}{dz^2} - (s^2 + s_{pq}^2)\tilde{B}_{pq} = s\frac{dF'_{pq}}{dz} + s^2E'_{pq} \quad (B\text{-}30)$$

where the boundary conditions, as for the "D" solution, are

$$\frac{d\tilde{B}_{pq}}{dz}(0) = 0\ , \quad \tilde{B}_{pq}(0) = \frac{P_{Apq}(0)}{\gamma}$$

For $p \neq \nu$, $q \neq h$, the solution is obtained by the method of variation of constants as

$$\tilde{B}_{pq} = \int_0^z \left(s\frac{dF'_{pq}}{dz} + s^2E'_{pq}\right)\frac{\sinh\sqrt{s_{pq}^2 - s_{\nu h}^2}\,(z-z')}{\sqrt{s_{pq}^2 - s_{\nu h}^2}}dz' + \frac{P_{Apq}(0)}{\gamma}\cosh\sqrt{s_{pq}^2 - s_{\nu h}^2}\,z \quad (B\text{-}31)$$

However, the solution of interest in determining the stability criteria is that for $p=\nu$, $q=h$, for which $s^2+s_{\nu h}^2 = O(\bar{u}_e)$. Then the equation for $\tilde{B}_{\nu h}$ is

$$\frac{d^2\tilde{B}_{\nu h}}{dz^2} = s\frac{dF'_{\nu h}}{dz} + s^2 E'_{\nu h} \qquad \text{(B-32)}$$

where to $O(\bar{u}_e)$, the functions $E'_{\nu h}$ and $F'_{\nu h}$ are

$$E'_{\nu h} = 0 \quad , \quad F'_{\nu h} = -H_{A\nu h}$$

Now $H_{A\nu h}$ is defined by

$$\sum_{p=0}^{\infty}\sum_{q=1}^{\infty} H_{Apq}(z)\,\Psi_{pq}(r)\,\Theta_p(\theta) = \int_0^z \rho\frac{d\bar{u}}{dz}\,p_1(z',r,\theta)\,dz'$$

and neglecting higher order terms,

$$H_{A\nu h} = \rho\,\bar{u}\,P_{00}$$

so that

$$\tilde{B}_{\nu h} = \frac{P_{A\nu h}}{\gamma} = s\rho\int_0^z P_{00}\,\bar{u}(z')dz' + B_{\nu h}(0)$$

or

$$\frac{P_{A\nu h}}{P_{00}} = -\gamma s\rho\int_0^z \bar{u}(z')\,dz' + \frac{P_{A\nu h}(0)}{P_{00}} \qquad \text{(B-33)}$$

This is the same result as presented in equations (2.49) and (3.12a). The solutions for $P_{B\nu h}$ and $P_{C\nu h}$ exhibit the same behavior, showing that although the velocity gradient $\frac{d\bar{u}}{dz}$ may be locally O(1), the overall effect is the same as if it were of the same order as the velocity itself.

APPENDIX C

Nozzle Admittance Coefficients

In Chapter III a relation between the pressure, velocity, and entropy perturbations at the entrance of the nozzle was introduced as the boundary condition at the nozzle end of the combustion chamber. This "admittance relation" for neutral oscillations in a supercritical nozzle was derived by Crocco, first for longitudinal modes of oscillation (Reference 1, Appendix B), and later extended by him to transverse modes. A brief description of the latter derivation is given in Reference 25. The purpose of this Appendix is to discuss the calculation of the admittance coefficients and to present the results obtained for two typical cases.

The transverse admittance relation for axisymmetric flow is

$$\frac{\gamma V_e}{P_{oo}} + \mathcal{A}\,\frac{P_e}{P_{oo}} + \mathcal{B}\,s_{vh}\,\frac{\gamma V_e}{P_{oo}} + \mathcal{C}\,\frac{\gamma S_e}{P_{oo}} = 0 \qquad \text{(C-1)}$$

where

$$\left.\begin{aligned} \mathcal{A} &= \frac{\sqrt{\frac{2}{\gamma+1}}\;\bar{u}\,\bar{c}^2(\xi_0\bar{c}^2-\zeta)}{\bar{u}^2(\xi_0\bar{c}^2-\zeta)-i\omega} \\ \mathcal{B} &= \frac{\frac{i\omega}{s_{vh}}\sqrt{\frac{\bar{u}}{\bar{c}^{2(\gamma+1)}}}\;\xi_0}{\bar{u}^2(\xi_0\bar{c}^2-\zeta)-i\omega} \\ \mathcal{C} &= \frac{\sqrt{\frac{2}{\gamma+1}}\;\bar{u}\left(f_3\zeta+\frac{1-\bar{u}^2}{2}\xi_0-i\omega\xi_2\right)}{\bar{u}^2(\xi_0\bar{c}^2-\zeta-i\omega} \end{aligned}\right\} \qquad \text{(C-2)}$$

are the admittance coefficients (the notation here differs somewhat fo that of Reference 25). In the expressions (C-2), $\bar{u}$, $\bar{c}$, ω , and γ refer to steady state gas velocity and sound velocity, oscillation frequency, and specific heat ratio, respectively, just as in Chapter III, although a different nondimensionalization scheme has been used. The auxiliary functions ζ , ξ_0 , ξ_2 , and f_3 will be discussed below.

The independent variable in the analysis of the oscillatory nozzle flow was taken as the steady state velocity potential ϕ , defined by the equation

$$\bar{u}(z) = \frac{d\phi}{dz} \tag{C-3}$$

The velocity profile in the nozzle is determined by the convergent section geometry, although it has been found convenient in this calculation to find a convenient analytical expression for $\bar{u}(z)$ which approximates well the actual velocity variation, which can be determined only by numerical methods.

The admittance coefficients may be obtained for an entire family of nozzles at one time. This family consists of all nozzles obtained from a single nozzle by a change of scale in the axial direction. That is, $\bar{u}(Kz)$ is specified rather than $\bar{u}(z)$, where K is an arbitrary multiplicative constant, and it is clear that

$$\bar{u}(Kz) = \frac{d(K\phi)}{d(Kz)}$$

The parameter of affinity K can be defined in many ways. In the present calculation it has been taken as the (dimensionless) velocity gradient at the throat, i.e.,

$$K = \left(\frac{d\bar{u}}{dz}\right)_t = \frac{1}{2}\left(\frac{d\bar{u}^2}{d\phi}\right)_t \tag{C-4}$$

Then the following transformation can be made in order to include all nozzles of the family in the calculation of the coefficients:

$$\left.\begin{aligned} X &= 2K\phi \\ \zeta' &= \zeta/2K \\ \omega' &= \omega/K \\ S'_{vh} &= S_{vh}/K \\ \xi_0' &= \xi_0/K \\ \xi_2' &= \xi_2 \\ f_3' &= f_3 \end{aligned}\right\} \tag{C-5}$$

Insertion of these expressions into the definitions of the admittance coefficients gives:

$$\mathcal{A} = \frac{\sqrt{\frac{2}{\gamma+1}}\ \bar{u}\,\bar{c}^2\left(\xi_0'\bar{c}^2 - \zeta'\right)}{\bar{u}^2\left(\xi_0'\bar{c}^2 - \zeta'\right) - i\frac{\omega'}{2}}$$

$$\mathcal{B} = \frac{\frac{i\omega'}{S_{2h}'}\sqrt{\frac{\bar{u}}{\bar{c}^{\frac{3}{\gamma-1}}}}\ \xi_0'}{\bar{u}^2\left(\xi_0'\bar{c}^2 - \zeta'\right) - i\frac{\omega'}{2}} \qquad \text{(C-6)}$$

$$\mathcal{C} = \frac{\sqrt{\frac{2}{\gamma+1}}\ \bar{u}\left(f_3'\zeta' + \frac{1-\bar{u}^2}{2}\xi_0' - i\frac{\omega'}{2}\xi_2'\right)}{\bar{u}^2\left(\xi_0'\bar{c}^2 - \zeta'\right) - i\frac{\omega'}{2}}$$

All quantities in the nozzle analysis have been nondimensionalized by corresponding values at the nozzle throat section: lengths by the throat radius, pressures by the throat (critical) pressure, velocities by the sonic velocity at the throat, etc. In order to match the nozzle conditions to the corresponding combustion chamber conditions at the entrance of the nozzle, the following relations are used,

$$S_{2h}' = \frac{1}{K}\left(S_{2h}\right)_{CHAMBER}$$
$$\bar{u} = \sqrt{\frac{\gamma+1}{2}}\left(\bar{u}_e\right)_{CHAMBER} \qquad \text{(C-7)}$$
$$\omega' = \frac{\sqrt{\frac{\gamma+1}{2}}\ f\ S_{2h}'}{\sqrt{A_c/A_t}}$$

where $f = \left(\frac{\omega}{S_{2h}}\right)_{CHAMBER}$ is the ratio of the actual chamber oscillation frequency to the frequency of acoustic oscillations, and A_c/A_t is the nozzle contraction ratio, which is uniquely related to the Mach number at the nozzle entrance $\bar{u}_e$.

Calculations have been carried out for two convergent section geometries, which will be referred to as the "linear" and "conical" nozzles, respectively. The physical profiles of the nozzles are shown in Figure C1,

and the corresponding velocity profiles in Figure C2. The linear nozzle is constructed so that the velocity varies linearly with distance along the axis in the converging section. The resulting expression for $\bar{u}(x)$,

$$\bar{u}^2 = 1 + X \tag{C-8}$$

where the throat section corresponds to $x=0$ and the positive X direction is the direction of flow, results in some simplification in the computations. The velocity profile in the conical nozzle is decidedly not linear, as shown in Figure C2. However, because of the circular arc throat section, the velocity variation can be taken as linear in the vicinity of the throat section, then between the throat section and a station a short distance away, the velocity can be represented by an expression of the form of equation (C-8). Beyond that station, a more complicated expression is necessary. For the 30° half-angle convergent section geometry used in the experimental phase of the transverse instability investigation, the following expressions have been found to approximate well the subsonic velocity distribution:

$$\left.\begin{aligned} \bar{u}^2 &= 1 + x, \qquad x_{tu} \le x \le 0 \\ \bar{u} &= \left(0.401\, x - \frac{0.0563}{x} + 0.9428\right), \qquad x_f \le x \le x_{tu} \end{aligned}\right\} \tag{C-9}$$

where x_{tu} is the station of changeover from the linear to the nonlinear velocity profile, and x_f is the limit of the range of interest of the calculations.

The calculation process may be thought of as having three stages: first, the solution of the differential equation for the auxiliary function ζ' , second, the calculation of the other functions ξ_0' , ξ_2' , and f_3' , and third, the computation of the admittance coefficients.

The function ζ' satisfies the complex Riccati equation

$$b_n\left(\frac{d\zeta'}{dx}+\zeta'^2\right)-(g_n+ih_n)\zeta'+j_n-ik_n=0 \qquad \text{(C-10)}$$

where

$$b_n = \bar{u}^2\left(\bar{c}^2-\bar{u}^2\right)$$

$$g_n = \frac{\gamma+1}{2}\frac{\bar{u}^2}{\bar{c}^2}\frac{d\bar{u}^2}{dx}$$

$$h_n = \omega'\bar{u}^2$$

$$j_n = \frac{\omega'^2}{4} - \frac{\bar{u}\bar{c}^{\frac{2\gamma}{\gamma-1}}S_{sh}^2}{4}$$

$$k_n = \frac{\gamma-1}{4}\frac{\bar{u}^2}{\bar{c}^2}\frac{d\bar{u}^2}{dx}\omega'$$

Equation (C-10) is equivalent to two real equations

$$\frac{d\zeta_r'}{dx} = \frac{1}{b_n}\left(g_n\zeta_r' - h_n\zeta_i' - j_n\right) - \zeta_r'^2 + \zeta_i'^2 \qquad \text{(C-11)}$$

$$\frac{d\zeta_i'}{dx} = \frac{1}{b_n}\left(h_n\zeta_r' + g_n\zeta_i' + k_n\right) - 2\zeta_r'\zeta_i' \qquad \text{(C-12)}$$

where $\zeta' = \zeta_r' + i\,\zeta_i'$. These differential equations are nonlinear, and have a singularity at the origin, which corresponds to the nozzle throat, where $\bar{u}=\bar{c}=1$. The boundary conditions for the functions ζ_r' and ζ_i' are taken from the physical condition that ζ' be regular at the sonic throat (see Reference 1, Appendix B). Therefore, the solution must be started at $X = 0$. This can be done by expanding ζ_r' and ζ_i' in power series about the origin. In a certain range, $x_1 \le X \le 0$, a suitable approximation is obtained by keeping only terms up to the first power in x. The solution in this range is found to be

$$\zeta_r' = \alpha_0 - \frac{x}{\left(\frac{\gamma+1}{2}\right)^2+\omega'^2}\left\{\alpha_0\left[\left(\frac{\gamma+1}{2}\right)^3+\omega'^2\right] - \frac{\gamma+1}{2}\beta_0\left[1-\frac{\gamma+1}{2}\omega'\right]\right.$$
$$\left. + \frac{\gamma^2-1}{8}\left(\omega'^2-S_{sh}^2\right) + \left(\frac{\gamma+1}{2}\right)^2\left(\alpha_0^2-\beta_0^2\right) + 2\left(\frac{\gamma+1}{2}\right)\omega'\alpha_0\beta_0\right\} \qquad \text{(C-13)}$$

$$\cdots - \frac{\kappa}{\left(\frac{\gamma+1}{2}\right)^2+\omega'^2}\left\{\frac{(\gamma+1)(3-\gamma)}{4}\omega'\alpha_0 + \beta_0\left[\left(\frac{\gamma+1}{2}\right)^2+\omega'^2\right]\right. \tag{C-14}$$

$$\left. + \frac{\gamma-1}{8}\omega'\left[\left(\frac{\gamma+1}{2}\right)^2 - S'^2_{yh}\right] - \frac{\gamma-1}{2}\omega'(\alpha_0^2-\beta_0^2) + 2\left(\frac{\gamma+1}{2}\right)^2\alpha_0\beta_0\right\}$$

where

$$\kappa_0 = \frac{\frac{\gamma+1}{2}\left(\frac{\omega'^2}{4} - \frac{S'^2_{yh}}{4}\right) - \frac{\gamma-1}{4}\omega'^2}{\left(\frac{\gamma+1}{2}\right)^2+\omega'^2}, \qquad \beta_0 = -\frac{\omega\left[\frac{\gamma^2-1}{8} + \left(\frac{\omega'^2}{4} - \frac{S'^2_{yh}}{4}\right)\right]}{\left(\frac{\gamma+1}{2}\right)^2+\omega'^2}$$

Beyond the station κ_1, the solution can proceed without difficulty because there are no other singularities in the range of interest. In the present computation, the differential equations were integrated by means of the method of Runge-Kutta, which evaluates the dependent variable at each x-step by means of the derivative calculated locally. That is, given

$$\frac{dy}{dx} = f(x, y)$$

then

$$y_{n+1} = y(x_{n+1}) = y_n + \frac{1}{6}(k_1 + 2k_2 + 2k_3 + k_4)$$

where

$$k_1 = \Delta x \cdot f(x_n, y_n)$$

$$k_2 = \Delta x \cdot f\left(x_n + \frac{\Delta x}{2}, y_n + \frac{k_1}{2}\right)$$

$$k_3 = \Delta x \cdot f\left(x_n + \frac{\Delta x}{2}, y_n + \frac{k_2}{2}\right)$$

$$k_4 = \Delta x \cdot f(x_n + \Delta x, y_n + k_3)$$

$$\Delta x = x_{n+1} - x_n$$

Explicit integral expressions can be found for the auxiliary variables ξ_0', ξ_2', and f_3': for example,

$$f_3'(x) = \frac{1}{2\tilde{c}^2}\exp\left(\frac{i\omega'}{2}\int_0^x \frac{dx'}{\tilde{u}^2}\right)\int_0^x \frac{d\tilde{u}^2}{dx}\exp\left(-\frac{i\omega'}{2}\int_0^{x'}\frac{dx''}{\tilde{u}^2}\right)dx' \tag{C-15}$$

However, because of the oscillatory nature of the integrand, it was decided to evaluate the auxiliary variables by direct numerical integration of the

following differential equations:

$$\frac{d}{dx}\left(\bar{c}^2 f_3'\right) - \frac{i\omega'}{2\bar{u}^2}\left(\bar{c}^2 f_3'\right) = \frac{1}{2}\frac{d\bar{u}^2}{dx} \tag{C-16}$$

$$\frac{d}{dx}\left[(1-\bar{u}^2)\xi_2'\right] + (1-\bar{u}^2)\xi_2'\left[\zeta' - i\omega'\left(\frac{1}{2\bar{u}^2} + \frac{2}{(\gamma+1)(1-\bar{u}^2)}\right)\right] =$$
$$= \left(\frac{2}{\gamma+1}\right)\left[\frac{df_3'}{dx} + \frac{s_{\nu h}'^2 \bar{c}^{\frac{2}{\gamma-1}}\bar{u}}{2i\omega'}\left(\frac{-\bar{u}^2}{2\bar{u}^2} + \frac{\bar{c}^2}{\bar{u}^2} f_3'\right)\right] \tag{C-17}$$

$$\frac{d}{dx}\left[(1-\bar{u}^2)\xi_0'\right] + (1-\bar{u}^2)\xi_0'\left[\zeta' - i\omega'\left(\frac{1}{2\bar{u}} + \frac{2}{(\gamma+1)(1-\bar{u}^2)}\right)\right] =$$
$$= \left(\frac{2}{\gamma+1}\right)\frac{s_{\nu h}'^2}{4}\frac{\bar{c}^{\frac{2}{\gamma-1}}}{\bar{u}} \tag{C-18}$$

The integration of equations (C-16) to (C-18) proceeds in the same manner as that discussed above for equations (C-11) and (C-12). The fact that this procedure leaves the functions ξ_0' and ξ_2' undetermined at the origin is unimportant in the calculation of the admittance coefficients.

Although it is convenient conceptually to divide the computation process into three stages, in practice it is possible to carry out the calculations of all stages in one operation, at each x-station. A single integration will thus give the coefficients for a wide range of chamber exit Mach number values, but for only one value of the fequency and mode parameters $\omega'/s_{\nu h}'$ and $s_{\nu h}'$. The oscillatory nature of the functions involved in the integration process make it necessary to use a small value of the integration step Δx. In order to cover a range of Mach numbers down to 0.05, with Δx =0.001, some 1900 integration steps are required. For use in comparing the theoretical and experimental results, especially in the case of the sector motor, a rather wide range is required for the parameter $s_{\nu h}'$, while the reduced frequency $\omega'/s_{\nu h}'$ is restricted to a fairly narrow range. However, in order to make the results more general, a much wider frequency range was used. The calculations were made for values of $s_{\nu h}'$ between 1 and 5, and for $\omega'/s_{\nu h}'$ between

0.1 and 1.0. It is interesting to compare the approximate times required by various computational methods to perform the calculations for 50 pairs of values of $1/S_{yh}$ and S_{yh} :

desk calculator ---- 1000 years
IBM 650 ---------- 500 hours
IBM 704 ---------- 6 hours
IBM 7090 ----------1-1/2 hours

Typical results of the calculations are shown in Figures C3 through C10. The coefficients plotted are $\mathcal{E}_r$ and $\mathcal{E}_i$, where

$$\mathcal{E} = \mathcal{E}_r + i\,\mathcal{E}_i = \mathcal{A} + i\,\mathcal{B} \tag{C-19}$$

since the nozzle admittance relation is used in the form

$$\frac{d}{d\bar{z}}\left(\frac{P_e}{P_{oo}}\right) - i\,S_{yh}\,\mathcal{E}\left(\frac{P_e}{P_{oo}}\right) = 0 \tag{C-20}$$

for the analysis of purely transverse modes with combustion complete at the nozzle entrance (see Chapter III). Figures C3 and C4 show $\mathcal{E}_r$ and $\mathcal{E}_i$ for a conical nozzle with a chamber exit Mach number of 0.05; Figures C5 and C6 are plotted for a Mach number of 0.10. Corresponding values of the admittance coefficients obtained for the linear nozzle are presented in Figures C7 to C10. The "range of interest" shown on the graphs of the coefficients is that corresponding to chamber oscillation frequencies within ±10 percent of the acoustical oscillation frequency. This restriction of the chamber frequency range has been observed experimentally, and is related to the theoretical assumption that the axial velocity perturbation is an order of magnitude smaller than the pressure and radial velocity perturbations. It can be seen that the admittance coefficients for the conical nozzle vary more rapidly with frequency than do those for the linear nozzle. However, in the range of interest of this study, the coefficients for the two nozzles are of approximately the same magnitude.

DISTRIBUTION LIST

TECHNICAL AND PROGRESS REPORTS

CONTRACT USN-BuWeps NOW 61-0686
(NASA) (CONFIDENTIAL)

U. S. Dept. of the Interior
Bureau of Mines
4800 Forbes Avenue
Pittsburgh 13, Pennsylvania
Attn: M. P. Beroy, Reports Libr.
Explosive Research Lab. (1)

Central Intelligence Agency
2430 E Street, N. W.
Washington 25, D. C.
Attn: OCD, Standard Dist. (1)

NASA
1512 H Street, N. W.
Washington 25, D. C.
Attn: Chief Div. of Res. Info. (5)

NASA
Langley Research Center
Langley Field, Virginia
Attn: E. R. Gilman, Librarian (1)

NASA
Lewis Research Center
21000 Brookpark Road
Cleveland 35, Ohio
Attn: Library (1)

Commander
Air Force Flight Test Center
Edwards AFB, California
Attn: FTRDL (1)
Attn: FTRPL (1)

Office of the Director of Defense
Research and Engineering
Washington 25, D. C.
Attn: D. B. Brooks
Off. of Fuels and Lubricants (1)

Dept. of the Air Force
Headquarters USAF, DCS/D
Washington 25, D. C.
Attn: AFDRT/AS (1)

Commander
Wright Air Development Division
Wright-Patterson AFB, Ohio
Attn: WCLJC (1)

Commander
Wright Air Development Div.
Wright-Patterson AFB, Ohio
Attn: WCLTLPE (1)

Commander
Air Force Ballistic Missile Div.
Air Force Unit Post Office
Los Angeles 45, California
Attn: WDSOT (1)

Commander
Air Force Missile Dev. Center
Holloman, AFB, New Mexico
Attn: MDGRT (1)

Commander
Air Force Missile Test Center
Patrick AFB, Florida
Attn: Technical Information and
Intelligence Br. (MTGRY) (1)

Commander
AF Office of Scientific Res.
ARDC 19th and E. Capitol Sts.
Washington 25, D. C.
Attn: SRCP, Dr. M. Slawsky (1)

Commander
Air Research and Dev. Command
Andrews Air Force Base
Washington 25, D. C.
Attn: RDRR-2 (1)

ASTIA
Arlington Hall Station
Arlington 12, Virginia
Attn: TIPCR (10)

Commander
Arnold Engg. Dev. Center
Air Research and Dev. Command
Tullahoma, Tennessee
Attn: AEOIM (1)

Commanding General
Aberdeen Proving Ground
Maryland
Attn: Ballistics Res. Lab.
ORDB-BLI (1)

Commander
Army Ballistics Missile Agcy.
Redstone Arsenal, Alabama
Attn: Tech. Documents Library
ORDAB-HT (3)

U. S. Army
Chemical Research and Dev. Labs.
Army Chemical Center, Maryland
Attn: Keith H. Jacobson
Medical Research (1)

Commanding Officer
Diamond Ord. Fuze Lab.
Washington 25, D. C.
Attn: ORDTL (012) (1)

Commanding General
Frankford Arsenal
Philadelphia 37, Pennsylvania
Attn: Mr. M. E. Levy, 1331
Research Division (1)

Commanding Officer
Office of Ord. Research
Box CM, Duke Station
Durham, North Carolina (1)

Commanding Officer
Picatinny Arsenal
Dover, New Jersey
Attn: Librarian (1)

Commander
Army Rocket and Guided Missile Agcy.
Redstone Arsenal, Alabama
Attn: Technical Library (2)

Commanding Officer
Picatinny Arsenal
Liquid Rocket Propulsion Lab.
Dover, New Jersey
Attn: Technical Library (2)
Attn: Mr. Jenkins (1)

Commanding General
White Sands Missile Range
New Mexico
Attn: Library (1)

Bureau of Naval Weapons
Dept. of the Navy
Washington 25, D. C.
Attn: RMMP-24 (3)

Bureau of Naval Weapons
Dept. of the Navy
Washington 25, D. C.
Attn: RRRSY-2 (1)

Bureau of Naval Weapons
Dept. of the Navy
Washington 25, D. C.
Attn: RMMP-4 (1)

Bureau of Naval Weapons
Dept. of the Navy
Washington 25, D. C.
Attn: ReS6 (1)

Commander
Pacific Missile Range
Point Mugu, California
Attn: Tech Library, Code 212 (2)

Commander
Naval Ordnance Lab.
White Oak
Silver Spring, Maryland
Attn: E. C. Noonan (1)

Commander (Code 753)
U. S. Naval Ord. Test Station
China Lake, California (2)

Director (Code 6180)
U. S. Naval Research Lab.
Washington 25, D. C.
Attn: H. W. Crhart (1)

Dept. of the Navy
Chief of Naval Research
Washington 25, D. C.
Attn: Propulsion Chemistry
Branch - Code 426 (1)

Commanding Officer
ONR Branch Office
1030 East Green Street
Pasadena, California (1)

Superintendent
U. S. Naval Postgraduate School
Naval Academy
Monterey, California (1)

Commanding Officer
U. S. Naval Underwater Ord. Station
Newport, Rhode Island
Attn: W W. Bartlett (1)

Aerojet-General Corporation
P. O. Box 296
Azusa, California
Attn: M. Grenier, Librarian (1)

Aerojet-General Corporation
Sacramento Plants
P. O. Box 1947
Sacramento 9, California
Attn: R. G. Weltz
Head, Tech. Info. Off. (1)

Aeronutronic
Div. of Ford Motor Company
Ford Road
Newport Beach, California
Attn: L. H. Linder, Div. Librarian (1)

Aeroprojects, Inc.
West Chester, Pennsylvania
Attn: W. Tarpley (1)

Air Reduction Company, Inc.
Murray Hill, New Jersey
Attn: Dr. Fred Balcar (1)

American Cyanamid Company
1937 W. Main Street
Stamford, Connecticut
Attn: Dr. A. L. Pelker (1)

Armour Research Foundation
Illinois Inst. of Technology
Chicago, Illinois
Attn: M. Klein (1)

Arthur D. Little, Inc.
Acorn Park
Cambridge 40, Massachusetts
Attn: D. C. Bowersock, Jr. (1)

Atlantic Research Corporation
Edsall Road & Shirley Highway
Alexandria, Virginia (2)

Bell Aircraft Corporation
Box 1
Buffalo 5, New York
Attn: T. Reinhardt (1)

Callery Chemical Company
Callery, Pennsylvania
Attn: Document Control (1)

The Dow Chemical Company
Midland, Michigan
Attn: M. S. Auro,
Tech. Serv. and Dev. Dept.
Abbott Road Buildings (1)

Esso Research and Engg. Co.
P.O. Box 51
Linden, New Jersey
Attn: Dr. J. P. Longwell
Spec. Project Unit (1)

Texaco Experiment, Inc.
P. O. Box 1-T
Richmond 2, Virginia
Attn: Elaine Weil, Library (1)

Food Machinery and Chem. Corp.
Special Projects Branch
P.O. Box 38
Buffalo 13, New York (1)

The Fulton-Irgon Corporation
P.O. Box 591
Dover, New Jersey
Attn: David Lippmann (1)

General Electric Company
Rocket Propulsion Units
Building 300
Cincinnati 15, Ohio
Attn: E. St. Clair Gantz (2)

Hughes Tool Company
Aircraft Division
Culver City, California
Attn: Dr. I. Shapiro (1)

Jet Propulsion Laboratory
4800 Oak Grove Drive
Pasadena 3, California
Attn: I. E. Newlan,
Chief Reports Group (1)

Liquid Propellant Information Agcy.
Applied Physics Laboratory
The Johns Hopkins University
Silver Spring, Maryland (3)

Marquardt Corporation
16555 Saticoy Street
Box 2013 - South Annex
Van Nuys, California (1)

Minnesota Mining & Mfg. Co.
900 Bush Avenue
St. Paul 6, Minnesota
Attn: J. W. Millin (1)

New York University
Dept. of Chemical Engg.
New York 53, New York
Attn: P. F. Winternitz (1)

Olin Mathieson Chem. Corporation
Research Library
New Haven, Connecticut
Attn: Mrs. Laura M. Kajuti (1)

Peninsular Chem-Research, Inc.
P. O. Box 3597
1207 N. W. Fifth Avenue
Gainesville, Florida
Attn: Paul Tarrant (1)

Pennsalt Chemical Corp.
P. O. Box 4388
Philadelphia 18, Pennsylvania
Attn: Dr. G. Bart-Wehrenalp (1)

Phillips Petroleum Co.
145 Chemical Laboratories Bldg.
Bartlesville, Oklahoma
Attn: Nadine G. Loge (1)

Purdue University
Lafayette, Indiana
Attn: M. J. Zucrow (1)

Reaction Motors Division
Thiokol Chemical Corporation
Denville, New Jersey
Attn: D. Mann (1)

Rocketdyne
North American Aviation, Inc.
6633 Canoga Avenue
Canoga Park, California
Attn: J. Silverman (2)

Rohm and Haas Company
Redstone Arsenal
Huntsville, Alabama
Attn: Librarian (1)

Shell Development Company
Emergyville, California
Attn: R. R. Ward (1)

Space Technology Labs
P. O. Box 95001
Airport Station
Los Angeles, 45, California
Attn: M. Goldman (1)

Stauffer Chemical Company
Chauncey, New York
Attn: J. R. Gould (1)

Sundstrand Turbo
Division of Sundstrand Corp.
10445 Glenoaks Blvd.
Pacoima, California
Attn: W. Unterberg (1)

Thiokol Chemical Corporation
Redstone Division
Huntsville, Alabama
Attn: Technical Director (1)

Wyandotte Chemical Corporation
Wyandotte, Michigan
Attn: R. A. Graham
Dept. of Cont. Research (1)

Monsanto Chemical Company
Research and Engg. Division
Spec. Proj. Dept. - 1 Chemical Lane
Everett Station, Boston 49, Mass.
Attn: K. Warren Easley (1)

Union Carbide Chemicals Company
Development Department
P. O. Box 8356
South Charleston, West Virginia
Attn: Dr. H. W. Schulz (1)

Dr. W. W. Wharton
Research Laboratory, Bldg. 4762
ARGMA
Redstone Arsenal
Huntsville, Alabama (1)

Commanding Officer
Office of Naval Research
346 Broadway
New York 13, New York
via
Office of Naval Research
Princeton, New Jersey
Attn: Julian Levy
Resident Representative (1)

Texaco, Inc.
Texaco Research Center
Beacon, New York
Attn: Technical Library (1)

United Aircraft Corporation
400 Main Street
East Hartford, Connecticut
Attn: Library (1)

Project Squid - Librarian (1)